Isosorbide as a building block for polyurethanes

Héloïse Blache

N°d'ordre NNT : xxx

THESE de DOCTORAT DE L'UNIVERSITE DE LYON
opérée au sein de
l'Institut National des Sciences Appliquées

Ecole Doctorale EDA 034
Matériaux de Lyon

Spécialité de doctorat : Matériaux
Discipline : Chimie des polymères

CONFIDENTIEL PENDANT 5 ANS (jusqu'au 29/03/2023)

Soutenue à huis clos le 29/03/2018, par :

Héloïse Blache

L'isosorbide en tant que composant pour les polyuréthanes

Isosorbide as a building block for polyurethanes

Devant le jury composé de :

ECEIZA, Arantxa	Professeure	Université du Pays Basque	Examinatrice
JOLY-DUHAMEL, Christine	Enseignant-Chercheur	ENSCM	Rapporteure
BUREL, Fabrice	Professeur	INSA-Rouen	Rapporteur
FLEURY, Etienne	Professeur	INSA-Lyon	Directeur de thèse
ROUSSEAU, Alain	Ingénieur de Recherche	INSA-Lyon	Encadrant
MÉCHIN, Françoise	Chargée de Recherche	CNRS	Encadrante
SAINT-LOUP, René	Docteur	Roquette Frères	Invité
JACQUEL, Nicolas	Docteur	Roquette Frères	Invité
PASCAULT, Jean-Pierre	Professeur Emerite	INSA-Lyon	Invité

Département FEDORA – INSA Lyon - Ecoles Doctorales – Quinquennal 2016-2020

SIGLE	ECOLE DOCTORALE	NOM ET COORDONNEES DU RESPONSABLE
CHIMIE	**CHIMIE DE LYON** http://www.edchimie-lyon.fr Sec. : Renée EL MELHEM Bât. Blaise PASCAL, 3e étage secretariat@edchimie-lyon.fr INSA : R. GOURDON	M. Stéphane DANIELE Institut de recherches sur la catalyse et l'environnement de Lyon IRCELYON-UMR 5256 Équipe CDFA 2 Avenue Albert EINSTEIN 69 626 Villeurbanne CEDEX directeur@edchimie-lyon.fr
E.E.A.	**ÉLECTRONIQUE, ÉLECTROTECHNIQUE, AUTOMATIQUE** http://edeea.ec-lyon.fr Sec. : M.C. HAVGOUDOUKIAN ecole-doctorale.eea@ec-lyon.fr	M. Gérard SCORLETTI École Centrale de Lyon 36 Avenue Guy DE COLLONGUE 69 134 Écully Tél : 04.72.18.60.97 Fax 04.78.43.37.17 gerard.scorletti@ec-lyon.fr
E2M2	**ÉVOLUTION, ÉCOSYSTÈME, MICROBIOLOGIE, MODÉLISATION** http://e2m2.universite-lyon.fr Sec. : Sylvie ROBERJOT Bât. Atrium, UCB Lyon 1 Tél : 04.72.44.83.62 INSA : H. CHARLES secretariat.e2m2@univ-lyon1.fr	M. Philippe NORMAND UMR 5557 Lab. d'Ecologie Microbienne Université Claude Bernard Lyon 1 Bâtiment Mendel 43, boulevard du 11 Novembre 1918 69 622 Villeurbanne CEDEX philippe.normand@univ-lyon1.fr
EDISS	**INTERDISCIPLINAIRE SCIENCES-SANTÉ** http://www.ediss-lyon.fr Sec. : Sylvie ROBERJOT Bât. Atrium, UCB Lyon 1 Tél : 04.72.44.83.62 INSA : M. LAGARDE secretariat.ediss@univ-lyon1.fr	Mme Emmanuelle CANET-SOULAS INSERM U1060, CarMeN lab, Univ. Lyon 1 Bâtiment IMBL 11 Avenue Jean CAPELLE INSA de Lyon 69 621 Villeurbanne Tél : 04.72.68.49.09 Fax : 04.72.68.49.16 emmanuelle.canet@univ-lyon1.fr
INFOMATHS	**INFORMATIQUE ET MATHÉMATIQUES** http://edinfomaths.universite-lyon.fr Sec. : Renée EL MELHEM Bât. Blaise PASCAL, 3e étage Tél : 04.72.43.80.46 Fax : 04.72.43.16.87 infomaths@univ-lyon1.fr	M. Luca ZAMBONI Bât. Braconnier 43 Boulevard du 11 novembre 1918 69 622 Villeurbanne CEDEX Tél : 04.26.23.45.52 zamboni@maths.univ-lyon1.fr
Matériaux	**MATÉRIAUX DE LYON** http://ed34.universite-lyon.fr Sec. : Marion COMBE Tél : 04.72.43.71.70 Fax : 04.72.43.87.12 Bât. Direction ed.materiaux@insa-lyon.fr	M. Jean-Yves BUFFIÈRE INSA de Lyon MATEIS - Bât. Saint-Exupéry 7 Avenue Jean CAPELLE 69 621 Villeurbanne CEDEX Tél : 04.72.43.71.70 Fax : 04.72.43.85.28 jean-yves.buffiere@insa-lyon.fr
MEGA	**MÉCANIQUE, ÉNERGÉTIQUE, GÉNIE CIVIL, ACOUSTIQUE** http://edmega.universite-lyon.fr Sec. : Marion COMBE Tél : 04.72.43.71.70 Fax : 04.72.43.87.12 Bât. Direction mega@insa-lyon.fr	M. Jocelyn BONJOUR INSA de Lyon Laboratoire CETHIL Bâtiment Sadi-Carnot 9, rue de la Physique 69 621 Villeurbanne CEDEX jocelyn.bonjour@insa-lyon.fr
ScSo	**ScSo*** http://ed483.univ-lyon2.fr Sec. : Viviane POLSINELLI Brigitte DUBOIS INSA : J.Y. TOUSSAINT Tél : 04.78.69.72.76 viviane.polsinelli@univ-lyon2.fr	M. Christian MONTES Université Lyon 2 86 Rue Pasteur 69 365 Lyon CEDEX 07 christian.montes@univ-lyon2.fr

*ScSo : Histoire, Géographie, Aménagement, Urbanisme, Archéologie, Science politique, Sociologie, Anthropologie

Remerciements

Je tiens tout d'abord à adresser mes plus sincères remerciements à mon directeur de thèse le professeur Etienne Fleury, et mes co-directeurs Alain Rousseau et Françoise Méchin, qui ont su me guider et me conseiller sur ce parcours semé d'embuches. Plus particulièrement, merci à Françoise pour son expertise et ses conseils avisés sur les polyuréthanes et leur technologie ainsi que sa réactivité pour la relecture de mes nombreuses présentations et divers rapports. Merci à Alain pour ses conseils plus particuliers concernant la RMN et l'IV, et merci à Etienne pour son expertise concernant l'isosorbide. Merci à tous les trois de m'avoir fait confiance !

J'aimerais également remercier l'entreprise Roquette et son financement, sans lequel ce projet n'aurait pas vu le jour. En particulier, merci également à René Saint-Loup et Nicolas Jacquel pour leur expertise sur l'isosorbide, et grâce à qui plusieurs brevets ont pu être déposés.

Nombres d'idées ont également été apportées par le professeur Jean-Pierre Pascault que je remercie pour avoir suivi ce projet. Merci, enfin, pour les nombreux conseils concernant la SEC et la synthèse de PU.

Je remercie également Pierre Alcouffe pour son travail inestimable sur la microscopie TEM et SEC, ainsi que Caroline Pillon pour son aide sur la SEC DMSO.

Je remercie Vincent Monti, qui par son travail de stage, a grandement contribué à la mise en place des tests mécaniques sur les revêtements.

Je remercie le service RMN et le CTμ pour nous avoir permis l'accès à leurs équipements et leur expertise.

Un laboratoire ne serait pas ce qu'il est sans un parc machine conséquent (et ses diverses pannes), je remercie donc Marion Colella, Raphaël Brunel, Guilhem Quintard, Julien Chatard et Pierre-Yves Renaud pour leur disponibilité au jour le jour et leur savoir-faire technique.

Merci à tous mes amis doctorants, et en particulier Raïssa, Matthieu, Benjamin et Thibaut pour les bons moments que nous avons passés ensemble. Merci pour votre soutien quotidien, les discussions scientifiques, votre bonne humeur et les pauses café !

Pour terminer, merci à mes parents pour leur soutien et leurs encouragements, et Laurent pour m'avoir supportée tout au long de ce dernier marathon.

Résumé en français de la thèse

INTRODUCTION

Dans les dernières décennies, le design de matériaux renouvelables est devenu une préoccupation majeure. Découvrir de nouveaux monomères biosourcés pour les plastiques est un enjeu important pour la transition vers des matériaux plus verts. Dans ce contexte, notre partenaire industriel, Roquette cherche à évaluer le potentiel d'une de ses molécules biosourcées, l'isosorbide. L'isosorbide a déjà été intégré avec succès dans divers polymères techniques tels que les polycarbonates ou les polyesters, auxquels il donne une température de transition vitreuse plus élevée et une plus grande dureté. Comme le polyuréthane est le 6ème polymère en termes de production dans le monde, et qu'il est habituellement utilisé pour des applications techniques, l'évaluation de l'intégration de l'isosorbide dans des polyuréthanes est du plus grand intérêt.

En effet, l'isosorbide pourrait devenir une alternative plus sûre à l'utilisation de 1,4-butanediol (qui peut aussi être biosourcé), et pourrait augmenter la boîte à outils disponible pour le design de polyuréthanes. Sa structure chimique en fait un bon candidat pour une utilisation en tant qu'allongeur de chaîne. Il est possible que l'isosorbide permette d'augmenter la dureté et la température de transition vitreuse dans les compositions polyuréthanes. Cependant, quelques propriétés intrinsèques de cette molécule la rendent aussi faiblement réactive et très hygroscopique.

Cette thèse a donc été orientée selon deux axes: l'incorporation d'isosorbide dans des copolymères linéaires à blocs, et l'incorporation d'isosorbide dans des matériaux polyuréthanes réticulés. Ce travail contient quatre chapitres principaux.

Le premier chapitre présente brièvement les polyuréthanes et leur chimie. En effet, la compréhension des mécanismes de réaction principaux, ainsi que les mécanismes à l'origine de la formation des microstructures, est essentielle pour leur bonne exploitation dans le reste des chapitres. Par ailleurs, ce chapitre contient également un court aperçu des méthodes de synthèse et des différents monomères disponibles commercialement pour la synthèse de polyuréthanes.

Les chapitres suivants présentent les résultats expérimentaux. L'isosorbide a été introduit dans plusieurs compositions polyuréthanes et chaque chapitre présente une application spécifique. Néanmoins, les chapitres progressent de l'étude de matériaux thermoplastiques microstructurés, au design de compositions plus homogènes et finalement au design de revêtements réticulés.

CHAPITRE 1

Dans le chapitre 1 sont résumés les paramètres importants à prendre en compte pour le design et la synthèse de matériaux polyuréthanes. Les principaux monomères utilisés industriellement pour la production de polyuréthanes sont également brièvement décrits.

La réaction menant à la formation d'une liaison uréthane à partir d'un alcool et d'un isocyanate a été utilisée pour la première fois pour la synthèse d'un polymère en 1937 par Otto Bayer. La versatilité de la chimie des polyuréthanes a permis par la suite d'obtenir une grande variété de matériaux, tels que des élastomères, des mousses ou encore des résines de coulée, et ce dès 1954. Cependant, la grande réactivité de la fonction isocyanate la rend également susceptible de réagir avec des fonctions autres que les alcools. Cette propriété est exploitée pour la production de polyurées avec la réaction isocyanates-amines. Les isocyanates sont également susceptibles de réagir avec d'autres entités chimiques telles que l'eau, les fonctions uréthanes ou encore les fonctions isocyanates. Ces réactions mènent en général à la formation de gaz ou de chaînes réticulées, ce qui peut être ou non désiré. La réaction uréthane est catalysée par diverses molécules, les plus courantes étant les organométalliques à base étain ou les amines. Il est également à noter que la fonction uréthane a une stabilité thermique variable selon sa structure chimique. Ainsi, une fonction du type alkyl-uréthane-aryl a une température de stabilité de dépassant pas 180°C.

Ensuite, la structure et la synthèse des élastomères polyuréthanes est décrite rapidement. Ce type de polymère est en effet un co-polymère à blocs statistiques comprenant un segment souple et un segment rigide. Il est obtenu par polyaddition entre un oligomère souple (généralement un polyéther ou un polyester) fonctionnalisé par des fonctions hydroxyle, un diisocyanate et un diol court appelé allongeur de chaîne. L'oligomère produit le segment souple alors que l'association diisocyanate et allongeur de chaîne produit le segment rigide. Ces deux segments sont en général incompatibles thermodynamiquement, ce qui permet d'obtenir une séparation de phase entre ces deux composants. Une grande variété de microstructures peut être obtenue selon l'affinité des composants l'un envers l'autre. En général, on cherche à obtenir une séparation de phase avec quelques cristaux de segments rigides, ce qui garantit un matériau élastomère avec de bonnes propriétés mécaniques et une certaine résistance thermique. La synthèse industrielle d'élastomères polyuréthanes se fait généralement en une étape lors de laquelle tous les composants sont incorporés en même temps pour obtenir la réaction alcool-isocyanate. Cependant, une synthèse en deux étapes comprenant d'abord la réaction du macrodiol avec le diisocyanate, suivi de l'ajout de l'allongeur de chaîne lors d'une seconde étape permet en général d'obtenir des segments rigides plus longs et donc de faciliter la séparation de phase.

Finalement, les monomères courants de l'industrie tels que polycaprolactone, polytétrahydrofurane, 1,4-butanediol, diisocyanate de toluène et 4,4'-diisocyanate de diphénylméthylène (MDI) sont décrits rapidement, avant de décrire l'obtention de revêtements polyuréthanes par ajout d'un agent réticulant, souvent un isocyanate ou un alcool à la fonctionnalité supérieure à 3. Les voies de synthèse poudre ou humide sont également décrites succinctement.

CHAPITRE 2

Une étude bibliographique présente d'abord l'isosorbide et ses propriétés, avant de s'intéresser aux élastomères polyuréthanes à base d'isosorbide. Il a ainsi été décidé de tester des compositions à base de MDI en tant que diisocyanate, et différents oligomères en tant que macrodiols tels que polycaprolactone, polytétrahydrofurane et oligomères dérivés d'huiles végétales.

De l'isosorbide pur a été utilisé avec succès en tant qu'allongeur de chaîne pour la synthèse de polyuréthanes thermoplastiques basés sur des macrodiols commerciaux et le MDI. Lors d'une première étape, la synthèse d'un prépolymère a été suivie pour obtenir la conversion totale des fonctions alcool, éviter des réactions parasites et s'assurer que l'allongement de chaîne serait contrôlé. Lors d'une seconde étape, les prépolymères ont été allongés avec de l'isosorbide (ISO) ou du 1,4-butanediol (BDO) à taux de segments rigides variables. Des masses molaires moyennes entre 11 $kg.mol^{-1}$ et 39 $kg.mol^{-1}$ ont été mesurées pour les polyuréthanes à base d'ISO. La teneur en segments rigides (SR) est un paramètre crucial pour la masse molaire finale des matériaux car une concentration en SR croissante provoque des masses molaires plus faibles. La méthode de synthèse des échantillons à base d'ISO a été optimisée pour obtenir un avancement plus grand de la réaction. Les masses molaires n'ont pas été significativement augmentées mais le protocole de synthèse était plus rapide et se passait de catalyseur. Ce protocole ne fonctionnait pas pour les compositions à base de BDO.

Les matériaux polyuréthane obtenus ont été caractérisés par DSC et DMA. Les températures de transition vitreuse obtenues étaient comprises entre -48°C et 7°C. Il a été observé qu'en moyenne, les échantillons basés sur ISO montraient une séparation de phase moindre et moins stable que l'allongeur modèle BDO, et comportaient un plateau caoutchouteux mal défini en DMA. La teneur en SR était critique pour la qualité de la séparation de phase également : globalement, une teneur en SR plus basse avait tendance à améliorer la stabilité de la T_g pendant les cycles de chauffe. Il a aussi été montré que le choix judicieux du segment souple utilisé en combinaison avec le SR MDI/ISO pouvait améliorer significativement la qualité de la séparation de phase et pouvait diminuer la rétention d'eau. Les meilleurs résultats ont ainsi été obtenus avec les macrodiols basés sur des huiles végétales (FADM), plus hydrophobes que polycaprolactone (PCL) et polytétrahydrofurane (PTMEG). En effet, la PCL était très miscible avec les SR MDI/ISO alors que le PTMEG montrait des propriétés entre celles de PCL et celles du FADM. Les échantillons à base d'ISO montraient des températures de fusion plus hautes dues aux propriétés intrinsèques de MDI/ISO avec des maximas du pic de fusion compris entre 174°C et 208°C, ce qui les rendait plus résistants thermiquement que d'autres polyuréthanes modèles basés sur le BDO. Les valeurs de dureté et de déformation rémanente en température étaient en accord avec ces conclusions.

Le comportement thermique des échantillons présentés dans ce chapitre était aussi caractérisé par la présence d'une transition ressemblant à une transition secondaire entre 50 et 80 °C, ainsi que des endothermes de fusion multiples à plus hautes températures. La nature et le mécanisme exacts à l'origine de ces transitions ne sont pas encore complètement compris dans les polyuréthanes. Cependant, ils sont probablement induits par des liaisons faibles ou des ordres à courte distance pour la transition intermédiaire, et des arrangements cristallins ou des séparations de phase pour le cas des endothermes de fusion multiples à plus hautes températures.

En conclusion, l'utilisation de l'isosorbide pour la synthèse de polyuréthanes est possible et de bonnes propriétés peuvent être obtenues par le choix judicieux du segment souple et du diisocyanate. Son utilisation pourrait être d'interêt pour des applications exigeant la non-toxicité et une part biosourcée.

CHAPITRE 3

Une étude bibliographique sur le diisocyanate d'isophorone (IPDI) est présentée dans la première partie. Malgré une faible réactivité, cet isocyanate peut potentiellement être utilisé pour la synthèse de polyuréthanes linéaires. Cependant, l'IPDI n'est pas favorable à la séparation de phase avec les allongeurs de chaîne courants tels que BDO, ce qui en fait un candidat intéressant à tester en synergie avec l'isosorbide. Les conclusions de cette étude ont amené à tester des formulations thermoplastiques basées sur les macrodiols PTMEG et FADM avec l'IPDI et l'ISO en tant que SR. Toutes les formulations ont aussi été synthétisées avec le BDO en tant qu'allongeur de chaîne afin de pouvoir comparer leurs propriétés respectives.

Tout d'abord, plusieurs SR purs ont été synthétisés pour sélectionner une combinaison appropriée de diisocyanate et d'allongeur de chaîne. L'isosorbide a été sélectionné car il menait à la plus haute T_g et sa chimie était mieux connue. L'isosorbide pur a ensuite été utilisé avec succès en tant qu'allongeur de chaîne pour la synthèse de polyuréthanes thermoplastiques basés sur des macrodiols commerciaux et l'IPDI. Lors d'une première étape, la synthèse du prépolymère a été suivie pour obtenir l'avancement maximal de la réaction entre le macrodiol et le diisocyanate et s'assurer que l'allongement de chaîne serait contrôlé. Lors d'une seconde étape, le prépolymère a été allongé par l'ISO ou le BDO à taux de SR variables. Des masses molaires moyennes ont été mesurées entre 16 $kg.mol^{-1}$ et 60 $kg.mol^{-1}$ pour les polyuréthanes basés sur ISO. Il a été déterminé que le taux de SR est un paramètre influençant fortement la masse molaire finale du matériau.

Les échantillons de polyuréthane thermoplastique obtenus ont ensuite été caractérisés par DSC et DMA. Les T_g mesurées étaient comprises entre -49°C et 94°C. La DSC a révélé qu'il y avait probablement une très faible séparation de phase pour tous les

échantillons basés sur le PTMEG au contraire des échantillons basés sur le FADM qui montraient une séparation de phase claire avec deux T_g. L'utilisation de l'ISO a aussi provoqué une large augmentation de la T_g des échantillons basés sur le PTMEG, et sur celle de la phase mélangée (phase mixte composée de segments souples et segments rigides) des échantillons basés sur FADM. Les mesures de DMA ont cependant révélé de faibles propriétés mécaniques aux températures supérieures à la T_g pour tous les échantillons, ce que l'on suppose provenir d'une séparation de phase insuffisante et d'un manque d'enchevêtrements dus à une masse molaire trop basse.

En conclusion, l'utilisation de l'isosorbide dans des formulations polyuréthanes à base d'IPDI a été réalisée. Il a été montré que ISO facilitait la survenue d'une séparation de phase et augmentait la T_g. Par ailleurs, une séparation de phase pouvait être initiée en choisissant judicieusement la combinaison SR et segment souples (SS). Cependant, les masses molaires doivent être augmentées pour pouvoir évaluer les propriétés mécaniques dans le futur, en choisissant bien le catalyseur et la température de réaction.

CHAPITRE 4

Dans une première partie de théorie sont présentés les phénomènes à l'origine de la formation de films appliqués aux polyuréthanes, puis les agents de réticulation choisis pour ce travail (trimères d'isophorone diisocyanate et trimère de pentamethylène diisocyanate) et le diméthyl éther d'isosorbide un solvant biosourcé et non toxique. Finalement, une rapide présentation de l'état de l'art sur l'incorporation d'isosorbide dans les revêtements est faite. On y voit notamment que l'isosorbide est en général modifié ou fonctionnalisé pour être intégré dans des revêtements.

A partir des résultats du chapitre 3, la formulation TII30, à base de PTMEG/IPDI/ISO (30% masse de SR) a été choisie comme base linéaire pour la formulation de revêtements transparents avec une séparation de phase minimale. Une partie des fonctions NCO de l'IPDI ont été remplacées par des fonctions NCO de trimères de diisocyanates. La synthèse de plusieurs nouveaux revêtements polyuréthanes contenant de l'isosorbide a été confirmée. La réticulation a été obtenue par l'intégration de trimères de diisocyanates aliphatiques. Une attention particulière a été prêtée à l'utilisation de composants biosourcés tels que le trimère de pentamethylène diisocyanate et le diméthyléther d'isosorbide.

L'extrusion réactive et un procédé par voie solvant ont été évalués en tant que moyens d'homogénéisation. Cependant, un contrôle insuffisant de la stœchiométrie des échantillons par extrusion réactive a mené au choix de la voie solvant.

Une formulation en voie solvant donnant lieu à la production de revêtements réticulés basés sur le DMI, solvant écologique choisi parmi une sélection de solvants

appropriés, a été mise au point. La formation d'un film a été optimisée par ajout d'un co-solvant (MEK) et d'un adjuvant siliconé (BYK 307). Le catalyseur dibutyl dilaurate d'étain (DBTDL) a été utilisé pour accélérer la réaction entre l'isosorbide et les fonctions -NCO des structures IPDI. Finalement, un cycle de réticulation en trois étapes consistant en 1h à 100°C, 1h30 à140°C et 30 min à 160°C avec une rampe de 2°C/min sous vide, a été choisi pour limiter l'évaporation des monomères car leur disparition précoce pendant le cycle de réticulation mène à des propriétés médiocres. Cependant, une étude poussée de la formation du film devrait être menée dans le style de celles rapportées par Monaghan et Dusek (ref. 136 et 139) dans le but de comprendre les paramètres importants pour la synthèse, le dépôt et la réticulation qui permettent d'obtenir des propriétés optimales.

Les revêtements obtenus contenaient moins de 2% de DMI résiduel, et les T_g des échantillons basés sur ISO étaient comprises entre 25 et 55°C. Notamment, des T_g plus basses ont été obtenues sur les échantillons basés sur BDO. L'incorporation de l'isosorbide a eu des effets bénéfiques sur les propriétés mécaniques telles que la résistance à l'impact et l'adhésion pratique.

CONCLUSION ET PERSPECTIVES

Au cours de cette thèse, de l'isosorbide biosourcé a été intégré dans des compositions polyuréthanes thermoplastiques et réticulées. Une attention particulière a été portée à l'incorporation d'autres composants biosourcés en combinaison de l'isosorbide dans certaines des compositions étudiées. Cela a permis d'obtenir des informations sur le potentiel de l'isosorbide pour la formulation de polyuréthanes avec une part biosourcée optimisée. Les propriétés chimiques et thermo-mécaniques des matériaux produits ont été évaluées et comparées à des compositions contenant du BDO. Plusieurs perspectives pour la suite de ce travail peuvent être proposées.

Premièrement, les résultats obtenus pour les élastomères basés sur les SR MDI/ISO ont mené à l'observation de microstructures caractéristiques et de transitions thermiques toujours mal comprises. Une étude approfondie de ces phénomènes pourrait amener une meilleure compréhension des mécanismes de séparation de phase à l'origine de la microstructure globulaire observée sur les échantillons FADM/MDI/ISO et éventuellement l'effet de cette microstructure sur les propriétés mécaniques telles que la dureté ou la résistance à la traction. Ceci exigerait des mesures systématiques en diffraction SAXS/WAXS combinées à de la thermo-microscopie et de l'AFM. Ce genre d'étude est cependant hors du champ d'étude de cette thèse.

Ensuite, des résultats encourageants ont été obtenus concernant les matériaux à base d'IPDI qui pourraient mener à la formulation de matériaux transparents et thermiquement stables. En effet, les échantillons à base de FADM/IPDI/ISO ont une séparation de phase intéressante mais souffrent de masses molaires faibles, peu propices à la formation d'enchevêtrements.

Enfin, le travail mené sur les revêtements a montré qu'il est possible d'obtenir des formulations de revêtements avec un haut taux de composants biosourcés (entre 60 et 85% en masse pour les systèmes étudiés), peu d'émissions volatiles (VOC) et en utilisant un solvant non toxique. D'après l'approche théorique de la formation des films présentée au début du chapitre 4, il pourrait être d'un grand intérêt d'appliquer les modèles de Dusek à ce système pour être capable de prédire les propriétés des revêtements selon les conditions de réticulation choisies. Cependant, les applications pratiques pour les films étudiés ici exigent probablement des T_g plus élevées (idéalement entre 80 et 100°C), une épaisseur plus importante et une caractérisation poussée en termes de dureté, adhésion et résistance à l'abrasion.

En conclusion, ce travail a démontré que l'isosorbide a le potentiel pour devenir un composant très utile pour la formulation de bio-polyuréthanes dans les années à venir, et il peut aussi être utilisé avec des composants non conventionnels pour obtenir des matériaux innovants tels que ceux obtenus avec l'IPDI ou les isocyanates biosourcés. Des applications

dans le secteur automobile, pharmaceutique, de l'habillement ou du sport sont envisageables.

TABLE OF CONTENTS

INTRODUCTION

Introduction

In recent years, sustainability has become a major concern when designing materials. Finding new bio-sourced monomers for plastics is a key issue for transition toward greener materials. In this prospect, our industrial partner Roquette Frères is seeking to evaluate the potential of one of its bio-based molecules isosorbide as a building block for polymeric materials. Isosorbide was already successfully integrated in diverse technical polymers such as polycarbonates or polyesters, to which it provides enhanced glass transition temperature and hardness. As polyurethanes are the sixth most produced polymers globally, and are usually used for technical parts, evaluation of the integration of isosorbide in polyurethane formulations is of the utmost interest.

Indeed, isosorbide could become a safer alternative to the widely used 1,4-butanediol (which is now also bio-sourced) and could enlarge available tool-box for design of polyurethanes. Its structure makes it a good candidate for use as a chain extender in block-copolymers. It is expected that isosorbide will bring both increase in hardness and glass transition temperature in polyurethane compositions. However, some intrinsic properties of this molecule may also render it weakly reactive and subject to water uptake.

This thesis was thus carried out with two main axes: incorporation of isosorbide in linear block copolymers, and incorporation of isosorbide in cross-linked polyurethane materials. This work consists in four main chapters.

The first chapter will consist in generalities about polyurethanes and their chemistry. Understanding of the main reaction mechanisms and conditions are indeed essential for synthesis and optimization, while understanding of phase segregation mechanisms and microstructure formation seems essential for interpretation of results. Moreover, a short overview of synthesis methods and commercially available building blocks will be made. A first part will thus explore polyurethane chemistry and more especially focus on urethane formation, isocyanate side-reactions and finally kinetics and stability of the urethane bond. A second part will deal with thermoplastic polyurethanes, and describe involved physico-chemical phenomena leading to the characteristic microstructure of such materials and finally an overview of available building blocks will be made. A third part will introduce polyurethane coatings from composition to deposition solutions.

The following chapters will present and discuss experimental results. Isosorbide was introduced in several polyurethane compositions and each of the following chapters will present a specific application. Chapters nonetheless progress successively from study of isosorbide-based phase segregating thermoplastic materials, to design of homogeneous isosorbide-based thermoplastics and finally to cross-linked isosorbide-based coatings.

The second chapter will thus focus on the synthesis and characterization of thermoplastic polyurethanes from isosorbide and the widespread 4,4’-methylenebis(phenyl isocyanate) as

components of the hard segments, associated with various oligomers as soft segments. As isosorbide is a secondary alcohol, optimization of the synthesis process will be explored. More specifically, synergies between classical oligomers such as linear polyesters and polyethers and the isosorbide-based hard segments will be compared to vegetable oil-issued oligomers, in terms of thermal behavior and phase segregation. Properties brought by isosorbide will also be compared to the more classical 1,4-butanediol chain extender. The first part will thus consist in a literature review about isosorbide structure and properties as well as a state of the art of its use as a chain extender for thermoplastic polyurethane materials. A second part will deal with synthesis of such materials and molar mass optimizations. Finally, thermo-mechanical behaviors and microstructure will be explored in the following parts, in terms of soft and hard segments association, and hard segment content.

The insights into the synergy of isosorbide-based hard segments with the different selected soft segments will be used to explore new thermoplastic polyurethane compositions in the next chapter. The third chapter will thus deal with incorporation of isosorbide in linear thermoplastic polyurethane compositions based on the aliphatic isophorone diisocyanate. Its aliphatic and asymmetrical nature makes it a preferred diisocyanate building block for clear polyurethane coatings. Several combinations of soft and hard segments will be studied in order to modify phase segregation. Properties of isosorbide-based polyurethanes will again be compared to the 1,4-butanediol models and thermo-mechanical properties of the resulting materials will be evaluated. A first part will thus present structure and properties of isophorone diisocyanate before presenting its use as a building block for linear block-polyurethane compositions, and in particular the state of the art of its incorporation along with isosorbide in such compositions. A second part will deal with synthesis of thermoplastic polyurethanes based on isosorbide and IPDI, and will in particular include a short study of several pure hard segments based on IPDI. A third part will present the thermo-mechanical characterization of the obtained materials and will focus on the particular synergy of the IPDI/Isosorbide-based hard segments with the two different soft segments.

Last but not least, in a final fourth chapter, clear polyurethanes varnishes will be obtained by incorporation of cross-linkers in one of the isosorbide-based formulations explored in Chapter 3. Bio-sourced content of some formulations will be increased by use of bio-mass issued trimer of pentamethylene diisocyanate. Especially, a greener deposition and film formation solution will be explored by careful choice of solvent and cure parameters. In a first part, a literature review about film formation of polyurethane coatings will be made, along with a short review on new bio-sourced components for the polyurethane coating industry as well as a state of the art in the use of isosorbide in cross-linked compositions. In a second part, the process for obtaining a defect free coating will be detailed. Finally, properties brought by isosorbide in such coatings will be evaluated by mechanical testing and compared to equivalent formulations obtained with 1,4-butanediol.

CHAPTER 1:
POLYURETHANE CHEMISTRY AND TECHNOLOGIES

Chapter 1. Polyurethane chemistry and technologies

1.1. POLYURETHANE CHEMISTRY

The reaction between isocyanate and alcohols allowing the synthesis of a polymer was first described by Otto Bayer in 1937 for fibers and elastomer synthesis applications. The versatility of the urethane chemistry soon allowed for the industrial production of expandable rigid and soft foams in 1954 along with other elastomers [1]. Polyurethane has become the sixth most commonly produced polymer globally with a forecast of annual growth rate by 2020 of 5% [2].

1.1.1. Route for the production of urethane functions

Urethane functions can be obtained classically by reaction of isocyanate with an alcohol function as shown in Figure 1.1. This type of synthesis is favored by industries in application requiring casting, as polyaddition does not require distillation of byproducts like polycondensation products. Isocyanates are compounds bearing one or several –N=C=O moieties. They are usually very reactive molecules as the carbon of the isocyanate function is highly electropositive due to its two electronegative adjacent atoms: oxygen and nitrogen [3]. This allows isocyanates to react with molecules having active hydrogens such as alcohols, amines or water. Favored reactions will then depend on the conditions: temperature, pressure and catalyst type.

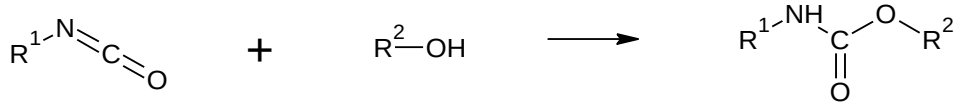

Figure 1.1: Chemical reaction of an isocyanate with an alcohol, producing a urethane function

At room temperature and under standard pressure conditions, the reaction of isocyanate with alcohol is slow and may be hindered by phase incompatibility between the components resulting in the formation of a crystalline urethane barrier at the interface in the absence of homogenization. Urethane synthesis is then usually carried out in temperature with the possible use of catalysts, and with a mean of phase homogenization (mixing or surfactants) [4].

Reactions of isocyanate with amine lead to the production of urea functions, as shown in Figure 1.2**.** Urea groups can thus be associated to polyurethane structures to form thermoplastic poly(urethane-urea) materials [5].

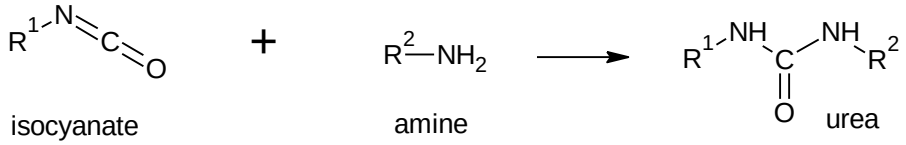

Figure 1.2: Chemical reaction of an isocyanate with an amine, producing a urea function

It was observed that a higher nucleophilicity of the active hydrogen generally enhances reactivity with isocyanate [6] in the following sequence:

Primary amine > aromatic amine > primary alcohol > H_2O > aromatic alcohol (phenol)

The reaction of isocyanate with amine will be favored over the one with alcohol if both are present in the reacting mixture.

1.1.2. Side Reactions

The high reactivity of isocyanate makes it a molecule subject to a wide variety of reactions [7], which may not be desirable when producing polyurethanes, as they result in the production of gases or cross-links in the case of polyisocyanates use.

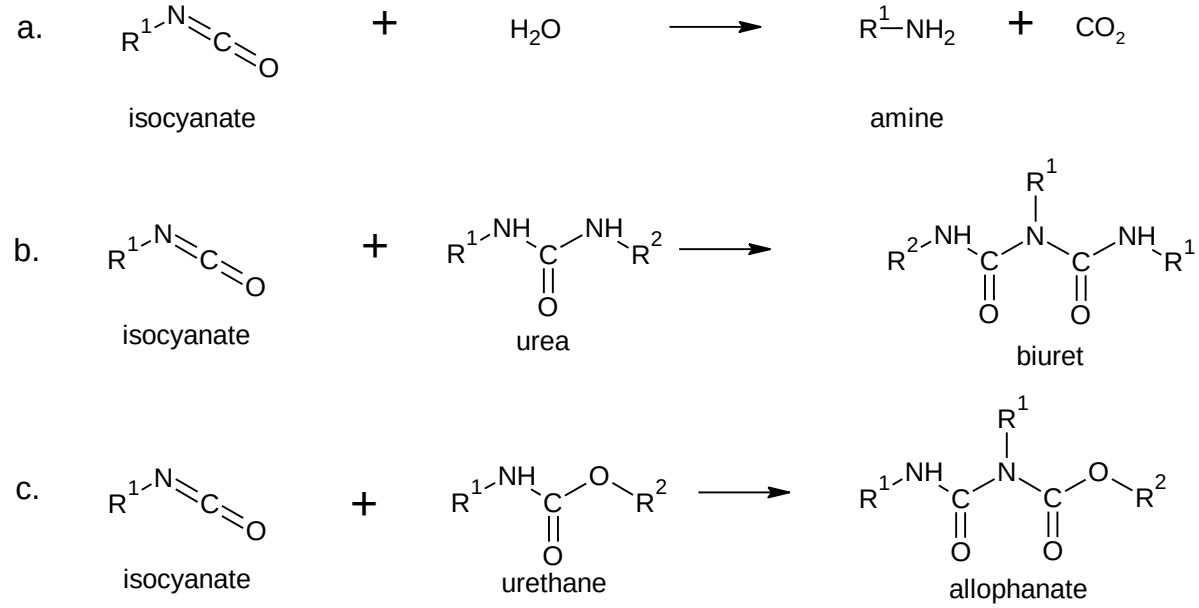

Figure 1.3: Isocyanate side-reactions – a. Reaction of an isocyanate with water, producing amine and carbon dioxide gas – b. Reaction of an isocyanate with urea groups, producing a biuret function – c. Reaction of an isocyanate with an urethane group, producing an allophanate function

Figure 1.3 a. presents the reaction of an isocyanate function with water, which results in the formation of carbon dioxide and an amine. This reaction is largely exploited in the production of polyurethane foams, as the produced CO_2 acts as a blowing agent. This reaction is however usually not wanted in other common polyurethane applications such as cast elastomers, cast thermosets, coatings or fibers as it results in unaesthetic and mechanically weak materials due to the formation of bubbles. The reaction with water is

however slow without the use of catalyst, but can be accelerated by tin or amine-based catalysts such as dibutyltin dilaurate or triethylenediamine [8].

Reaction of isocyanate with urea and urethane groups leads to formation of biuret or allophanate respectively. The extent of those reactions depends on the used catalyst [9], and the quantity of excess isocyanate and temperature [10], but such reactions at room temperature are usually very limited [11]. Specifically, allophanate functions were shown to appear by Lapprand *et al.* [12] in a non-catalyzed reaction of an equimolar ratio of urethane and isocyanate functions at 170°C.

1.1.3. Kinetics and catalysts for the urethane formation

The rate of reaction between isocyanate and hydroxyl groups is critically influenced by the steric hindrance and position of the reacting function on the carbon chain back-bone.

Alcohol structures thus display a decreasing reactivity [13], as shown below:

Primary alcohols > Secondary alcohols > Phenols

In the same way, -NCO groups positioned on aromatic rings are more reactive than chain-ends –NCO functions, and in the case of polyisocyanates, if one function has reacted, the reactivity of the others is usually reduced.

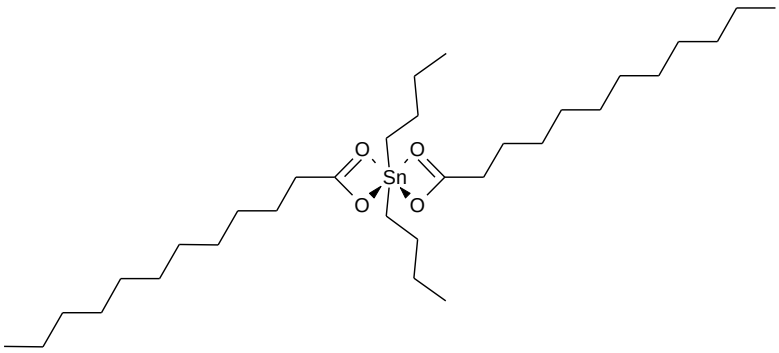

Figure 1.4: Structure of Dibutyltin dilaurate

Two types of catalysts are used for the synthesis of urethanes: amine-based catalysts and organometallic-based catalysts. They are respectively Lewis bases intended to increase reactivity of the hydroxyl, or Lewis acids to increase the reactivity of the isocyanate function [14]. Amine catalysts are in majority used for foam applications and may act as chain extenders [8]. Organotin based catalysts such as tributyltin oxide or dibutyltin dilaurate, were shown to accelerate the reaction of primary and secondary alcohols and much less affect the reaction with water [15]. Organotin catalysts are generally known for their excellent acceleration of hydroxyl/isocyanate reaction in water- and solvent-free systems [8]. Low concentration levels of dibutyltin dilaurate (DBTDL, Figure 1.4) are usually used for cast elastomers and reactive injection molding [16].

1.1.4. Stability of the isocyanate reaction products

Upon heating, urethane links can be subject to a wide array of dissociations [17], resulting in the formation of:

- Alcohol and isocyanate
- Primary amine, olefin and carbon dioxide
- Secondary amine and carbon dioxide
- Various transesterifications

Table 1.1: Thermal stability of urethane groups as a function of isocyanate and polyol constituents from [19]

Urethane Structure	Approximate limit of thermal stability (°C)
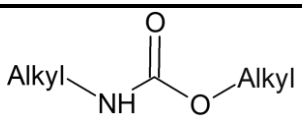	250
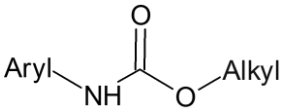	200
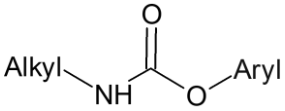	180
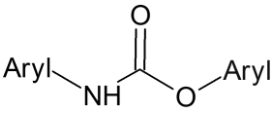	120

The thermal reversibility of urethane functions can be used for some applications such as blocked isocyanates [18]. However, this reversibility can also be a limiting factor for thermal stability and resistance, as products of degradations can in turn take part in the various reactions involved in urethane chemistry described in the previous sections. This may significantly modify the material chemical structure and composition. It was thus observed by Yang *et al.* [19] that the annealing over 160°C of a polyurethane obtained from 1,4-butanediol and 4,4'-diphenylmethane diisocyanate resulted in the formation of higher molar mass entities. Approximate thermal stability as a function of the urethane link substituents are reported in Table 1.1. In general, it is safe to consider that urethanes derived from the more reactive isocyanate such as aromatic isocyanates, are also the less stable [17].

Thermal processing of polyurethanes must be carefully monitored to ensure that no side reactions linked to degradation occur, or in the case they do, that they are well controlled.

1.2. THERMOPLASTIC POLYURETHANES

Thermoplastic polyurethanes are linear chain thermoplastics containing urethane links. They are usually thermally processable elastomer materials, which make them essential for rubber replacement applications.

1.2.1. Block copolymers

Thermoplastic polyurethanes are linear block copolymers resulting from the reaction of difunctional alcohol and isocyanate building blocks. As such, they are composed of a statistical sequence of alternative hard segments (HS) and soft segments (SS). Soft segments are usually long and flexible oligomeric diols also called macrodiols, while hard segments are composed of a succession of stiff diisocyanates and short diols, called chain extenders. The three alternating building blocks are linked by urethane bonds, as shown by Figure 1.5.

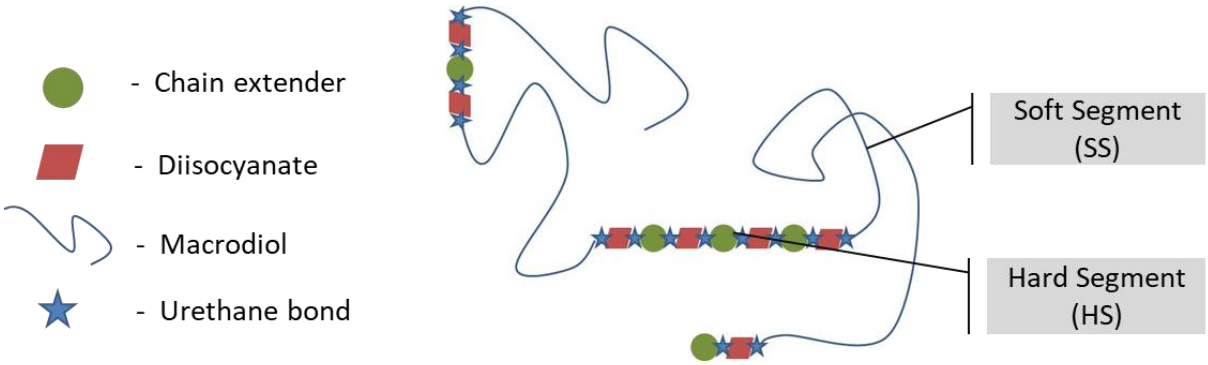

Figure 1.5: Scheme of the linear copolymer structure of a thermoplastic polyurethane

As the macrodiols are oligomers of average molar mass usually between 500 and 3000 $g.mol^{-1}$, synthesized separately from the polyurethane synthesis, they usually have molar-mass dispersity close to 1 for polyether oligomer diols, or close to 2 for polyester oligomer diols. This inherent dispersity of the building blocks of polyurethane results in a typical dispersity of 2 or higher for those materials [1].

Practically, uniform mass distribution of the hard segments cannot be achieved and the polyurethane chain usually follows a statistical Flory distribution [20]. This results in the formation of hard segments with a higher degree of polymerization than theoretically predicted [13].

It was also shown by Peebles *et al*. that the length distribution of the hard segment is hugely influenced by general relative reactivity of components, kinetics and stoichiometry as well as reaction conversion and is very difficult to measure experimentally [21], [22].

1.2.2. Synthesis methods

Solvent-free synthesis of thermoplastic polyurethanes is generally preferred over solvent synthesis for economic and environmental concerns. There are essentially two methods: the one-shot process and the prepolymer process, also called the two-step synthesis [8].

1.2.2.1. One-shot process

The one-shot process is usually preferred for industrial manufacturing as it is a very fast and efficient synthesis process. It simply consists first in mixing both hydroxyl terminated building blocks (macrodiol and chain extender) along with catalyst if needed. The diol mixture is then dried to ensure limited side reaction with water, and then mixed in a stoichiometric ratio along with the diisocyanate at the appropriate temperature (usually between 80°C and 130°C) [8] for 2 to 30 min [13]. The resulting material is then poured or injected into preheated moulds. Depending on the reaction conversion and industrial process, subsequent curing and post-curing time may be needed.

The reactivity of the two types of hydroxyls from the macrodiol and chain extender with the chosen diisocyanate must be the same. On the contrary, the resulting material may have a large dispersity and polymer chain compositions may be very heterogeneous resulting in poor mechanical properties.

The main drawback of the one-shot process is the exothermic release due to the reaction. As all reactions occur at the same time, depending on the batch size, the temperature rise of the reacting mixture can be non-negligible. If the temperature rises above the upper stability limit of the weakest urethane bonds, there is a higher risk of uncontrolled side-reactions leading to cross-links, thermal degradation or increase in dispersity.

1.2.2.2. Two-step synthesis

Two-step synthesis is not as fast as the one-shot procedure but allows for the maximization of the length and size distribution of the hard segments [21], [22]. Moreover, catalysts are not as essential in a two-step procedure as in a one-shot synthesis thanks to the sequenced procedure that erases the competition between macrodiol and chain extender reactivity [13].

The first step consists in the reaction of the hydroxyl-terminated macrodiol with an excess of diisocyanate at a temperature up to 130°C and in inert atmosphere [8]. This reaction leads to the production of a –NCO terminated soft segment, with excess diisocyanate and the production of higher oligomers by reaction of both –NCO functions of some of the diisocyanate molecules, as illustrated by Figure 1.6 a. They are thus usually characterized by their molar mass dispersity and their –NCO ratio.

The formed prepolymer is then degassed. Such mixtures usually have a limited stability and the longer the waiting time before the second step, the poorer the end-product properties [13].

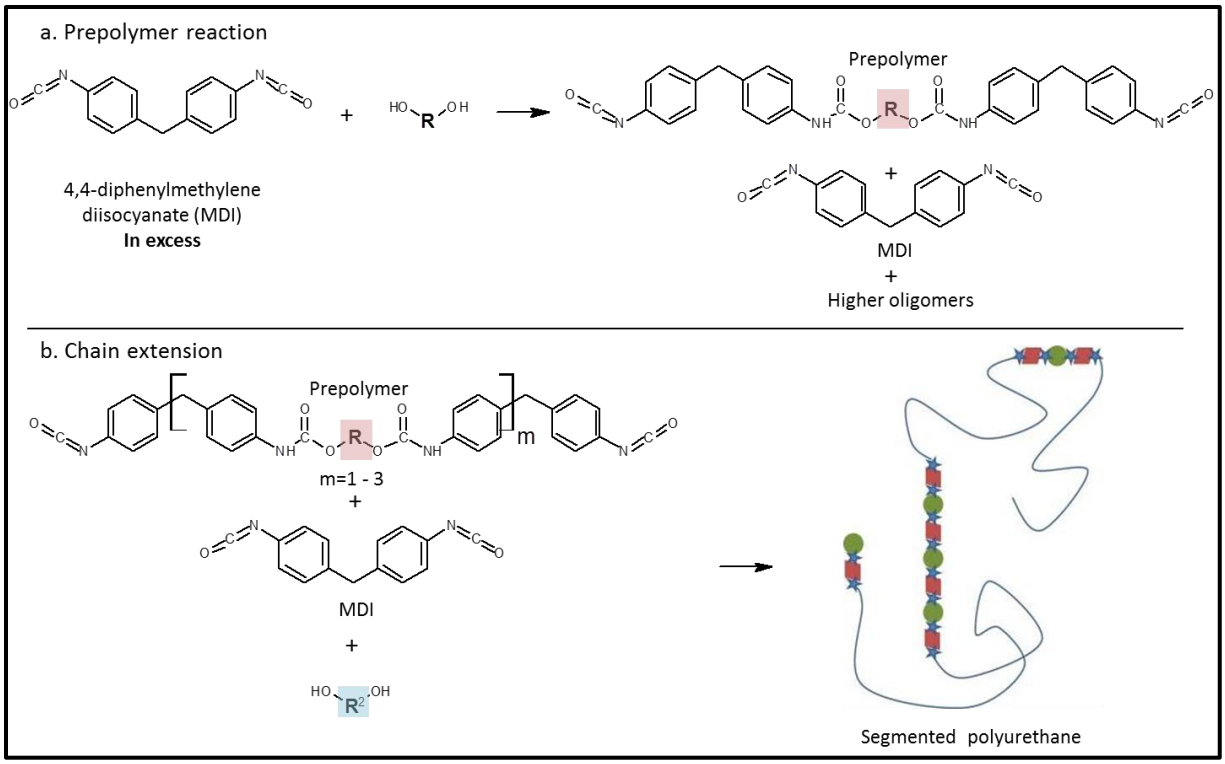

Figure 1.6: Example of the preparation of NCO terminated prepolymers and thermoplastic polyurethanes by a two-step procedure with – a. Prepolymer synthesis – b. Chain extension

In a second step, see Figure 1.6 b., the liquid chain extender is added to the prepolymer mixture in stoichiometric ratio with vigorous stirring. Upon addition of the chain extender, the mixture has a limited pot life due to the onset of phase segregation and is degassed for 2 to 5 min if possible. The mixture is then molded. As in the case of the one shot procedure, additional curing or post curing time might be required. As the synthesis is sequenced, the control over the exothermic release is better than with the one-shot process.

1.2.3. Microstructure

The heterogeneous structure of the thermoplastic polyurethane chains induces a phase segregation as hard and soft segments are usually non-miscible. Cooper *et al.* in the 60's were the first to show that polyurethane elastomers' outstanding properties were due to phase segregation [23]. This feature is essential in the design of non-covalently bonded elastomers, as the soft segments with a very low glass transition temperature (in most cases below 0°C, usually between -70 and -40°C) provide a soft matrix and hard segments with a higher glass transition temperature, form non-covalently bound hard domains which provide good mechanical properties and thermal resistance. Those very specific features allow for thermal reversibility of the bounding, and thus guarantee thermal re-processing of polyurethane elastomers in the case of a temperature range low enough to preserve the urethane function stability. They moreover induce the appearance of several scales of order in the materials, from inter-chain interactions followed by micro-phase segregation, to lamellar structures.

1.2.3.1. Concept of phase segregation

As the segments along the polyurethane chains are covalently bound, macroscopic phase segregation can never be achieved, unlike the case of more classical polymer blends [24]. Several theoretical studies in the late 1980s have predicted the appearance of multiple phases in block copolymer materials [25]–[27].

Camberlin *et al*. [28]–[30] designed a method for evaluating the quality and kinetics of phase segregation in polyurethanes, by measuring the variation of the calorific capacity ΔC_p at the glass transition of the soft segment-rich phase. By comparison with the ΔC_p of the pure soft segment, they were able to calculate the amount of hard segments mixed in the soft phase thanks to the Fox equation:

$$\frac{1}{T_g} = \frac{w^{SS}}{T_g^{ss}} + \frac{w^{HS}}{T_g^{HS}} \qquad \textbf{Equation 1}$$

where w^{SS} and w^{HS} are weight fractions of the soft and hard segments respectively, and T_g, T_g^{SS}, T_g^{HS} are the glass transition temperatures of the studied materials, the pure soft segments and the pure hard segments respectively. Thus, the closer the glass transition temperature of the thermoplastic polyurethanes to the glass transition temperature of the pure soft segments, the better the phase segregation. By studying this parameter as a function of time and temperature of annealing, they were able to conclude that the phase segregation is linked to the interaction parameter between the hard and soft segments and that the equilibrium time depends on the chain mobility.

Those theories were confirmed and completed by Koberstein *et al.* [31] by combining Small Angle X-ray Scattering (SAXS) with Differential Scanning Calorimetry (DSC).

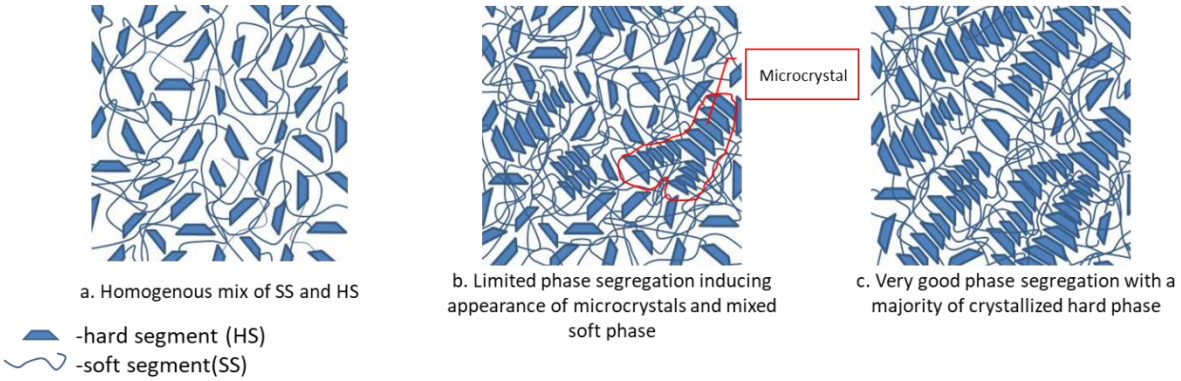

Figure 1.7: Schematic representation of several phase segregation states in segmented polyurethanes – a. continuous amorphous mixed phase – b. Intermediate microstructure comprising amorphous pure or mixed phases, and limited crystallization of hard segments – c. Ideal microstructure with good phase segregation and a majority of crystallized hard phase, from Koberstein *et al.* theory in [31]**.**

However, additional crystallization phenomena associated to the hard block segments further complicate the understanding of the mechanism behind phase segregation of polyurethanes. Depending on the affinity between soft and hard segments as well as the

thermal history of the material, they found that a wide array of microstructures can be obtained, as shown in Figure 1.7.

1.2.3.2. Crystallization

Several other scales of order can be observed in polyurethanes. The smaller one is dependent on the inter-chain interactions. As a matter of fact, the chemical structure of the urethane bond makes it very prone to form hydrogens bonds [32], which usually induces ordering of hard segments as Figure 1.8 illustrates.

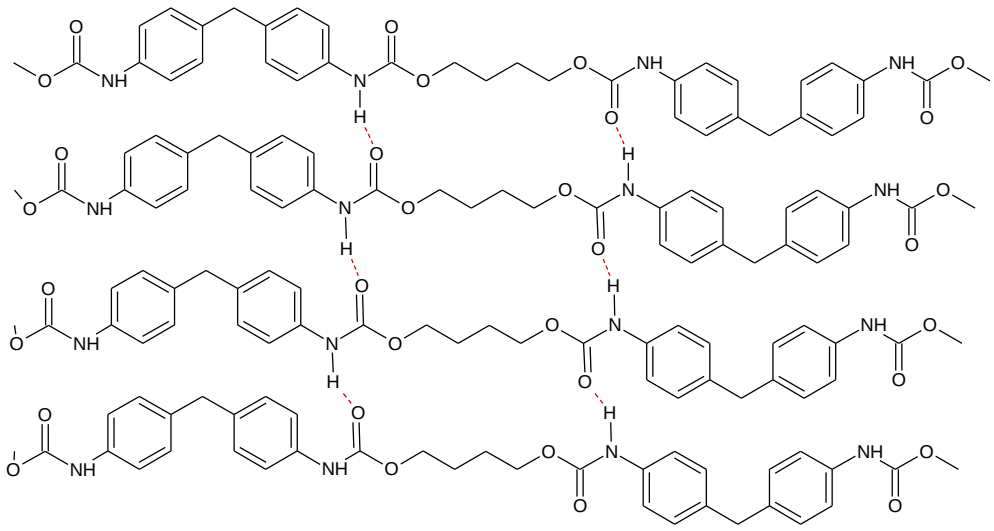

Figure 1.8: Schematic representation of the hydrogen bonding between hard segments composed of 4,4'-diphenylmethylene diisocyanate and 1,4-butanediol

Hydrogen bonding is another one of the driving forces controlling crystallization, and thus also plays a role in phase segregation. The ordering due to hydrogen bonding is critically influenced by the choice of the combination of diisocyanate and chain extender as the amount and strength of the formed H-bonds is dependent on the molecular structure of the hard segments [33]. The appearance of notable crystalline structures such as fibrils, spherules or lamellae in polyurethanes was reported by several authors [33]–[36].

1.2.4. Building blocks

This section is a quick overview of some of the most frequently used building blocks and commercial bio-sourced solutions.

1.2.4.1. Diisocyanates

In 2011, the total world consumption of isocyanates was 6.6 million metric tons [1]. A large majority of the globally produced polyurethanes are based on aromatic diisocyanates, namely toluene diisocyanate (TDI) and methylenebis(phenyl isocyanate) (MDI) whose production is very cost efficient. Both of them are however produced from fuel stocks and as of today no renewable route for their synthesis has been discovered. They are both subject

to yellowing due to their aromatic structure [37] but they are both extremely reactive polyisocyanates.

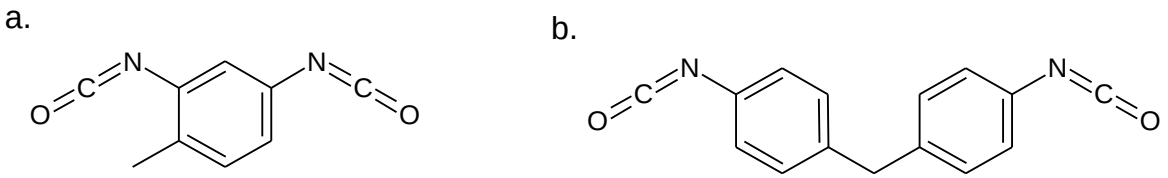

Figure 1.9: Chemical structures of a. toluene diisocyanate – b. methylenebis(phenyl isocyanate)

TDI is obtained from toluene and its main application (85% of the TDI production) is flexible foams. MDI is synthesized from aniline and formaldehyde and it is mainly used for synthesis of both rigid and flexible foams, adhesives, sealants, coatings and elastomers. It can be used for a majority of polyurethane applications and its global consumption is thus 2.5 times higher than TDI.

A mere 3% of the global production of isocyanate is represented by aliphatic isocyanates, such as hexamethylene diisocyanate (HDI), isophorone diisocyanate (IPDI) or hydrogenated MDI (HMDI), and they are mainly used in coating applications.

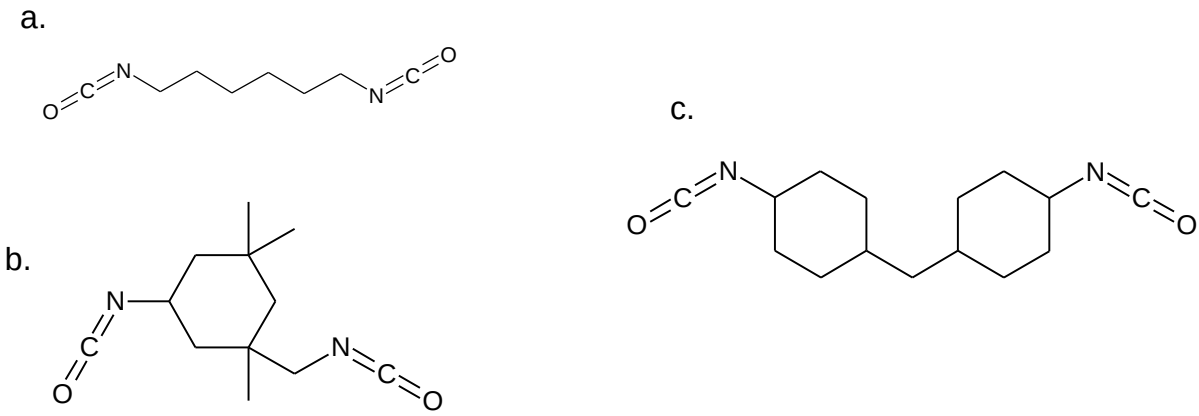

Figure 1.10: Chemical structures of a. hexamethylene diisocyanate – b. isophorone diisocyanate – c. hydrogenated methylenebis(phenyl isocyanate)

To our knowledge, there are only three commercially available bio-sourced diisocyanates: 2-Heptyl-3,4-bis(9-isocyanatononyl)-1-pentylcyclohexane (DDI) [38], L-lysine diisocyanate ethyl ester (EELDI) [39], [40] and derivatives of pentamethylene diisocyanate (PMDI), which are obtained from bio-based feedstocks [2] and their use for polyurethane synthesis is still anecdotic.

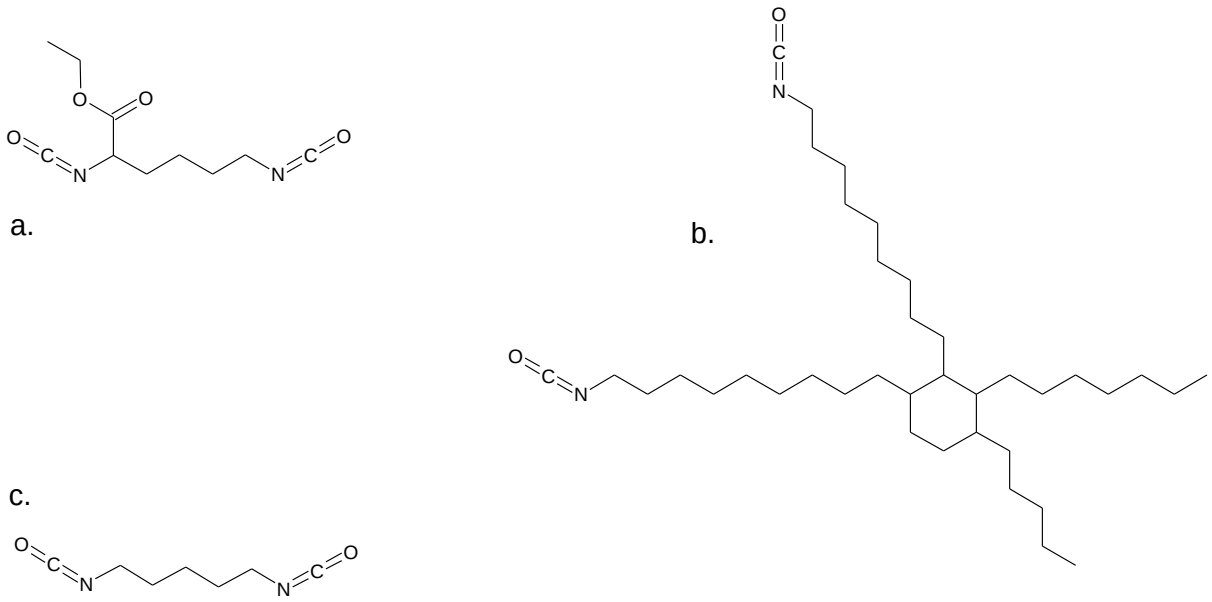

Figure 1.11: Chemical structures of a. Ethyl ester L-lysine diisocyanate – b.– 2-Heptyl-3,4-bis(9-isocyanatononyl)-1-pentylcyclohexane (DDI) – c. pentamethylene diisocyanate

1.2.4.2. Soft segments

Soft segments are oligomers of average molar mass between 500 and 3000 g.mol^{-1} and hydroxyl terminated. A wide commercial selection of soft segments is available for synthesis of polyurethanes and structures can be tailored to meet specific needs, which make polyurethane design very versatile. This section does not intend to give a comprehensive list of possible soft segment architecture. Focus will be made on some bio-sourced solutions and especially on seed oil derivatives.

In 2011, 75% of the global polyol production was polyether-based, 5% of which were solely poly(tetrahydrofuran) diols, and 21% and 2% were for polyester and acrylic-based building blocks respectively [1]. Out of those types, several bio-sourced solutions are already available, such as for example polytrimethylene ether glycol (Cerenol) from Dupont [41]. Other bio-based polyesters can as well be easily obtained from already green monomers such as for example 1,4-butanediol, ethanol or ferulic acid, but numerous new ones are also being explored such as for example tetrahydrofurandimethanol or sorbitol [42], [43]

In recent years, focus was made on building blocks obtained from seed oils. As a matter of fact, seed oils are mostly composed of triglycerides or fatty acids which can be easily used for the synthesis of polyesters after modification [44]. In some cases, hydroxyl functions are already available on the backbones of the fatty acids, as is the case of the ricinoleic acid obtained from castor oil. This allows for the direct use of castor oil in some polyurethane applications [45], [46].

Moreover, fatty acids obtained from oils can be used to produce fatty acid dimers of various architectures by formation of covalent bonds across both fatty acids carbon backbones [47], as shown in Figure 1.12. The obtained polyesters are very hydrophobic, they are thus

considered very interesting to limit water adsorption of polyurethane materials and may promote phase segregation.

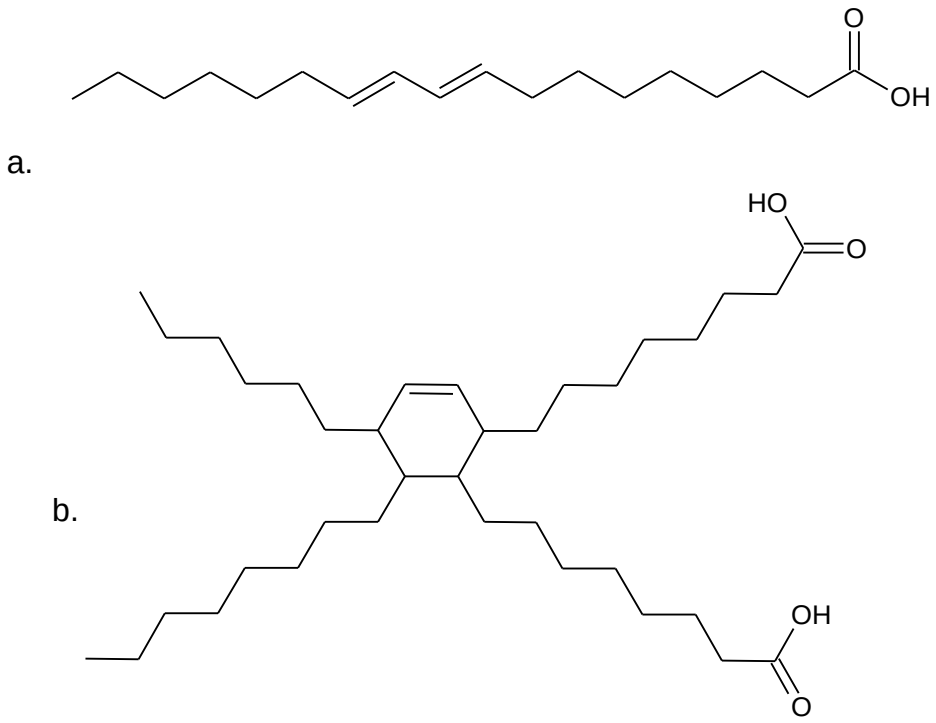

Figure 1.12: Chemical structure of fatty acid (a.) and fatty acid dimer (b.), from [47]

Use of fatty acid dimer-derived polyester soft segments for synthesis of thermoplastic polyurethanes were reported by various authors [35], [48]–[51]. However, most materials obtained were amorphous except when associated with MDI and BDO, resulting in poor mechanical properties.

1.2.4.3. Chain extenders

Chain extenders serve as spacers between diisocyanate units and they are often low molar mass monomers. They play a crucial role in hydrogen bonding and crystallization of the hard segments [24], [25], [52].

There is a huge list of potential diol molecules that can be used as chain extenders. However, the two industrially most significant are water, used as a foamer and extender for foam applications, and 1,4-butanediol commonly used for elastomer hard segments [1].

A more thorough review of isosorbide as a chain extender will be presented in the following sections.

1.3. POLYURETHANE COATINGS

The previous section allowed showing that polyurethane chemistry allows for the design of very varied structures to answer to specific need due to its versatility. Polyurethanes are also used for the production of coatings, which are particularly recognized for their durability, abrasion resistance, aesthetics and formulation flexibility [1].

1.3.1. Cross-linker solutions

Cross-links used for coating technologies are usually covalent inter-chain bonds, as they guarantee dimensional and mechanical properties over a large range of temperatures.

Cross-links may be obtained by using the isocyanate side-reactions, as was done by Lapprand *et al.* [12], [53], or by using multifunctional building blocks.

The range of commercially available multifunctional building blocks is wide, as they can be short polyols, long oligomers or multifunctional isocyanates and the choice of one or another only depends on technical and formulation issues. It seems however worth noting that as coatings are usually intended for applications requiring color stability in exposed environment, aliphatic isocyanates are preferred over aromatic ones, and multifunctional units were obtained by manufacturers through homoligomerization of aliphatic diisocyanates.

1.3.2. Coating deposition technologies

Polyurethane coating formulation versatility allows it to be processed for deposition with varied method. Focus will be made in this section on powder and solvent borne coating deposition which are relevant for Chapter 4.

1.5.2.1. Powder coatings

The principal requirement for powder coating deposition is that all the monomers or components mixture must be solid at room temperature and it must be possible to process it into a powder [54]. The powder is then sprayed onto a substrate which is subsequently heated to coalesce and/or cure the powder particles to obtain a uniform surface.

Polyurethane components blending is usually done by extrusion with partially blocked isocyanates to protect those functions until the deposition and curing step [1] in order to obtain a partially cross-linked solid. The advantage of powder coating deposition is that it is completely solvent-free, which can turn into a huge ecological and toxicological benefit.

1.5.2.2. Solvent borne

Solvent-borne coating formulations are also very varied. Classical solutions are one- or two-part solvent-borne formulations in which the isocyanate and alcohol fractions are either mixed or separated to optimize shelf-life of the formulations and industrial workflow. As

coatings formulations often use low reactivity aliphatic isocyanate, deposition is made at room temperature and curing is usually carried out at the appropriate temperature [1].

In recent years, research was more focused on reducing volatile organic compounds (VOC) and thus efforts are being made to limit use of organic solvents or replace them by non toxic ones. Ultimately, solvent choice is linked to the formulation components solubility. In this context, invention of water-borne polyurethanes by Dupont de Nemours [55] allowed for the use of an alternative to toxic solvent uses.

1.4. CONCLUSION

In summary, an overview of the general literature on polyurethanes allowed to understand the general chemistry and physical phenomena to consider when designing polyurethane formulations. In particular, side reactions of isocyanates and stability of the urethane bonds must be taken into account during synthesis and processing of polyurethane materials.

Moreover, it was shown that polyurethanes are a key component of plastic industry as they allow for the design of very diverse materials ranging from elastomers, adhesives, coatings and various foams. However, there is nowadays a need of exploring new building blocks to enhance sustainability of polyurethane materials.

The potential of a new bio-sourced building block will be explored in the following chapters for both thermoplastic and thermoset polyurethane materials. Effect of isosorbide in MDI-based thermoplastic formulations will be first explored in chapter 2, before incorporation in IPDI-based thermoplastic formulations in chapter 3 and subsequent design of VOC-free solvent-borne coating formulations based on isosorbide in chapter 4.

CHAPTER 2:

ISOSORBIDE AS A CHAIN EXTENDER FOR THERMOPLASTIC POLYURETHANES BASED ON MDI

CHAPTER 2. ISOSORBIDE AS A CHAIN EXTENDER FOR THERMOPLASTIC POLYURETHANES BASED ON MDI 26

Chapter 2. Isosorbide as a chain extender for thermoplastic polyurethanes based on MDI

2.1. STATE OF THE ART IN INCORPORATION OF ISOSORBIDE IN THERMOPLASTIC POLYURETHANE COMPOSITIONS

2.1.1. Isosorbide

2.1.1.1. 1,4:3,6-Dianhydrohexitols

Isosorbide is a renewable molecule from the 1,4:3,6-dihanhydrohexitol isomers group along with isomannide and isoidide. Studies about this group of molecules were first reported in the late 40's [56], [57]. The three isomers differ by the placement of their two hydroxyl groups, as illustrated with Figure 2.1. The alcohol functions of isosorbide are placed in endo and exo position across the two fused tetrahydrofuranic rings. Subsequently, both functions are placed either in the endo position for isomannide, or the exo position in the case of isoidide, which imparts differing reactivity to the isomers.

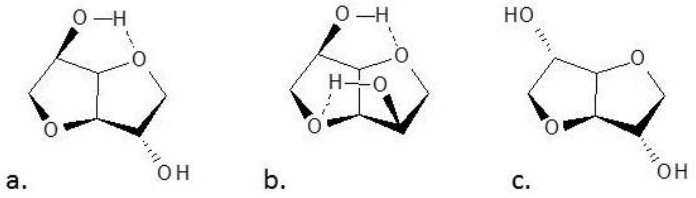

Figure 2.1: Molecular structures of isosorbide (a.), isomannide (b.), isoidide (c.)

Isoidide is thus the most reactive of the group. However, for now, isoidide can only be obtained from L-iditol, which is unfortunately not readily available from nature and makes isoidide a very expensive building block [58]. A mix of isosorbide and isomannide is usually obtained industrially by dehydration of sorbitol. It was only from the early 2000's [59], [60], that economically viable processes allowing the production of isosorbide with a sufficient purity were invented, thus enabling the use of isosorbide for polymer synthesis.

2.1.1.2. Synthesis of Isosorbide

Isosorbide is obtained from renewable sources. The synthesis route is described in Figure 2.2. The first step in its production is the enzymatic hydrolysis of starch to obtain D-glucose (1), followed by its subsequent hydrogenation into D-sorbitol (2). Isosorbide (3) is then obtained from the dehydration of sorbitol.

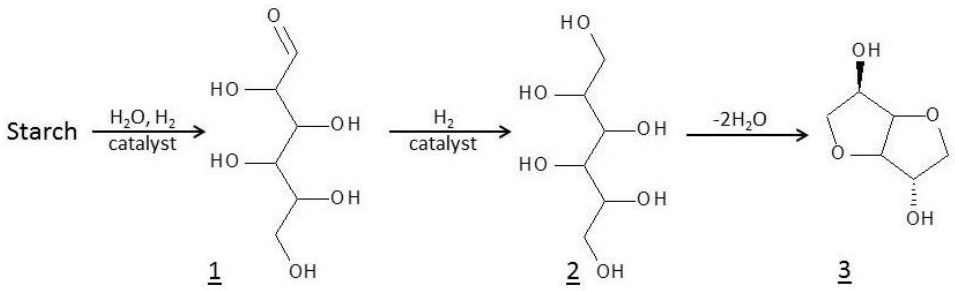

Figure 2.2: Synthesis route for the production of isosorbide from starch from [59], [60]

2.1.1.3. Chemical structure and properties of Isosorbide

Isosorbide is a chiral and cycloaliphatic molecule. It is composed of two planar and fused tetrahydrofuranic rings. These two rings form a 120° angle, thus inducing an open book-shaped molecule, as shown in Figure 2.3. The two hydroxyl moieties are placed across the V-shaped core on the C2 and C5 carbons. The endo hydrogen of the alcohol function on C5 notably forms a hydrogen bond with the oxygen of the adjacent furanic ring.

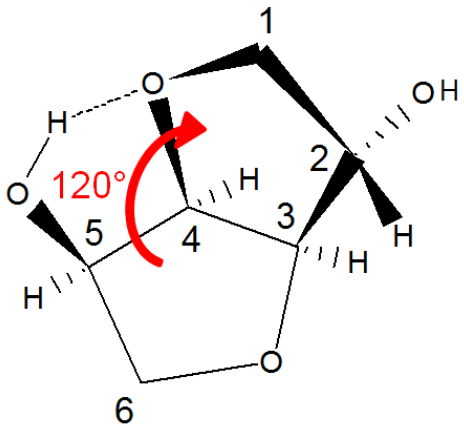

Figure 2.3: Spatial representation of isosorbide

This spatial structure was described by Hopton *et al.*, Goodwin *et al.* and Jacquet *et al.* in the 70's and 80's [61]–[63]. Its physical properties were then reported by Flèche *et al.* [59] and are summarized in Table 2.1.

Table 2.1: Key physical properties of isosorbide from [59]

Molar mass	($g.mol^{-1}$)	146.14
Melting temperature	(°C)	61-62
Boiling temperature	(°C) at 10 mmHg	160

They also have shown that isosorbide is thermally stable up to 270°C. Moreover, isomerization of isosorbide toward isoidide or isomannide is only possible in the presence of nickel at high pressure (150 bar) and temperature (220°C) [64]. It is however highly

hygroscopic under standard atmospheric conditions at relative humidity levels over 26%. Those properties make isosorbide a suitable candidate for synthesis of polyurethanes.

2.1.2. Reactivity and model reactions

2.1.2.1. Reactivity of isosorbide with isocyanates

The asymmetric placement of the two hydroxyl functions of isosorbide and their respective steric environment impart different reactivities. The results of several experiments studying this effect in the case of esterification reactions were reported [65]. It was shown that the kinetics of the reaction and the reactivity of either the endo or exo alcohol with acids and anhydrides were heavily dependent on the reaction conditions. This could also be the case for polyurethane reactions.

Ionescu *et al.* [66] have studied the reaction of isosorbide with phenyl isocyanate in 1,4-dioxane solution without catalyst. They indeed have shown a difference in reactivity between the two functions of isosorbide with isocyanates. This question was also addressed by Cognet-Georjon *et al.* in 1995 [67] by studying the reaction of isosorbide first with a mono-functional aromatic isocyanate (p-tolyl isocyanate) in tetrahydrofuran solution and catalyzed by dibutyltin dilaurate (DBTDL) at 50°C, then with the di-functional 4,4'-diphenylmethylene diisocyanate (MDI) in the same conditions. Authors concluded that in the presence of a very reactive isocyanate and/or catalyst there is no difference of reactivity between the two alcohol functions of isosorbide.

A similar study was carried out by Li *et al.* [68] by reaction of isosorbide with ethyl ester L-lysine diisocyanate (EELDI) in acetone solution at 40°C catalyzed by DBTDL; they also demonstrated the quasi equi-reactivity of both hydroxyl functions of isosorbide.

From these results, it can be considered that in the presence of a highly reactive isocyanate and at high temperature or with catalyst, the hydrogen bond of the endo-hydroxyl becomes as reactive as the exo hydroxyl function.

2.1.2.2. Synthesis and properties of hard segments from isosorbide and di-functional isocyanates

Before discussing complete thermoplastic polyurethanes, it seems important to study the properties of pure hard segments based on isosorbide. Hence, the first documented record of the synthesis of polyurethanes made of isosorbide and a bifunctional isocyanate – namely the synthesis of hard segments – was in the form of a patent of the mid 80's from Dirlikov *et al.* [69] in which were described the reactions in solution of isosorbide with 1,6-hexamethylene diisocyanate (HDI), 4,4'-diphenylmethylene diisocyanate (MDI) and toluene diisocyanate (TDI). Shortly after, Thiem *et al.* [70] also reported the synthesis of several polyurethanes from isosorbide by an interfacial polycondensation route. However, this method required the modification of isosorbide into aminated and chlorinated acid monomers in order to enable the Schotten-Baumann reaction (the reader is invited to see

ref. 70 for more information on this reaction), which added a lot of steps to the synthesis, and the polyurethanes were not obtained from a classical isocyanate-alcohol reaction. They however synthesized polyurethanes exclusively composed of isosorbide moieties and were able to study their glass transition, which was found around -20°C. From these results, hard segments composed only of isosorbide blocks without involving diisocyanates with a different chemical structure do not seem very interesting for use in thermoplastic elastomer applications.

Table 2.2: Summary of the physical properties of polyurethane hard segments based on isosorbide and a bifunctional isocyanate (values obtained from literature)

Bifunctional isocyanate block		**Molar mass** M_n (g.mol^{-1})	**T_f (°C)**	**T_g (°C)**	**Reference**
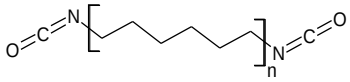 Linear aliphatic diisocyanate	n=2	3150	140	30	[70]
	n=4	2400	144	118	[70]
	n=6 (HDI)	/	190	110	[69]
		/	/	77	[71]
		4000	/	74	[72]
		18000	170	77	[73]
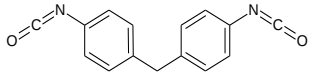 4,4'-diphenylmethylene diisocyanate (MDI)		2400	235	187	[67]
		/	/	183	[71]
		7000	/	179	[72]
		18500	217	183	[73]
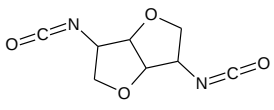 Isosorbide based diisocyanate		3200	120	-20	[70]
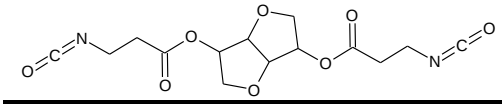		14300	/	78	[74]

Isosorbide based diisocyanate				
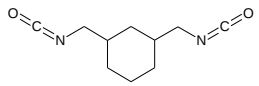 1,3-bis(isocyanatomethyl)cyclohexane	7000	/	134	[72]
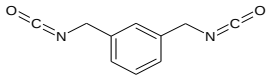 1,3-bis(isocyanatomethyl)benzene	6000	/	119	[72]
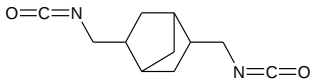 2, 5(2,6)-bis(isocyanatomethyl)bicyclo[2.2.1]heptane	7000	/	152	[72]
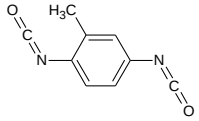 Tolylene-2,4-diisocyanate (TDI)	5000	/	182	[72]
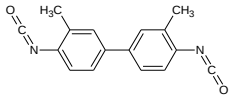 4,4'-diisocyanato-3,3'-dimethylbiphenyl	4000	/	133	[72]

Cognet-Georjon *et al.* [67] also studied the hard segments (HS) obtained from MDI and isosorbide, both from bulk and solutions synthesis. It has been reported in their work that those hard segments display a glass transition temperature of 187°C and melting temperature of 235°C, which is very interesting for improving thermo-stability of the thermoplastic polyurethanes. They also studied the relationship between the length of the hard segments and their glass transition temperature and confirmed that this parameter was critical in order to improve their thermal behavior and stability.

In the late 2000's, the interest for those compounds was renewed, and Beldi *et al.* [71] thus synthesized various hard segments based on isosorbide. Polyaddition reactions of isosorbide with HDI or MDI were performed in dimethylacetamide and catalyzed with tin based DBTDL catalyst. Lee *et al.* [72] also did a similar study, using a wide range of different diisocyanates.

The syntheses were also carried out in heated solution and catalyzed. A summary of the synthesized hard segments based on isosorbide and their properties is reported in Table 2.2.

Similar results were obtained by Marìn *et al.* [73], by catalyzed synthesis in DMF solution. Marìn moreover studied the crystals obtained from such materials, and concluded that the hard segments obtained by reaction of isosorbide with MDI or HDI do not easily crystallize, but in the case they do, the obtained phase is semi-crystalline with a hexagonal packing in the case of the HDI-ISO hard segments. The highest glass transition temperatures (T_g) were obtained by reaction of isosorbide with aromatic diisocyanates such as tolylene-2,4-diisocyanate (TDI) or 4,4'-diphenylmethylene diisocyanate (MDI), but some aliphatic diisocyanates such as 1,3-bis(isocyanatomethyl)cyclohexane or 2,5(2,6)-bis(isocyanatomethyl)bicyclo[2.2.1]heptane also displayed T_g over 130°C. More recently, Zenner *et al.* [74] studied the possibility of synthesizing polyurethanes from the 1,4:3,6-dihanhydrohexitols isomer group. They thus modified isosorbide with succinic anhydride to obtain an isocyanate terminated di-ester molecule with an isosorbide core. The synthesized polymer displayed a glass transition of 78°C and was potentially hydrolysable due to its ester functions, which makes it a valuable option for the synthesis of polyurethane biomaterials.

From the literature, it appears that isosorbide can be reacted with a variety of bifunctional isocyanates in order to produce hard segments. The highest glass transition temperature was measured on the hard segments synthesized with MDI, but isosorbide in general induces a glass transition over 100°C with a lot of diisocyanates. However, the resulting hard segments do not easily crystallize.

2.1.3. Thermoplastic polyurethanes (TPU) based on Isosorbide

In order to obtain thermoplastic polyurethanes, it is required to synthesize linear block copolymers composed of alternating hard and soft segments, the soft segments being composed of a flexible oligomer diol with a molar mass between 500 and 3000 $g.mol^{-1}$, while the hard segments are composed of an alternating pattern of diisocyanates and short diols. Several examples of soft segments used for the synthesis of isosorbide-based polyurethanes were found in the literature and are presented and discussed hereafter.

2.1.3.1. Poly(tetrahydrofuran) as a soft segment for isosorbide-based TPUs

Poly(tetrahydrofuran) (PTMEG) is a polyether resulting from the acid-catalyzed polymerization of tetrahydrofuran, its chemical structure is presented in Figure 2.4. PTMEG is a very wide-spread soft segment for the synthesis of thermoplastic polyurethanes. Its industrial uses range in particular from textile fibers to fake leather.

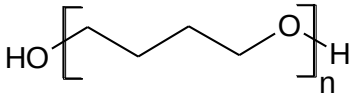

Figure 2.4: Chemical structure of hydroxy functionalized poly(tetrahydrofuran)

The first synthesis of a polyurethane based on a diol combination of PTMEG and Isosorbide was carried out by Cognet-Georjon *et al.* [75] in the mid-90's. They used a two-step bulk polycondensation procedure in order to obtain the isosorbide, MDI and PTMEG based materials. The first step was a classical prepolymer synthesis, during which the soft diol was reacted with an excess of bifunctional isocyanate. The second step was then either carried out in bulk or in a tetrahydrofuran solution with dibutyltin dilaurate (DBTDL).

Table 2.3: Summary of the properties of PTMEG and Isosorbide-based thermoplastic polyurethanes as a function of the difunctional isocyanate from literature

Diisocyanate	M_n^{PTMEG} (g.mol^{-1})	wt% HS	M_n a) (kg.mol^{-1})	T_g^{SP} b) (°C)	T_m^{HS} c) (°C)	Reference
MDI	/	100	2.4	/	235	[67]
	2000	48	10	-79	193	[75]
	2000	35	20	-76	180	[75]
	1000	51	17	/	181	[75]
	650	61	13	/	181	[75]
	1400	30	26	-59	/	[76], [77]
	1400	50	19	-64	206	[76], [77]
HDI	/	100	18	/	170	[73]
	2000	20	153	-48	20	[78]
	2000	25	68	-46	20	[78]
	2000	32	64	-42	20	[78]
	2000	43	16	-39	20	[78]

a) Number average molar mass of the materials (various methods used throughout the studies, numbers may not always be comparable) – b) Glass transition temperature of the soft domains – c) Melting temperature of the hard segment crystals

Cognet-Georjon reports that longer soft diols, regardless of the amount of hard segments, seem to promote phase segregation. Moreover, the use of isosorbide in such thermoplastic polyurethanes allows to obtain better mechanical properties at higher temperatures, in comparison to polyurethanes based on more classical diols such as 1,4-butanediol or hydroquinone bis(2-hydroxyethyl) ether.

Interest for those materials was only renewed in the mid- 2010's when the team of Javni *et al.* [76] also synthesized polyurethanes based on Isosorbide, PTMEG and MDI. They used a

two-step method in bulk without catalyst. They moreover studied the effect of using both isosorbide and 1,4-butanediol (BDO) and their blends as chain extenders. They report that increasing isosorbide content in the synthesized materials results in lower molar masses, with molar mass dispersities around 2. They also found that hard segments based on MDI and isosorbide were likely to crystallize, which is consistent with the results of previous studies on isosorbide based hard segments that showed that crystallization was however kinetically slow. Dynamic mechanical analysis (DMA) performed on those materials features a typical elastomer behavior, with seemingly improved mechanical properties compared to BDO-based samples, as can be seen in Figure 2.5. Optical microscopy and atomic force microscopy (AFM) associated with small angle x-ray scattering (SAXS) show that a high isosorbide content tends to promote the formation of smaller and more globular HS domains as compared to equivalent BDO based materials [77].

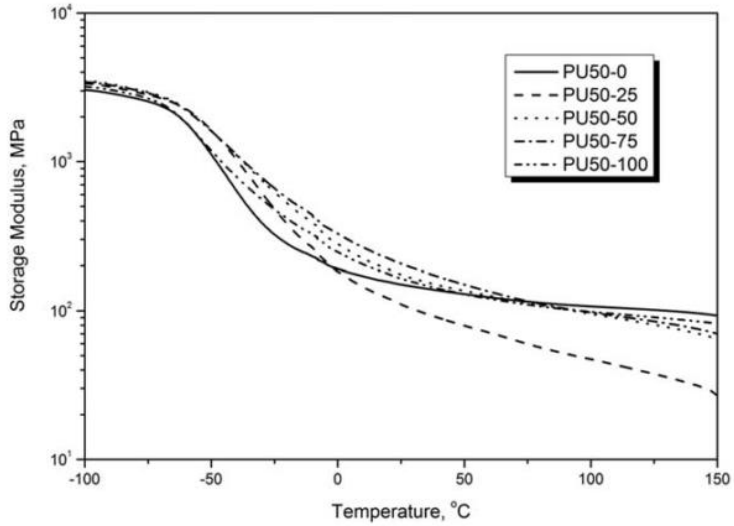

Figure 2.5: Example of DMA temperature scan as a function of the BDO/ISO ratio (PU50-0 contains only BDO as the chain extender, while PU50-100 is based on 100% ISO as the chain extender) – reproduced from [76]

Kim *et al.* [78] synthesized polyurethanes based on PTMEG, isosorbide and HDI in a one shot method without catalyst. Table 2.3 summarizes the main properties of materials studied in this literature screening. Overall, the glass transition temperature of the soft phase obtained with HDI/isosorbide hard segments seems to be higher than that obtained with MDI, but this could also originate from the choice of the synthesis method that is different between studies [75], [76] and that from Kim *et al*. Kim has also shown that the PTMEG/HDI/Isosorbide based polyurethanes are suitable for cell culture and that a higher content in isosorbide also seems to promote degradation in phosphate buffer solutions. Thus, those materials can have bio-medical applications.

In summary, PTMEG- and isosorbide-based polyurethanes were successfully synthesized by several teams. The main features of such polyurethanes are that phase segregation in PTMEG/MDI/Isosorbide is in part promoted by the length of the macrodiol; in other words, the longer the soft segment, the better the phase segregation. A higher content of

isosorbide based HS seems to induce a decrease in the average molar masses of the polyurethane copolymer in all the studies cited here, probably due to the lower reactivity of isosorbide.

2.1.3.2. Poly(ε-caprolactone) as a soft segment for isosorbide based TPUs

Poly(ε-caprolactone) (PCL) is a polyester obtained from ring opening polymerization of ε-caprolactone. Its chemical structure is shown in Figure 2.6.

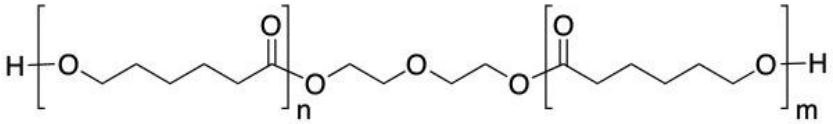

Figure 2.6: Example of the chemical structure of hydroxy functionalized poly(ε-caprolactone)

Hydroxyl-terminated bifunctional poly(ε-caprolactone) oligomers as soft segments were used in combination with isosorbide in materials aimed at medical applications, thanks to the hydrolysable nature of the ester bonds.

Table 2.4: Summary of the properties of thermoplastic polyurethanes based on PCL and isosorbide as a function of the bifunctional isocyanate from literature

Diisocyanate	M_n^{PCL} (g.mol^{-1})	wt% HS	M_n [a] (kg.mol^{-1})	T_g^{SP} [b] (°C)	T_m^{HS} [c] (°C)	Reference
HDI	530	60	225	/	153	[79]–[81]
	3000	33	37	-57	188	[82]
	2000	14	51	31	/	[83]
	2000	26	28	32	/	[83]
	2000	36	20	32	/	[83]
	2000	54	17	43	/	[83]
MDI	3000	38	33.1	-31	220	[82]

a) Number average molar mass of the materials (various methods used throughout the studies, numbers may not always be comparable) – b) Glass transition temperature of the soft domains – c) Melting temperature of the hard segment crystals

Those properties were used in the mid-2000's by Gorna *et al.* [79][81] in order to synthesize bone scaffolds based on isosorbide polyurethane and hydroxyapatite as a solid and biocompatible filler. They synthesized some thermoplastic polyurethane based on PCL (M_n= 530 g.mol^{-1}), HDI and isosorbide with a content of 60 wt% of hard segments. The synthesis first involved the reaction in bulk of isosorbide with HDI to form a prepolymer, which was subsequently dissolved in DMF and the reaction with PCL was carried out in this solution.

The resulting average molar mass was measured to be around 225 kg.mol^{-1} and the polymer was subsequently processed (by combination of invert-phase casting and salt leaching, the reader is invited to consult the reference for more details on this method) to obtain microporous materials, which were evaluated as biocompatible and favorable to cell colonization [81]. The same material was also used by Tsui *et al.* [80] to produce microporous biodegradable membranes intended as healing grafts for cartilage wounds.

Marìn *et al.* [82] made a very thorough study of PCL (M_n=3000 g.mol^{-1}) and isosorbide based polyurethane systems. They investigated the effect of the synthesis method from bulk or solution, as well as the nature of the diisocyanate used, which was either MDI or HDI. They found that polymerization in bulk allowed to obtain higher average molar masses than the polymerization in solution, for a similar dispersity. Furthermore, the feed ratio was maintained in the resulting polymer by bulk synthesis, contrary to solution where some PCL reactant was lost (probably during purification and recrystallization). The study of the thermal behavior of those polyurethanes showed both melting of soft phase domains in the 40-50°C range, and melting of the isosorbide based hard segments at higher temperatures, which were dependent on the nature of the isocyanate used. The corresponding values are reported in Table 2.4.

The last study found on polyurethanes based on HDI, PCL and isosorbide was led by Park *et al.* [83] and devoted to the synthesis of catalyst-free biodegradable thermoplastic elastomers. The materials were obtained from a one-shot synthesis in bulk at 150°C for 12h and then purified in DMF. The isosorbide based polyurethanes displayed a single glass transition temperature between 30°C and 40 °C and no melting of hard segments could be detected on the thermograms, which seems to indicate that the phase segregation in those materials was poor. They moreover showed that the stronger hydrophilicity brought by the presence of isosorbide seemed to accelerate the hydrolysis of the poly(caprolactone) segments in water.

In summary, thermoplastic polyurethanes based on PCL and isosorbide aimed at biomedical applications have been synthesized by several teams. Bulk synthesis is the main synthesis method used by the authors. Overall, the glass transition of the soft domains seems to be higher than that presented in Table 2.3 for PTMEG based equivalent TPU, which seems consistent with respective Tg of PTMEG and PCL with a transition temperature between -90°C and 80°C for PTMEG oligomers [84] and around -70°C for PCL oligomers [85].

2.1.3.3. Polycarbonate diols

Hydroxylated polycarbonate (PCD) oligomers are, similarly to PCL, macrodiols intended for applications requiring biodegradation. An example of a polycarbonate oligomer is presented in Figure 2.7.

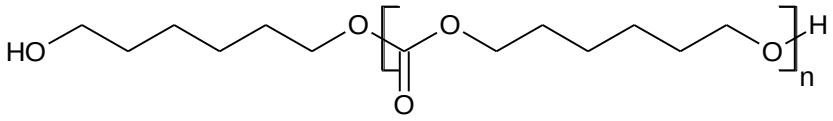

Figure 2.7: Chemical structure of bi-functional hydroxyl terminated poly(hexamethylene carbonate) from [86]

The only mention of the use of a polycarbonate polyol in association with isosorbide for the synthesis of polyurethane was the work of Oh *et al*.[86].

Table 2.5: Summary of the properties of thermoplastic polyurethanes based on polycarbonate and isosorbide as a function of the bifunctional isocyanate according to ref [86]

Isocyanate	M_n^{PCD} (g.mol^{-1})	wt% HS	M_n a) (kg.mol^{-1})	T_g^{SP} b) (°C)	T_m^{HS} c) (°C)
HDI	2000	20	126	-38	63
	2000	25	97	-37	65
	2000	30	78	-36	66
	2000	50	56	-34	71

a) Number average molar mass of the materials (various methods used throughout the studies, numbers may not always be comparable) – b) Glass transition temperature of the soft domains – c) Melting temperature of the hard segment crystals

Their study was very similar to the work of Kim *et al*. and Park *et al*. [78], [83]. The synthesis was carried out in a one-shot fashion: both macrodiol and isosorbide were loaded in the reaction vessel at the same time to react with HDI. The properties of the obtained materials are reported in Table 2.5. Relatively high molar masses were obtained. Moreover, it seems that the soft phase glass transition temperature, and the hard phase melting temperature slightly increase as the hard segment content increases. These phenomena are understood to be arising from the quality of the phase segregation. These materials were moreover shown to have a biocompatible as well as biodegradable character.

2.1.3.4. Isocyanate-free isosorbide based thermoplastic polyurethanes

The non-isocyanate synthesis route also has been explored by some authors in order to obtain isosorbide-based polyurethanes. By carbonatation of isosorbide diglycidyl ether, Besse *et al*. [87] were able to obtain oligomers as shown in Figure 2.8, which were then reacted with an amine in order to obtain polyhydroxyurethanes.

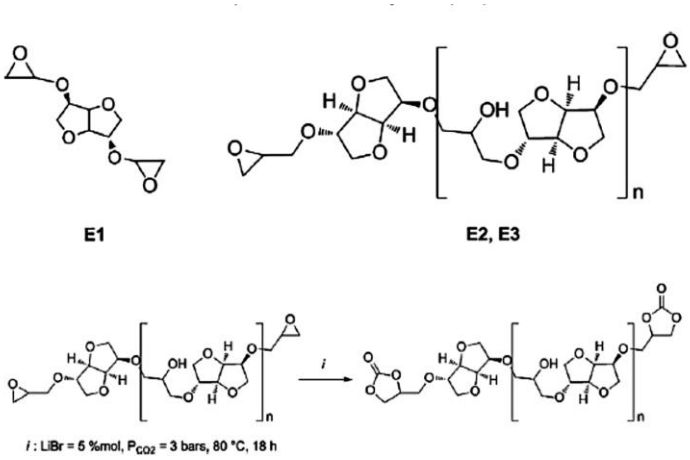

Figure 2.8: Synthesis of isosorbide dicyclocarbonate, reproduced from [87]

However, this synthesis route yielded isosorbide-containing polymers with molar masses smaller than 10 kg.mol^{-1} and with T_g in the -10°C to 60°C range deemed suitable for coatings applications. Last but not least, it was confirmed by the team that the degradation of those materials did not involve the release of harmful isocyanates.

2.1.3.5. Bio-based polyurethanes

As isosorbide is a bio-sourced molecule, it is a very interesting candidate for the synthesis of entirely bio-sourced polyurethanes. In 2014, Charlon *et al*. [88] synthesized a biobased polyurethane from isosorbide and a vegetable oil-based diisocyanate called 2-heptyl-3,4,-bis(9-isocyanatononyl)-1-pentylcyclohexane (DDI), shown in Figure 2.9. DDI was simply reacted with a mix of ISO and BDO in order to form a block polymer.

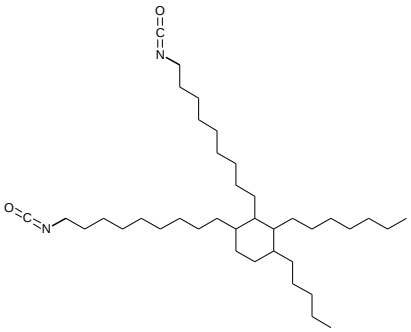

Figure 2.9: Chemical structure of 2-heptyl-3,4,-bis(9-isocyanatononyl)-1-pentylcyclohexane (DDI), obtained from fatty acids dimer

As can be noted in Table 2.6, as the isosorbide content increases, the number average molar mass decreases, as already shown by other teams.

Table 2.6: Summary of the properties of thermoplastic polyurethanes based on DDI, 1,4-butanediol and isosorbide according to ref [88]

Isocyanate	wt% ISO	M_n a) (kg.mol^{-1})	T_g^{SP} b) (°C)	T_m^{HS} c) (°C)	Maximum strain (%)	Reference
DDI	0	17.6	-15	60	700	[88]
	5	12.8	-13	50	350	[88]
	10	8	-36	50	100	[88]
	15	9.8	2	84	150	[88]
	20	3.9	-1	82	30	[88]

a) Number average molar mass of the materials (by SEC)– b) Glass transition temperature of the soft domains – c) Melting temperature of the hard segment crystals

The glass transition temperature increases as well as the melting temperature of the hard domains. However, the mechanical properties of such materials are rather poor as it is not possible to obtain hard segments with a significant number of units, which hinders phase segregation.

The team of Oulame *et al*. [89] has also synthesized bio-sourced polyurethanes in 2015. They synthesized polyester oligomers based on ferulic acid (Figure 2.10) and isosorbide that were subsequently reacted with HDI or toluene diisocyanate (TDI).

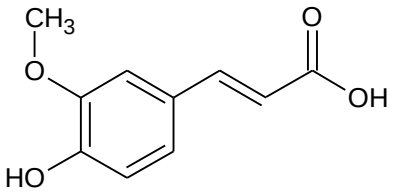

Figure 2.10: Chemical structure of ferulic acid

The glass transition temperatures of the obtained materials ranged from 67°C to 106°C, which means that those products did not display an elastomeric behavior at room temperature.

2.1.3.6. Conclusion

The literature search made on the topic of isosorbide and more specifically isosorbide in polyurethanes compositions has allowed reviewing the state of the art in this field. The first thing of note is that isosorbide is a very good candidate for bio-based production of polyurethanes. It is also a non-toxic monomer, which makes it very interesting for compositions requiring biocompatibility. However, the structure of this molecule gives it a

limited reactivity which can be counteracted by a proper choice of reactants and reaction conditions.

Nonetheless, it has also been seen from literature that isosorbide based hard segments generally have high glass transition temperatures and crystallization seems to be more readily obtained when isosorbide is associated with MDI or HDI.

A large array of thermoplastic polyurethanes obtained from isosorbide was described in the literature. Commonly found compositions were based on PTMEG, PCL and polycarbonates as soft segments associated with MDI or HDI as the isocyanate. Significant differences in the value of the temperature of the soft domains glass transition were observed throughout the studies reported previously, which depends mainly on the quality of the phase segregation [52]. The nature of components of the polyurethane associated to isosorbide, the synthesis method, the soft segment length and the hard segment content are thus critical parameters.

New trends in polyurethane compositions include isocyanate-free synthesis of polyurethanes and entirely bio-based polyurethanes. The non-isocyanate synthesis route requires the reaction of a carbonate with an amine, which means that isosorbide cannot be used in its native –OH terminated state for production of polyurethanes. Moreover, this route does not produce high molar masses due to side reactions [90], which is detrimental for the mechanical properties of the end material. Then, the only viable route at the moment toward greener isosorbide polyurethane seems to lay in the use of bio-based soft segments and isocyanate. Soft segments can be relatively easily obtained from renewable sources such as sugars and vegetable oils. Isocyanates are more difficult to obtain from nature. DDI is for example partially bio-based, but its chemical structure does not make it by itself a suitable component for the production of elastomeric TPUs with good mechanical properties due to the hindrance brought to phase segregation by DDI.

This chapter will then study the synthesis of isosorbide-based thermoplastic polyurethanes in association with soft segments of differing nature. The properties of the isosorbide-based polyurethane will be as well compared to those of 1,4-butanediol-based polyurethanes, which is a classical industrial chain extender.

Isosorbide will be used as a chain extender for the synthesis of thermoplastic polyurethanes by a two-stage method. The aim of this chapter is more specifically to study the synthesis of isosorbide-based polyurethanes in terms of molar mass, and kinetics, as well as to study the quality of the phase segregation of isosorbide-based compositions as a function of the soft segment nature and of the hard segment content. Moreover, the isosorbide-based materials will be compared to 1,4-butanediol-based models. The diisocyanate chosen for this study is MDI as it was clear from literature that this monomer readily forms hard segment crystallites and is a very common and highly reactive industrial monomer. Soft segments were selected from the literature as poly(ε-caprolactone), poly(tetrahydrofuran); to increase the bio-

sourced ontent, a fatty acid dimers-based polyester was also tested. This chapter will thus contain:

- Characterizations of the starting reactants
- A study of the two-step synthesis of polyurethane materials as a function of the soft segment and the chain extender
- An optimization of said synthesis of isosorbide-based polyurethanes after careful examination of the condition effects
- A synthesis of polyurethane materials with increasing hard segment contents
- A study of the quality of the phase segregation in the materials as a function of the chain extender, soft segment and hard segment weight ratio.
- Other mechanical characterizations including permanent set and hardness, and swelling in water.

2.2. SYNTHESIS OF THERMOPLASTIC POLYURETHANES

2.3.1. Two-stage synthesis of TPUs

The two-stage synthesis used for synthesis of the thermoplastic polyurethane is presented schematically in Figure 2.11.

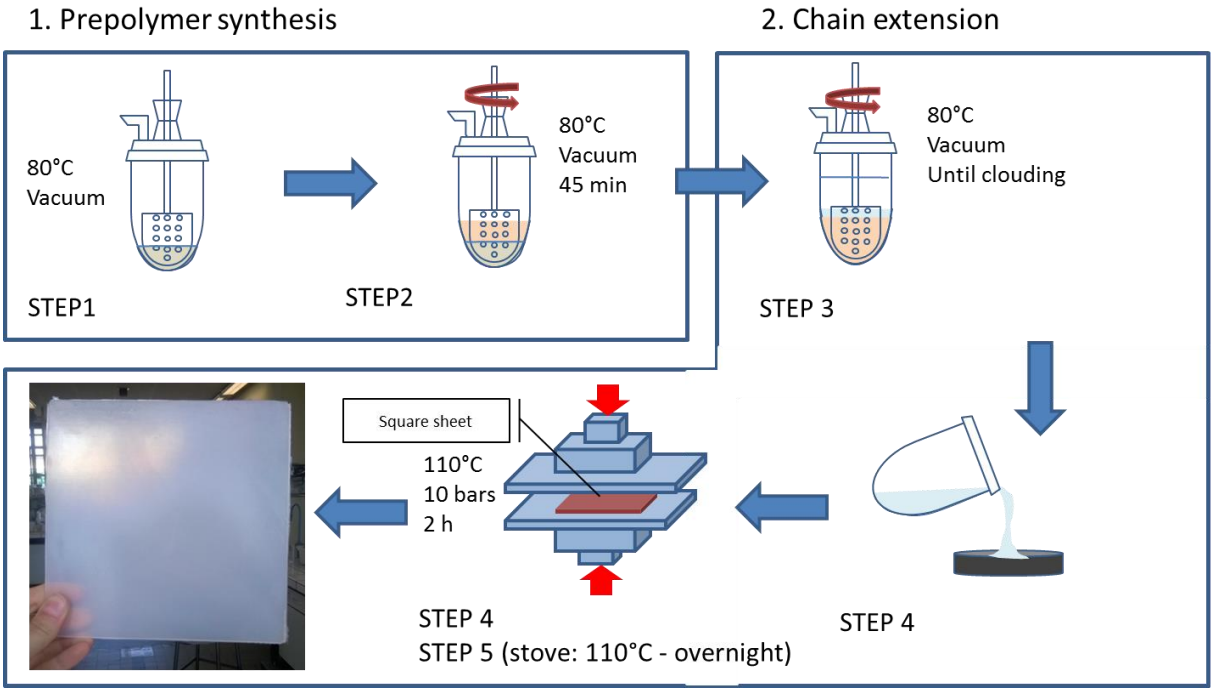

Figure 2.11: Scheme of original synthesis. In a first step, the prepolymer is obtained from the reaction of a macrodiol (PTMEG) with an excess of bifunctional isocyanate (MDI). Then, in a second step, the chain extender (ISO) is added in order to form hard segments.

The synthesis yields around 150 g of material.

- STEP 1: MDI is weighed and inserted in the reactor and the reactor is then put under vacuum, heated at 80°C with an oil bath and mechanically stirred at a low speed (around 50 rpm) in order to melt the MDI.

- STEP2: The vacuum is broken by nitrogen flushing and the reactor is subsequently opened, put on a scale and the melted macrodiol is weighed directly in the reactor bottom for accuracy. The reactor is then closed, put under vacuum, with 80°C heating and a high-speed (between 200-300 rpm) mechanical stirring. The prepolymer reaction is left to proceed for 45 min.

- STEP 3: The vacuum is broken by nitrogen flushing and reactor is opened again and installed on a scale. The melted isosorbide (melted in a stove at 80°C prior to use) containing DBTDL catalyst is weighed, and the reactor closed, put back under vacuum and stirred at high speed at a temperature of 80°C. The chain extending reaction is left to proceed until a clouding of the reaction mixture (sign of the beginning of the phase separation) and/or a thickening of the mixture preventing further mixing is

observed. In the case of BDO chain extender, due to higher reactivity, the heating bath was removed, and the reaction occurred for 2-5 min before clouding of the reacting mixture, with high speed mixing (between 200-300 rpm) and vacuum.

- STEP 4: The vacuum is broken by nitrogen flushing and the reactor is opened. The reaction mixture is poured into molds (sheets of 2mm thickness). The molds are then pressed at 110°C at a pressure of 10 bars for 2 hours.

- STEP 5: The molds are removed from the press and put in a stove at 110°C for 16 hours (overnight) in order to increase the degree of conversion of the reaction to its maximum.

2.3.1.1. Prepolymers

A two-stage synthesis of block polyurethanes first involves the synthesis of prepolymers based on the macrodiols and an excess of diisocyanate. The reaction thus results in the production of a distribution of –NCO terminated macrodiols as shown in Figure 2.12.

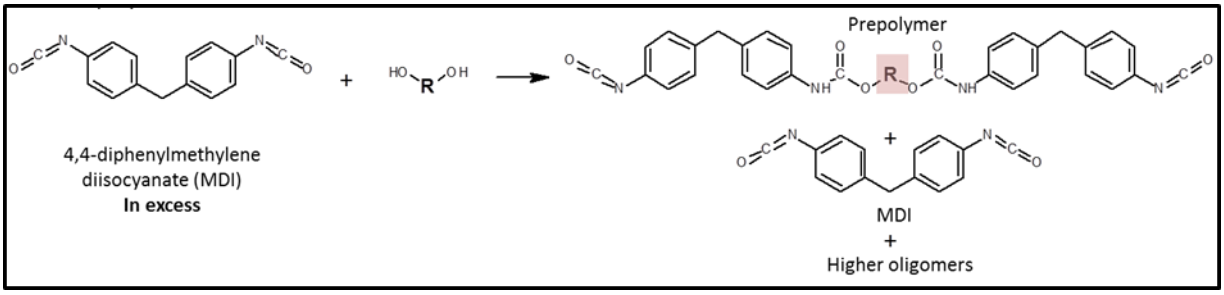

Figure 2.12: General scheme of MDI reaction with a macrodiol (R) being either poly(tetrahydrofuran), poly(ε-caprolactone) or fatty acid dimers based polyester in order to obtain a –NCO terminated prepolymer.

The synthesis of the prepolymer has been studied to obtain stable and suitable prepolymers for the second step of the polyurethane synthesis. All reactants used in this section are characterized and presented in the material section (see section 5.1., p. 167 in the experimental section).

2.3.1.1.1. Synthesis of the prepolymers

In order to prepare polyurethanes with a molar ratio of macrodiol/diisocyanate/extender diol of 1:3:2 respectively, the synthesis of prepolymers with a ratio of NCO/OH = 3 was studied. Table 2.7 reports the composition of those prepolymers. The NCO functions were added in a slight 0.05 molar excess from the expected final ratio to obtain the longest possible polymer chains. All the reactants are presented in the material section 5.1. (see p. 167). The prepolymers were prepared by reaction of MDI with a macrodiol being either poly(ε-caprolactone), poly(tetrahydrofuran) or vegetable oil-based macrodiol (FADM) in a reactor under vacuum and heated by an oil bath at 80°C; samples were taken periodically for analysis over a two hours course.

Table 2.7: Composition of prepolymers based on MDI and NCO equivalents, after a 45 min reaction time at 80°C

Sample	Polyol Type	Polyol mass (g)	MDI mass (g)	NCO/OH initial ratio (-)	Experimental Eq_{NCO}[a)] ($mol.kg^{-1}$)	Free –NCO function percentage[a)] (%mol)	Free MDI percentage[b)] (%mol
PTMEG-pp	PTMEG	20.72	15.60	3.040	2.22	65	34.7
PCL-pp	PCL	19.61	14.73	3.120	2.28	66	36.4
FAMD-pp	FADM	26.91	10.57	3.203	Not obtained	Not measured	37.3

a) Obtained by chemical titration as described in the experimental section– b) Obtained by SEC as described in the experimental section

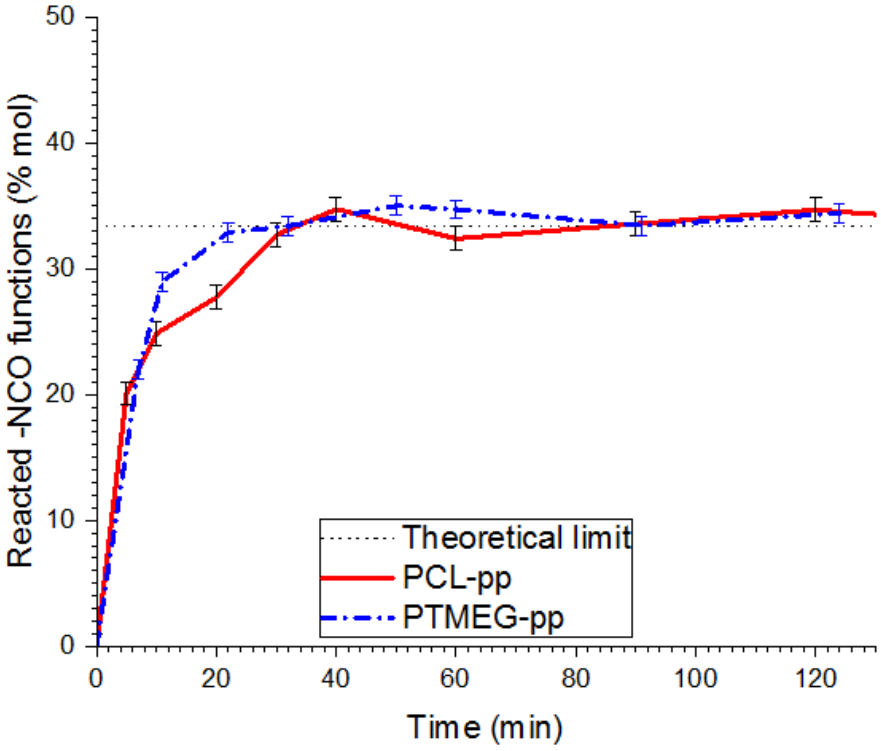

Figure 2.13: Conversion of NCO groups (1 - $Eq_{NCO}(t)/Eq_{NCO}$ (t=0))x100) as a function of time during prepolymer reaction, obtained by chemical back titration of NCO functions. The theoretical limit was calculated from initial reactant masses and stoichiometry

In order to check the stability of the prepolymers, a follow-up of the reaction was done by titration of the NCO groups for the prepolymers based on PTMEG and PCL. Figure 2.13 presents the obtained curve. At the completion of the reaction for prepolymers with NCO/OH ratio 3.05, the expected NCO conversion is 33%. This limit is reached after 20 min reaction time at 80°C in the case of PTMEG-pp, and after 30 min in the case of PCL-pp. From

there on, the percentage of reacted -NCO functions does not increase significantly, which means that the prepolymers are stable for at least two hours under the synthesis conditions. It was then decided to set the time of the chain extender addition at 45 min in order to have a reasonable synthesis reaction time.

After 45 min, the NCO index (Eq_{NCO}) and the free –NCO function percentage were then measured by chemical titration, and the percentage of free MDI was measured by size exclusion chromatography using a refractometric detection (Table 2.7). Eq_{NCO} and free –NCO functions percentage were not possible to obtain by chemical titration for FAMD-pp, however it was possible to measure the free MDI percentage.

2.3.1.1.2. Characterization of prepolymers

SEC curves of the prepolymers and macrodiols are presented in Figure 2.14. As the exclusion volume of the columns is around 16.5 mL, all molecules appearing before this volume are not properly separated, inducing errors in the molar mass measurements.

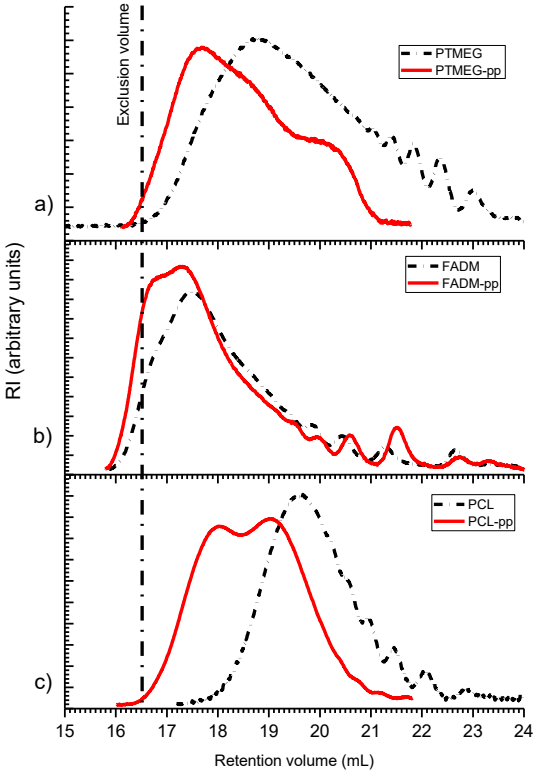

Figure 2.14: SEC RI curves of the prepolymers and the corresponding macrodiols in THF (1mL/min) a) PTMEG and PTMEG-pp – b) FADM and FADM-pp – c) PCL and PCL-pp

This case was encountered for the sample FADM-pp and even for the starting FADM which displayed a very broad range of molar masses. All the other samples seem to have been correctly separated. The high resolution of the SEC columns even allowed to separate the low mass entities, whose peaks clearly appear as separate on the higher retention volume range (>20 mL).

PTMEG-pp and PCL-pp curves both present shoulders at smaller retention volumes, which seems to indicate the presence of two distinct size populations. This could either originate from chain lengthening of the prepolymer or from the formation of aggregates. It is very well known that TPUs are difficult to dissolve in organic solvents due to their strong H-bonds, hence the formation of aggregates. FADM display small peaks at high retention volumes that are still present in the FADM-pp sample. They however do not appear at smaller retention volumes than those of the FADM-pp curve, which suggests the corresponding chemical entities in FADM do not react with MDI and are thus probably not –OH functionalized. Those small peaks seem to appear at smaller retention volumes in FADM than FADM-pp. The value difference between two FADM and FADM-pp small peaks was calculated to be around 10%, which is within the 10% error of the SEC and is thus considered the limit of the SEC reproducibility.

In order to obtain reliable molar mass values for the FADM-based samples, some SEC measurements were carried out with separation columns with a bigger porosity using a 0.01M solution of bis(trifluoromethane)sulfonimide lithium salt ($LiNTf_2$) in dimethyl formamide (DMF) as eluent. The obtained curve is presented in Figure 2.15. However, the resolution of this column did not allow precisely distinguishing the different size populations. FADM-pp is logically shifted toward the smaller retention volumes. Both samples display a small shoulder at the higher retention volumes. The corresponding molar mass was (Table 2.8) calculated from polystyrene standards and reflects the overall tendencies shown in the SEC curves.

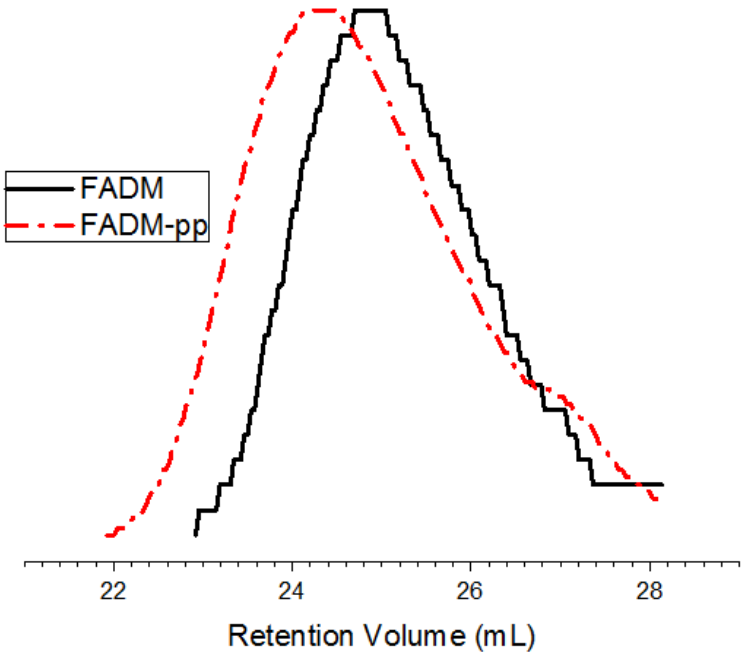

Figure 2.15: SEC RI curves of the FADM prepolymers and the corresponding macrodiols in DMF LiNTf2 0.01M (1mL/min)

As the calibration used is the conventional method with polystyrene standards, the macrodiols average molar mass is higher than the theoretical value M_n=1000 g.mol^{-1} (for PTMEG and PCL) or 2200 g.mol^{-1} (for FADM) given by the suppliers. The dispersity of the samples is not hugely impacted by the MDI functionalization: overall, the value of Đ is stable between PTMEG and PTMEG-pp on the one hand, and PCL and PCL-pp on the other hand. FADM-pp displays a slight increase in Đ with respect to FADM.

Table 2.8: Molar mass distribution of prepolymers and macrodiols (Polystyrene conventional calibration) obtained in THF for the PCL and PTMEG based samples, and in DMF LiNTf$_2$ 0.01M for the FADM based samples.

Sample	M_n (g.mol^{-1})	M_w (g.mol^{-1})	Đ (M_w/M_n)
PTMEG	1680 ±170	2990 ±300	1.8
PTMEG-pp	3140 ±310	5440 ±540	1.7
PCL	1550 ±160	1920 ±190	1.2
PCL-pp	2980 ±300	4450 ±450	1.5
FADM	3760 ±370	6650 ±660	1.8
FADM-pp	4040 ±400	8970 ±900	2.2

The characterization of prepolymers has allowed seeing that the chosen synthesis protocol produced prepolymers with the expected number of free –NCO groups. It is however also probable that some limited lengthening of the macrodiols and dimerization of MDI occurred during this step of the synthesis.

2.3.1.2. Chain extension reaction

The synthesis of the prepolymers then allowed to proceed to the second part of the thermoplastic polyurethanes synthesis: the addition of the chain extenders. Three series of polyurethanes were synthesized, based on PCL, PTMEG or FADM macrodiol and with MDI as the diisocyanate. For isosorbide-based compositions, dibutyltin dilaurate (DBTDL) catalyst was used. A solution of 0.07 wt% DBTDL was made in melted isosorbide (80°C).

Table 2.9 presents the composition and molar mass of the series of polyurethanes synthesized with PCL, MDI and either ISO or BDO as the chain extender. Similarly, Figure 2.16 shows the SEC curves of the said polyurethanes. It is to be noted that at an equivalent stoichiometry, the weight fraction of hard segments in the material is lower for BDO-based samples due to a smaller molar mass of this chain extender compared to ISO.

Table 2.9: Composition and molar mass of poly(ε-caprolactone) (PCL)-based polyurethanes series – obtained by SEC in $LiNTf_2$ 0.01 M solution at 1 mL/min and calculated from polystyrene standards

Sample	Chain extender	wt% HS	Stoichiometry	M_n	M_w	Đ
			SS/MDI/Diol	(kg.mol^{-1})	(kg.mol^{-1})	(M_w/M_n)
CMI50	ISO	51	1:3:2	16.5 ±2	40.5 ±4	2.5
CMB50	BDO	48	1:3:2	30.7 ±3	76.8 ±8	2.5

From the SEC curves and the values of the molar masses, the CMI50 sample has smaller number and weight average molar masses than the equivalent BDO based CMB50 sample but has a similar dispersity index. This difference can be attributed to the lower reactivity of ISO compared to BDO.

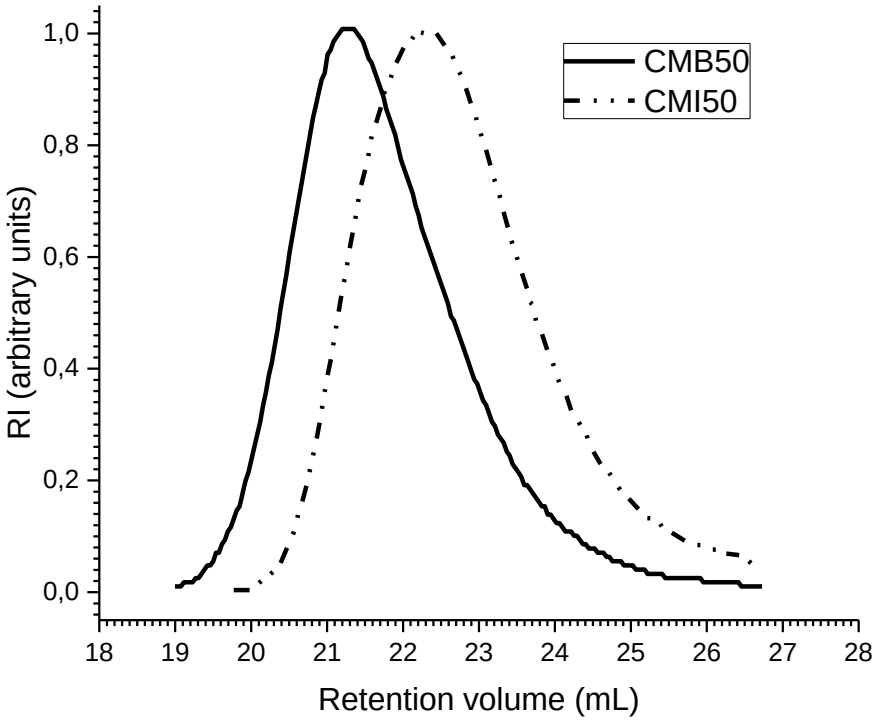

Figure 2.16: SEC curves of PCL based polyurethanes, in DMF 0.01 $LiNTf_2$

Table 2.10 presents the composition and molar mass of a series of samples based on PTMEG and either ISO or BDO as a chain extender. The stoichiometry was changed to obtain samples containing around 40, 50 and 60 wt% of hard segments. Figure 2.17 presents the SEC curves of the samples.

First of all, it can be noted that the increase in the hard segment content is linked to a decrease in the average molar mass of all the PTMEG-based samples. This is also the case on

the weight average molar mass of the TMB series of samples. The weight average molar mass of the series of samples based on PTMEG and ISO (TMI) is stable around 60 kg.mol^{-1} if the error is taken into consideration. Those numbers can be investigated by comparing the SEC curves of the two series of samples, in Figure 2.17.

Table 2.10: Composition and molar masses of poly(tetrahydrofuran) (PTMEG)-based polyurethanes series – obtained by SEC in $LiNTf_2$ 0.01 M solution at 1 mL/min and calculated from polystyrene standards

Sample	Chain extender	wt% HS	Stoichiometry SS/MDI/Diol	M_n (kg.mol^{-1})	M_w (kg.mol^{-1})	Đ (M_w/M_n)
TMI40	ISO	40	1:2:1	31.4 ±3	64.6 ±6	2.1
TMI50	ISO	51	1:3:2	22.8 ±3	63.9 ±6	2.8
TMI60	ISO	59	1:4:3	16.4 ±2	54.3 ±5	3.2
TMB40	BDO	37	1:2:1	128 ±13	316 ±32	2.5
TMB50	BDO	48	1:3:2	48.6 ±5	135 ±14	2.8
TMB60	BDO	56	1:4:3	23.5 ±2	59.9 ±6	2.5

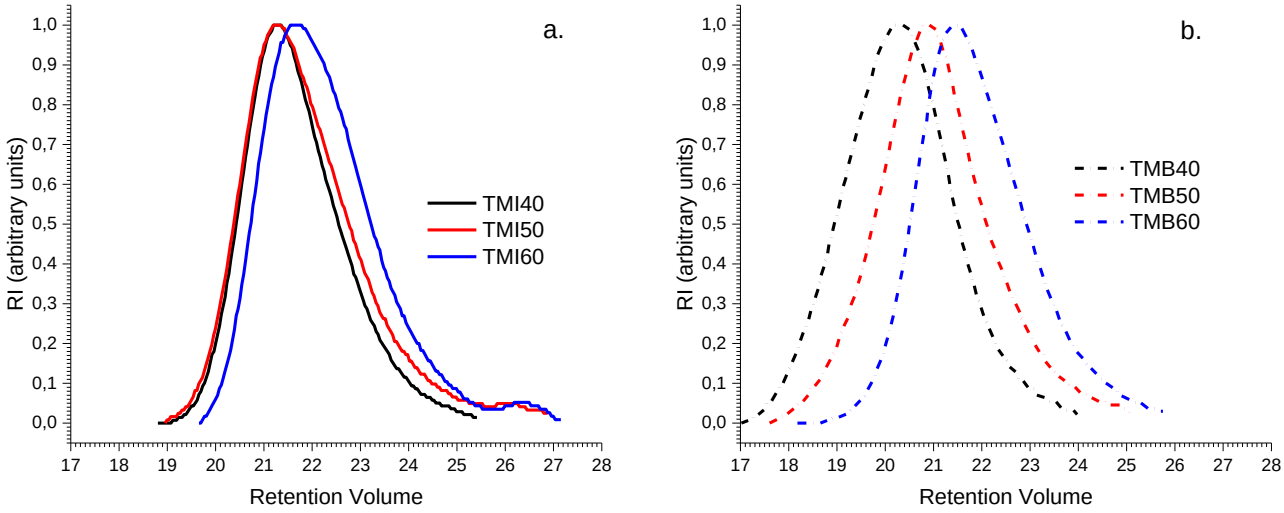

Figure 2.17: SEC curves of PTMEG based polyurethanes, in DMF 0.01 $LiNTf_2$ – a. with ISO as the chain extender – b. with BDO as the chain extender.

It is obvious that the curves are shifted toward the higher retention volumes as the fraction of hard segment increases considering the TMB40, TMB50 and TMB60 samples. This is not the case for the series of samples based on ISO: the increase in hard segment content is linked to the appearance of a small shoulder at the higher retention volumes. That probably originates from pure hard segments that are not bound to any PTMEG soft segment and has a pronounced effect on the value of M_n for those materials. The products appearing at the

smaller retention volumes are not greatly influenced by the weight fraction of hard segments.

A third series of polyurethanes was synthesized, based on a fatty acid dimer polyester (FADM) and either BDO or ISO as the chain extender. Hard segment contents were as well varied. Compositions and molar masses of the samples are presented in Table 2.11 and Figure 2.18.

Table 2.11: Composition and molar masses of fatty acid dimers polyester (FADM)-based polyurethane series – obtained by SEC in $LiNTf_2$ 0.01 M solution at 1 mL/min and calculated from polystyrene standards

Sample	Chain extender	wt% HS	Stoichiometry SS/MDI/Diol	M_n (kg.mol^{-1}))	M_w (kg.mol^{-1})	Đ (M_w/M_n)
FMI25	ISO	24	1:2:1	39.0 ±4	120 ±12	3.1
FMI35	ISO	34	1:3:2	18.1 ±2	56.5 ±6	3.1
FMI40	ISO	42	1:4:3	15.9 ±2	50.2 ±5	3.2
FMI50	ISO	53	1:6:5	11.6 ±1	40.7 ±4	3.5
FMB25	BDO	23	1:2:1	34.1 ±3	90.1 ±9	2.6
FMB35	BDO	32	1:3:2	30.3 ±3	97.5 ±10	3.2
FMB40	BDO	39	1:4:3	23.5 ±2	76.1 ±8	3.2
FMB50	BDO	49	1:6:5	18.1 ±2	60.4 ±6	3.3

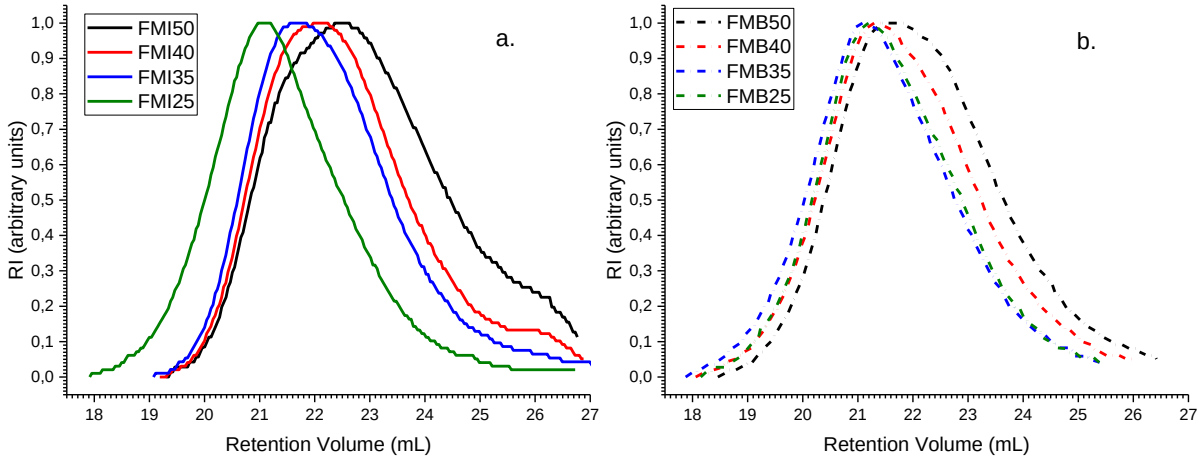

Figure 2.18: SEC curves of FADM based polyurethanes, in DMF 0.01 $LiNTf_2$ – a. with ISO as the chain extender – b. with BDO as the chain extender.

First of all, it can be noticed that the molar mass dispersity index of the series of samples based on FADM is globally higher than for the PTMEG series studied above in Figure 2.17 and

Table 2.10. This can be explained by the branched nature of FADM as well as the higher dispersity of the prepolymer based on FADM shown previously in Figure 2.18**.**

The same trends can be observed with FADM and PTMEG: the increase in fraction of hard segments is linked to a decrease in the molar mass of both series based on ISO and BDO. The appearance of a shoulder and the stagnation of the higher mass fraction values at a similar retention volume as the hard segment content (see samples FMI35-50) increases in the case of ISO are also to be noted. The variation of the molar mass of the FMB25-50 series of samples is however smaller than that obtained in the same condition with PTMEG as a soft segment on the TMB40-60 sample series.

In summary, thermoplastic polyurethanes based on isosorbide, 4,4'-diphenylmethylenediisocyanate and various soft segments were obtained. The number average molar mass was at least 11 $kg.mol^{-1}$, with an average 20 $kg.mol^{-1}$. At equivalent stoichiometry, the molar masses of the ISO-based samples were however significantly smaller than the BDO-based equivalents, which is due to the lower reactivity of the hydroxyl functions of isosorbide. Molar masses were also found to decrease with the weight fraction of hard segments in all sample series (based on ISO and BDO), in accordance with several studies on isosorbide [76]–[78], [83], [86].

Better properties could potentially be obtained by optimizing the synthesis of the ISO-based polyurethanes in order to increase molar mass and get rid of the independent hard segments found at high retention volumes in the SEC curves. This could be achieved by the study of the synthesis process and its significant parameters.

2.3.2. Optimization of the synthesis of a TPU based on MDI and Isosorbide

From the molar mass study presented in 2.3.1.2, it was decided to study the optimization of the synthesis for a TPU based on PTMEG, MDI and Isosorbide, at a stoichiometry 1:3:2. In the following sections, the process of the original synthesis will be recalled in order to list the parameters that can be studied before presenting the results of the effects of those parameters on the molar masses. Eventually, the results of the optimized synthesis of PTMEG/MDI/ISO 1:3:2 will be compared to the BDO based equivalent polyurethanes, obtained with a synthesis as close as possible to that used for ISO.

2.3.2.1. Original synthesis procedure

The two-stage synthesis presented in 2.3.1 was used for most of the TPU presented in 2.3.1.2. STEP 1 and STEP 2 were well studied in 2.3.1.1. Thus, they will not be modified in order to optimize the molar mass of the polyurethanes. Two parameters of STEP 3 could be of major importance: the temperature of the chain extension in the reactor, and the quantity of DBTDL catalyst used at this point. During STEP 4, the shape of the mold can have an impact on the heat repartition and exothermal heat release of the reaction during the press cure. STEP 5 could be optimized in order to reduce the post cure time and thus

improve the overall synthesis time. Those parameters will be studied in the following sections.

2.3.2.2. Effect of the temperature during the chain extension

The influence of the reaction temperature on the molar mass of the isosorbide based polyurethanes was studied by testing three different temperatures during STEP 3, STEP 4 and STEP 5. In order to save materials, the batches for the parameters screening were of 40 g instead of 150 g and the smaller samples were poured into polypropylene cylindrical molds instead of sheets at STEP 4. The press was not used and the samples were directly cured in the stove at the end of STEP 4. The three synthesis protocols were named A, B and C.

The temperature used during STEP 3, STEP 4 and STEP 5 was 80°C for Method A, 110°C for Method B, and 130°C for Method C, respectively. The molar masses were measured by SEC in a 0.01M solution of bis(trifluoromethane)sulfonamide lithium salt ($LiNTf_2$) at a flow rate of 1 mL/min. The SEC was measured after solvation of the samples, four days after the synthesis. The results are presented in Figure 2.19 and Table 2.12. Method C samples were not soluble in any solvent and thus no data could be gathered, it is however probable that this temperature led to unwanted cross-linking reactions due to side-reactions of the isocyanates.

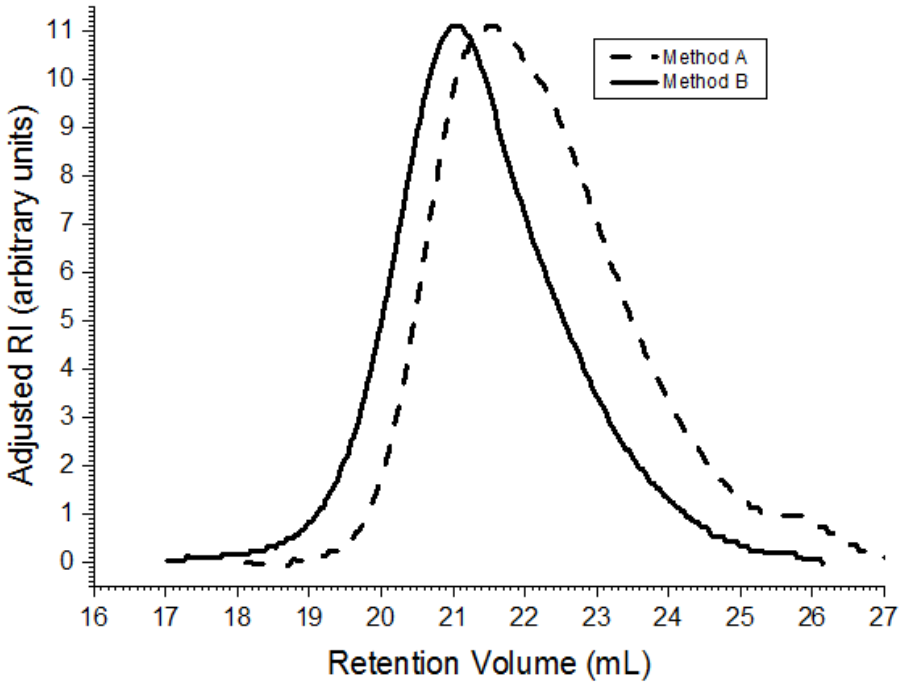

Figure 2.19: SEC curves of isosorbide based polyurethanes (PTMEG/MDI/ISO 1:3:2) synthesized with two synthesis methods A (80°C) and B (110°C), in DMF 0.01 $LiNTf_2$

The SEC curve profiles for method A and B are not gaussian, and the curves tend to be shifted toward the higher retention volumes, which means that the two samples obtained with method A and B have an important population of oligomers. The shoulder visible around 26 mL for method A and to a smaller extent for method B is probably due to independent MDI/ISO hard segments.

Table 2.12: Molar masses values for PTMEG/MDI/ISO 1 :3 :2 as a function of the synthesis method A or B, in DMF 0.01 $LiNTf_2$ and conventional calibration with polystyrene standards

Synthesis method	Sample mass (g)	Mixing time before phase separation (STEP 3)	Temperature at steps 3 to 5 (°C)	M_n ($kg.mol^{-1}$)	M_w ($kg.mol^{-1}$)	Đ (M_w/M_n)
Method A	40	1h30	80	8.3 ±1	30.7 ±3	3.7
Method B	40	45 min	110	23.6 ±2	72.6 ±7	3.1

Those observations are confirmed by Table 2.12, which presents the molar mass values obtained from the previous curves. It is very apparent from the SEC data that the temperature of the chain extension is a major parameter: with 30°C of difference, the average molar mass of the samples can be increased three-fold. The best results are obtained with the higher temperature 110°C.

It can be noted that the dispersity of both samples is higher than 3, which is somewhat surprising and can be attributed to the fact that H-bond interactions were still present in the solutions at the time of the SEC measurement. This problem will however be discussed in further details in Annex A.

2.3.2.3. Effect of the catalyst concentration

The influence of the reaction kinetics on the molar mass of the isosorbide-based polyurethanes was studied by testing the effect of the catalyst concentration during STEP 3, STEP 4 and STEP 5.

Similarly to the previous temperature screening, the batches for the catalyst concentration screening were also of 40 g instead of 150 g, the smaller samples were poured into polypropylene cylindrical molds, and the samples were put directly in a stove to maximize the conversion of the reaction.

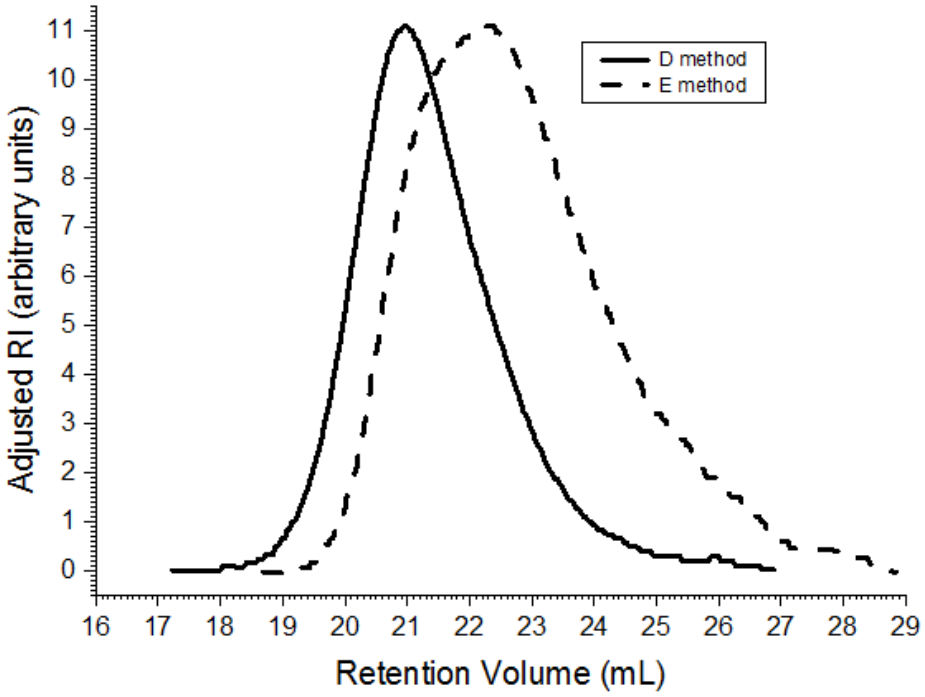

Figure 2.20: SEC curves of isosorbide based polyurethanes (PTMEG/MDI/ISO 1:3:2) synthesized with two synthesis methods D (100 ppm DBTDL) and E (60 ppm DBTDL), in DMF 0.01 $LiNTf_2$

Two catalyst concentrations were tested. In Method D, 100 ppm of DBTDL catalyst from the total mass of the reacting mixture, in solution in the melted isosorbide were added at STEP 4. The reaction was carried out subsequently at 80°C for 7 min. At STEP 5, the sample was heated at 110°C for 16 h (overnight) in the stove. In Method E, 60 ppm of DBTDL catalyst in solution in the melted isosorbide were added at STEP 4. In order to obtain comparable kinetics to Method D, the temperature of STEP 4 was 90°C for 7 min, and STEP 5 was carried out at 110°C in the stove for 16 h (overnight). Those reaction times allowed the appearance of the phase segregation (cloudy mixture).

Table 2.13: Molar masses values for PTMEG/MDI/ISO 1:3:2 as a function of the synthesis method D or E, in DMF 0.01 $LiNTf_2$ and calculated from conventional calibration with polystyrene standards

Synthesis method	Sample mass (g)	DBTDL catalyst (ppm over the total mass of the monomers)	Temperature at step 3 (°C)	M_n ($kg.mol^{-1}$)	M_w ($kg.mol^{-1}$)	Đ (M_w/ M_n)
Method D	40	100 (1DBTDL/12500 -NCO)	80	20.7 ±2	65.8 ±7	3.2
Method E	40	60 (1DBTDL/21700 -NCO)	90	8.1 ±1	46.7 ±5	5.8

Figure 2.20 shows the profiles of the SEC curves recorded for Method D and E. Compared to D, E is shifted toward the higher retention volumes with a well-defined shoulder, which

means it has smaller molar masses. Moreover, the peak of E is very broad and asymmetric compared to D, which suggests the presence of a lot more lone hard segments and small length chains.

Those observations are supported by the values in Table 2.13. The average molar masses obtained with method D are almost three-fold larger than those obtained with E. The dispersity of E is very high, around 6, as was suggested by the SEC curve profile. It is supposed that the poor results from method E originated from a fast reaction that quickly hindered transport and mixing of the reaction mixture. The molar masses obtained with Method D are comparable to the results of Method B. The addition of catalyst allowed to quicken the STEP 3 (7 min instead of 45 min) and to use a lower temperature of reaction (80°C instead of 110°C). However, the addition of a catalyst may not always be suitable depending on the application. The DBTDL catalyst used here is indeed very toxic and would for example not be allowed in materials intended for biomedical use. It was however chosen to continue testing both B and D method for scale-up effects and post-cure optimization.

2.3.2.4. Effect of the scale-up

The formation of polyurethane bonds from an isocyanate and an alcohol function is very exothermic. Since the shape of the sample and the total mass of the reacting mixture can influence the temperature of the bulk during the reaction, the effect of the scale-up must be studied.

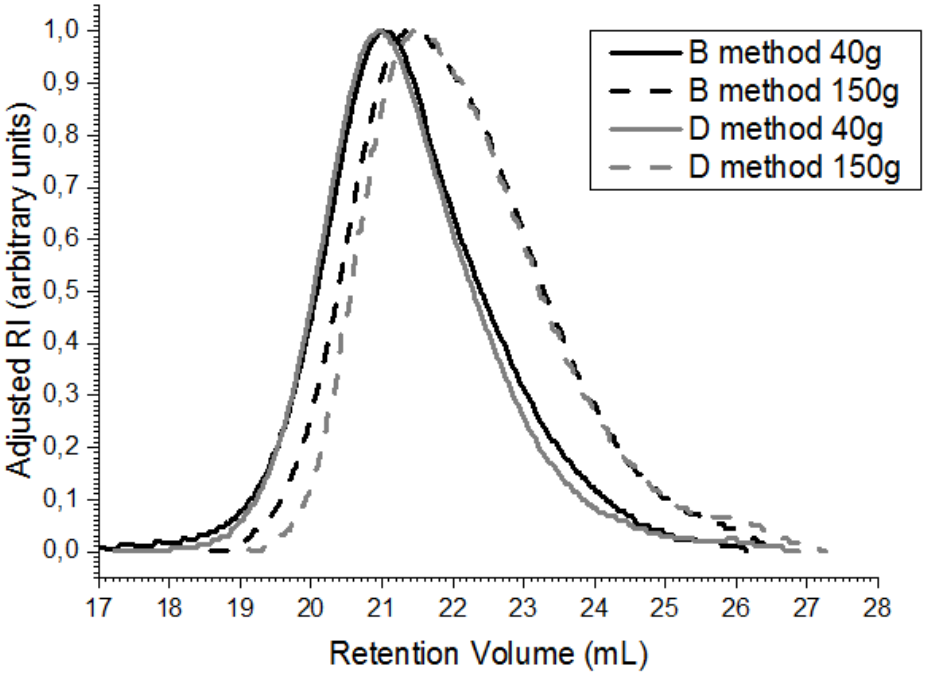

Figure 2.21: SEC curves of isosorbide based polyurethanes (PTMEG/MDI/ISO 1:3:2), synthesized with two synthesis methods B (110°C) and D(80°C/100 ppm DBTDL) and two batch sizes, in DMF 0.01 $LiNTf_2$

Batches of samples of 150 g were made with method B and D to be compared to the 40 g batches discussed previously in 2.3.2.3. The samples were subsequently poured into square

sheet molds at STEP 4 and pressed at 10 bars and 110°C for 2h. They were then post-cured for 16 h at 110°C in the stove. Figure 2.21 shows the profiles of the SEC curves obtained.

First of all, it is obvious that the samples obtained from the 150 g batches will display lower molar masses, as the profiles are shifted toward the higher retention volumes. The original method B and D from 40 g batches are equivalent and their curves overlap almost perfectly. However, it seems that in the 150 g batch series, method B displays slightly higher molar masses than D, while their low masses are almost equivalent.

These observations are confirmed by the average molar masses values in Table 2.14. As previously, the presence of lone hard segments composed only of ISO and MDI can be suspected by the appearance of a shoulder at the higher retention volumes. This phenomenon seems to be increased by the use of Method D. For both methods B and D, scale-up was detrimental to the molar masses of the material, as the temperatures used from STEP 1 to STEP 3 cannot be increased because of side reactions and exotherm during reaction is difficult to control. This result is probably due to the change in the geometry of the mold used for STEP 4 and 5 which induces a different heat distribution in the sample. Solutions must be found by optimization of the following steps.

Table 2.14 : Molar masses values for PTMEG/MDI/ISO 1:3:2 polyurethane as a function of the synthesis method B or D and the batch size, in DMF 0.01 $LiNTf_2$ and calculated from conventional calibration with polystyrene standards

Synthesis method	Sample mass (g)	DBTDL catalyst (ppm)	Temperature at step 3 (°C)	M_n ($kg.mol^{-1}$)	M_w ($kg.mol^{-1}$)	Đ (M_w/M_n)
Method B	40	0	110	23.6 ±2	72.6 ±7	3.1
Method B	150	0	110	15.2 ±2	48.8 ±5	3.2
Method D	40	100	80	20.7 ±2	65.8 ±7	3.2
Method D	150	100	80	9.2 ±1	32.7 ±3	3.5

2.3.2.5. Effect of post cure time and temperature

In order to further increase the molar masses of the up-scaled samples, the effect of a post cure was studied. The temperature should be set between 110°C and 160°C since the polyurethane bonds become unstable at higher temperatures.

The square sheets obtained from the 150 g batches of method B and D were cut in half and were heated in a stove at 140°C for 1 hour in the case of B1 and D1, and 2 hours in the case of B2 and D2. The subsequent SEC results are presented in Figure 2.22 and Table 2.15.

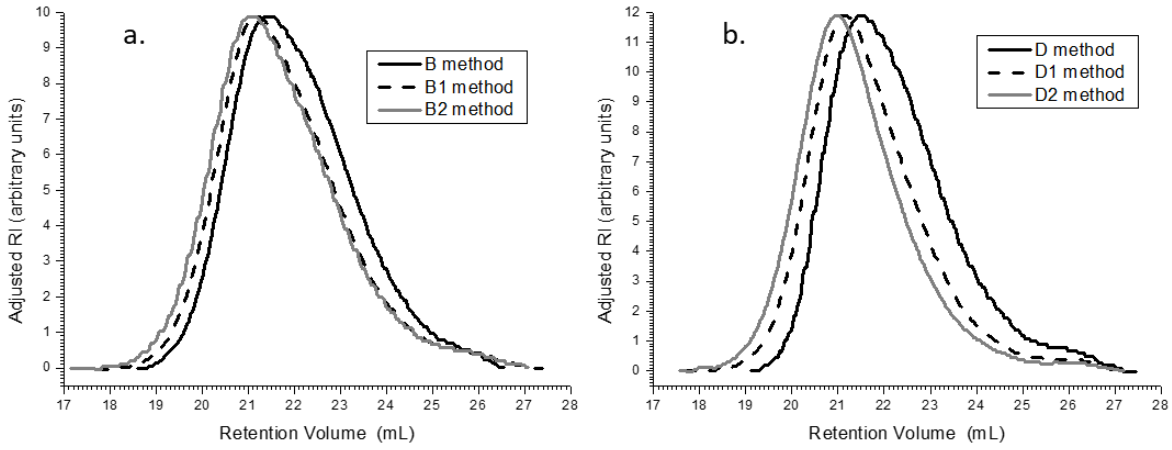

Figure 2.22: SEC curves of isosorbide based polyurethanes (PTMEG/MDI/ISO 1:3:2) in DMF 0.01 $LiNTf_2$ – a. synthesis with method B as a function of the post-cure time – b. synthesis with method D as a function of the post-cure time.

Figure 2.22 a. presents the SEC curves of the B series. Both post cured samples B1 and B2 curves are shifted toward the smaller retention volumes, which indicates that the polymer chains were indeed lengthened. There is however not significant differences between samples B1 and B2. The same observations can be made on Figure 2.22 b. between the samples obtained from D method and D1 and D2. There is however a more significant effect of the post-cure time in the D series: overall, D2 curve is shifted toward the smaller retention volumes compared to D1. The post cure also has a noticeable effect on the high retention volumes shoulder: it is greatly reduced from method D curve to D1.

Table 2.15: Molar masses values for PTMEG/MDI/ISO 1:3:2 polyurethane in DMF 0.01 $LiNTf_2$ and calculated from conventional calibration with polystyrene standards as a function of the post cure time.

Synthesis method	Sample mass (g)	DBTDL catalyst (ppm)	Post-cure time (140°C)	Temperature at step 3 (°C)	M_n ($kg.mol^{-1}$)	M_w ($kg.mol^{-1}$)	Đ (M_w/M_n)
Method B	150	0	0	110	15.2 ±2	48.9 ±5	3.2
Method B1	150	0	1 h	110	18.4 ±2	69.0 ±7	3.7
Method B2	150	0	2 h	110	20.2 ±2	74.9 ±7	3.7
Method D	150	100	0	80	9.2 ±1	32.7 ±3	3.5
Method D1	150	100	1 h	80	13.6 ±1	47.8 ±5	3.5
Method D2	150	100	2 h	80	24.2 ±2	83.9 ±8	3.5

These observations are reflected by the values calculated from the curves and reported in Table 2.15. In both cases, the average molar mass values of the isosorbide based polyurethanes are measured to be around 20 $kg.mol^{-1}$ after two hours post cure at 140°C.

Better results may be obtained if the post-cure is not carried out after 16h in the stove at 110°C but at an earlier time during the synthesis. This will be studied in the following section.

2.3.2.6. Combined effects

In order to enhance the effects of the post-cure at 140°C, Method F was suggested, which is a variation of B2. Changes were made on STEP 5. No catalyst was used in order to produce an optimized, greener and potentially biocompatible polyurethane based on isosorbide. The synthesis protocol of method F was as follow:

- STEP 1 and STEP 2 were not changed and are described in details in 2.3.2.1.
- STEP 3: The vacuum is broken by nitrogen flushing and the reactor is opened again and installed on a scale. The melted isosorbide (melted in a stove at 80°C prior to use) is weighed, and the reactor closed, put back under vacuum and stirred at high speed at a temperature of 110°C. The chain extending reaction is left to proceed until a clouding of the reaction mixture (sign of the beginning of the phase separation), which usually happened after 45 min under these conditions.
- STEP 4: The vacuum is broken by nitrogen flushing and the reactor is opened. The reaction mixture is poured into molds (sheets of 2mm thickness). The molds are then pressed at 110°C at a pressure of 10 bars for 2 hours.
- STEP 5: The molds are removed from the press and put in a stove at 140°C for 2 hours in order to increase the reaction conversion to its maximum. The samples are subsequently taken out of the stove and left to cool down at room temperature before being opened.

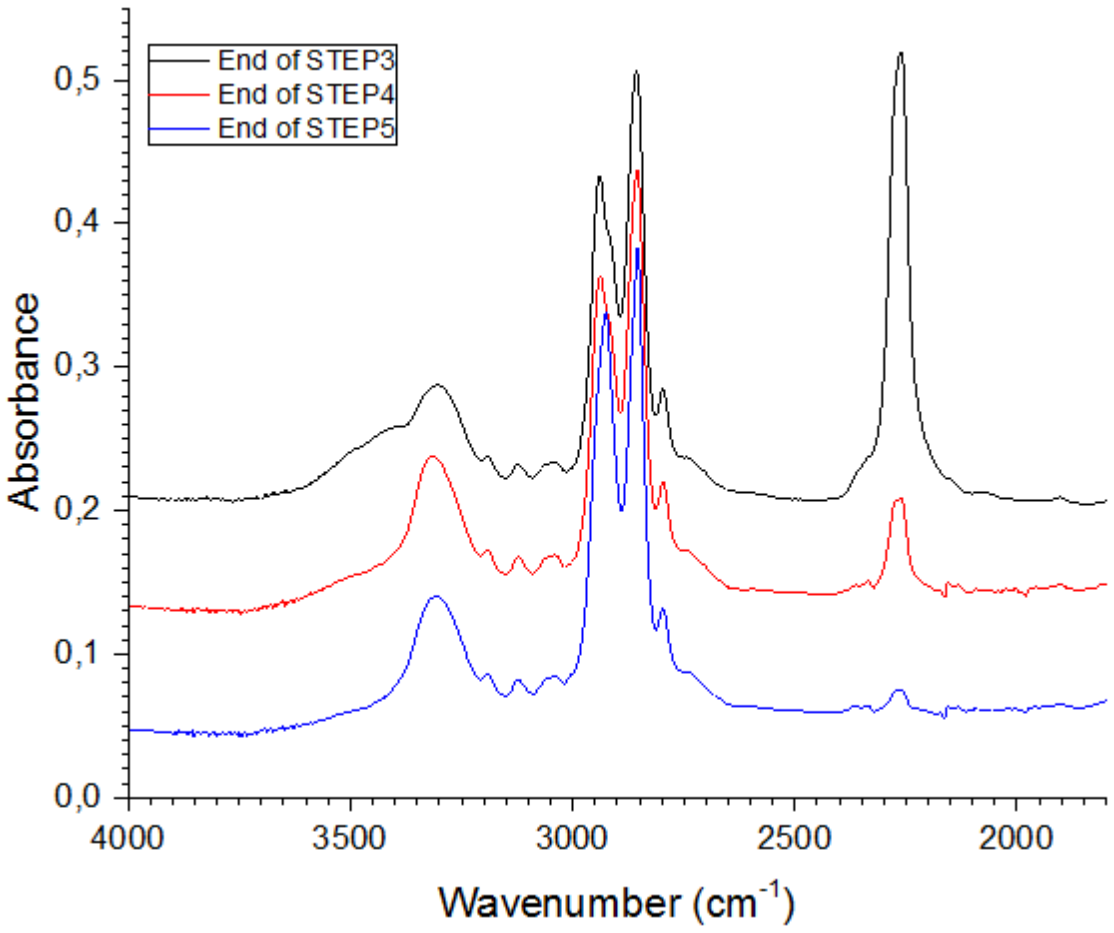

Figure 2.23: FT-IR attenuated total reflexion (ATR) spectra measured at key steps during the synthesis of a PTMEG-MDI-ISO 1:3:2 polyurethane using the protocol of method F

As those changes on the synthesis method are only significant if free NCO functions are still present in the material, all throughout the different steps of the bulk synthesis, some Fourier-transform infrared spectra (FT-IR) were recorded at the end of the steps 3 to 5 and are presented in Figure 2.23. It can be seen that as the synthesis proceeds, the free –NCO absorbance band at 2260 cm^{-1} progressively disappears. This is accompanied by a disappearance of the large free –OH band at 3395 cm^{-1}, partially fused with the –NH band at 3310 cm^{-1}. As the MDI was inserted in the reaction vessel with a slight (0.05 mol) excess, the NCO band at STEP 5 is still present. The CH_2 bands between 2900 and 2800 cm^{-1} are not affected by the reaction as expected.

Table 2.16: Infrared bands attribution in PTMEG-MDI-ISO 1:3:2 polyurethane

Wavenumber (cm^{-1})	Functional groups
3395	Free -OH
3310	-NH from urethane
2940	CH_2 asymmetrical elongation
2855	CH_2 symmetrical elongation
2260	free -NCO

In order to obtain reproducible SEC values, the DMF solutions of the samples were analyzed 21 days after their making. This is explained in further detail in Annex A. The results are reported in Figure 2.24 and Table 2.17.

The results of Method F were compared to those of the original method presented in 2.3.2.1.

Protocol used for the Original Method are recalled here for ease of reading purpose.

The synthesis yields around 150 g of material.

- STEP 1: The MDI is weighed and inserted in the reactor and the reactor is then put under vacuum, heated at 80°C with an oil bath and mechanically stirred at a low speed (around 50 rpm) in order to melt the MDI.

- STEP2: The vacuum is broken by nitrogen flushing and the reactor is subsequently opened, put on a scale and the melted macrodiol is weighed directly in the reactor bottom for accuracy. The reactor is then closed, put under vacuum, with 80°C heating and a high-speed (between 200-300 rpm) mechanical stirring. The prepolymer reaction is left to proceed for 45 min.

- STEP 3: The vacuum is broken by nitrogen flushing and reactor is opened again and installed on a scale. The melted isosorbide (melted in a stove at 80°C prior to use) containing DBTDL catalyst is weighed, and the reactor closed, put back under vacuum and stirred at high speed at a temperature of 80°C. The chain extending reaction is left to proceed until a clouding of the reaction mixture (sign of the beginning of the phase separation) and/or a thickening of the mixture preventing further mixing is observed. In the case of BDO chain extender, due to higher reactivity, the heating bath was removed, and the reaction occurred for 2-5 min before clouding of the reacting mixture, with high speed mixing (between 200-300 rpm) and vacuum.

- STEP 4: The vacuum is broken by nitrogen flushing and the reactor is opened. The reaction mixture is poured into molds (sheets of 2mm thickness). The molds are then pressed at 110°C at a pressure of 10 bars for 2 hours.

- STEP 5: The molds are removed from the press and put in a stove at 110°C for 16 hours (overnight) in order to increase the degree of conversion of the reaction to its maximum.

First of all, the SEC curves show that the use of Method F for synthesis had a beneficial effect on the molar masses since the overall peak is shifted toward the smaller retention volumes compared to those of the original method. Moreover, the dispersity seems to be equivalent for both cases.

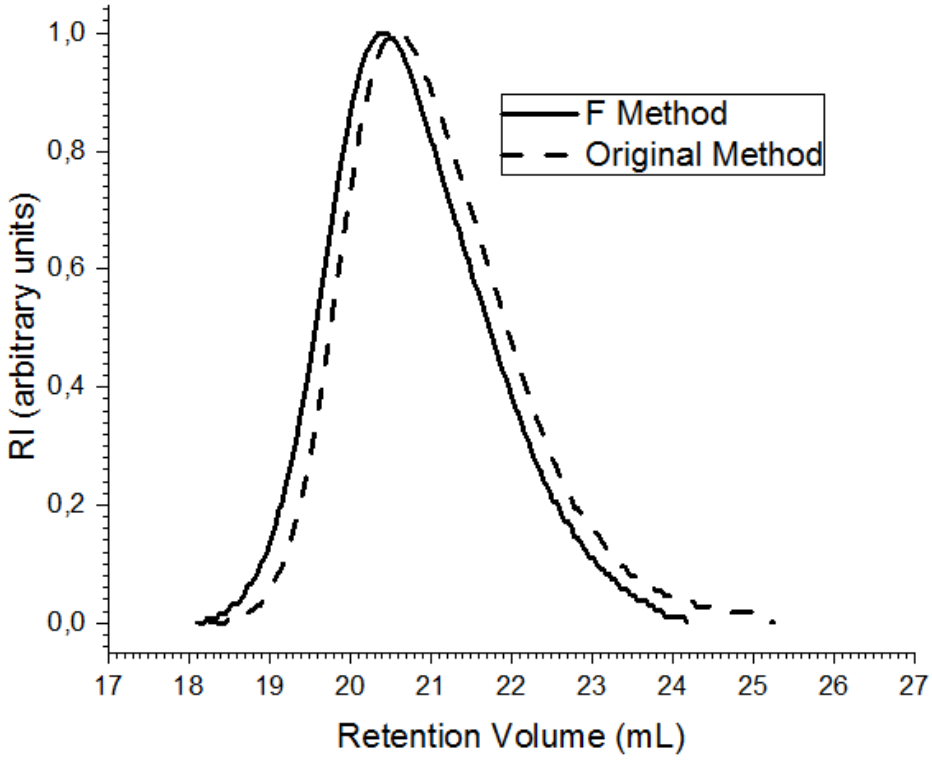

Figure 2.24: SEC curves of isosorbide based polyurethanes (PTMEG/MDI/ISO 1:3:2) in DMF 0.01 $LiNTf_2$, comparison between method F and the original synthesis.

These observations are confirmed by the values reported in Table 2.17. A precision of only ±10% on the values is expected with SEC analysis method, however there is indeed a slight improvement of around 25% of the values of the number average and weight average molar masses, and a disappearance of the shoulder at high retention volumes brought by method F.

Table 2.17 : Molar masses values for PTMEG/MDI/ISO 1:3:2 polyurethane in DMF 0.01 $LiNTf_2$ and calculated from conventional calibration with polystyrene standards, comparison between method F and the original synthesis.

Synthesis method	Sample mass (g)	DBTDL catalyst (wt%)	Temperature at step 3 (°C)	M_n ($kg.mol^{-1}$)	M_w ($kg.mol^{-1}$)	Đ (M_w/M_n)
Method F	150	0	110	22.7 ±2	58.5 ±6	2.6
Original	150	0	80	17.0 ±2	45.3 ±5	2.7

Moreover, the synthesis lapse time was significantly improved (around 3.5 hours, instead of one whole day) and does not involve the use of a catalyst any more.

Table 2.18 : Summary of the DSC results for PTMEG-MDI-ISO 1:3:2 samples synthesized with method F compared to the original method.

Sample	1st Heating Cycle			2nd Heating Cycle
	T_g (°C)	T_f (°C)	ΔH_f (J/g)	T_g (°C)
Original	-44	187	20.5	-31
Method F	-40	202	12.1	-29

Since thermal treatments are known to induce changes in the phase morphology, the thermal behavior of the material obtained through synthesis method F was studied and compared to that obtained with the non-modified method. Results are presented in Figure 2.25 and Table 2.18. It can be noted that the melting temperature of the hard domains is increased for polyurethanes obtained through method F. Moreover, the transition at 59°C (discussed in section 2.4.5) present in the DSC of the original sample does not seem to be present for the Method F sample. This tends to prove that the length of the hard segments has been increased by the synthesis process, thus increasing the melting temperature of the hard domains.

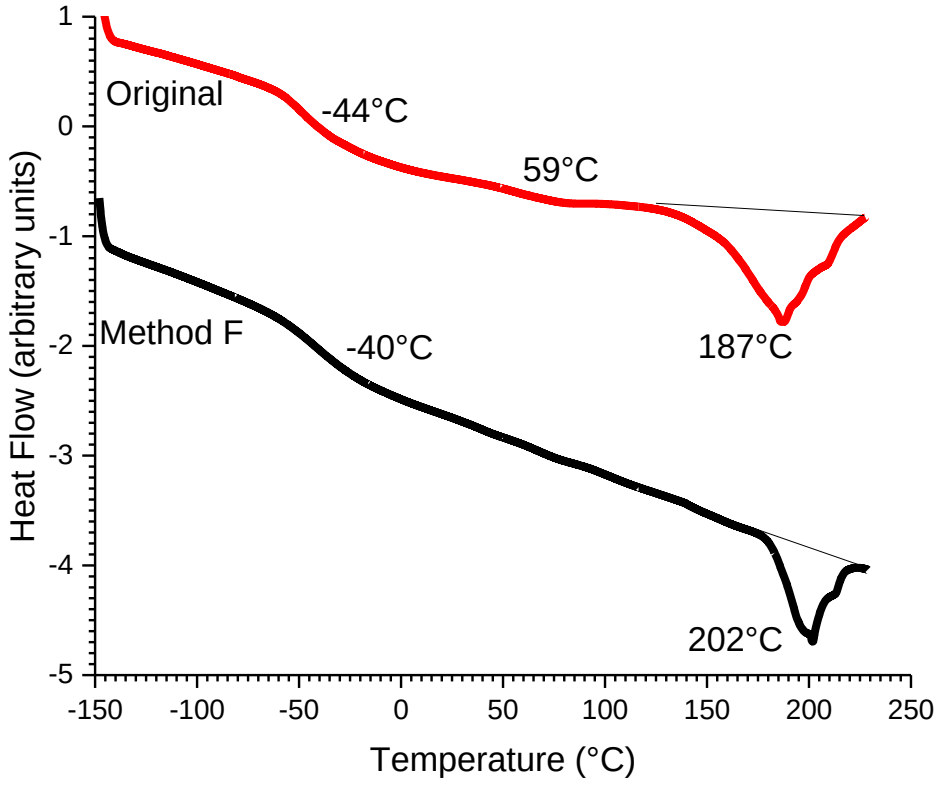

Figure 2.25: Differential Scanning Calorimetry, first heating ramp recorded at 20°C/min from -150°C to 250°C for PTMEG-MDI-ISO 1:3:2 samples synthesized with method F compared to the original method.

It should also be noted that the melting enthalpy has decreased on the Method F curve. This could be explained by the fact that the synthesis optimization has allowed reducing the lone small mass chains found at the high retention volume on the SEC curves and thus those longer segments may be less mobile and crystallize with difficulty. However, as they also may separate more easily from the soft segments due to their length, the formed crystalline phase will contain less impurities and defects and thus its melting temperature may increase.

2.3.2.7. Comparison with 1,4-butanediol

In order to compare the results of the optimization of the synthesis of isosorbide-based polyurethane to more classical materials widely used in industry, a polyurethane of composition PTMEG-MDI-BDO 1:3:2 was synthesized with a protocol as close as possible to method F. As BDO is much more reactive with MDI than ISO, method F was adapted to method G, as follow:

One should note that no DBTDL was used in either the Original Method or the Method G with BDO as chain extender, contrary to what was done with ISO. Indeed, reactivity of BDO was very high and only allowed for a stirring of a few minutes before the mixture was removed from the reactor.

- STEP 1 and STEP 2 were not changed and are described in details in 2.3.2.1.

- STEP 3: The vacuum is broken by nitrogen flushing and the reactor is opened again and installed on a scale. 1,4-butanediol at room temperature is weighed, and the reactor closed, put back under vacuum and stirred at high speed with no heating. The chain extending reaction is left to proceed until a clouding of the reaction mixture (sign of the beginning of the phase separation), which usually happened after only 2 to 5 min under these conditions (depending on exact room temperature on the synthesis day).

- STEP 4 and STEP 5 are similar to Original Method presented in 2.3.1. for the Original Method using BDO, or to Method F in the case of Method G.

FT-IR reflection spectra were recorded in ATR mode at key points during the synthesis and the results are presented below in Figure 2.26**,** in order to monitor the disappearance of the NCO functions along the synthesis process.

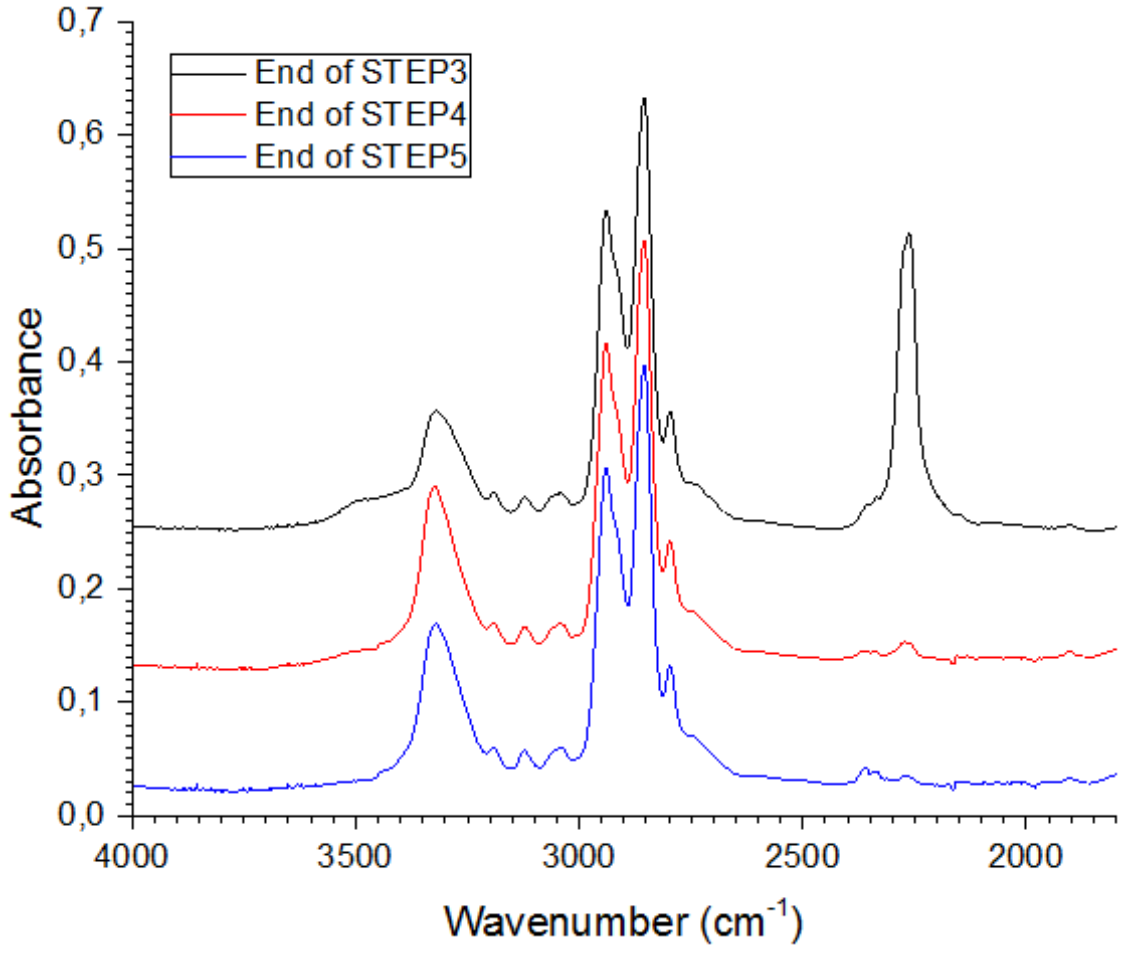

Figure 2.26: FT-IR attenuated total reflection (ATR) spectra recorded at key steps during the synthesis of a PTMEG-MDI-BDO 1:3:2 polyurethane using the protocol of method G

It can be noted that the free NCO band has almost completely disappeared at the end of STEP 4 and has not evolved a lot at the end of STEP 5. This disappearance is matched with that of the large –OH band at 3410 cm^{-1}. It is probable that the optimized synthesis used for

ISO-based materials won't have an effect as pronounced on the molar mass distribution of the BDO-based materials.

Table 2.19: Infrared bands attribution in PTMEG-MDI-BDO 1:3:2 polyurethane

Wavenumber (cm^{-1})	Functional groups
3410	Free -OH
3322	-NH from urethane
2942	CH_2 asymmetrical elongation
2855	CH_2 symmetrical elongation
2261	free -NCO

Molar mass distribution was then obtained by SEC. In order to obtain reproducible values, the DMF solutions of the samples were measured 21 days after their making. The results are reported in Figure 2.27 and Table 2.20.

Table 2.20: Molar masses values for PTMEG/MDI/BDO 1:3:2 polyurethane in DMF 0.01 $LiNTf_2$ and calculated from conventional calibration with polystyrene standards as a function of the post cure time, comparison between method G and the original synthesis.

Synthesis method	**Sample mass (g)**	**Highest annealing temperature (°C)**	**DBTDL catalyst (wt%)**	**M_n ($kg.mol^{-1}$)**	**M_w ($kg.mol^{-1}$)**	**Đ (M_w/ M_n)**
Method G	150	140	0	57.6 ±6	155 ±16	2.7
Original	150	110	0	48.6 ±5	135 ±14	2.7

The results of Method G were compared to those of the original method using BDO. First of all, the SEC curves show that the use of Method G for synthesis had a small effect on the molar masses since the overall peak is shifted toward the smaller retention volumes compared to that of the original method. Moreover, the dispersity seems to be equivalent for both cases. These observations seem confirmed by the values reported in Table 2.20. However, as a precision of only 10% on the values is expected with SEC analysis, the increase in molar mass obtained with method G is not significant enough to be considered as due to the synthesis method, whereas that obtained with method F on ISO-based samples clearly displays increased molar masses.

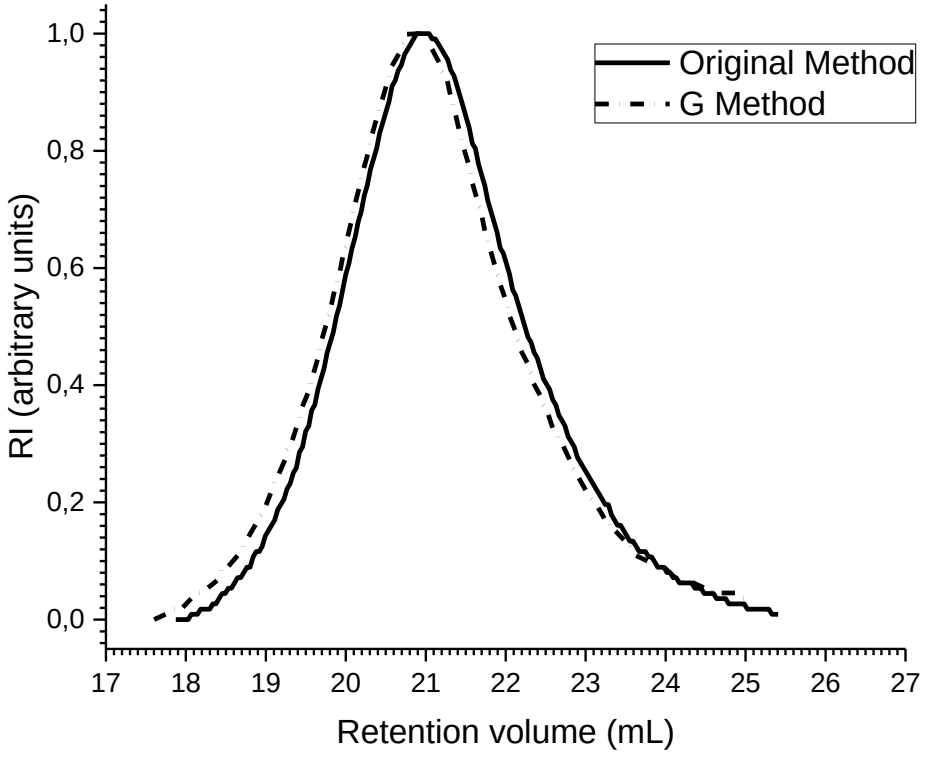

Figure 2.27: SEC curves of isosorbide based polyurethanes (PTMEG/MDI/BDO 1:3:2) in DMF 0.01 $LiNTf_2$, comparison between method G and the original synthesis.

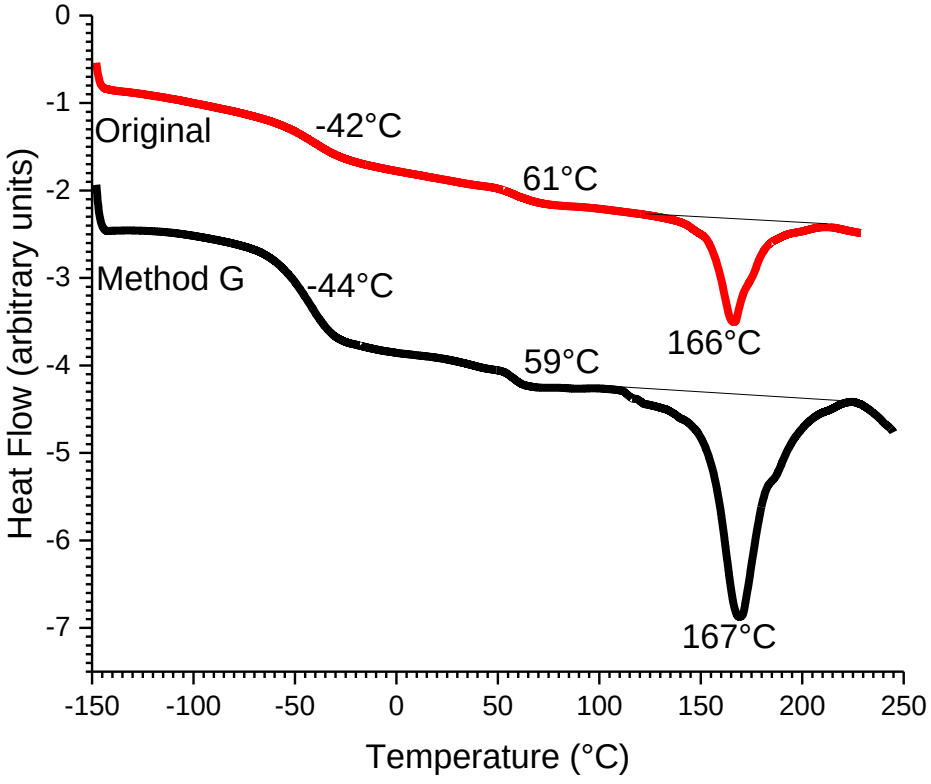

Figure 2.28: Differential Scanning Calorimetry, first heating ramp measured at 20°C/min from -150°C to 250°C for PTMEG-MDI-BDO 1:3:2 samples synthesized with method G compared to the original method.

The effect of the thermal treatment on the thermal behavior of the BDO-based polyurethane was also studied by DSC. The results are presented in Figure 2.28 and Table 2.21. The behavior of the method G sample does not display any remarkable difference from the original sample. The exact same transitions are visible, but they seem to be more pronounced. The melting enthalpy of the hard domains is higher for method G curve with 23.5 J/g compared to 20.6 J/g, and the glass transition temperature is slightly lower as well (see Table 2.21).

There is no significant difference as well in the values of the glass transition temperature found in the 2nd heating cycle between the two methods, as what has been seen with isosorbide based-samples.

Table 2.21 : Summary of the DSC results for PTMEG-MDI-BDO 1:3:2 samples synthesized with method G compared to the original method.

Sample	1st Heating Cycle			2nd Heating Cycle
	T_g (°C)	T_f (°C)	ΔH_f (J/g)	T_g (°C)
Original	-42	166	20.6	-39
Method G	-44	169	23.5	-36

As was expected from the FT-IR curves, the improved synthesis process used for isosorbide-based materials does not bring significant differences on the BDO-based model except for improved crystallization of hard domains, since almost all NCO functions have disappeared before the post-cure step.

2.3.2.8. Conclusion

The synthesis of a thermoplastic polyurethane based on PTMEG/MDI/ISO at a stoichiometry of 1:3:2 respectively was optimized on laboratory scale. The average molar mass of this material was slightly improved by the disappearance of lone hard segments, but is still lower than the M_n of the model material based on PTMEG/MDI/BDO at the same stoichiometry. Determination of the molar mass of entanglement would have allowed to evaluate the suitability of this polymer for physical testing. However, as true molar mass values were not obtained, it was not possible to obtain this value. Nonetheless, an average molar mass of 22.7 $kg.mol^{-1}$ (polystyrene standards) was obtained for the ISO-based polyurethanes with the improved synthesis method, which is a mass sufficient to consider that the material is not composed of oligomers and that its physical properties can be compared to those of the BDO-based material. It was also demonstrated that the optimized synthesis process is suited to the production of isosorbide-based polyurethane formulations. Moreover, this new method is catalyst-free and faster.

2.4. THERMAL BEHAVIOR AND MICROSTRUCTURE OF THERMOPLASTIC POLYURETHANES

The following section will report the thermal behavior displayed from DSC and DMA of the thermoplastic polyurethane series presented in the previous section 2.3.1.1.1.

2.4.1. Poly(ε-caprolactone) based thermoplastic polyurethanes

The measurements carried out on the series of samples based on poly(ε-caprolactone) are presented in Figure 2.29 and Table 2.22. First of all, similar phenomena are visible in the DSC curves of the CMI50 and CMB50 samples.

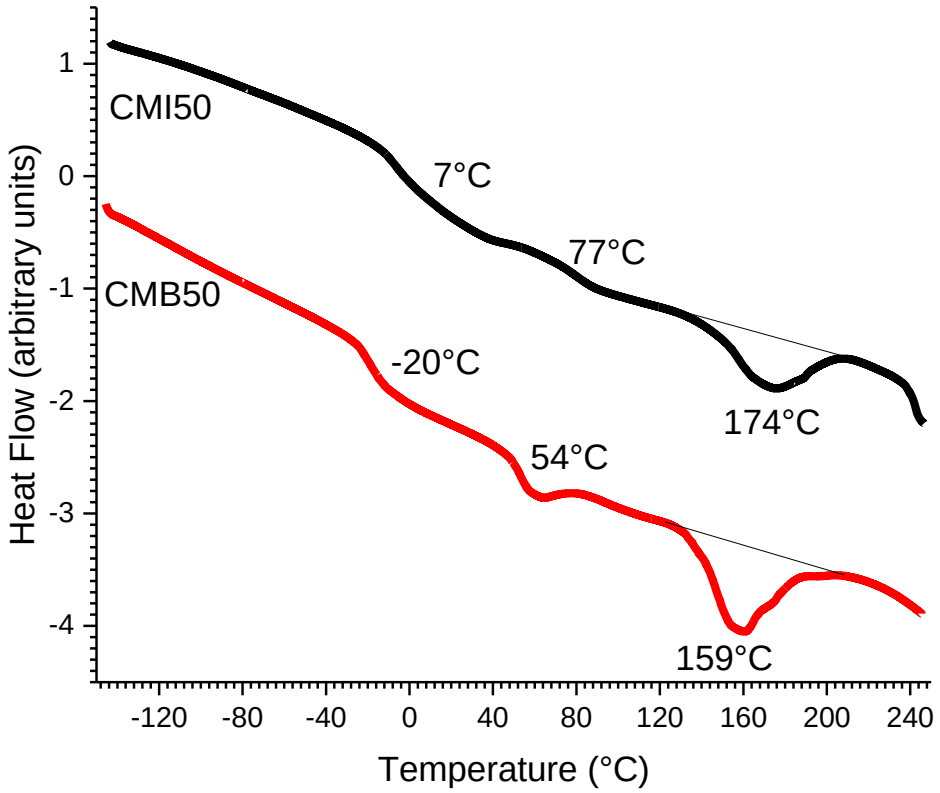

Figure 2.29: Differential Scanning Calorimetry, first heating ramp measured at 20°C/min from -150°C to 250°C for the sample series based on PCL, MDI and ISO or BDO.

A first glass transition appears at low temperature for both samples, followed by a second transition, the nature of which will be further discussed in 2.4.5, and eventually, a melting peak at relatively higher temperature. This behavior is typical of thermoplastics, and the first glass transition can be attributed to a soft segment rich phase, while the melting peak is due to the "melting" or order disrupting of hard-segments rich crystallites.

It is important to note that the isosorbide-based sample CMI50 displays its transitions at higher temperatures compared to the model BDO-based CMB50. The first glass transition of CMI50 is indeed 27°C higher than that of CMB50. This behavior can be partly explained by a poorer phase segregation in the case of CMI50: the higher concentration of isosorbide/MDI-

based hard segments in the soft phase is at the origin of an increase in this phase glass transition temperature [30]. The endothermic peak due to the hard segment crystallites is also at higher temperature on the CMI50 sample, which is due to the fact that pure isosorbide/MDI segments have higher glass transition and melting temperatures (around 180°C and 210°C respectively, as reported by [67]) compared to those of BDO/MDI segments (T_g= 107°C and T_m=198-225-240°C as reported by [91]).

Table 2.22 : Summary of the DSC results for the sample series based on PCL and MDI

Sample	1st Heating Cycle			2nd Heating Cycle		
	T_g (°C)	T_f (°C)	ΔH_f (J/g)	T_g (°C)	T_f (°C)	ΔH_f (J/g)
CMI50	7	174	10.2	26	196	6.2
CMB50	-20	159	16.6	-7	165	13.0

In order to qualitatively evaluate the stability and kinetics of the phase segregation, the glass transition temperature was measured with a second heating cycle after a cooling ramp of 20°C/min from 250°C. The obtained values are reported in Table 2.22. The glass transition temperatures of both samples have been influenced by the heat treatment: there is an increase of 19°C and 13°C for CMI50 and CMB50, respectively. One can also note that the enthalpy of fusion on the second run are lower for both samples, which shows that crystallization was not favored in the test condition, especially for the ISO-based sample. Overall the materials based on PCL did not display a very stable phase segregation in the test conditions, but there is again a sensible difference between the isosorbide and BDO-based samples.

Table 2.23: Summary of DMA results for the sample series based on PCL

Sample	T_α	25°C			T_α + 50°C		
	(°C)	G' (MPa)	G''(MPa)	tan δ	G'(MPa)	G''(MPa)	tan δ
CMI50	0	77	20	0.26	33	4.9	0.15
CMB50	-7	41	7.8	0.19	34	4.9	0.14

In order to further characterize the thermal behavior, CMI50 and CMB50 were tested with DMA. The obtained curves are presented in Figure 2.30, and some numerical values are reported in Table 2.23 for ease of reading purposes.

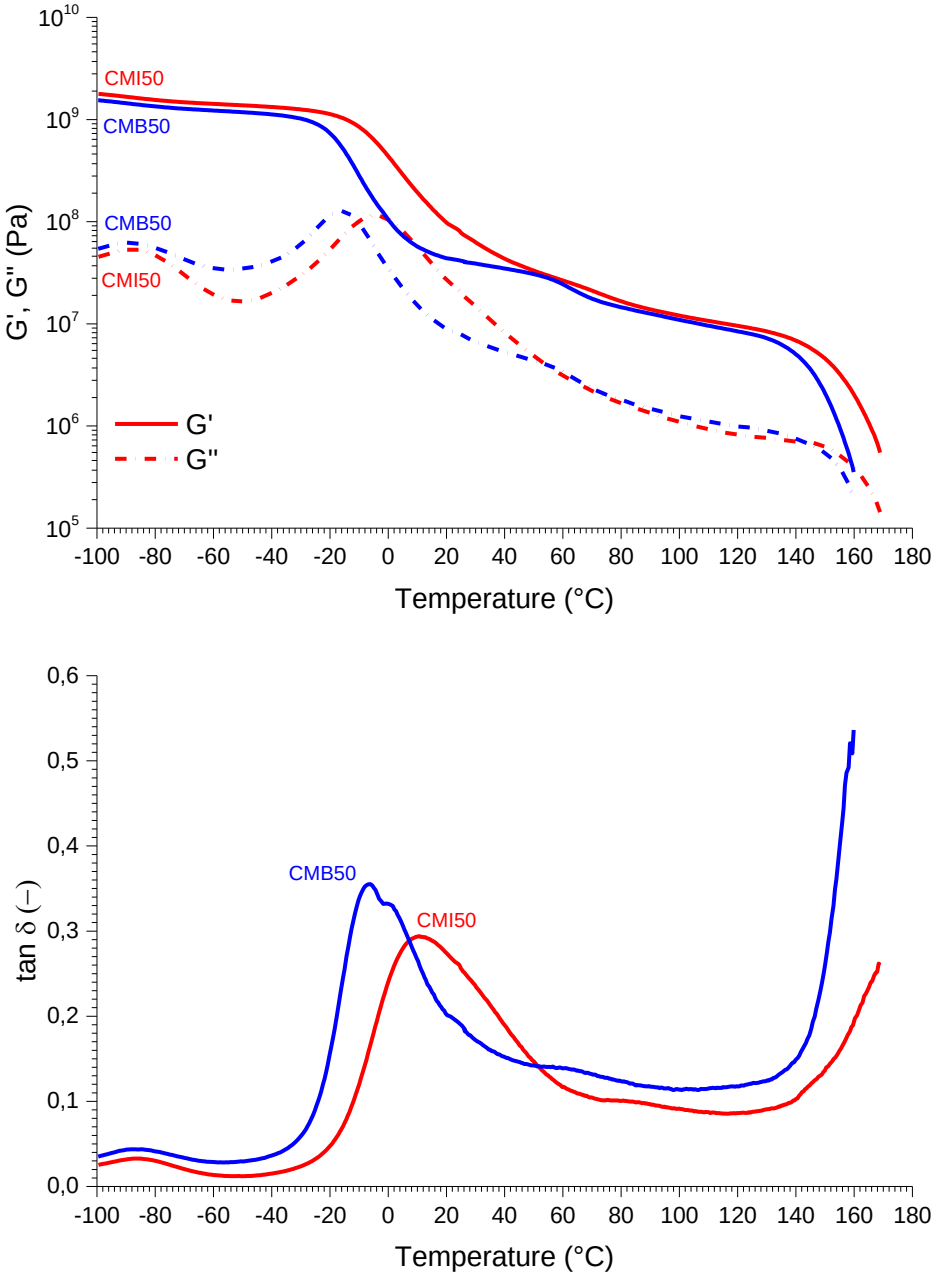

Figure 2.30: Dynamic Mechanical Analysis of PCL-based samples CMB50 and CMI50, at a frequency of 1 Hz and 0.1% strain, with a heating ramp of 3°C/min.

The DMA curves are consistent with the observations made in the DSC scans: the α transition (maximum of tan δ), which is related to the DSC glass transition is 7°C higher for the CMI50 sample, and it is as well very broad. One can also see a second transition on both CMI50 and CMB50 curves, as an inflexion on the G' trace and a slight increase on the tan δ curve at the same temperature between 40 and 90°C. This second transition appears again at a higher temperature in the case of the CMI50 sample between 70 and 120°C. Moreover, the flow limit onset is clearly delayed for CMI50, starting around 140°C compared to 120°C for CMB50.

All these observations confirm the one made on the DSC curves. When associated with PCL, isosorbide/MDI hard segments do segregate, however this separation does not occur as

readily and is not as stable as when PCL is associated with BDO. It is however important to note that in spite of smaller molar masses, the samples based on isosorbide display mechanical properties (i.e. value of the plateaus) that are slightly superior to those obtained with the BDO-based models.

2.4.2. Poly(tetrahydrofuran) based thermoplastic polyurethanes

The measurements carried out on the series of samples based on poly(tetrahydrofuran) are presented in Figure 2.31-2.32 and Table 2.24. The effect of the hard segment content and the properties brought by the use of isosorbide were studied.

The glass transition temperature of the isosorbide-based series of sampleTMI40, TMI50 and TMI60 was measured at -46°C and was not influenced by the hard segment content, as can be seen in Figure 2.31. As the hard segment content in the materials increases, the mean length of those segments also increases. Thus, the crystalline phase in the hard domains can be influenced. This can be seen by the change in the temperature of the minimum of the melting peak: this temperature is increasing, and a melting in several steps is occurring, especially in the case of TMI60.

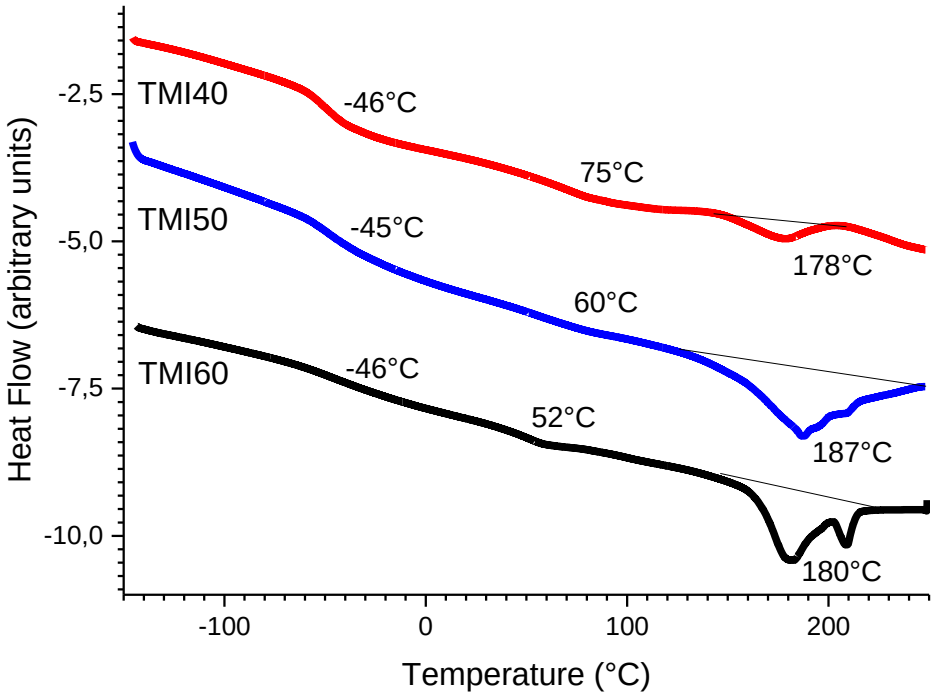

Figure 2.31: Differential Scanning Calorimetry, first heating ramp measured at 20°C/min from -150°C to 250°C for the sample series based on PTMEG, MDI and ISO.

Lastly, the temperature of the second transition decreases with the hard segment content: at 75°C for TMI40 to 52°C for TMI60.

In the case of the BDO-based series of samples shown in Figure 2.32, the glass transition temperature is not influenced by the hard segment concentration, as well as the second transition around 60°C which seems more stable than for isosorbide. However, the melting peak minimum temperature in the case of the model BDO-based samples is decreasing with

the hard segment concentration, unlike what was seen for isosorbide samples TMI40 and TMI50 for which it was slightly increasing. This phenomenon is principally controlled by the length of the hard segments that can have significant impact on phase segregation, crystallinity and glass transition of the hard segment (HS) [52].

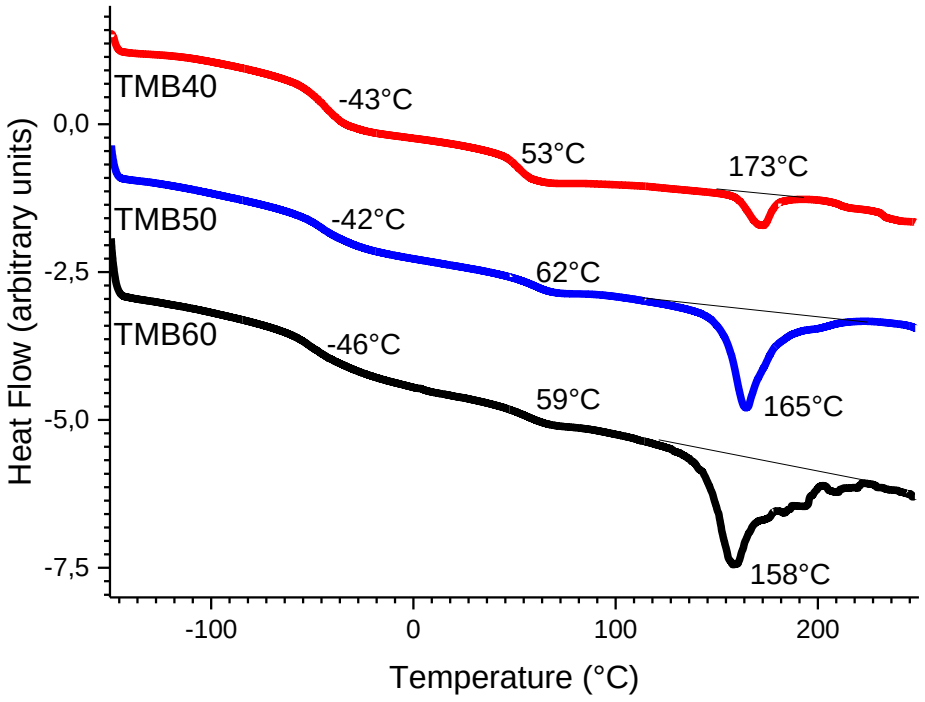

Figure 2.32 : Differential Scanning Calorimetry, first heating ramp measured at 20°C/min from -150°C to 250°C for the sample series based on PTMEG, MDI and BDO.

In order to evaluate the stability and kinetics of the phase segregation, the glass transition temperature was measured on a second heating cycle after a cooling ramp of 20°C/min from 250°C. The obtained values are reported in Table 2.24. The glass transition temperatures of both series of samples have been influenced by the heat treatment: there is an overall increase in the values of the glass transition temperature. This increase is larger in the case of the isosorbide-based series of samples. It is moreover more pronounced as the hard segment content increase. There is also a small increase in the T_g in the second heating cycle in the case of the BDO-based samples, but it is far more limited and does not seem to be linked to the hard segment content. Melting on the second scan was not always present and could not be detected on samples TMI40 and TMB40; it was replaced by a glass transition at 164°C and 105°C, respectively. As before, melting enthalpy values were lower than during the first heating scans, and this was especially true for the samples based on isosorbide.

Table 2.24 : Summary of the DSC results for the sample series based on PTMEG and MDI

Sample	1st Heating Cycle			2nd Heating Cycle		
	T_g (°C)	T_f (°C)	ΔH_f (J/g)	T_g (°C)	T_f (°C)	ΔH_f (J/g)
TMI40	-46	178	5.6	-31	/	/
TMI50	-45	187	19.8	-6	160	4.5
TMI60	-46	180	21.5	15	171	8.3
TMB40	-43	173	3.4	-28	/	/
TMB50	-42	165	20.5	-39	169	14.2
TMB60	-46	158	29.7	-35	176	19.3

To further characterize the thermal behavior, both series of PTMEG-based materials were tested with DMA. The obtained curves are presented in Figure 2.33 and Figure 2.34, and some numerical values are reported in Table 2.25 for ease of reading purposes.

Table 2.25 : Summary of DMA values for the sample series based on PTMEG

Sample	T_α	25°C			T_α + 50°C		
	(°C)	G' (MPa)	G''(MPa)	tan δ	G'(MPa)	G''(MPa)	tan δ
TMI40	-30	16	1.3	0.08	17	1.5	0.09
TMI50	-17	51	6.1	0.12	44	4.7	0.11
TMI60	8	178	16.2	0.09	98	9.2	0.09
TMB40	-27	9.6	0.3	0.03	9.6	0.3	0.03
TMB50	-27	30	1.8	0.06	30	1.9	0.06
TMB60	-28	75	5.4	0.07	78	5.8	0.07

Overall, the DMA results are consistent with the results obtained by DSC. Figure 2.33 presents the DMA curves of the isosorbide and PTMEG-based samples. The maximum of the tan δ is progressively shifted and is becoming larger as the HS content is increasing. The sample TMI60 is especially notable as tan δ does not display a single maximum anymore: it seems to be split in two parts and it spans on almost 160°C, suggesting a very weak phase segregation.

Figure 2.34 presents the DMA of the BDO-based models. It can be noted that the α transition temperature is very stable as the HS fraction increases. The flow limit does not seem to be significantly influenced by the HS fraction. TMI40 and TMB40 began to flow early on and the scan had to be interrupted at the very beginning of the flow limit.

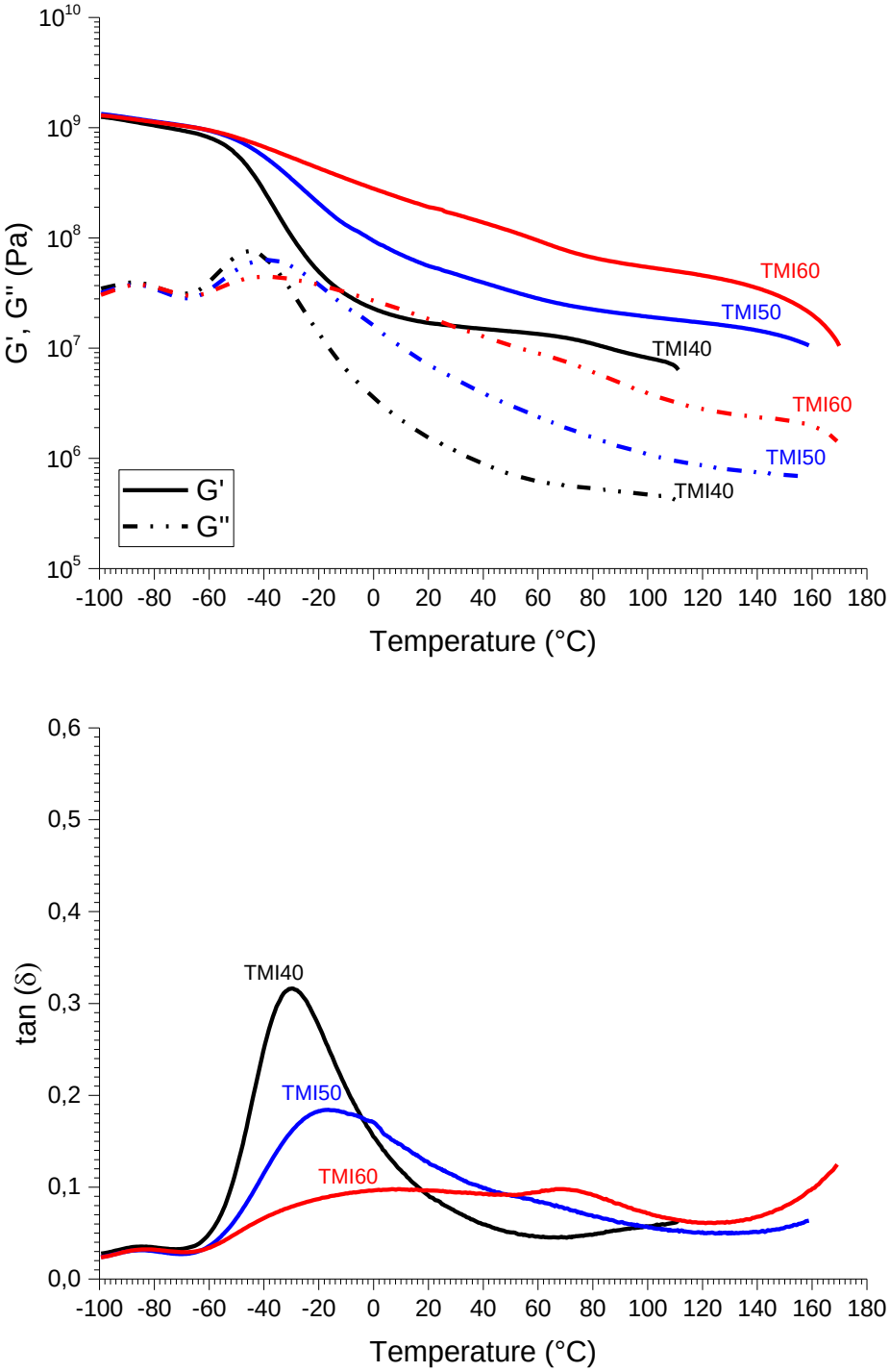

Figure 2.33: Dynamic Mechanical Analysis of PTMEG and isosorbide-based samples TMI40, TMI50 and TMI60, at a frequency of 1 Hz and 0.1% strain, with a heating ramp of 3°C/min.

The second transition found between 50°C and 70°C on both series of samples can be seen on the BDO-based series as a small inflexion of G' and G'' in the same range of temperatures,

but it is not as visible as on the isosorbide-based series. It may however be at the origin of the second peak of tan δ and the inflexion of G' and G'' around 70°C for the TMI60 sample.

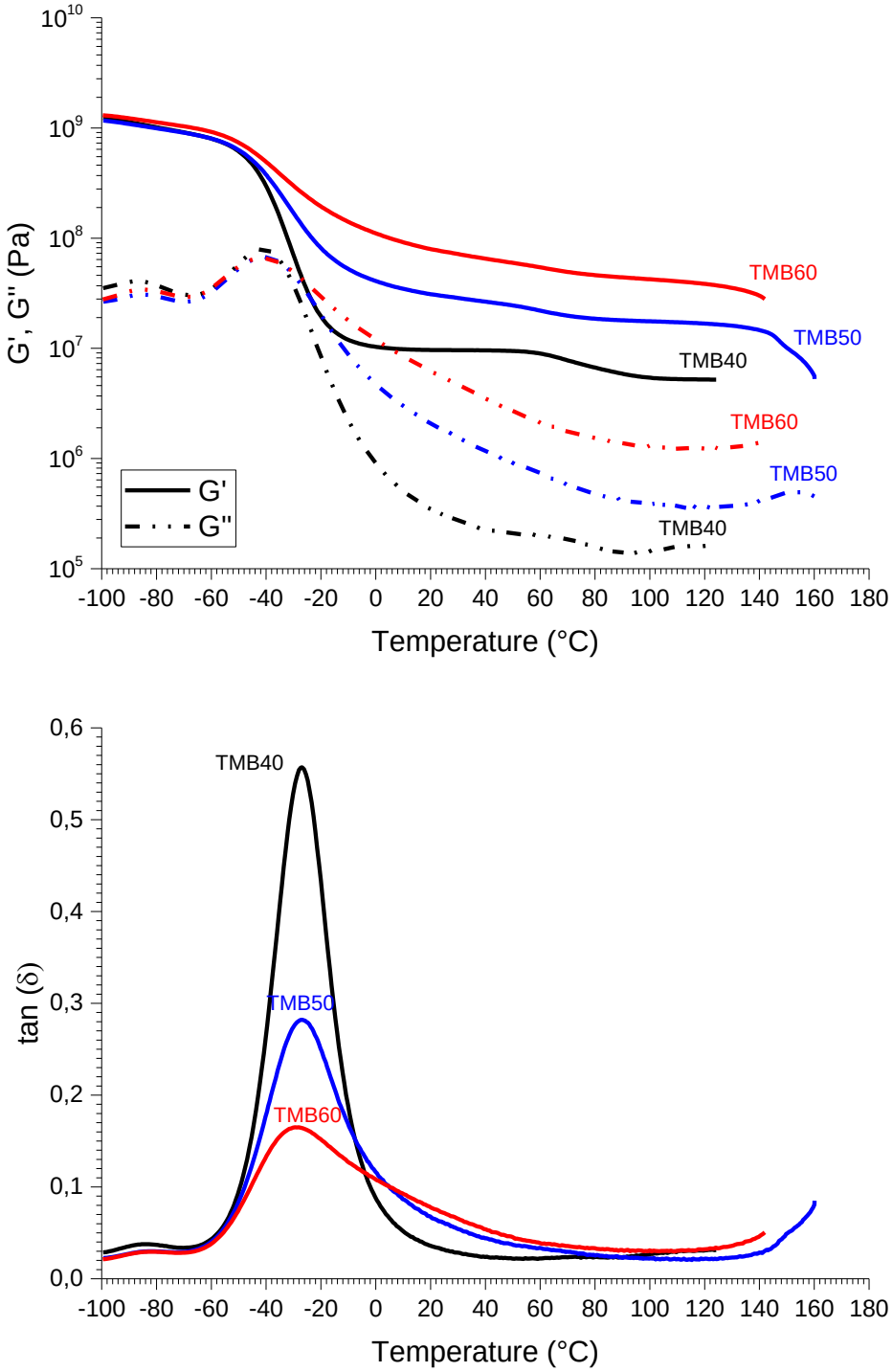

Figure 2.34: Dynamic Mechanical Analysis of PTMEG and BDO-based samples TMB40, TMB50 and TMB60, at a frequency of 1 Hz and 0.1% strain, with a heating ramp of 3°C/min.

In summary, when associated with PTMEG, isosorbide/MDI hard segments do also segregate, the glass transition obtained by DSC on the isosorbide series is equivalent to that obtained for the model BDO. As for the PCL-based materials, the samples based on isosorbide display mechanical properties (i.e. value of the plateaus) that are slightly superior

to those obtained with the BDO-based models. However, the broader peak of tan δ and the shifting of T_g after heat treatment of the isosorbide-based samples show that the phase segregation is not as complete or as stable as the model BDO-based samples, as was seen previously with PCL-based polyurethanes. Moreover, this phenomenon is enhanced by the HS concentration.

2.4.3. Thermoplastic polyurethanes based on polyester containing fatty acid dimers

The measurements carried out on the series of samples based on fatty acid dimers polyester (FADM) are presented in Figure 2.35**,** Figure 2.36 and Table 2.26. Here also, the effect of the hard segment content and the properties brought by the use of isosorbide were studied.

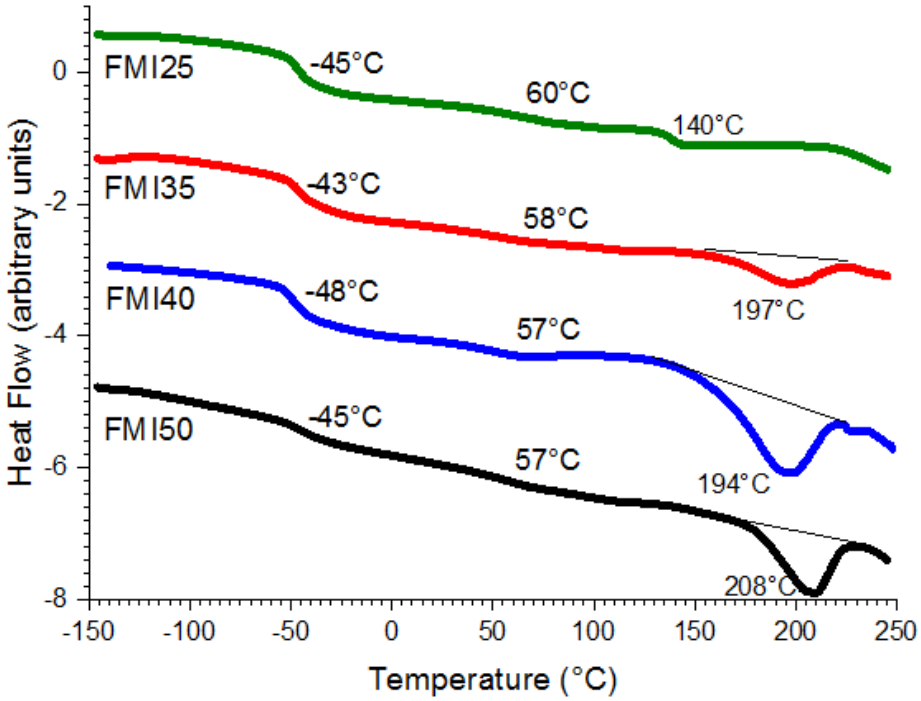

Figure 2.35:Differential Scanning Calorimetry, first heating ramp measured at 20°C/min from -150°C to 250°C for the sample series based on FADM, MDI and ISO.

The glass transition temperature of the isosorbide-based series of samples FMI25, FMI35, FMI40 and FMI50 was measured around -45°C and was not influenced by the hard segment content, as can be seen in Figure 2.35. As was seen with the PTMEG and isosorbide-based samples, the length and concentration of the HS influences the maximum melting peak of the HS crystals: the temperature of the minimum is increasing from 194°C to 208°C for the FADM and isosorbide-based samples. It can be noted as well that no crystallization nor melting was obtained for the FMI25 sample. The presence of the HS phase can only be detected by a glass transition at 140°C. This low value considering the T_g of the pure MDI/ISO HS (around 195°C [67])could originate from a HS rich phase mixed with some soft phase, or also shorter HS, or a mix of those situations.

Lastly, the second secondary transition is quite stable as well with the hard segment content: it can be found around 55°C for all eight isosorbide-based and BDO-based samples.

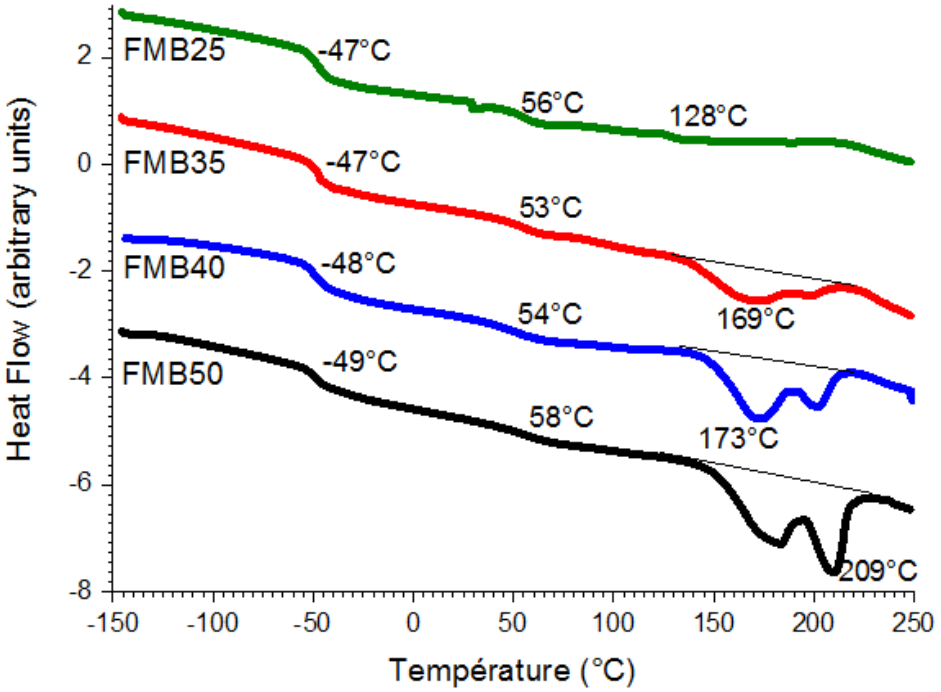

Figure 2.36 : Differential Scanning Calorimetry, first heating ramp measured at 20°C/min from -150°C to 250°C for the sample series based on FADM, MDI and BDO.

In the case of the BDO-based series of samples shown in Figure 2.36, the glass transition temperature is not influenced by the hard segment concentration. The melting peak minimum temperature in the case of the model BDO-based samples is increasing as well with the hard segment concentration. Overall, from DSC curves, the behavior of isosorbide based samples is remarkably similar to that of the model BDO-based samples.

From Table 2.26, it can also be noted that all eight samples of the FADM-based series display a quite stable T_g throughout the heating cycles, which is an indicator of a kinetically favorable and stable phase segregation. However, crystallization during the second heating scan is only obtained for a HS concentration over 40 wt% for ISO-based samples, while this limit is over 25 wt% in the case of BDO-based samples.

Further characterizations were performed by DMA, results of which are presented in Figure 2.37 and Figure 2.38, and some numerical values are reported in Table 2.27.

Table 2.26: Summary of the DSC results for the sample series based on FADM and MDI

Sample	1st Heating Cycle			2nd Heating Cycle		
	T_g (°C)	T_f (°C)	ΔH_f (J/g)	T_g (°C)	T_f (°C)	ΔH_f (J/g)
FMI25	-45	-	-	-42	-	-
FMI35	-43	197	6.3	-43	-	-
FMI40	-48	194	13.1	-44	-	-
FMI50	-45	208	18.1	-41	219	3.7
FMB25	-47	-	-	-47	-	-
FMB35	-47	169	14.3	-48	168	7.4
FMB40	-48	173	18.0	-48	187	12.5
FMB50	-49	209	33.6	-50	209	18.3

Table 2.27: Summary of DMA results for the sample series based on FADM

Sample	T_α	25°C			T_α + 50°C		
	(°C)	G' (MPa)	G''(MPa)	tan δ	G'(MPa)	G''(MPa)	tan δ
FMI25	-31	5.5	0.6	0.11	5.4	0.7	0.13
FMI35	-32	19	2.4	0.13	21	2.7	0.13
FMI40	-34	46	4.7	0.10	51	5.8	0.11
FMI50	-35	100	9.0	0.09	114	11	0.10
FMB25	-33	4.9	0.5	0.10	5.3	0.6	0.11
FMB35	-35	12	0.9	0.08	13	1.1	0.09
FMB40	-36	25	2.0	0.08	28	2.5	0.09
FMB50	-37	82	5.7	0.07	93	8.3	0.09

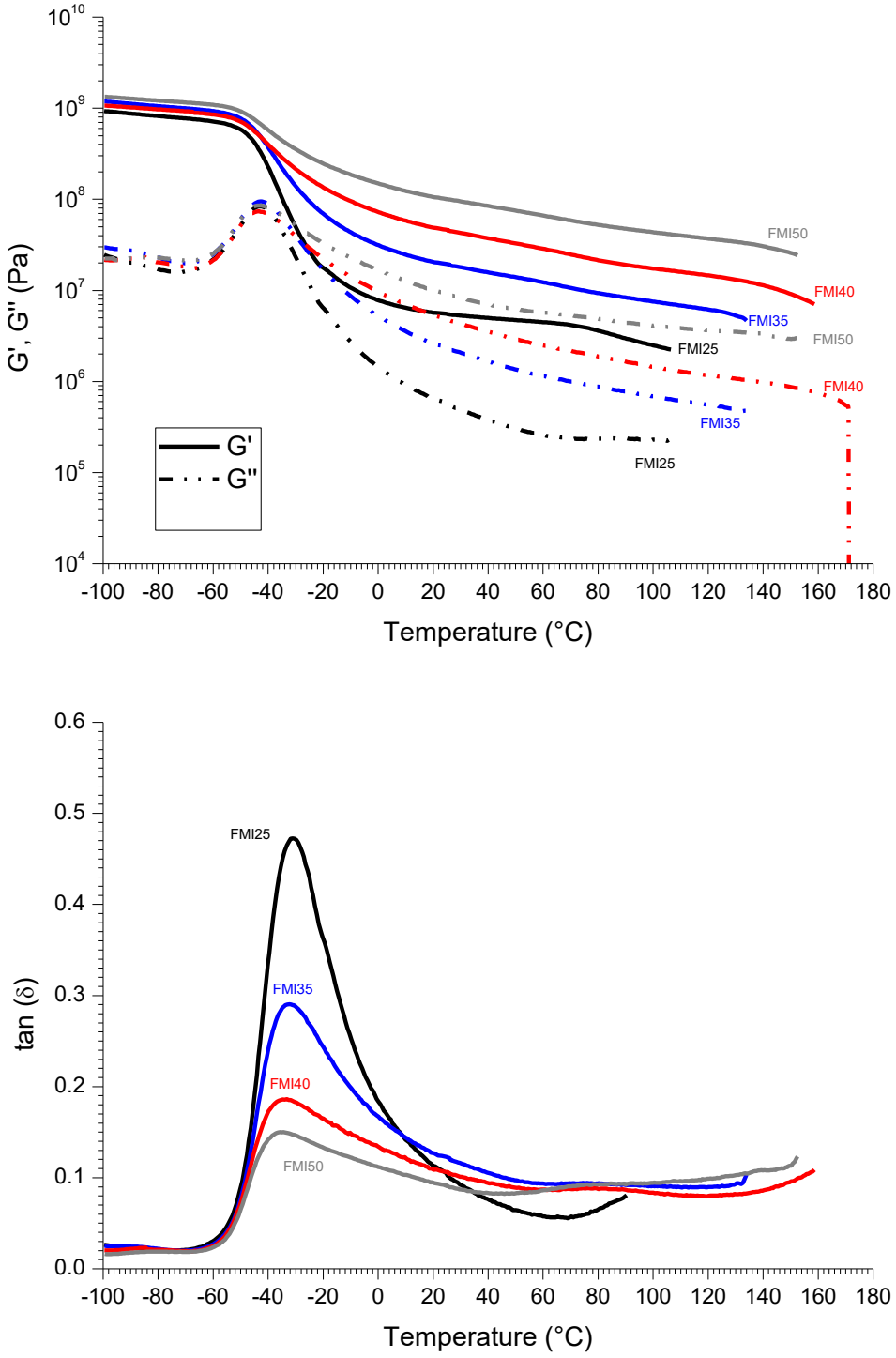

Figure 2.37: Dynamic Mechanical Analysis of FADM and ISO-based samples FMI25, FMI35, FMI40 and FMI60, at a frequency of 1 Hz and 0.1% strain, with a heating ramp of 3°C/min.

Overall, the DMA results are consistent with the results obtained by DSC. Figure 2.37 presents the DMA curves of the isosorbide and FADM-based samples. The maximum of the tan δ is very stable. The relaxation is as well becoming broader as the HS content is increasing and is almost transforming into a plateau for samples FMI40 and FMI50. Flow limit onsets of the isosorbide-based series could not be obtained because the samples broke before it was reached. It is supposed that oxidation in air atmosphere may be induced during

the DMA analysis, thus leading to early breakage of the samples. Longer scans may have been recorded in nitrogen atmosphere.

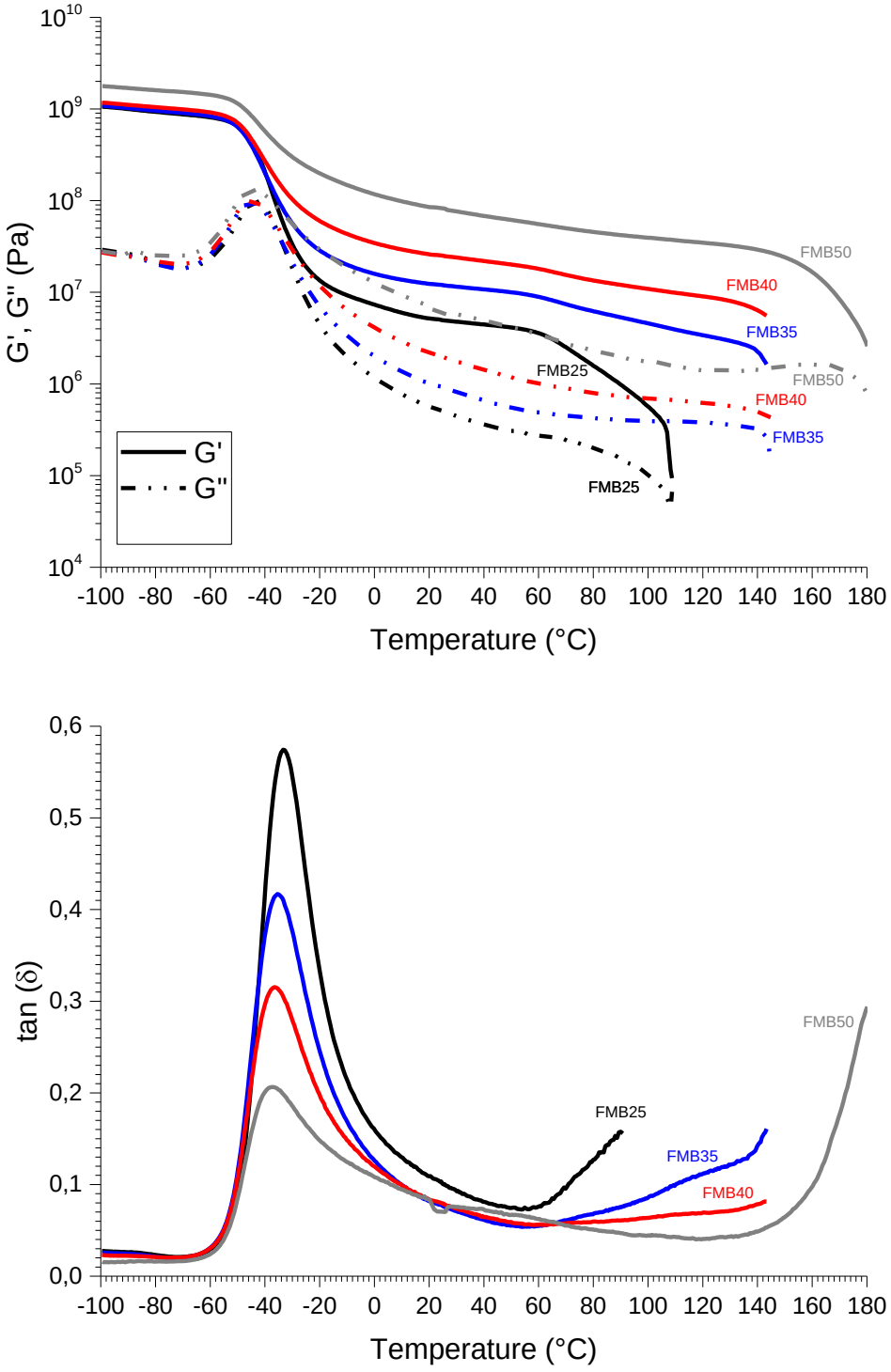

Figure 2.38: Dynamic Mechanical Analysis of FADM and BDO-based samples FMB25, FMB35, FMB40 and FMB60, at a frequency of 1 Hz and 0.1% strain, with a heating ramp of 3°C/min.

Figure 2.38 presents the DMA of the BDO-based models. It can be noted that the α transition temperature is also very stable as the HS fraction increases. The flow limit onset was only obtained for the FMB50 sample as the other samples of the series broke earlier.

The second transition found between 50°C and 70°C on both series of samples can be seen on the BDO-based series as a small inflection of G' and G'' in the same range of temperatures on FMIB40 and FMB35 samples, but it is not as visible on the isosorbide-based series.

In summary, when associated with FADM, isosorbide/MDI hard segments do segregate, the glass transition obtained by DSC on the isosorbide series is equivalent to the one obtained for the model BDO and is well defined. However, the large maxima of tan δ and the poor definition of the rubber plateau of the isosorbide-based samples show that even with this less polar soft segment, the phase segregation is not as favorable for ISO-based materials, as the model BDO-based samples. Crystallization of isosorbide-based hard segments is also less kinetically favorable than the BDO-based model, and it is especially visible on the DSC second heating scans. However, the overall phase segregation of the ISO/MDI HS seems to be more stable with FADM than with the other studied soft segments. Bio-sourced content was thus increased by use of FADM while maintaining elastomeric behavior and thermal properties. Choice of ISO over BDO chain extender depends on the end product property requirements, and thus ISO is a valuable addition to the PU formulation tool box.

2.4.4. Origin of the multiple melting endotherms (MME)

Samples CMB50, TMI50, TMI60, FMB35, FMB40 and FMB50 presented in 2.4.1 to 2.4.3 display multiple melting endotherms. Such thermal behaviors were studied by Koberstein *et al.* [92], Li *et al*. [93], Saiani *et al.* [94]–[96], Fernandez-d'Arlas *et al.* [97], and their studies showed a large influence of both thermodynamic and structural parameters. Koberstein *et al.* [92] studied polyurethane copolymers based on a copolymer of poly(oxyethy-1-ene-b-oxypropylene-b-oxyethylene) glycol (PEO-PPO) as a soft segment, associated to 40 wt% MDI/BDO hard segments. They showed that multiple endotherms were due to distinct crystal populations with different melting temperatures. Moreover, the appearance of multiple endotherms was also linked to the rate of heating and time of isothermal annealing, which means that those endothermal peaks are strongly dependent on the processing and thermal history.

Li *et al.* [93] studied a polyurethane system based on polyester soft segments, MDI and BDO with 45 wt% HS content, and linked the appearance of the melting endotherms to changes in the length of the -NH and C=O bond, indicating dissociation.

Saiani *et al.* [94] studied this phenomenon in further details in several works in the case of materials containing over 60 wt% HS (PPEO-PPO soft segments and MDI/2-methyl-1,3-

propanediol hard segments). They first showed in 2001 that depending on the material composition, one of the endothermal peak was due to the melting of the ordered structure present in the hard phase, while the other peak was due to the microphase mixing of soft and hard segments. Furthermore, for samples with high content of HS, the phase separation is the first process to start followed by the ordering of the hard phase. They later [95] focused on polyurethanes with high hard segment content and showed that the rate of phase separation depends on the HS content, and that in the particular case of their material of choice (PPEO-PPO of M_n ~ 3100 $g.mol^{-1}$ as soft segment with MDI/2-methyl-1,3-propanediol (MPDO) as hard segment), there was a delay of the start of the phase segregation for materials containing more than 65 wt% of HS. At a structural level, samples with a HS content higher than 65 wt% were shown to be composed of a continuous hard segment phase containing domains of mixed soft and hard segments at a concentration of 65 wt% HS. Further studies of annealing on those materials [96] have shown that the phase segregation occurred at all annealing temperatures tested, and that the delay of phase segregation start was decreasing with increasing annealing temperature, while the maximum degree of phase segregation reached at long annealing times was increased with annealing temperature.

Fernandez-d'Arlas *et al.* [97], [98] studied MME in the case of materials based on MDI/BDO hard segments with soft segments based on PTMEG or polyadipate, containing between 30 and 43 wt% HS, and they as well showed that double melting peaks appeared thanks to a thermal history enabling self-nucleation and annealing.

All samples presented in 2.4 were subjected to the same thermal treatment during their synthesis, and as such were all annealed for the same time and temperature. Multiple melting endotherms (MME) were observed for series of samples based on MDI/BDO HS coupled with either FADM or PCL, or with MDI/ISO HS coupled with PTMEG, at HS content of 50 wt% in the case of PCL and PTMEG, and 35 wt% in the case of the FADM series. The more frequent occurrence of this phenomenon in samples containing BDO supports the fact that MDI/BDO HS does separate more easily from the soft segment than MDI/ISO, however this is not true for the PTMEG sample series where TMI50 and TMI60 samples show a well-defined MME, while TMB50 and TMB60 MME are poorly defined if indeed present at all. One should not forget that MME are also dependent on the sample composition and can only appear after a time delay during annealing and at a certain HS content threshold (found to be 65 wt% HS by Saiani *et al*. [95] for their particular polyurethane composition), which is likely to be different for all the compositions tested in this chapter.

MME appearance and kinetics in the studied samples could help characterize the kinetics of phase segregation of ISO and BDO but would require thorough thermal, spectral and microscopic study and is not the object of this work.

2.4.5. Nature of the intermediate secondary transition of TPUs based on BDO and ISO

A transition appearing between 50°C and 80°C was observed by DSC on most sample curves, and the corresponding temperatures are reported in Table 2.28. Its temperature of appearance seems to be influenced by the combination of SS/HS and by the HS content and it is particularly well-defined in the CMB and TMB curve series. A wide array of physical phenomena could be at the origin of this transition, including the T_g of a hard phase, H-bond interactions or annealing-induced order.

This transition cannot be attributed solely to the hard domains of pure HS, as the glass transition of such HS was measured by Cuvé *et al.* [99] for BDO/MDI to be around 100-110°C and by Cognet-Georjon *et al.* for MDI/ISO to be around 187°C [67]. Moreover, it was shown by Klinedinst *et al.* [100] that partial crystallization of the soft phase (PTMEG in their case) only occurred for soft segments length of 2000 $g.mol^{-1}$ and above. However, the appearance of an amorphous phase composed of the mix of some hard segments with soft segments cannot be ruled out.

Yilgör *et al*. [52] also mention the breakage of hydrogen bonds between urethanes –NH and the oxygens of the ether or ester carbonyl functions along the soft segments occurring in the same range of temperatures, which are found in all soft segments studied here. Christenson *et al.* [101] showed that this type of H bonds disappeared and were replaced by H bonds between urethane –NH and–CO groups when the phase segregation increased.

Such intermediate transitions could also be found in the works of other authors like the work of Hwang *et al.* [102] in 1984 or Leung *et al*. [103] in 1986. In 1986, Hesketh *et al.* [104] observed the appearance of a T_g-like transition between 30°C and 50°C in PTMEG/MDI/BDO based polyurethanes, and explained it by the breakage of short-range order induced by room temperature annealing. In 2009, Ponkitwitoon *et al.* [105] also studied materials of the same composition and saw an event around 50°C, which was demonstrated by FT-IR and SAXS to be linked to an increase in the HS inter-domain spacing and a change in the H-bond spacing.

For the moment, the exact nature of this transition is unresolved. It is however interesting to note that its temperature of appearance seems to be linked to the HS content in the isosorbide and PTMEG based samples. More input could be obtained from annealing and spectral analysis (such as WAXS, SAXS and IR) studies on those samples.

Table 2.28: Summary of composition and temperature of endothermic secondary transition for TPU samples series from DSC measurements

Sample	Soft segment nature	Chain extender	wt% HS	Temperature of transition °C
CMI50	Poly(ε-caprolactone)	ISO	51	77
CMB50		BDO	48	54
TMI40	Poly(tetrahydrofuran)	ISO	40	75
TMI50		ISO	51	60
TMI60		ISO	59	52
TMB40		BDO	37	53
TMB50		BDO	48	62
TMB60		BDO	56	59
FMI25	Fatty acids based polyester	ISO	24	60
FMI35		ISO	34	58
FMI40		ISO	42	57
FMI50		ISO	53	57
FMB25		BDO	23	56
FMB35		BDO	32	53
FMB40		BDO	39	54
FMB50		BDO	49	58

2.4.6. Microstructure of thermoplastic polyurethanes based on FADM

In order to get insight into the microstructure and to relate it to the thermal behavior, both TEM and AFM were performed on the FADM and ISO-based samples.

TEM images are presented in Figure 2.39. The FMB35 sample is displaying a continuous soft phase (light contrast) and globular hard phase domains (dark contrast, around 2-3 µm diameter). By comparison, FMI35 is also displaying those features, but the 2 µm hard phase domains have more homogeneous size dispersion and are stacked in a hexagonal-like fashion. This stacking is even more obvious and regular for FMI40, which features smaller

domains (around 1.2 µm diameter). The FMI50 is still displaying a continuous soft phase with hard phase domains. However, the hard phase domains seem to be in a coalescing dynamic, with very huge domains (up to 10 µm diameter) and broad size dispersion, suggesting that the system is getting close to phase inversion.

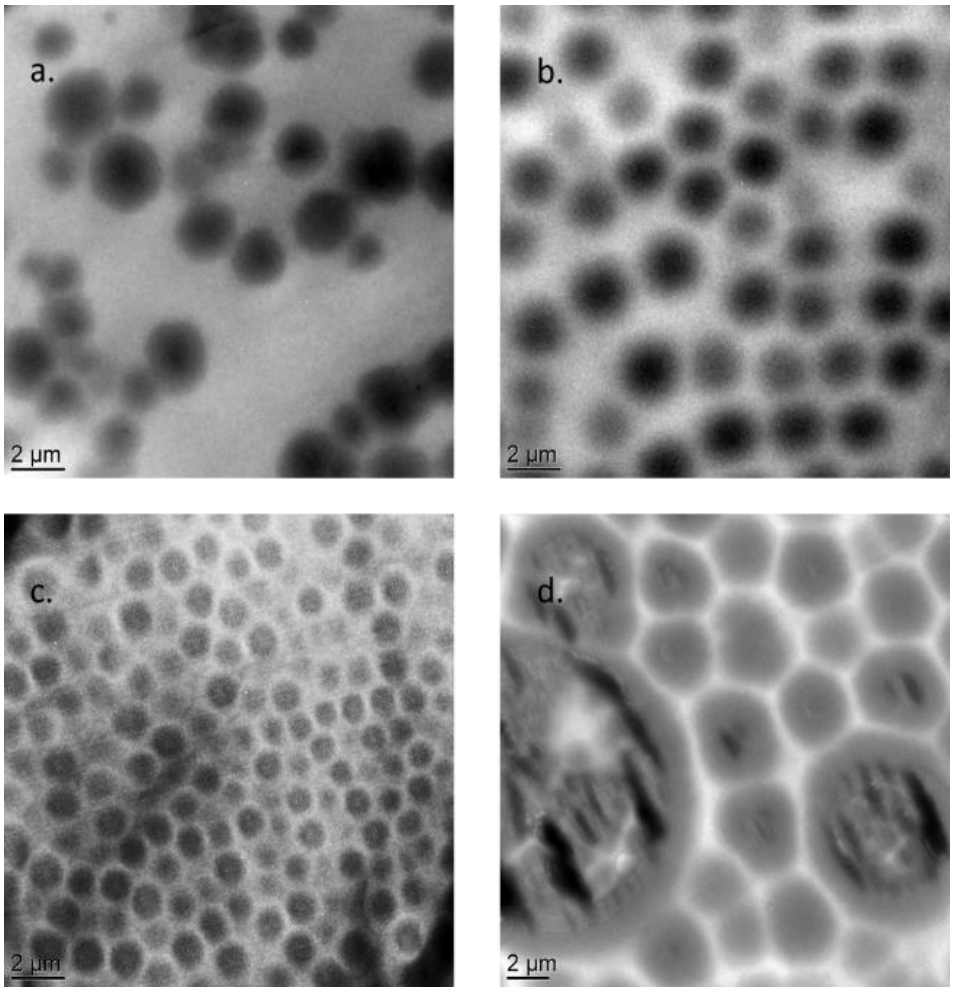

Figure 2.39 : TEM images on cryo-microtomy films a. FMB35 – b. FMI35 – c. FMI40 – d. FMI50

No information could be obtained by TEM on the homogeneity of the hard domains due to poor contrast. It was thus decided to perform AFM imaging.

Similar morphologies were observed on AFM phase images, shown in Figure 2.40, with two magnifications. By comparison, the morphology of sample FMI25 is closer to FMB35 than the latter is to FMI35 in terms of hard domains volume concentration. Rays on the images a. to d. are artifacts originating from the preparation method. Some texture appeared in the hard domain, but it was not possible to determine its exact nature.

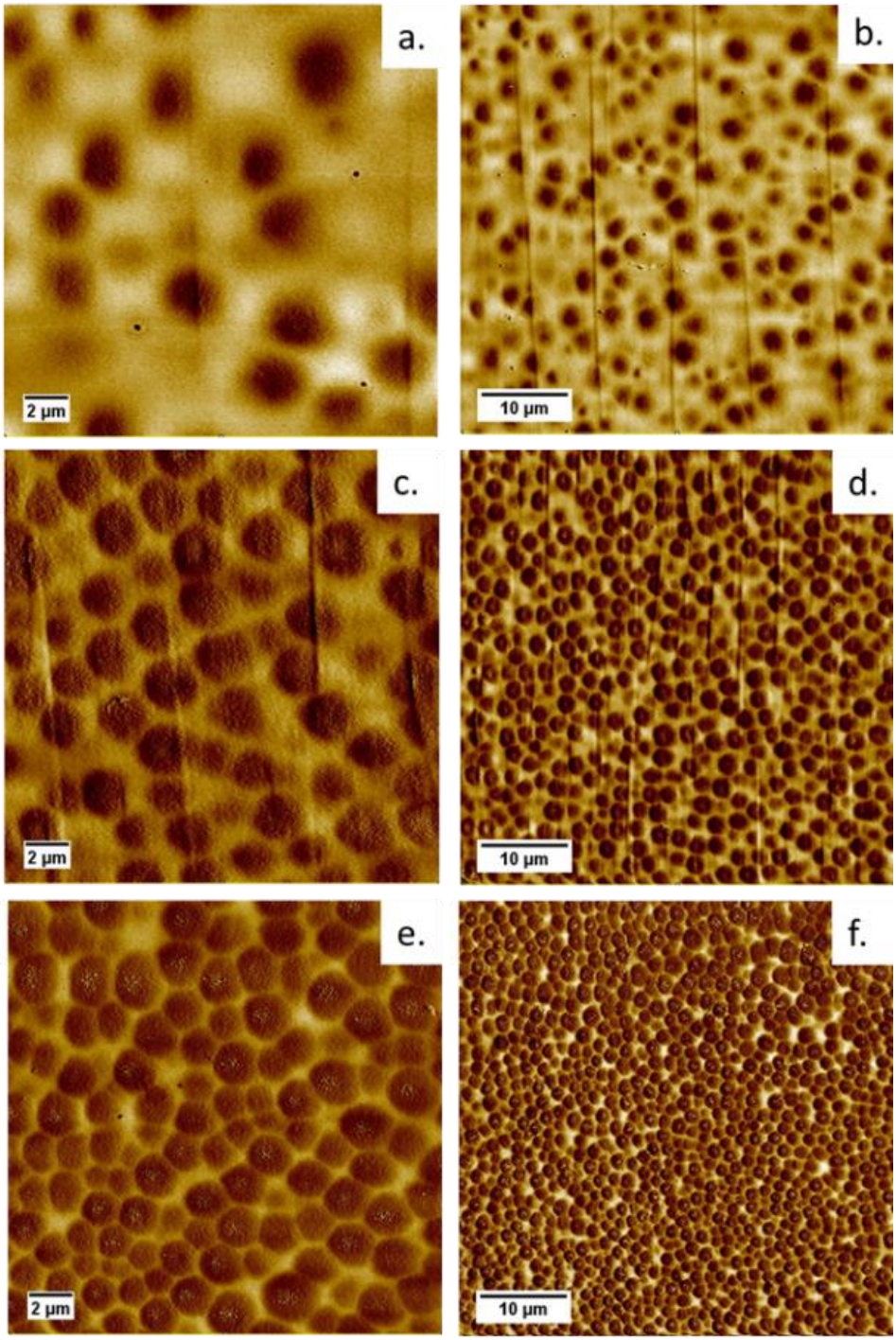

Figure 2.40: AFM images on cryo-microtomy surfaces at two different magnifications (first row: 20x20µm, second row: 50x50 µm) – a. and b. FMI25 – c. and d. FMI35 – e. and f. FMI40

2.5. WATER UPTAKE AND OTHER MECHANICAL CHARACTERIZATIONS

In order to go further in the characterization of the TPUS based on ISO and BDO, thermal characterization tests were completed by hardness and compression set tests, as well as some characterization of the water uptake of the samples.

2.5.1. Mechanical properties : Hardness and Compression set

Shore D hardness was measured on puck shaped samples of 40 mm diameter and 10 mm thickness, with a manual shore D durometer from Zwick-Roell. It was determined as the mean of fifteen measurements, spaced by at least 5 mm.

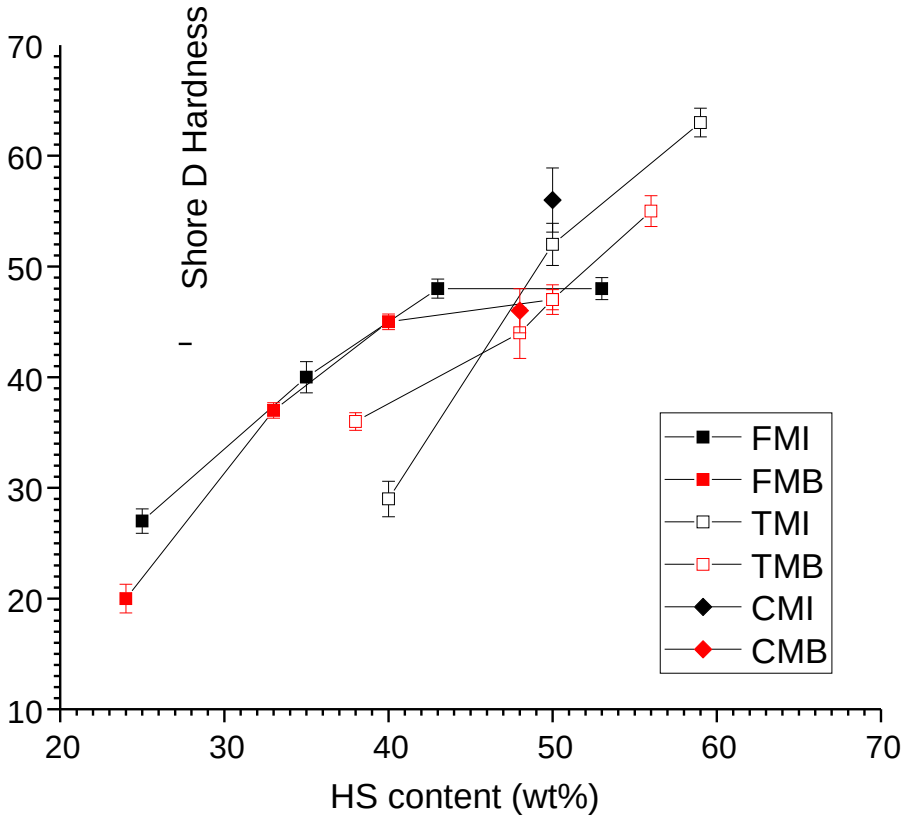

Figure 2.41: Shore D hardness as a function of HS content in wt% for samples based on MDI, measured at room temperature

Figure 2.41 presents the results as a function of the HS content. Overall, the sample series based on isosorbide display a slightly higher hardness than the equivalent BDO-based series (order of magnitude between 5 and 10 units), which is explained by the poorer phase segregation obtained with ISO-based samples, and the higher T_g and T_m of the MDI/ISO HS. Indeed, this difference in hardness is smaller for the FMI and FMB sample series which are the most separated samples in this study. One should also note that due to the difference in molar masses between ISO and BDO, at equivalent stoichiometry, the weight percent of HS is higher in the case of ISO. A test was performed at exact same HS mass proportion (exactly 50 wt%) for samples TMI50 and TMB50, but TMB hardness was still found to be lower than TMI in this case. Those results can be put in perspective to the DMA curves, as it was shown

that on most ISO-based samples, the rubber plateau was higher than the equivalent BDO due to overall poorer purity of the soft phase. However, Hardness is a completely different measurement compared to DMA as it does not differentiate between plasticity and elastic modulus and therefore should not be understood as an equivalent measurement.

Compression set was determined as described in the experimental section. The thermal treatment was performed in the stove for 24h at 70°C. The results are presented in Figure 2.42.

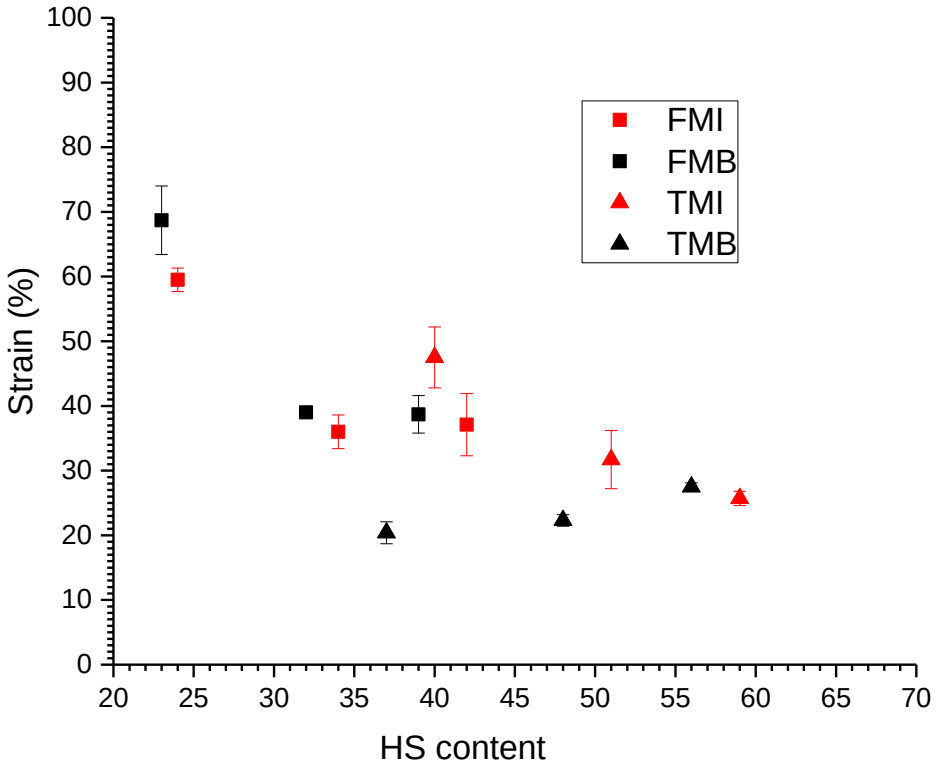

Figure 2.42: Compression set as a function of the HS content in wt%

In the case of the FADM based sample series, the use of isosorbide chain extender seems to be favorable to a better shape retention compared to BDO (Figure 2.42). This is not the case for TMI and TMB sample series in which the behavior seems to be much more HS content-dependent: for isosorbide, the more HS, the more the shape of the sample is stable under stress while TMB seems to display the opposing behavior. This inconsistency could be explained by the thermal instability of phase segregation in PTMEG-based samples compared to the use of more hydrophobic soft segments such as FADM.

2.5.2. Swelling in water of isosorbide based polyurethanes

Swelling in deionized water of some TPUs was monitored over the course of fifty days. The results are reported in Figure 2.43.

First of all, one can note that the water uptake of the tested samples was always below 2 wt%, and that the uptake of isosorbide-based sample is on average only superior to the

model BDO-based samples by 25%. Even if pure isosorbide is highly hygroscopic, it does not induce a large water uptake compared to model polyurethanes and different other types of polymers.

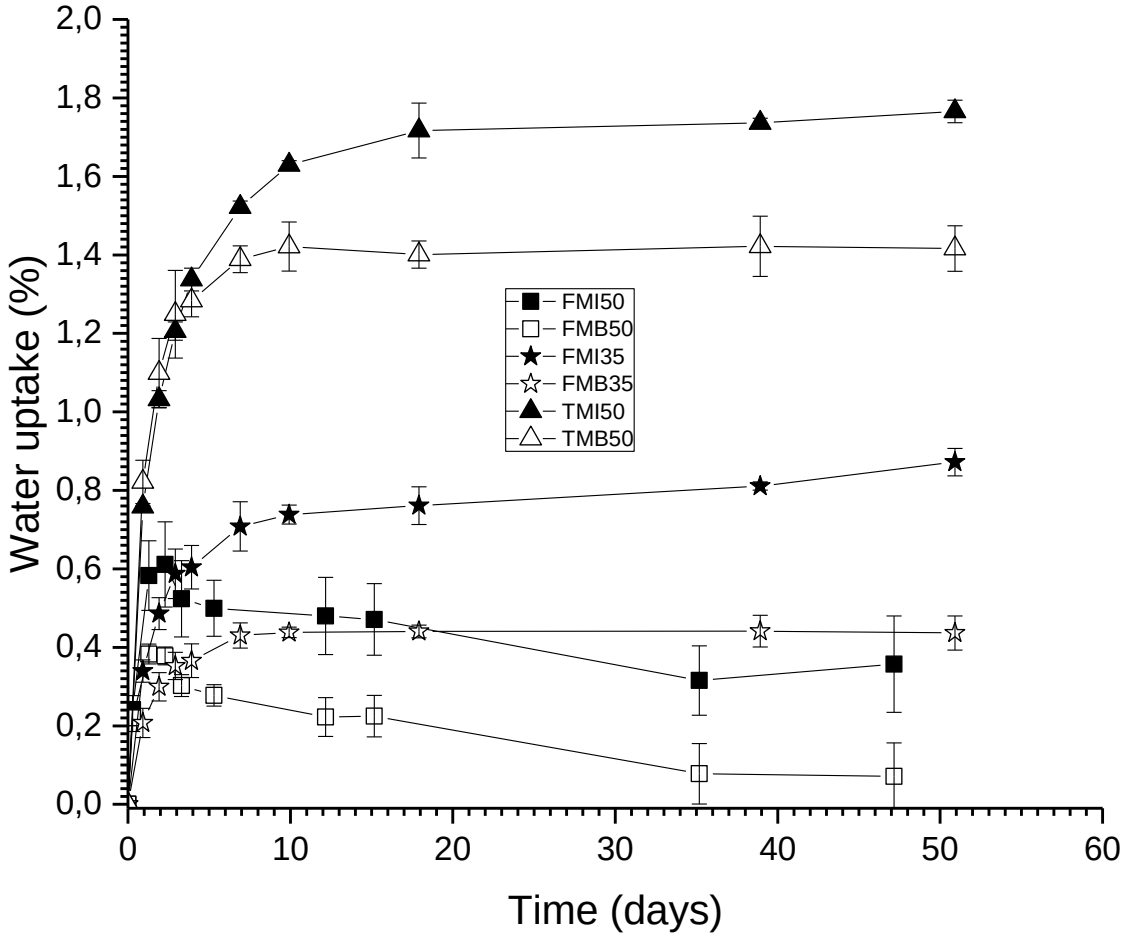

Figure 2.43: Swelling in water test – Water uptake (wt%) as a function of time for samples based on PTMEG or FADM with either BDO or ISO chain extender.

A difference in water uptake can also be seen between TMI50 and TMB50 on the one hand, and FMI50 and FMB50 on the other hand: mass gain at 50 days is larger in the case of the PTMEG-based sample series. This is mainly due to the very hydrophobic nature of FADM which repels water. At equivalent stoichiometry, TMB50 is more hygroscopic than FMI50.

By comparison of FMI50 and FMI35, one can also see that the HS content has an influence on the water uptake, as MDI/ISO HS tends to be more hygroscopic than the FADM SS. Water uptake is decreasing on FMI35 and FMB35 curves after 35 days, which is probably due to the start of hydrolysis of the ester functions of the FADM soft segment, which induces the solubilization of small molecules in water and thus a mass loss. These modification in molar mass should be confirmed by SEC.

Finally, the water uptake test has shown that isosorbide does not induce a critical swelling in water and that this effect can be controlled by a careful choice of the HS and SS combination.

2.6. CONCLUSION

Pure isosorbide was successfully used as a chain extender in the synthesis of thermoplastic polyurethanes based on commercial macrodiols and MDI. In a first step, the synthesis of the prepolymer was carefully monitored to obtain the completion of the reaction between the macrodiols and the MDI and avoid side reactions, and to make sure the chain lengthening was controlled. In a second step, the prepolymers were chain extended with either ISO or BDO at varying HS content. Average molar masses between 11 $kg.mol^{-1}$ and 39 $kg.mol^{-1}$ were measured for ISO based polyurethanes. HS content was shown to be a critical parameter in the final molar mass of the material, as increasing HS concentration resulted in smaller molar masses.

The synthesis method of isosorbide-based samples was optimized in order to reach a higher conversion of the reaction. Molar masses were not significantly increased but the improved synthesis protocol was faster and did not involve the use of a catalyst. Thermal analysis seemed to indicate more stable phase segregation. It was also shown that this protocol was ineffective on the molar masses for BDO chain extenders.

The obtained thermoplastic polyurethane sample series were subsequently characterized by DSC and DMA. The obtained T_g ranged from -48°C to 7°C. It was shown that on average ISO-based samples displayed poorer and less stable phase segregation than with the model chain extender BDO, thus inducing poorly defined rubbery plateaus on DMA. HS content was critical to the quality of the phase segregation as well: on average, lower HS content of MDI/ISO tended to improve the stability of the T_g throughout heating cycles. It was also demonstrated that a careful choice of the soft segment used in combination of the MDI/ISO HS could significantly improve the quality of the phase segregation and could help improve water uptake as well. The best results were thus obtained with the most hydrophobic FADM oligomers. PCL was very miscible with MDI/ISO HS, while PTMEG displayed properties between those of PCL and FADM. ISO-based samples however displayed higher melting temperatures due to the intrinsic properties of the MDI/ISO HS with melting peak maxima ranging between 174°C and 208°C, and thus displayed better temperature resistance than other model polyurethanes based on BDO. Hardness and compression set results were in accordance with those observations.

The thermal behavior of the samples studied in this chapter also displayed a secondary glass transition-like step between 50 and 80°C as well as multiple melting endotherms at higher temperatures. The nature and mechanisms at the origin of those transitions are not yet fully understood in polyurethanes but are likely to be originating from weak bonds or short-range order in the case of the intermediate temperature transition, and crystal ordering or phase separation for the multiple melting transitions at higher temperatures.

In conclusion, the use of Isosorbide in polyurethane synthesis is possible and good properties can be obtained by a careful choice of the soft segment and di-isocyanate combination, and its use could be essential in applications requiring non-toxicity and bio-sourced content.

CHAPTER 3:

ISOSORBIDE AS A CHAIN EXTENDER FOR THERMOPLASTIC POLYURETHANES BASED ON IPDI

Chapter 3. Isosorbide as a chain extender for thermoplastic polyurethanes based on IPDI

3.1. INTRODUCTION

3.1.1. Structure and properties of isophorone diisocyanate

Isophorone diisocyanate, also known as 3-Isocyanatomethyl-3,5,5-trimethylcyclohexyl isocyanate, is a cycloaliphatic diisocyanate [106]. Its physical properties are summarized in Table 3.1. Its structure does not contain any double bond as shown in Figure 3.1. Its two isocyanate functions are not equivalent: one is a primary-NCO while the other is secondary. Those two functions thus do not have the same reactivity, with a rate factor difference between the two of 2.5 [107], and it was shown also that one was favored over the other as a function of the catalyst used [108], [109]. Lewis bases thus induce a higher reactivity of the primary -NCO function, while Lewis acids promote the reaction of the secondary –NCO function [110]. This reactivity difference between the NCO functions is however valued, as it can be used to control prepolymer reactivity and architecture as well as prepolymer viscosity [1].

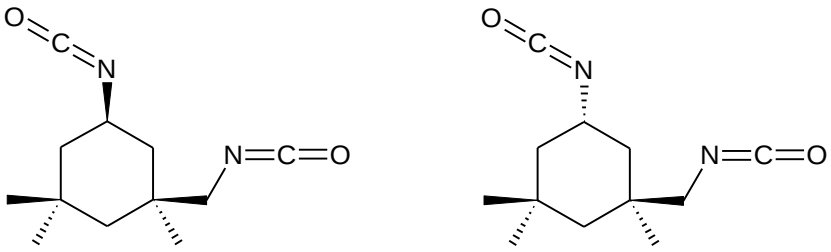

a. *Cis*-isophorone diisocyanate b. *Trans*-isophorone diisocyanate

Figure 3.1: Isophorone diisocyanate isomers

Commercial isophorone diisocyanate is usually available as a mixture of *cis* and *trans* isomers. Spectral studies have shown that the usual ratio is of 75% *cis* and 25% *trans*.

Table 3.1: Key physical properties of isophorone diisocyanate from [111]

Molar mass	($g.mol^{-1}$)	222.2
Melting temperature	(°C)	-60°C
Boiling temperature	(°C) at 1.33 kPa	158

IPDI is a clear and colorless liquid at standard temperature, due to its low melting point. Its low boiling temperature can however be an issue with high temperature processes, making this molecule very volatile and thus harmful for the operator.

3.1.2. Synthesis

Isophorone, the starting molecule of isophorone diisocyanate, is usually obtained through trimerization of acetone [112]. As shown in Figure 3.2, three steps lead classically to IPDI. First, isophorone (4) is converted to isophorone nitrile (5) by reaction with hydrogen cyanide [113] or calcium ethoxide [114].

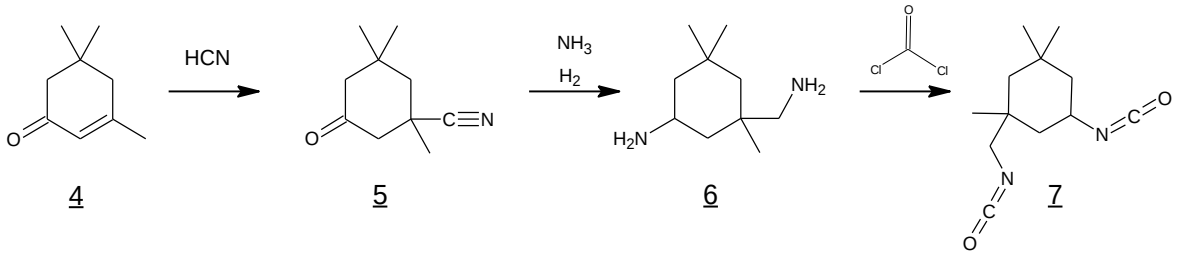

Figure 3.2: Synthesis route of isophorone diisocyanate from isophorone

Isophorone nitrile is subsequently hydrogenated to isophorone diamine (6) through catalytic reductive amination. Finally, IPDI (7) is obtained usually by phosgenation of the amine functions [115], but other routes involving the reaction of amine with urea and alcohol have been reported in order to avoid the use of phosgene gas [116].

3.1.3. Use of Isophorone diisocyanate in polymer synthesis

Due to its aliphatic and asymmetrical nature, IPDI is readily used for synthesis of materials requiring color stability and transparency. Nevertheless, literature about its use in non-cross-linked materials was searched in order to get insight into the properties IPDI brings in PU or other polymers, and its potential when coupled to isosorbide.

3.1.3.1. Classical linear block polyurethanes

Although IPDI is usually employed to the production of coatings and thermosets, few mentions of thermoplastic polyurethanes made out of IPDI were found. In the mid 80's, Jadhav *et al.* [45] have studied systems of linear block copolymers from IPDI coupled to phenyl isocyanate-modified bifunctional castor oil and various linear aliphatic diols such as ethylene glycol, 1,2-propylene glycol or BDO. The obtained materials had softening points between 85 and 105°C, but no melting temperatures were reported by the authors. Ten years later, Cascella *et al.* [117] also synthesized linear polyurethanes from IPDI. They used a mix of PTMEG and PCL (3:1 molar ratio respectively) with an average molar mass around 2000 $g.mol^{-1}$ in a two-stage synthesis and used isophorone diamine (the amine from which IPDI is derived) as a chain extender to obtain polyurethane urea materials. As reported in Table 3.2, the resulting materials displayed a melting peak and were probably phase separated contrary to those studied in [45] that were composed of castor oil, IPDI and chain extended with small glycols. Around the same time, Nikles *et al.* [118] prepared linear PU from PCL, IPDI and 2,5-bis(N-2-hydroxymethyl-N-methylamino)-1,4-benzoquinone diol (AQD) (see structure in Figure 3.3), as amino-quinone compounds are known for being water repellent and thus can be used for metal coatings. The T_g temperature of the HS segments

based on AQD and IPDI was reported to be 170°C, which is exceptionally high considering the asymmetrical structure of IPDI.

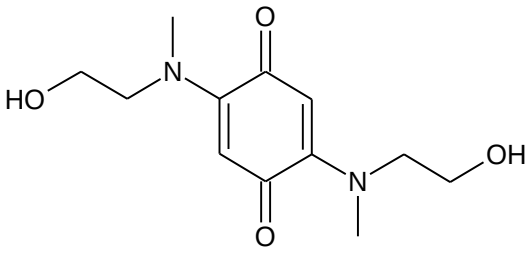

Figure 3.3: Structure of 2,5-bis(N-2-hydroxymethyl-N-methylamino)-1,4-benzoquinone diol (AQD)

In 2014, Jang *et al.* [119] studied polyurethanes simply made of IPDI and 3,5-bis(1,3-oxathiolan-2-yl)- 1,2-cyclopentanedimethanol (OTPDM) and its isomers, presented in Figure 3.4. Those materials displayed optical properties useful for applications as optical switches, filters or attenuators, as Jang *et al*. were able to demonstrate a linear variation of the refractive index as a function of temperature, low optical losses and low birefringence.

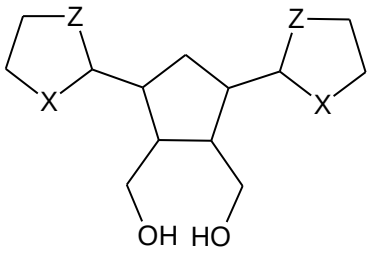

Figure 3.4: Structure of 3,5-bis(1,3-oxathiolan-2-yl)- 1,2-cyclopentanedimethanol, with X, Z= S,S or S,O or O,O atoms (OTPDM, X,Z)

From a thermal point of view, those materials exhibited reasonable T_g temperatures between 133 and 70°C. Wenwen *et al.* [120] synthesized polyurethanes for electrospun fibers based on various polyester diols carrying functionalizable carbon-carbon double bonds, IPDI and BDO as the hard segments. Those PU nano-fibers were intended as carrier for immobilized catalysts. Molar masses between 7 and 35 kg.mol^{-1} were reported.

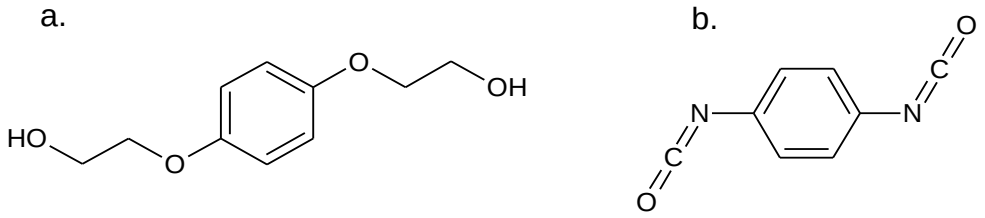

Figure 3.5: Structure of a. hydroquinone bis(2-hydroxyethyl) ether (HQEE) – b. 1,4-phenylene diisocyanate

Since 2016, IPDI-based TPU also have been studied for their shape memory properties, as nonplanar ring structures have been demonstrated to increase recovery after large deformation [121], [122]. Xu *et al.* [121] have studied systems composed of PTMEG, IPDI and hydroquinone bis(2-hydroxyethyl) ether (HQEE) (see Figure 3.5 a.) as a chain extender. By

comparison with planar ring structure of 1,4-phenylene diisocyanate-based polyurethanes (Figure 3.5 b.), they suggested that the shape memory effect obtained with IPDI was due to a higher degree of deformability of IPDI hard domains. Srivastava *et al.* [122] synthesized polyurethanes based on PCL, IPDI and BDO as a chain extender with a nanoclay filler (methyl tallow bis-hydroxyethyl quaternary ammonium ion exchanged montmorillonite). It was found that the filler had a beneficial impact on the recrystallization of the polyurethane material after deformation.

Table 3.2: Summary of the properties of thermoplastic polyurethanes based on IPDI as a function of the soft segment and chain extender combination, from literature

Soft segment	M_n^{SS} (g.mol^{-1})	Chain extender	wt% HS	M_n a) (kg.mol^{-1})	T_g^{SP} b) (°C)	T_m^{HS} c) (°C)	Ref.
Castor oil	1000	Ethylene glycol	-	-	100-105	-	[45]
	1000	1,2-propylene glycol	-	-	85-90	-	[45]
	1000	BDO	-	-	95-100	-	[45]
PTMEG/PCL mix	2000	Isophorone diamine	-	-	-68	19	[117]
PCL	1250	AQD	55	15.6	95	-	[118]
-		OTPDM S,S	100	19.4	133	-	[119]
		OTPDM O,S	100	19.5	78	-	[119]
		OTPDM O,O	100	16.4	71	-	[119]
Polyester containing carbon-carbon double bonds	1870	BDO	30	6.9	-	-	[120]
	578	BDO	30	34.5	-	-	[120]
	714	BDO	30	23.4	-	-	[120]
PTMEG	2000	HQEE	43	5.3	-	-	[121]
PCL	2000	BDO	30	69	-	53	[122]

a) Average molar mass – b) glass transition temperature of the soft phase – c) Glass transition temperature of the hard segments

A thorough study of the literature allowed for the screening of several IPDI-based linear compositions of polyurethanes. Phase segregation of SS and HS was in general not achieved. When measured, the melting point of IPDI-BDO-based HS is also rather low at 53°C [122], which is detrimental to the mechanical properties of the materials at higher temperatures. IPDI-based systems can however be interesting when specific optical and shape recovery properties are required.

3.1.3.2. Toughening of bio-based thermoplastics

IPDI has also been used for the toughening of bio-based polymers such as starches or poly(lactic acid) materials. Linear waterborne PU dispersions are notably used to toughen water miscible polymers such as starch [123], but other examples involving IPDI-based prepolymers were found to toughen starches [124] and poly(lactic-acid) materials [125]. Lu *et al.* [123] were able to enhance mechanical and water-resistance properties of thermoplastic starch by blending in a waterborne PU dispersion. The TPU was based on castor oil, IPDI and 2,2-bis(hydroxymethyl)propionic acid (DMPA) and dispersed in water. Zhang *et al.* [124] more especially studied the effect of the diisocyanate type on such starch blends by adding castor oil and IPDI-based prepolymer. They demonstrated the enhancement of mechanical properties of thermoplastic starch with IPDI, however the effect was smaller than that obtained with toluene diisocyanate. In the same fashion, Gurunathan *et al.* [125] mixed a castor oil and IPDI based prepolymer to poly(lactic-acid) and subsequently demonstrated enhanced mechanical properties (tensile modulus, elongation at break and impact resistance) and the presence of two separate glass transitions due to incomplete compatibility between both components.

3.1.3.3. Waterborne polyurethanes based on IPDI

IPDI is readily used for the formulation of waterborne polyurethanes. The examples presented in this part were specifically chosen among a variety of others because they present waterborne linear polyurethane systems obtained from IPDI. You *et al.* [126] produced waterborne polyurethane-amide dispersions. Soft segments were either poly(1,4-butylene adipate) – a linear polyester oligomer, or a polyethylene glycol, associated with IPDI, and either 1,4-butanediol or various dicarboxylic acids as chain extenders. Dispersion was ensured by incorporation of DMPA along the polymer chains. Such materials are however subject to an important water swelling (up to 13%) due to the incorporation of ionized DMPA along the chain and the use of polyesters as soft segments.

Fang *et al*. [127] enhanced the mechanical properties of such waterborne thermoplastic polyurethanes by incorporating acrylic chain-end functions to the IPDI-based polyurethanes chains. They were thus able to obtain clear elastomeric pourable materials. Control over the PU - PMMA hybrids ratio in the dispersion, allowed them to tailor tensile strength, strength hardening modulus, elongation at break and recoverable elasticity as well as water uptake.

Wan *et al.* [128] used IPDI-based polyurethane waterborne formulations in order to obtain self-healing materials. The soft segment was PCL (1000 $g.mol^{-1}$) and the chain extender was 2-hydroxyethyl disulfide (see Figure 3.6), as the rupture of disulfide bond promotes the creation of new covalent bonds through reaction of thiolate anions and sulfonyl radicals.

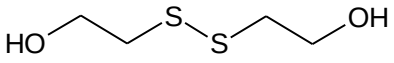

Figure 3.6: Structure of 2-hydroxyethyl disulfide

Self-healing of a scratch was achieved by heating the film at 60°C for 10 min. As the ratio of 2-hydroxyethyl disulfide increased, the surface quality was restored. However, since the glass transition temperature of such films is around -25°C with a melting peak between 50 and 100°C, the resulting materials probably had a poor thermal resistance in spite of displaying phase segregation.

Finally, Hajializadeh *et al.* [129] tried to strengthen linear waterborne polyurethanes by adding amide functionalized multi-walled carbon nanotubes (MWCNT) fillers to the water dispersions, and obtained cast polyurethane films from them. The polyurethane water dispersion was based on PCL (2000 $g.mol^{-1}$), IPDI and DMPA with a molar ratio of 1:3:2 respectively. The presence of MWCNT resulted in an increase in crystallinity of the soft segments, and a slight increase in the T_g. The conductivity of the material was also enhanced.

3.1.3.4. Association with isosorbide

No literature using both isosorbide and *stricto sensu* IPDI could be found to this date. However, one example of polyurethane synthesis involving the use of isosorbide in relation to isophorone diamine (the diamine obtained from isophorone – see Figure 3.7) was reported by Ménard *et al.* [130].

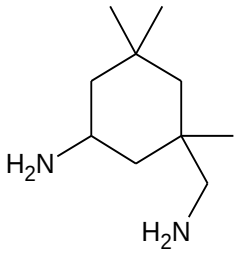

Figure 3.7: Structure of isophorone diamine

Thermoplastic polyhydroxyurethanes were obtained through a non-isocyanate route involving the reaction of cyclocarbonate functions with amines to form urethanes. Isosorbide hydroxyl functions were reacted with ferulic acid (see Figure 2.10 chap 2) to form esters, and the resulting oligomers were functionalized with cyclocarbonates. Finally, those cyclocarbonate ending oligomers were reacted with isophorone diamine (IPDA) in order to

obtain linear poly(hydroxyurethanes). Overall, materials containing IPDA had higher T_g than other similar materials based on linear primary amines. Moreover, the same trend could be observed with isosorbide containing precursors compared to other linear diols. The isosorbide and IPDA based material displayed a T_g of 51°C with M_n of 3500 $g.mol^{-1}$.

3.1.3.5. Conclusions

The literature search made on the topic of IPDI associated to polyurethanes has allowed reviewing the state of the art in this field.

In spite of a low reactivity due to its chemical structure, IPDI can be used to control the kinetics of the polymerization reaction and the viscosity of prepolymers, however it also usually results in low molar masses. Its aliphatic nature makes it an interesting building block for applications requiring UV resistance, hence its use for the synthesis of coatings. Moreover, its hydrophobicity and low reactivity makes it a very common monomer for formulation of water-borne polyurethane dispersions.

Due to the poor phase segregation of polyurethanes based on IPDI and common industrial diols such as BDO, the examples of linear block polyurethanes made from IPDI are scarce. In the recent years, some examples of it being used for its interesting optical properties and shape recovery, or as a bio-based material toughener were reported. However, those remain very specialized applications.

Finally, IPDI is widely used for synthesis of waterborne polyurethane suspensions intended for thermoset coating applications. However, some examples of waterborne thermoplastics made from IPDI were obtained. Such materials needed to be strengthened by various routes as their mechanical properties were overall poor.

In summary, in order to use IPDI as a building block for the synthesis of block polyurethanes, it is required to obtain a high molar mass to induce phase segregation between HS and SS, which will impart better mechanical properties. Moreover, thermal stability could be improved by the use of a diisocyanate/chain extender combination with a high glass transition temperature.

After the study of the properties of several hard segments based on IPDI and various diols, this chapter will study the synthesis of IPDI-based thermoplastic polyurethanes in association with soft segments of different nature. The properties of the isosorbide-based polyurethanes will be as well compared to 1,4-butanediol-based polyurethanes, which is a classical industrial chain extender. A model linear thermoplastic formulation based on IPDI will be chosen as a base for formulation of new cross-linked polyurethane coatings in a following chapter.

The aim of this chapter is to synthesize thermoplastics from IPDI displaying phase segregation and good thermal resistance. As such, hard segments made from IPDI and diols such as isosorbide, a polyether oligomer made from isosorbide, 1,4-butanediol and 2,5-

bis(hydroxymethyl)tetrahydrofuran will first be synthesized and their properties will be assessed in order to choose the best candidate. IPDI will then be used as a diisocyanate for the synthesis of thermoplastic polyurethanes by a two-step method. The aim of this chapter is more specifically to study the synthesis of IPDI/isosorbide-based polyurethanes in terms of molar mass, and kinetics, as well as to study the quality of the phase segregation of isosorbide-based compositions as a function of the soft segment and the hard segment content. Moreover, the isosorbide-based materials will be compared to 1,4-butanediol-based models. Soft segments were selected from previous chapter as poly(tetrahydrofuran) and a fatty acid dimer-based polyester. This chapter will thus contain:

- Characterizations of the starting reactants
- Synthesis of several hard segments based on IPDI/diol with a 1:1 stoichiometry
- Study of the two-step synthesis of polyurethane materials as a function of the soft segment and the chain extender
- Synthesis of polyurethane materials with increasing hard segment content
- Study of the quality of the phase segregation in the materials as a function of the chain extender, soft segment and hard segment weight ratio.

3.2. SYNTHESIS OF POLYURETHANES

3.2.1. Study of the hard segments based on IPDI

3.2.1.1. Synthesis of hard segments based on IPDI

Hard segments were synthesized in a THF solution. The ratio of OH/NCO used was 1. DBTDL was used to catalyze the urethane formation reaction at a concentration between 0.3 wt% and 5 wt% of the total mass of monomers. Exact compositions of the samples are reported in Table 3.3**.** Very viscous or solid diols at standard temperature such as a polyether oligomer based on isosorbide (IsoOP, presented in the material section) and isosorbide (ISO or IsoBD) were liquefied at 80°C in a stove prior to use. DBTDL, IPDI and the liquid diol were inserted in a 100 mL round bottom flask equipped with a water-cooled condenser, together with 20 mL of tetrahydrofuran. The reaction was carried out at 50°C (oil bath). The disappearance of the NCO peak was periodically monitored by FT-IR throughout the reaction, at the end of which the THF solution of polyurethane was precipitated in 300 mL of ice-cooled petroleum ether with a very fast magnetic stirring. The precipitate was filtered and subsequently washed twice with 100 mL of petroleum ether. The precipitate was then heated at 50°C under vacuum for 2 hours in order to evaporate remaining petroleum ether. The resulting samples were white powders.

Table 3.3 : Composition and reaction parameters of the synthesized IPDI-based hard segments for 20 mL of THF – OH/NCO = 1.05

Sample name	Diol type	Concentration of monomers in THF (g/mL)	Mass of IPDI (g)	Mass of Diol (g)	Mass of DBTDL (g)	Reaction time at 50°C (hours)
IPDI-THFDM	THFDM	0.25	3.19	1.85	0.016	6
IPDI-IsoOP	IsoOP	0.13	1.23	1.41	0.020	6
IPDI-BDO	BDO	0.26	3.67	1.50	0.251	6
IPDI-IsoBD	ISO	0.25	3.02	1.96	0.227	12

3.2.1.2. Characterization of hard segments based on IPDI

After synthesis, hard segment samples were dissolved in a 0.01M $LiNTf_2$ solution in DMF in order to obtain the SEC curves presented in Figure 3.8. The highest molar mass was obtained for the IPDI-BDO sample as indicated by the smaller retention volumes of the curve. This was expected since BDO is a primary alcohol, which is more reactive than secondary alcohols

such as ISO or IsoOP. Small shoulders are present at higher retention volumes for all four curves, which seems to indicate that some very short chains of a few units were synthesized.

Molar masses were calculated by means of a polystyrene calibration curve, and are reported in Table 3.4, along with a theoretical average polymerization index deduced from average molar mass and the theoretical mass of the monomers. Glass transition was obtained from 20°C/min heating scans.

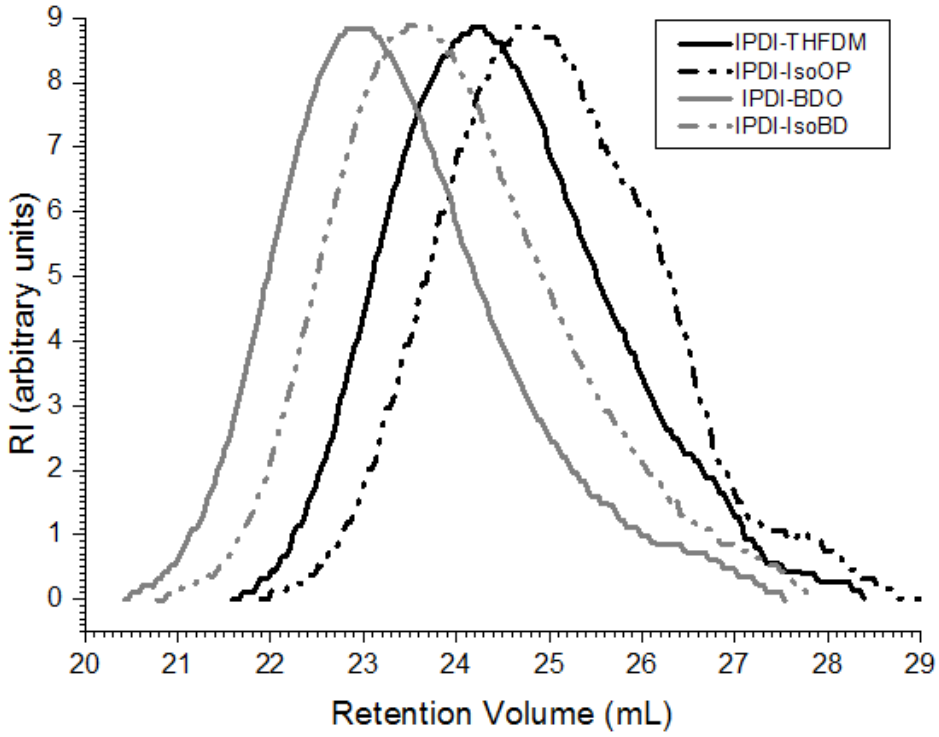

Figure 3.8: SEC RI curves of the pure hard segments based on IPDI in DMF 0.01M LiNTf2 (1 mL/min)

Table 3.4 : Composition and molar mass distribution of pure hard segments (Polystyrene conventional calibration) obtained in DMF $LiNTf_2$ 0.01M (1 mL/min), the average polymerization degree was calculated from the theoretical molar mass of the monomers

Sample	Diol	Stoichiometry	M_n	M_w	Đ	Average polymerization Degree*	T_g
		IPDI/Diol	($g.mol^{-1}$)	($g.mol^{-1}$)	(M_w/M_n)	DP_n	(°C)
IPDI-THFDM	THFDM	1.05:1	2410 ±241	5930 ±593	2.5	14	53
IPDI-IsoOP	IsoOP	1.05:1	1060 ±106	3940 ±394	2.4	4	41
IPDI-BDO	BDO	1.05:1	6800 ±680	16040 ±1604	2.7	44	24
IPDI-ISO	ISO	1.05:1	3600 ±360	9660 ±966	2.3	20	121

* calculated from SEC data

Consistently with the properties of linear PU materials using IPDI and BDO as hard segments from the literature study, the hard segments based on IPDI and BDO have a glass transition around standard room temperature in spite of achieving reasonable molar masses and DP_n during the synthesis. The hard segments based on IPDI and ISO on the contrary display a glass transition 100°C higher than the model IPDI-BDO in spite of a DP_n half that of IPDI-BDO. IPDI-THFDM has a DP_n in the order of magnitude of the IPDI-ISO HS, but its glass transition temperature is only around 50°C. Finally, very low molar masses were obtained for the IPDI-IsoOP, but the glass transition of this material is still higher than that of IPDI-BDO.

In conclusion, the best chain extender candidates for enhancing thermal properties of hard segments based on IPDI are IsoOP and ISO. Good properties could probably be displayed by IPDI-IsoOP if sufficiently long hard segments can be obtained. As the properties and kinetics of ISO are better known from the work carried out in Chapter 2, and the hard segments properties of the IPDI-ISO system seem to be very interesting due to its high T_g, it was chosen to study the synergy between this type of hard segments and two different SS in the following sections.

3.2.2. Synthesis of TPUs based on IPDI

3.2.2.1. Prepolymers

In a similar manner to the work done in chapter 2 on MDI-based polyurethanes, a two-step synthesis was used for the production of IPDI-based polyurethanes. The reaction was carried out with an excess of 5 mol% of NCO functions. This reaction results in the production of -NCO-terminated macrodiols as shown in Figure 3.9. As the –NCO functions of IPDI are not equivalent and the molecule is not symmetrical, it is possible to form a wide range of structures.

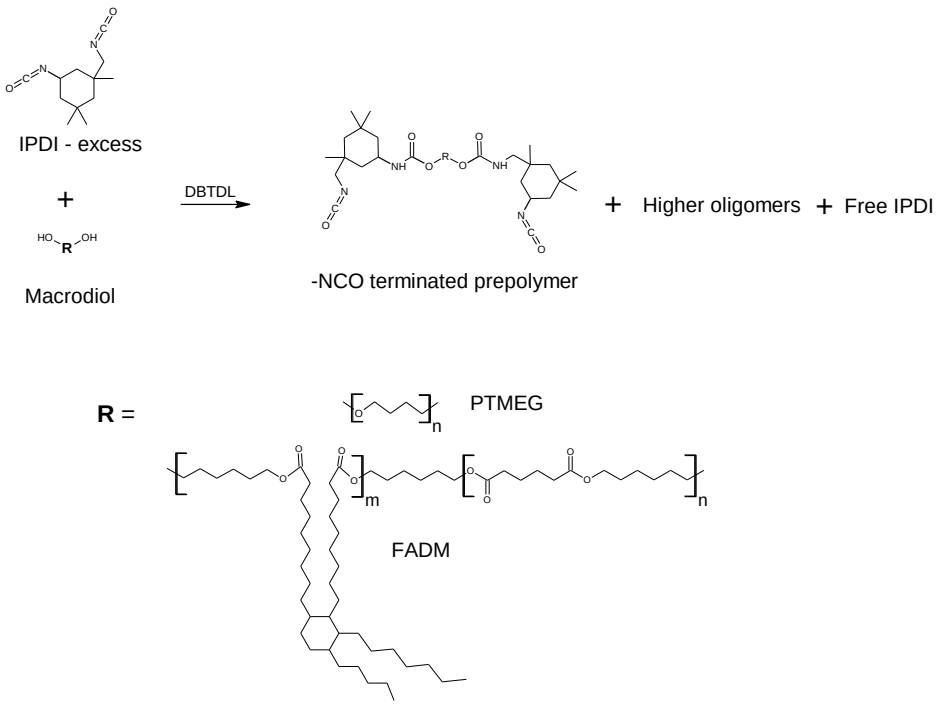

Figure 3.9 : Reaction of IPDI with a macrodiol being either poly(tetrahydrofuran) (PTMEG) or fatty acid dimer-based polyester (FADM) in order to obtain a –NCO terminated oligomer (the structure presented here is an example of possible structures).

As IPDI is far less reactive than MDI as well, it was necessary to use a catalyst. The stability of the poly(tetrahydrofuran) and IPDI-based prepolymer has been studied in order to check the completion of the reaction and the stability of the prepolymer for the second step of the polyurethane synthesis.

In order to prepare polyurethanes with a ratio of macrodiol/diisocyanate/extender diol of 1:3:2 respectively, the synthesis of a prepolymer with a NCO/OH ratio of 3 was studied. Table 3.5 reports the composition of those prepolymers. The NCO functions were added in a slight excess of 0.05 molar from the expected final ratio in order to obtain the longest possible polymer chains. The prepolymer was prepared by reaction of IPDI with poly(tetrahydrofuran) with 0.04 wt% of DBTDL catalyst in a reactor under vacuum and heated by an oil bath at 80°C; samples were taken periodically for analysis over a two-hour course.

Table 3.5: Composition of a prepolymer based on IPDI and PTMEG, and NCO equivalents, after 45 min of reaction at 80°C with 0.04 wt% of DBTDL

Sample	Polyol mass (g)	IPDI mass (g)	NCO/OH ratio (-)	Experimental Eq_{NCO} [a] ($mol.kg^{-1}$)
PTMEG-IPDI	26.8	17.2	2.9	2.32

a) Obtained by chemical titration as described in the experimental section

In order to check the stability of the prepolymers, a follow-up of the reaction was performed by titration of the NCO groups for the prepolymers based on PTMEG and IPDI. Figure 3.10 presents the obtained curve. At the completion of the reaction for prepolymers of NCO/OH ratio of 2.9, the expected molar percentage of reacted NCO is around 35%. This limit is reached in less than 10 min of reaction at 80°C. From there on, the percentage of reacted -NCO functions does not increase significantly until 60 min at which point a slight but steady deviation can be seen. This could be due to evaporation of IPDI through vacuum or side reactions like IPDI dimerization. However, the IPDI-based prepolymer is stable for at least one hour under those synthesis conditions. It was then decided to set the time of the chain extension at 45 min in order to have reasonable synthesis reaction time.

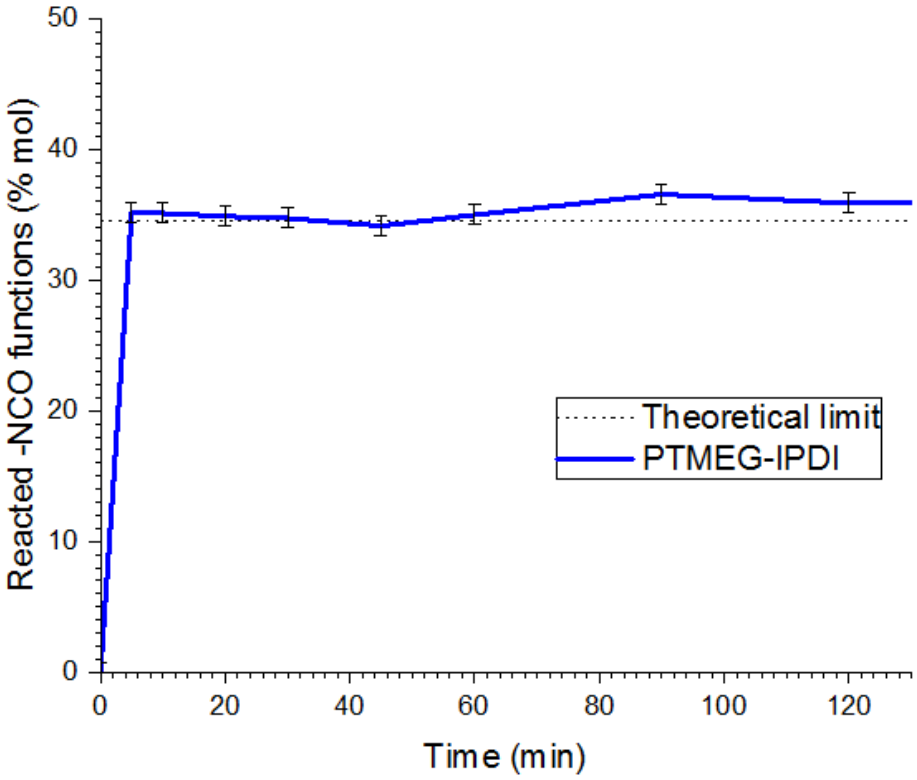

Figure 3.10: Molar percent of reacted NCO (1 - $Eq_{NCO}(t)/Eq_{NCO}$ (t=0)) functions as a function of time during PTMEG-IPDI prepolymer reaction, obtained by chemical back titration of NCO functions. The theoretical limit was calculated from initial reactant masses and stoichiometry

3.2.2.2. Chain extender addition

The synthesis of the prepolymers based on IPDI with either PTMEG or FADM allowed to then proceed to the second part of the thermoplastic polyurethanes synthesis: the addition of the chain extenders ISO or BDO. Two series of polyurethanes were synthesized, based on PTMEG or FADM macrodiol and with IPDI as the diisocyanate. Two HS ratios were also tested in each case. The chain extenders were in the molten form, ISO was melted at 80°C prior to use while BDO is liquid at room temperature and was thus added as it is. After addition of the chain extender in the reactor, the reacting mixture was put under vacuum and heated at 80°C with a fast-mechanical stirring. The reaction was left to proceed until an increase in

viscosity preventing mixing was noticed. At this point, the material was taken out of the reactor and poured in 50 mL plastic containers. The containers were put in a 110°C stove for 16 hours (overnight). The following day, the samples were pressed in the form of square sheets or cylindrical molds at 120°C with a hydraulic press at a pressure of 40 kN. The resulting samples were clear and uncolored polymer sheets of thickness 2mm in the case of the PTMEG SS, or slightly yellow transparent sheets for the FADM SS due to intrinsic coloration of the starting FADM macrodiol.

Table 3.6: Composition and molar mass of poly(tetrahydrofuran) (PTMEG) and IPDI-based polyurethanes series – obtained by SEC in $LiNTf_2$ 0.01 M solution at 1 mL/min and calculated from polystyrene standards

Sample	Chain extender	wt% HS	Stoichiometry SS/MDI/Diol	M_n ($kg.mol^{-1}$)	M_w ($kg.mol^{-1}$)	Đ (M_w/M_n)
TII45	ISO	49	1:3:2	60.4 ±6	135 ±14	2.2
TII60	ISO	63	1:5:4	40.0 ±4	89.9 ±9	2.2
TIB45	BDO	46	1:3:2	78.2 ±8	161 ±16	2.1
TIB60	BDO	60	1:5:4	63.6 ±6	133 ±13	2.1

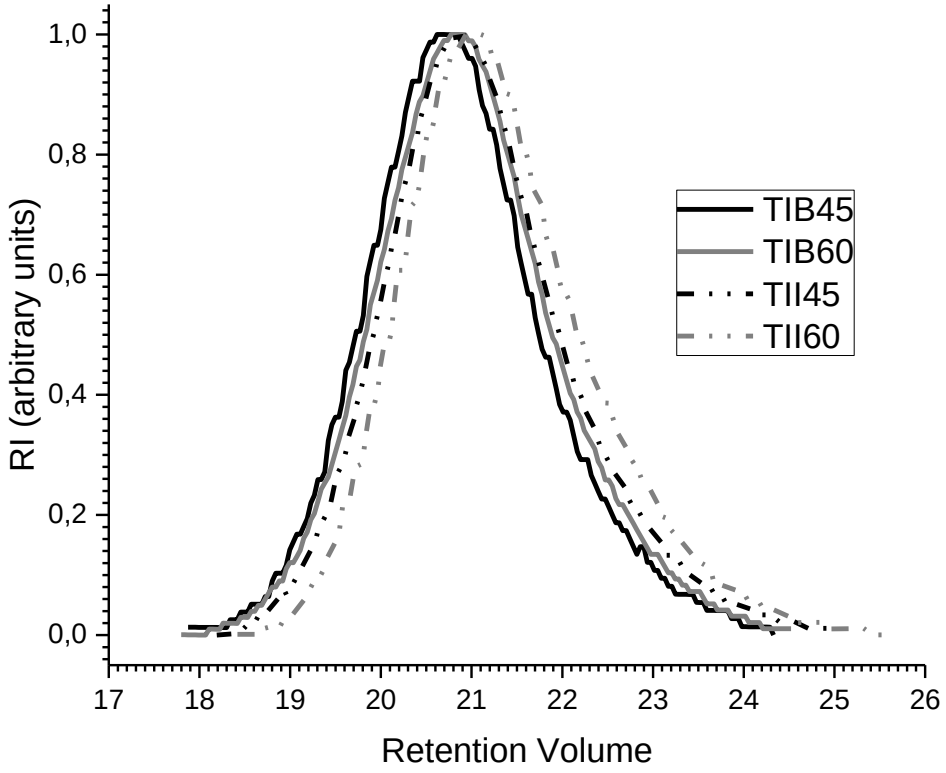

Figure 3.11: SEC curves of PTMEG and IPDI-based polyurethanes, in DMF 0.01 $LiNTf_2$ with either ISO or BDO as the chain extender

Table 3.6 presents the composition and molar masses of the series of samples obtained from PTMEG, IPDI and a chain extender chosen between ISO and BDO. The SEC curves are presented in Figure 3.11. From the stacking of the curves, it is already apparent that very similar molar masses were achieved regardless of the nature of the chain extender, with a slight shift toward the lower masses for the samples containing a higher HS ratio such as TII60 and TIB60.

From the values presented in Table 3.6, the samples based on isosorbide TII45 and TII60 present slightly lower molar masses than the corresponding BDO-based TIB45 and TIB60, however the values are in the same order of magnitude. This phenomenon can again be explained by the difference in reactivity of BDO in relation to ISO as was seen in Chapter 2. The dispersity in this sample series is as well very close to the theoretical value of 2 expected from polyaddition synthesis. Finally, it can be noted that the molar mass decreases with the HS ratio in both ISO and BDO-based sample series.

Table 3.7 presents the composition and molar masses of the series of samples obtained from FADM, IPDI and a chain extender chosen between ISO and BDO. The SEC curves are presented in Figure 3.12.

Table 3.7: Composition and molar mass of fatty acid dimer polyester (FADM) and IPDI-based polyurethanes series – obtained by SEC in $LiNTf_2$ 0.01 M solution at 1 mL/min and calculated from polystyrene standards

Sample	Chain extender	wt% HS	Stoichiometry SS/MDI/Diol	M_n ($kg.mol^{-1}$))	M_w ($kg.mol^{-1}$)	Đ (M_w/M_n)
FII30	ISO	32	1:3:2	23.5 ±2	66.6 ±7	2.8
FII45	ISO	46	1:5:4	16.4 ±2	45.6 ±5	2.8
FIB30	BDO	28	1:3:2	55.5 ±6	158 ±16	2.8
FIB45	BDO	42	1:5:4	44.0 ±4	122 ±12	2.8

From the spread of the different curves over a large range of retention volume, it is apparent that the sample series based on FADM presents more heterogeneous molar masses. One can note that the samples FIB45 and FIB60, based on BDO as the chain extender are almost overlapping, which means that their molar mass is close, with FIB45 a bit shifted toward the small retention volumes**.** Samples based on ISO are both shifted to higher retention volumes as their HS ratio increases. However, no shoulder is present at high retention volume on any curves of the FADM series as well, which indicates that no small mass entities were synthesized and that the produced materials are very homogeneous in size, similarly to what was seen for the PTMEG-based sample series presented previously.

From the values presented in Table 3.7, the samples based on isosorbide FII30 and FII45 present more than twice lower molar masses than the corresponding BDO-based FIB30 and FIB45. FII30 and FII45 present however average molar masses over 15 kg.mol^{-1}, which is sufficient to consider them as polymers. This phenomenon can again be explained by the difference in reactivity of BDO in respect of ISO as was seen in Chapter 2. The dispersity of this sample series is slightly higher than 2, which could be explained by the higher dispersity of the starting macrodiol FADM as was seen in Chapter 2. Finally, the molar mass decreases with the HS ratio in both ISO and BDO-based sample series.

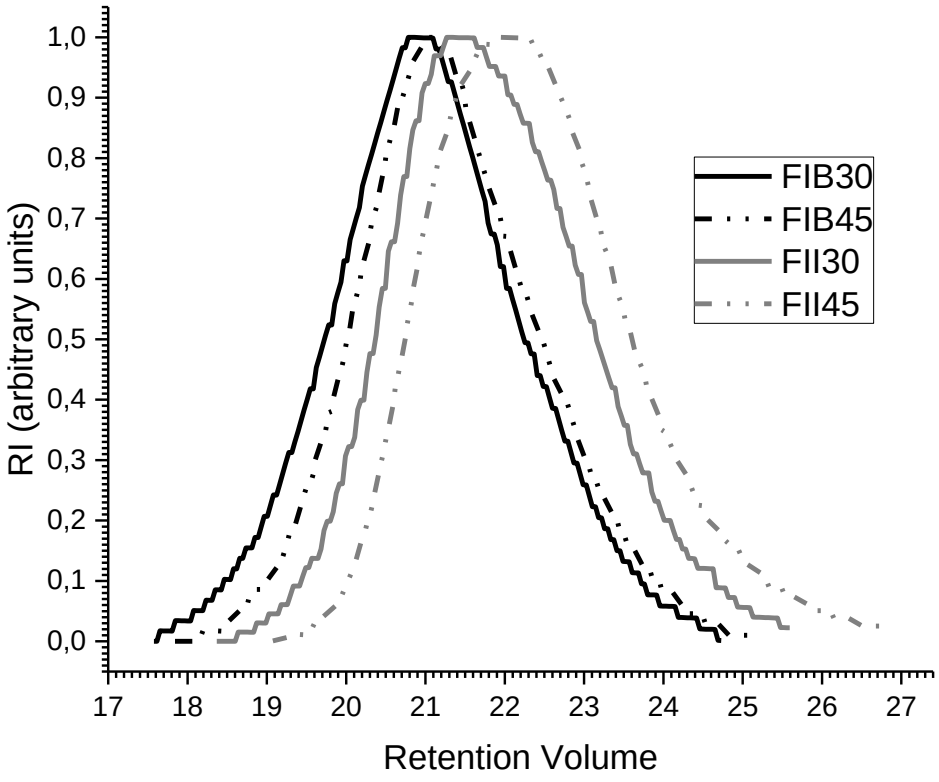

Figure 3.12: SEC curves of FADM and IPDI-based polyurethanes, in DMF 0.01 $LiNTf_2$ with either ISO or BDO as the chain extender

In summary, synthesis of linear polyurethanes based on IPDI associated with ISO or BDO as chain extender, and either FADM or PTMEG as soft segments was achieved. After SEC characterization, it was confirmed that the obtained materials have molar masses sufficient to be considered as polymers.

3.3. THERMAL BEHAVIOR AND MECHANICAL PROPERTIES CHARACTERIZATION

The following section will report the thermal properties obtained from DSC and DMA of the thermoplastic polyurethane series presented in the previous section.

3.3.1. Thermal behavior of samples based on PTMEG and IPDI

The DSC and DMA measurements carried out on the series of samples based on poly(tetrahydrofuran) are presented in Figure 3.13 to Figure 3.16 and Table 3.8. The scans were carried out at 20°C/min from -100°C to 150°C, and two heating scans were carried out successively.

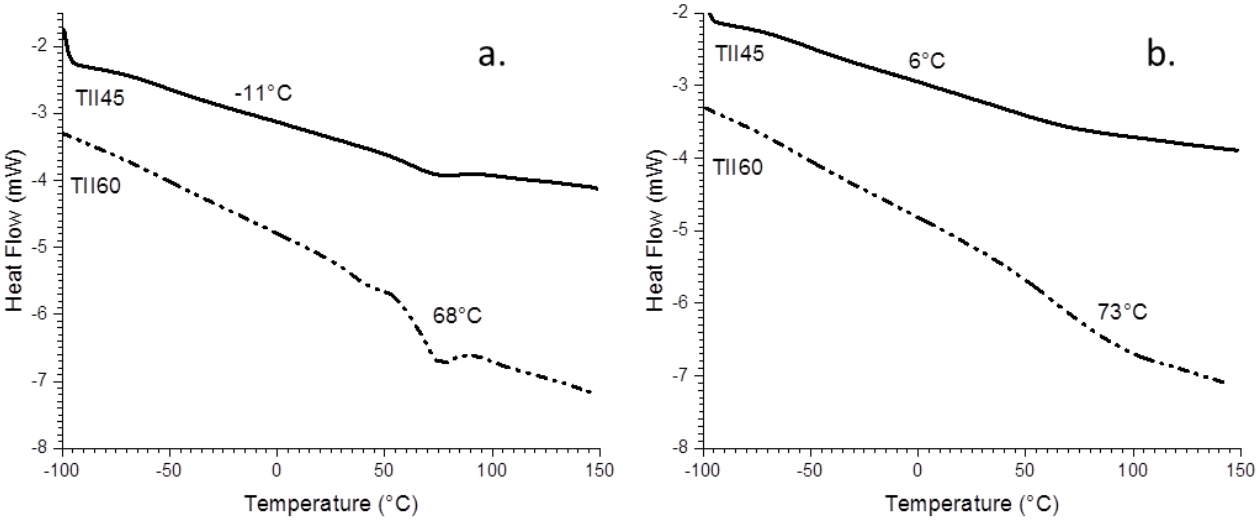

Figure 3.13: Differential Scanning Calorimetry of polyurethanes based on PTMEG, IPDI and ISO – a) first heating ramp performed at 20°C/min from -100°C to 150°C – b) second heating ramp performed at 20°C/min after a cooling at 20°C/min

From the first heating scans of the sample series based on ISO (Figure 3.13 a.), it is apparent that the glass transition of the TPUs based on PTMEG, IPDI and ISO is spread on a very large range of temperature. It is however not very clear if this T_g is unique for sample TII45 or if the sample displays in fact two T_g (one around -50°C and the second one around 65°C) that are not well defined. The second case would mean that the system is very close to phase segregation. There is also a very large effect of the HS ratio between sample TII45 and TII60, with a T_g that increases of almost 80°C.

However, from the second heating scan (Figure 3.13 b.) and the presence of only one T_g, it seems that the PTMEG SS are homogenizing with the IPDI-ISO HS, which means that, the potential phase segregation is not stable at all.

The same trend can be observed in the first and second heating scans of the BDO-based sample series (Figure 3.14). The effect of the HS ratio on the T_g is however more limited in this case with an increase of only 40°C between TIB45 and TIB60.

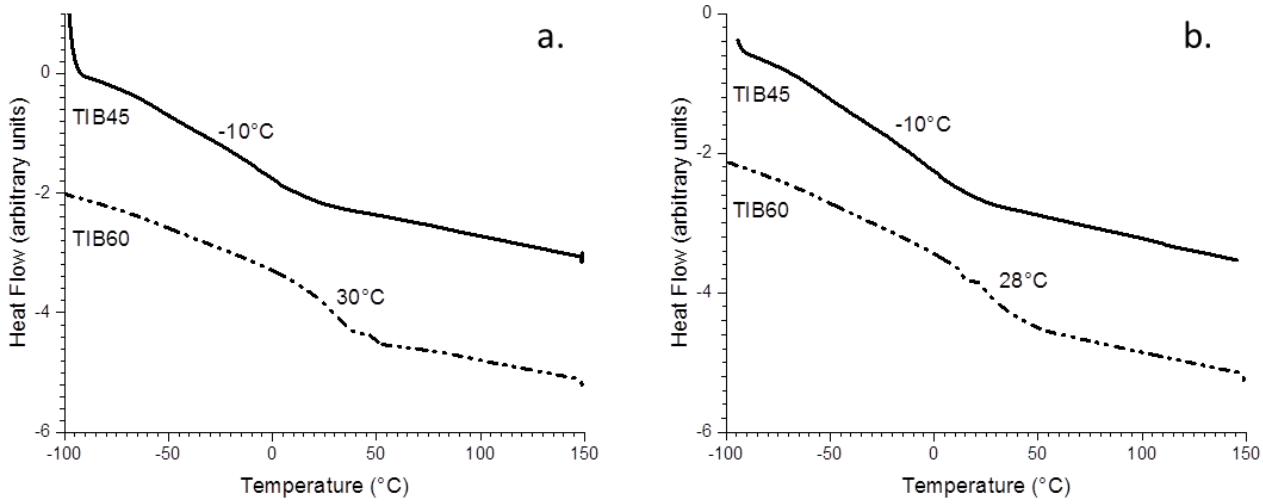

Figure 3.14: Differential Scanning Calorimetry of polyurethanes based on PTMEG, IPDI and BDO – a) first heating ramp performed at 20°C/min from -100°C to 150°C – b) second heating ramp performed at 20°C/min after a cooling at 20°C/min

In order to further characterize the thermal behavior, both series of PTMEG-based materials were tested with DMA. The obtained curves are presented in Figure 3.15 and 3.16, and some numerical values are reported in Table 3.8 for ease of reading purposes.

Table 3.8 : Summary of DMA results for the sample series based on PTMEG

Sample	T_α	25°C			T_α + 50°C		
	(°C)	G' (MPa)	G''(MPa)	tan δ	G'(MPa)	G''(MPa)	tan δ
TII45	60	91	23	0.25	-	-	-
TII60	100	553	32	0.06	-	-	-
TIB45	14	1.3	0.6	0.50	0.51	0.11	0.22
TIB60	43	128	50.3	0.39	0.38	0.12	0.34

Overall, the DMA results are consistent with the results obtained by DSC. Figure 3.15 presents the DMA curves of the isosorbide and PTMEG-based samples. The maximum of tan δ is highly dependent of the HS ratio for both series of samples, as was observed previously with T_g on the DSC curves. A well-defined glassy plateau and T_α are visible on all four curves. However, the rubbery plateau is not present for the isosorbide-based series TII45 and TII60, while TIB45 and TIB60 display a very short one. The isosorbide samples seem to immediately flow at the end of the α transition. It is very likely that the polymer chains of isosorbide-based materials do not form entanglements, thus inducing a lack of rubbery plateau [131]. Moreover, the T_α of sample TII45 is a lot higher than the -11°C supposed T_g on the DSC scans.

The tan δ curve of this sample also seems to display a secondary maximum around -35°C. This seems to support theory of a limited phase segregation in this sample, composed of a majority of HS/SS mix and a small amount of purer SS, with two weekly defined T_g on the DSC scan.

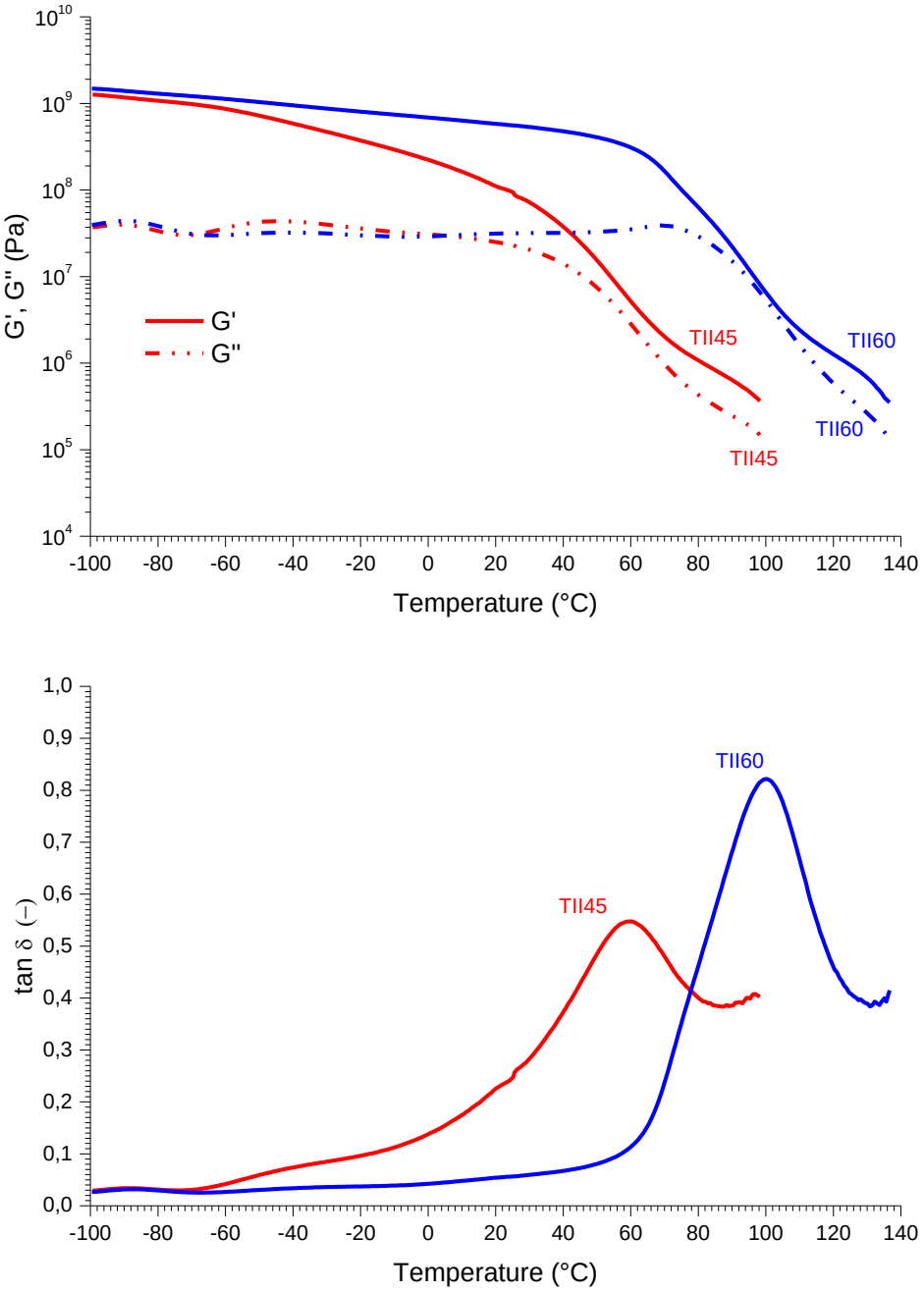

Figure 3.15: Dynamic Mechanical Analysis of PTMEG and ISO-based samples TII45 and TII60 at a frequency of 1 Hz and 0.1% strain, with a heating ramp of 3°C/min.

As the BDO-based model does display a short rubbery plateau and has a comparable molar mass to the ISO-based material, it seems likely that replacement of BDO by ISO also changes the space conformation of the polymer chains, thus inducing a decrease in entanglement density. This consideration can be further developed if one remembers that IPDI and ISO are both asymmetrical and nonplanar molecules likely inducing a coiled conformation of the

polymer chains. Wu *et al.* [132] demonstrated in 1992 that it was possible to predict the entanglement molar mass (that is, the molar mass of an entanglement strand between two adjacent entanglement junctions) from the chemical structure of polymers. This value can be extremely high (over 200 000 g.mol^{-1}, in some of Wu's examples) and thus can easily exceed the average molar mass of the polymer.

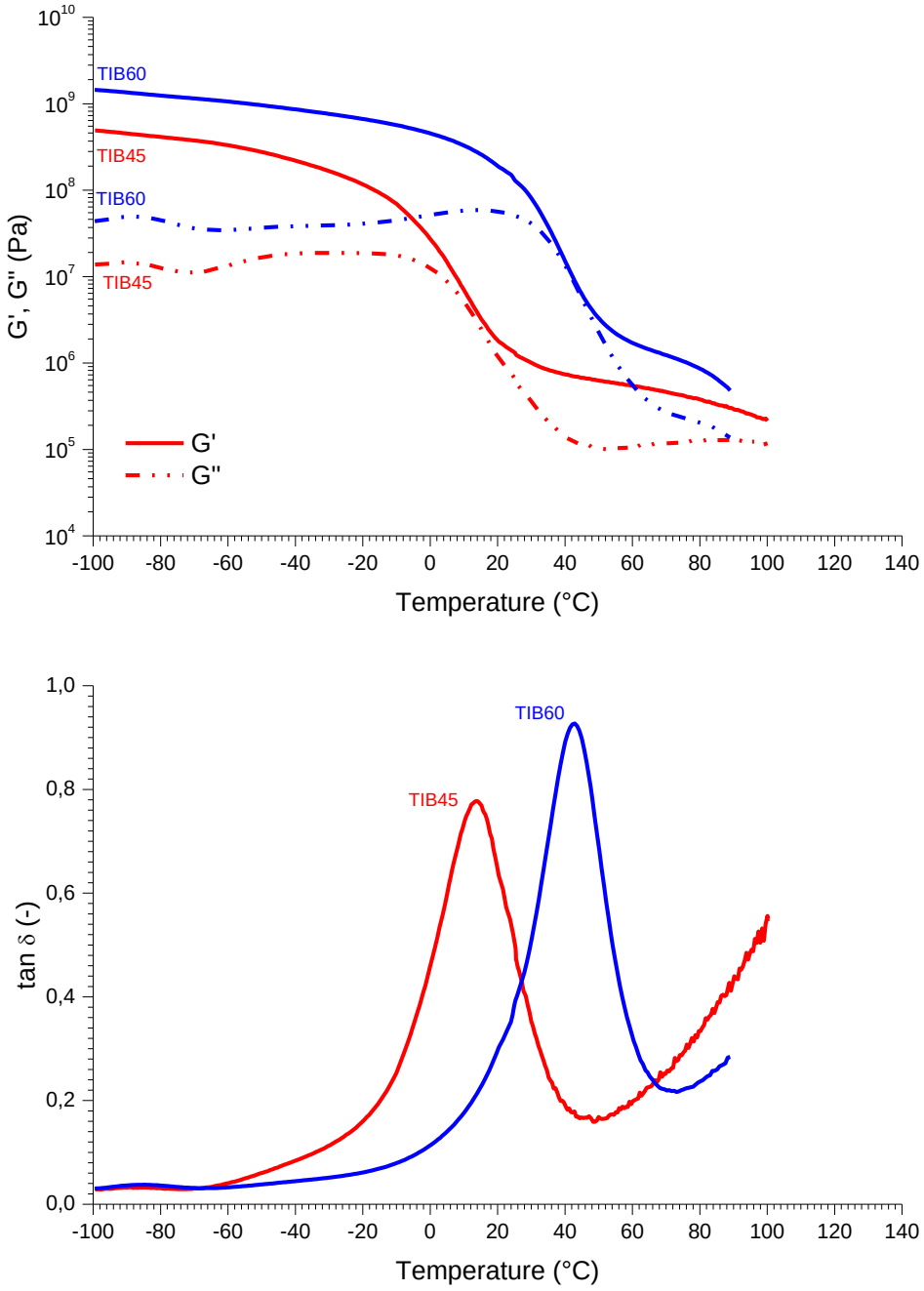

Figure 3.16: Dynamic Mechanical Analysis of PTMEG and BDO-based samples TIB45 and TIB60 at a frequency of 1 Hz and 0.1% strain, with a heating ramp of 3°C/min.

In summary, when associated with PTMEG, isosorbide/IPDI hard segments very poorly segregate, and a strong effect of the hard segment ratio could be observed on the glass transitions of the tested materials. The use of ISO in place of the classical BDO allowed to

raise the glass transition by 40°C in the case of the TII60 compared to TIB60. However, the lack of phase segregation and/or entanglements decreases their mechanical properties at temperatures over their T_g. They are very transparent and not colored, which could be very interesting for coating related applications.

3.3.2. Thermal behavior of samples based on FADM and IPDI

The DSC and DMA measurements carried out on the series of samples based on fatty acid dimer polyester oligomers are presented in Figure 3.17 to 3.20 and Table 3.9. The scans were carried out at 20°C/min from -100°C to 150°C, and two heating scans were carried out successively.

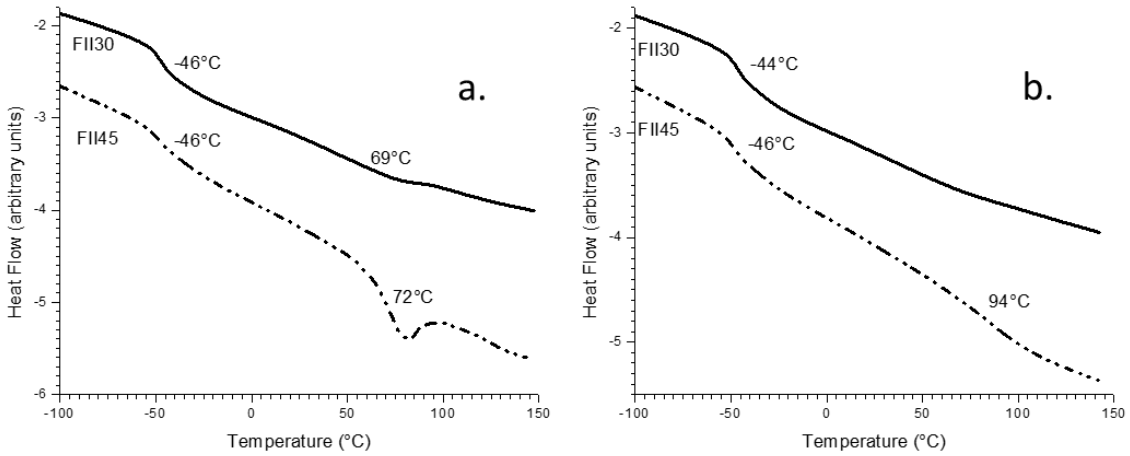

Figure 3.17: Differential Scanning Calorimetry of polyurethanes based on FADM, IPDI and ISO – a) first heating ramp performed at 20°C/min from -100°C to 150°C – b) second heating ramp performed at 20°C/min after a cooling at 20°C/min

From the first heating scans of the sample series based on ISO (Figure 3.17 a.), it is apparent that the TPUs based on FADM, IPDI and ISO display two glass transitions, with the second one being more defined for FII45. The effect of the HS ratio is minor between sample FII30 and FII45, with two very stable T_g as the HS ratio increases. The first T_g is around -46°C, which is the same as the soft phase domains T_g values obtained for the FMI series of samples in Chapter 2. This indicates that this sample series based on FADM and ISO displays phase segregation to some extent with a soft phase composed of FADM and a harder phase probably composed of a mix of SS and HS, as the value of the T_g attributed to IPDI/ISO-based HS is lower that the value measured on the pure hard segments at 121°C.

However, in the second heating scan (Figure 3.17 b.), the high T_g tends to spread on a very large temperature range, making it difficult to measure. This is the sign of a poorly stable phase segregation and homogenization of HS in the SS. However, it is to note that the soft phase T_g is still present and stable.

The exact same trend can be observed on the first and second heating scans of the BDO-based sample series (Figure 3.18). The soft phase T_g is overall a few degrees lower compared to the equivalent ISO-based samples. As expected, the T_g attributed to the BDO-based HS is lower than that of the ISO-based HS.

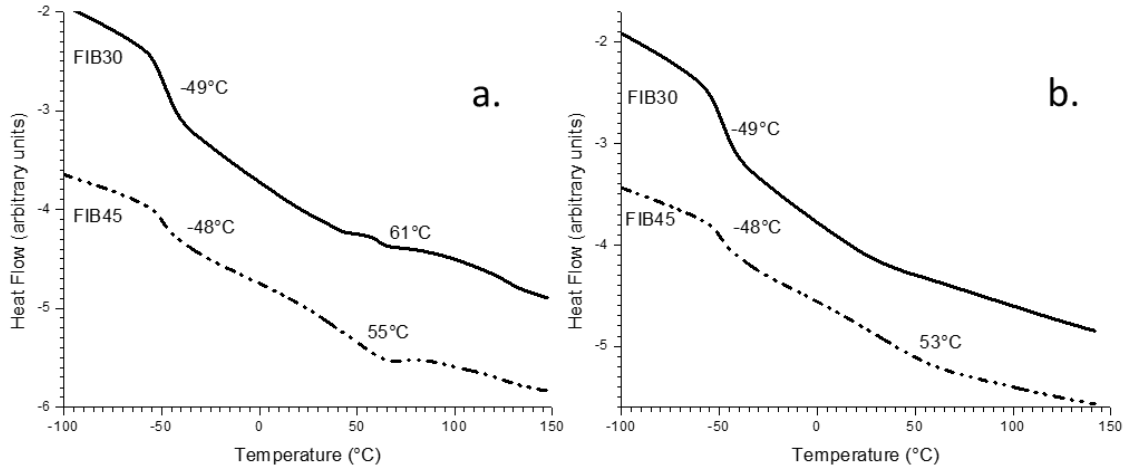

Figure 3.18: Differential Scanning Calorimetry of polyurethanes based on FADM, IPDI and BDO – a) first heating ramp performed at 20°C/min from -100°C to 150°C – b) second heating ramp performed at 20°C/min after a cooling at 20°C/min

However, this temperature is around 30°C higher than that measured at 24°C on the pure BDO/IPDI-based HS presented in 3.2.1, which could be due to the formation of very long HS.

In order to further characterize the thermal behavior, both series of PTMEG-based materials were tested with DMA. The obtained curves are presented in Figure 3.19 and 3.20, and some numerical values are reported in Table 3.9 for ease of reading purposes.

Table 3.9 : Summary of DMA results for the sample series based on FADM

Sample	T_α	25°C		T_α + 50°C	
	(°C)	G' (MPa)	tan δ	G'(MPa)	tan δ
FII30	-34	13	0.38	22	0.30
FII45	-28	161	0.12	173	0.11
FIB45	-27	39	0.32	43	0.30

Figure 3.19 presents the DMA curves of the isosorbide and FADM-based samples. As was expected from the DSC, the maximum of the tan δ depends only slightly on the HS ratio for both FII30 and FII45. The transition α was not visible for FIB30, as the sample was prone to

ambient temperature creep inducing flow temperature close to 0°C on DMA. No conclusion could be drawn on the BDO-based samples.

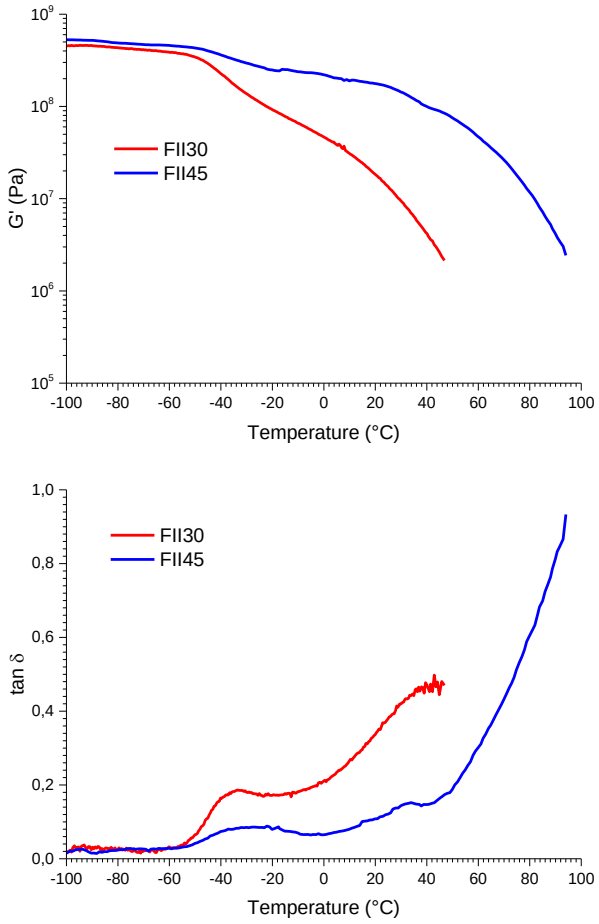

Figure 3.19: Dynamic Mechanical Analysis of FADM and ISO-based samples FII30 and FII45 at a frequency of 1 Hz and 0.1% strain, with a heating ramp of 3°C/min.

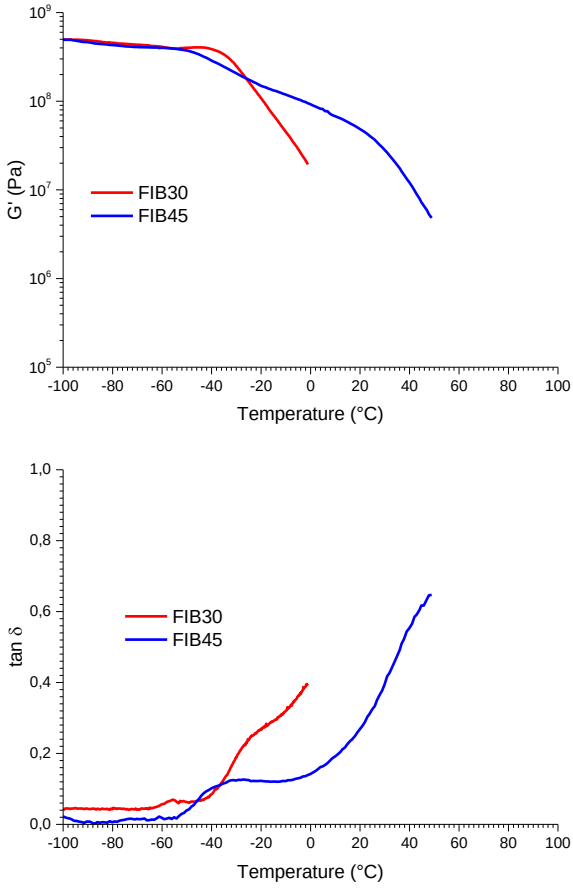

Figure 3.20: Dynamic Mechanical Analysis of FADM and ISO-based samples FIB30 and FIB45 at a frequency of 1 Hz and 0.1% strain, with a heating ramp of 3°C/min.

For both sample series however, there is no clear limit between the end of the transition α and the beginning of the flow limit. No clear rubbery plateau was observed as well, which can be due to lack of entanglements, as was explained in the previous section.

In summary, when associated with FADM, isosorbide/IPDI hard segments partially segregate. The use of ISO in place of the classical BDO allowed to raise the glass transition of the hard phase by 20°C in the case of the FII60 compared to FIB60. However, the lack of phase segregation and entanglements decreases their mechanical properties at temperatures over their T_g. They could however display interesting transparency while maintaining good mechanical properties if higher molar masses could be obtained.

3.3.3. Mechanical properties

Shore D hardness was measured on puck-shaped samples of 40 mm diameter and 10 mm thickness, with a manual shore D durometer from Zwick-Roell. It was determined as the

mean of fifteen measurements with a standard deviation of less than 5 units, spaced by at least 5 mm.

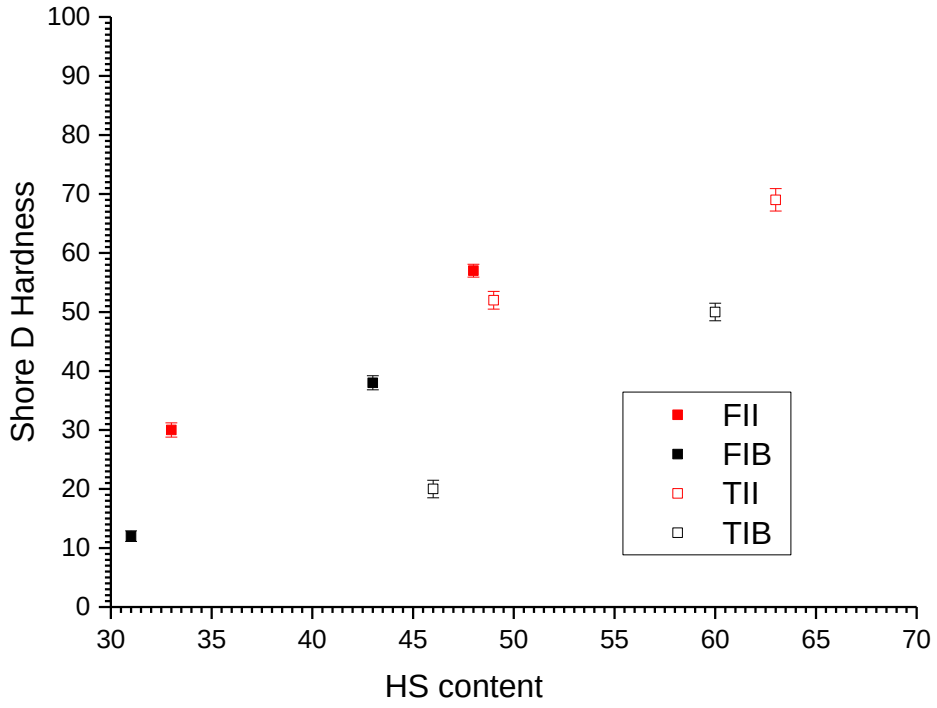

Figure 3.21: Shore D hardness as a function of HS content in wt% for samples based on IPDI at room temperature – standard deviation is presented as error bars on the data points.

Figure 3.21 presents the results as a function of the HS content. Overall, the sample series based on isosorbide display a clearly higher hardness than the equivalent BDO-based series (order of magnitude between 20 and 30 units), which is explained by the higher glass transition obtained with ISO-based samples and the higher T_g of the IPDI/ISO HS. This difference in hardness is more stable for the FII and FIB sample series which are the best separated samples in this study. In the TII and TIB case, the hardness difference between ISO and BDO chain extender depends more on the HS ratio. The FADM-based samples FII45 and FIB45 are also both harder than the PTMEG samples TII45 and TIB45 at equivalent HS ratio.

3.4. CONCLUSION

Several pure HS were synthesized in order to select a suitable combination of diisocyanate and chain extender. Isosorbide was chosen because it led to the highest T_g and its kinetics and chemistry were better known. Pure isosorbide was then successfully used as a chain extender in the synthesis of thermoplastic polyurethanes based on commercial macrodiols and IPDI. In a first step, the synthesis of the prepolymer based on PTMEG was carefully monitored to obtain the completion of the reaction of the macrodiols and the IPDI and to make sure the chain lengthening was controlled. In a second step, the prepolymers were chain extended with either ISO or BDO at varying HS content. Average molar masses between 16 $kg.mol^{-1}$ and 60 $kg.mol^{-1}$ were measured for ISO-based polyurethanes. HS content was shown to be as well a critical parameter in the final molar mass of the material.

The obtained thermoplastic polyurethane sample series were subsequently characterized by DSC and DMA. Measured T_g ranged from -49°C to 94°C. DSC revealed a lack of phase segregation for all tested samples based on PTMEG, while FADM-based samples displayed some phase segregation. Use of ISO also brought a large increase in the T_g of the PTMEG-based samples, and on the T_g of the mixed phase for FADM-based samples. The DMA measurement however revealed weak mechanical properties at temperatures over the T_g for all samples, which is supposed to originate from both lack of sufficient phase segregation and entanglements.

In conclusion, the use of isosorbide in IPDI polyurethane formulations was achieved. ISO was shown to enhance T_g, and phase segregation could be initiated by a careful choice of SS and HS combination. However, molar masses must be increased for the future assessment of the mechanical properties of such materials, by careful choice of catalyst and temperature of reaction.

CHAPTER 4:
POLYURETHANE COATINGS BASED ON ISOSORBIDE

Chapter 4. Polyurethane coatings based on isosorbide

3.1. INTRODUCTION

In this section will be presented the phenomena at the origin of the film formation in solvent borne coating systems as well as some building blocks and new solvents used for the preparation of isosorbide-based coated surfaces. A short review of the use of isosorbide in coating compositions will also be reported.

3.1.1. Film formation in solvent-borne polyurethane coating systems

In solvent-borne one component coating systems, two main phenomena are in competition. First, the monomers at the origin of the network formation react, thus gradually increasing the T_g of the material. Second, at the same time, the solvent gradually evaporates, thus increasing further the T_g of the coating by reduction of plasticizer concentration. As solvent also promotes reactant mobility, thus enabling higher conversion, those two phenomena are competing. Moreover, retained solvent will change mechanical properties of the resulting coating. The following section will review the available literature on the subject, as control of the rate of conversion and solvent evaporation is crucial for synthesis of solvent-borne coatings.

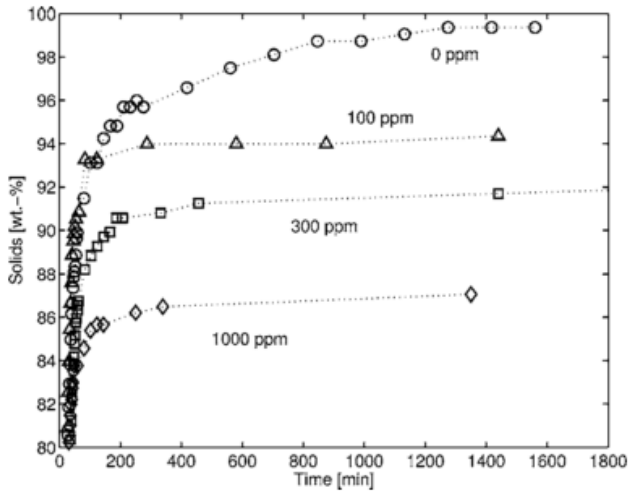

Figure 4.1: Weight loss in a polyurethane system of t-HDI and a tetra-hydroxyl-functionalized star oligomer of the type described in [133] **due to solvent loss, as a function of time and catalyst concentration, reproduced from** [134]**. Rate of reaction influences the solvent retention.**

The first study on this subject applied to polyurethane systems, was led by Dusek *et al.* in the 2000s [134]–[136]. They showed theoretically that as a polymer film is anisotropically deformed (due to cure as well as solvent evaporation), the vapor pressure of solvent over the film decreases, thus increasing solvent retention inside the film. This also means that faster conversion is expected to decrease solvent evaporation rate and increase its retention in the network [135], as can be seen in Figure 4.1.

They later completed this first theory by studying the theoretical influence of other parameters such as thermodynamics, cross-linking kinetics, solvent diffusivity, evaporation mode and network build-up on the vapor pressure of the solvent, and experimentally demonstrating some of them on cross-linked polyurethane model systems [134]. They were thus able to show that some solvent remained trapped in the film at long times, and that it was not dependent on the non-volatile fraction of the starting solution (i.e. the monomer concentration of the starting solution).

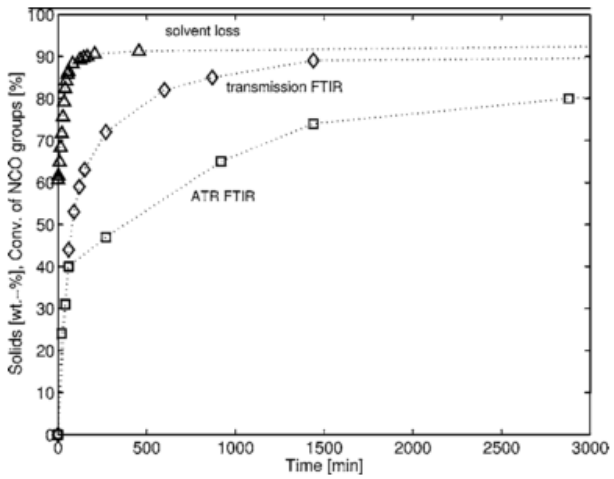

Figure 4.2: Conversion of the NCO groups in the file and the surface layer and weight loss due to solvent evaporation as a function of the time, reproduced from [134]

Moreover, study of the -NCO group conversion in the film and at the surface layer coupled to monitoring of the solvent evaporation, as shown in Figure 4.2., allowed for the description of the “skin” or “gradient” formation phenomenon.

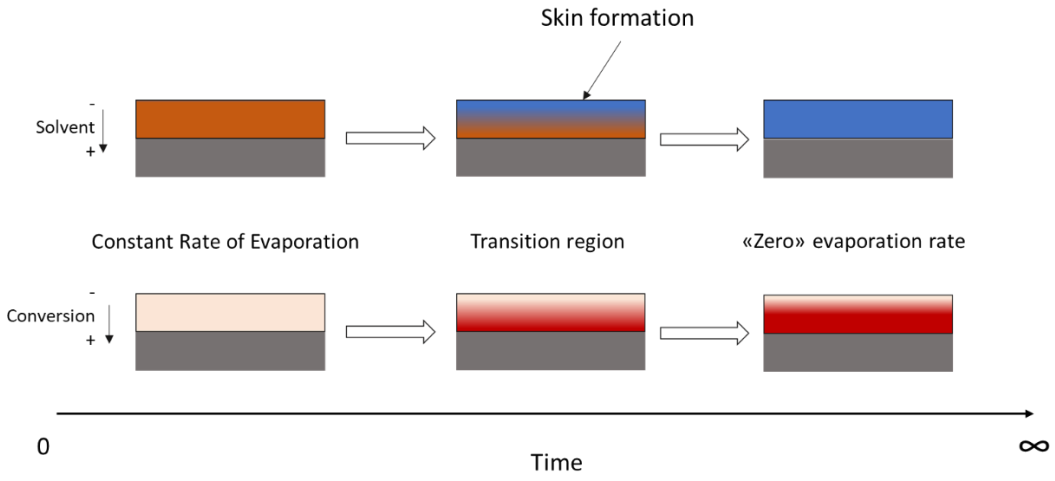

Figure 4.3 : Schematic representation of the gradient effect as a function of time.

As a matter of fact, evaporation and diffusivity rate of the solvent results in the formation of a glassy layer at the surface of the film and the formation of a gradient of solvent in the bulk of the film, as shown in Figure 4.3. The trapped solvent can be at the origin of various

defects such as bubbles, delamination or poor mechanical properties. This solvent gradient results in conversion gradient as well inside the film.

In 2003, they also showed that conversion (resulting in functional group consumption and increase in structure connectivity) could induce changes in solvent affinity toward the developing network, resulting in possible phase segregation in closed systems, depending on thermodynamic affinity of both solvent and network components [136]. However, they also showed that the increase in conversion increased solvent activity, meaning that the diffusion and evaporation rate increased along with conversion, assisting steady evaporation.

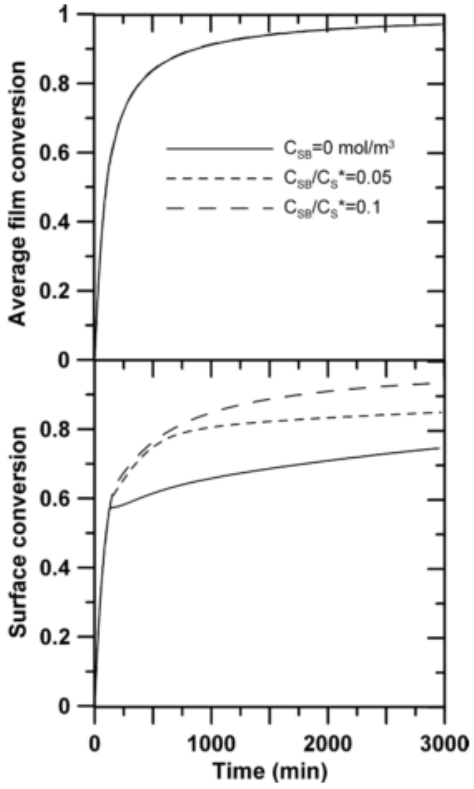

Figure 4.4 : Effect of solvent concentration in air on the average and surface conversion of a film, as a function of time, reproduced from [137]**, with C_{SB} the bulk air concentration of solvent, and C_S* the saturated vapor concentration of solvent in air**

Kiil *et al*. [137], [138] also modeled the simultaneous effect of conversion and solvent evaporation. They used principles demonstrated by the previous studies of Dusek et *al.* to predict solvent evaporation over time, effect on solvent concentration on the average conversion of the film and the conversion at the film surface, effect of solvent concentration on the gel time, and effect of initial film thickness on conversion. Their models were compared to the experimental data of Dusek and were shown to be in very good agreement. Lastly, they investigated the effect of wind velocity on solvent evaporation, film conversion and time to vitrification. They thus showed that higher solvent concentration in air (due to low wind velocity) resulted in longer drying time but increased film conversion at its surface.

Monaghan *et al*. [139] more recently demonstrated those same principles on a different polyurethane system, composed of a trifunctional aliphatic diisocyanate derivative (t-HDI) and a acrylate-styrene copolymer polyol [140]. They put in evidence three distinct phases in the solvent evaporation process by monitoring the modulus change of a paper substrate coated with the reacting solution, as shown in Figure 4.5. The first phase (1) is due to paper wetting, the second phase (2) is characterized by an increase in modulus linked to the solvent evaporation, while the modulus'increase found on phase (3) is mainly due to conversion. Even though they are quite remarkable, those results cannot be compared to those obtained on non-porous substrates.

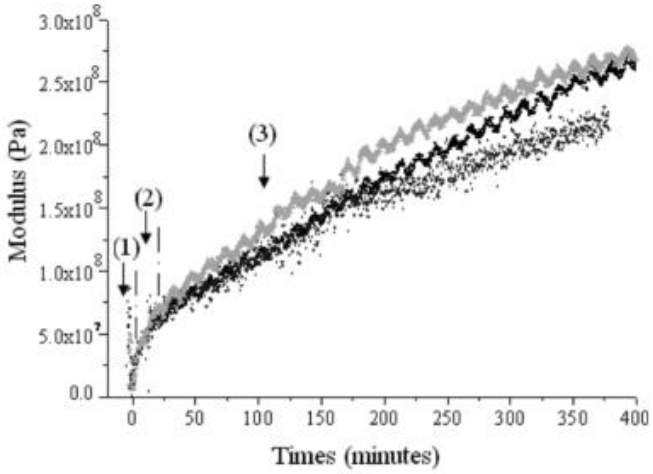

Figure 4.5: Modulus of a paper substrate coated with 2K polyurethane system mixture in ethyl acetate solvent, as a function of time, reproduced from [139]

By other techniques such as dielectric conductivity and DMA, they moreover showed that even if solvent type, concentration and rate of evaporation had an impact on the cure kinetics, for long post-cure times, the coating end-properties such as T_g, were very similar.

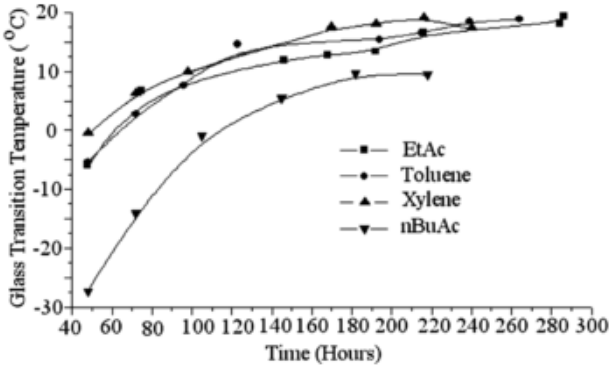

Figure 4.6: Glass transition temperature as a function of the post-cure time and solvent type. End-properties are very similar except for n-butyl acetate solvent which coating displays a lower T_g at long post-cure time, figure reproduced from [139]

Review of the literature on film formation for polyurethane coatings allowed to understand that the solvent evaporation rate is mainly dependent on thermodynamic affinity with the coating components, coating thickness, wind velocity and coating conversion. Conversion, on the other hand, is also impacted by solvent evaporation, coating thickness through skin formation, as well as solvent diffusivity as conversion increases. Interestingly, at long post-cure times, coatings reach a limit at which properties do not evolve further independently of the solvent type. However, the control of all the parameters at work in the film formation of coating is very complex and would require systematic study of each considered system.

3.1.2. Diisocyanate trimers

In order to impart functionality over 2 to common diisocyanates, diisocyanate oligomers are formed through the production of isocyanurate rings. Aliphatic diisocyanate trimers commonly found in industry are isophorone diisocyanate trimer (t-IPDI) and hexamethylene diisocyanate trimer (t-HDI) and mixes of those two components [1]. They impart increased crosslinking density to coating formulations, but it was also shown that they can improve flame retardancy [141], thermal and chemical resistance [142], film formation [143] and worker safety by reduction of volatile isocyanate fraction [144]. From their ring containing structures, IPDI and its trimer impart higher hardness and mechanical properties when used for polyurethane synthesis, however, they are not available from renewable sources. From a patent from Arco Chemical Technology [145] in 1997, trimerization of isophorone diisocyanate is obtained by homopolymerization at 85°C using an appropriate quaternary ammonium carboxylate catalyst, which controls the amount of higher oligomers such as penta- or heptamers in the final product. Commercial t-IPDI can thus contain up to 29 wt% of oligomers with functionality over 3, as was shown by Burel *et al.* [146].

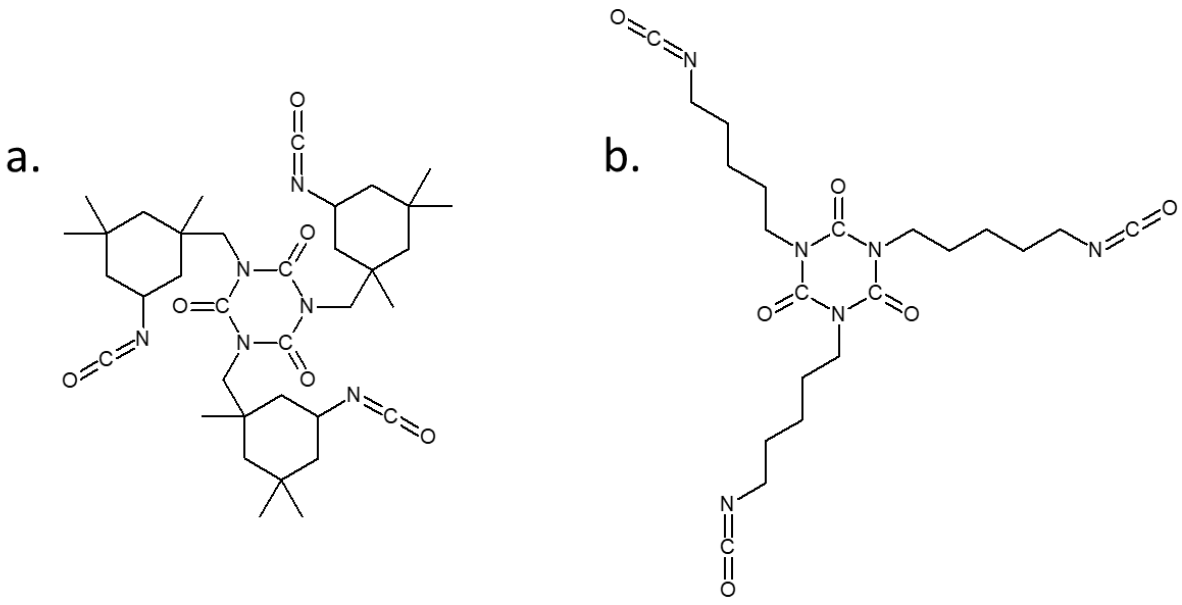

Figure 4.7: a. Example of a possible structure of isophorone diisocyanate trimer (t-IPDI) – b. Structure of the pentamethylene diisocyanate trimer (t-PMDI)

Very recently in 2016, Covestro launched the commercial production of a partially bio-sourced isocyanate building block called pentamethylene diisocyanate trimer (t-PMDI), which structure is presented in Figure 4.7. Pentamethylene diisocyanate is obtained by classical phosgenation of pentamethylene diamine, which can be produced by biochemical routes from biomass [147]. Pentamethylene diisocyanate trimer is then obtained similarly to isophorone diisocyanate trimer by homopolymerization with various quaternary ammonium carboxylate catalysts. Its structure is very close to that of t-HDI, which makes it a suitable bio-sourced substitute for t-HDI. Almost no example of its use for coating formulations is available to this date, it is nonetheless expected that t-PMDI will not impart high hardness compared to t-IPDI.

3.1.3. Isosorbide dimethyl ether (DMI)

Isosorbide dimethyl ether (DMI) is a solvent derived from isosorbide. Its structure is presented in Figure 4.8. It is a recently available green solvent [148] obtained from D-glucitol [149], [150]. It has a low volatility as its boiling point under standard conditions is comprised between 234 and 246°C (and 93-95°C under 0.1 mmHg [149]). Moreover it is nontoxic which makes it a very interesting solvent for pharmaceutical and cosmetic applications [151], [152].

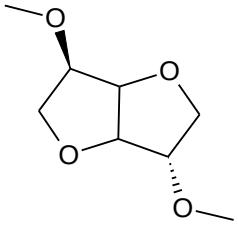

Figure 4.8: Structure of isosorbide dimethyl ether (DMI)

Very few examples of use in coating applications have been found. Durand *et al.* [153] studied its potential as a coalescent for water-borne paints and showed that it could be used in combination with other isosorbide derived ethers to control film formation kinetics and film quality. Some patents using DMI in coating formulations were as well reviewed. In a similar manner to Durand *et al.*, Rood *et al.* [154] included ethers derived from dianhydrohexitols as possible solvents for waterborne polyurethane coatings. In 2013, Messant *et al.* [155] designed a bio-sourced varnish used to prevent graffiti over urban infrastructures, and claimed DMI as a possible cleaning agent. In 2014, Nordstorm *et al.* [156] used DMI as a solvent for hardening nail varnish.

In summary, DMI is a very interesting prospective candidate for use in coating formulations as it is green and nontoxic. Moreover it can easily solubilize isosorbide and would be nonreactive in a urethane reaction. It hasn't ever been used to date for polyurethane coating formulations.

3.1.4. Use of isosorbide in coatings

A literature search was performed in order to obtain more insight into the integration of isosorbide in polymer coating formulations.

3.1.4.1. Vegetable oils-based and mercaptan-based coating systems

Use of isosorbide was reported in coating formulations with a high renewable content. Pan *et al.* [157] obtained a green coating by reacting a maleic anhydride and isosorbide-based dicarboxylic ester with an epoxidized sucrose ester of fatty acids (see Figure 4.9). Deposition on steel substrates was made through solvation in a mix of ethanol and water, thus further increasing bio-sourced content.

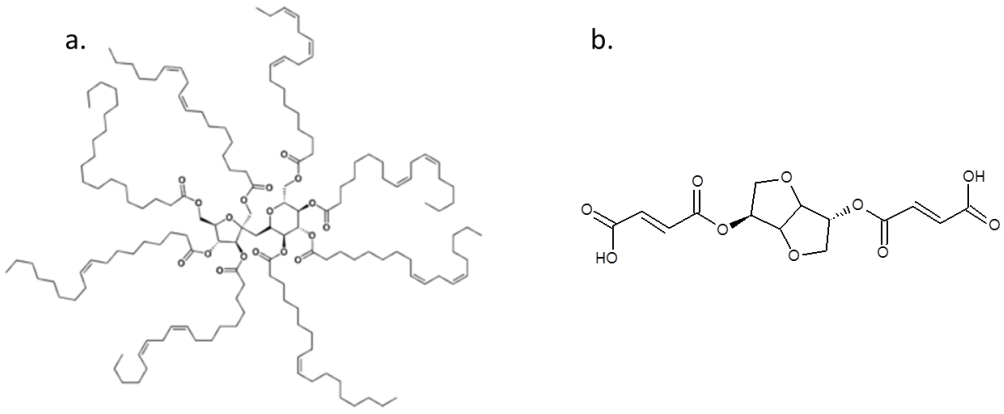

Figure 4.9: Structures of a. sucrose ester of fatty acids [158] **and b. isosorbide functionalized by maleic acid** [157]

Modjinou *et al.* [159] also functionalized isosorbide in order to photo-induce a thiol-ene reaction with mercaptan and terpenes derived from vegetable oils (see Figure 4.10). Isosorbide was thus functionalized with allyl bromide which allowed obtaining allyl terminations. Polymer networks were then synthesized by reaction of the allyl functions of the isosorbide derivatives and linalool with a trifunctional mercaptan. The coating synthesis was solvent-free and performed under very mild conditions, as it only required UV light and standard room conditions. The resulting cross-linked polymers were shown to possess antibacterial properties (preventing attachment and growth of bacterial colonies on surfaces) and glass transitions between -25°C and 0°C, which makes them attractive elastomers for pharmaceutical applications.

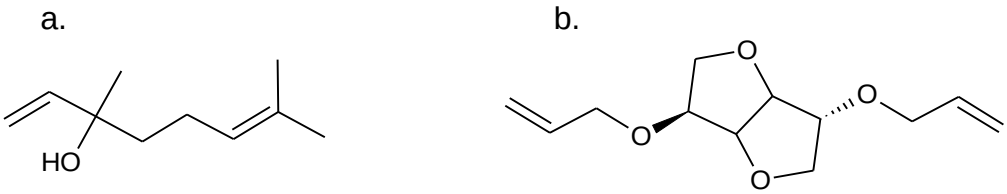

Figure 4.10: Structure of the allyl monomers used in [159] **- a. linalool is a terpene derived from essential oils – b. allyl-functionalized isosorbide**

In the same manner, Lorenzini *et al.* [160] used allyl-functionalized isosorbide, trifunctional mercaptan (also known as tri-thiol) and 2,2-dimethoxy-1,2-diphenylethan-1-one (DMTPA) to produce films and coatings. Some of the tested samples were as well filled with silver nanoparticles to enhance antimicrobial properties without hampering cell attachment. Finally, the obtained coatings displayed rubberlike properties and were thus judged appropriate for coating of rubber pharmaceutical devices such as catheter tubes.

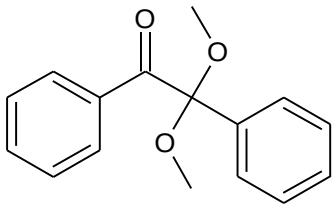

Figure 4.11: Structure of 2,2-dimethoxy-1,2-diphenylethan-1-one (DMTPA)

Similarly to what was seen in the literature screening for the use of ISO in linear TPUs, ISO is usually incorporated in green formulations. It is however very often modified.

3.1.4.2. Coatings based on oligomers containing isosorbide

Other examples of use of isosorbide for the synthesis of coatings include isosorbide-based oligomers. Gioia *et al.* in 2014 and 2016 studied the recycling of polycarbonate from Compact Discs (CD) [161] and the recycling of poly(ethylene terephthalate) (PET) [162].

In the case of polycarbonate (PC) recycling, the first step was to depolymerize PC through addition of ethylene carbonate and alcoholysis by isosorbide to both reduce average molar mass and functionalize the produced oligomers with hydroxyl chain-end functions (see Figure 4.12) intended for use in powder coating applications.

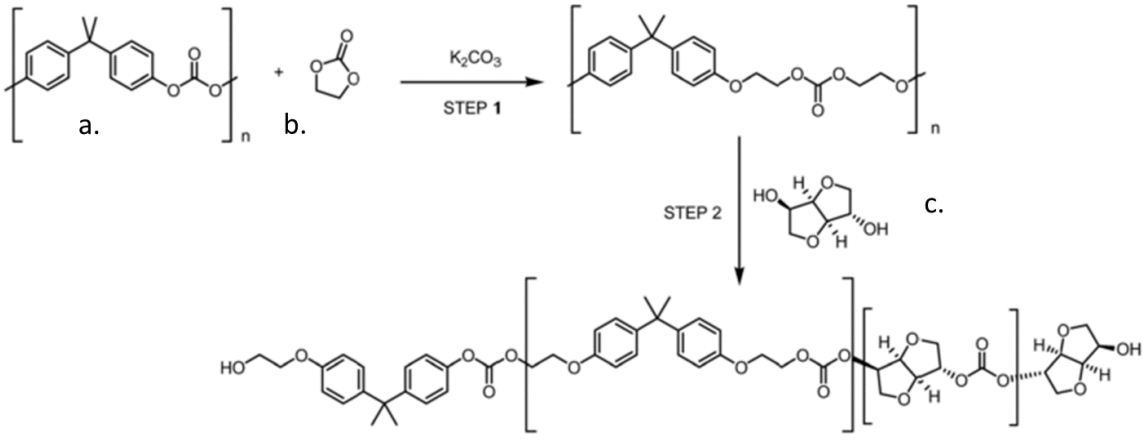

Figure 4.12: Synthesis of polycarbonate oligomers from a. Bisphenol A-based polycarbonate – b. Ethylene carbonate and c. Isosorbide from [161]

Powder coating precursors were also synthesized by Gioia *et al.* [162] through depolymerization of PET and reaction of the resulting adducts with both bio-sourced

isosorbide and succinic acid in order to produce polyester oligomers, as can be seen in Figure 4.13.

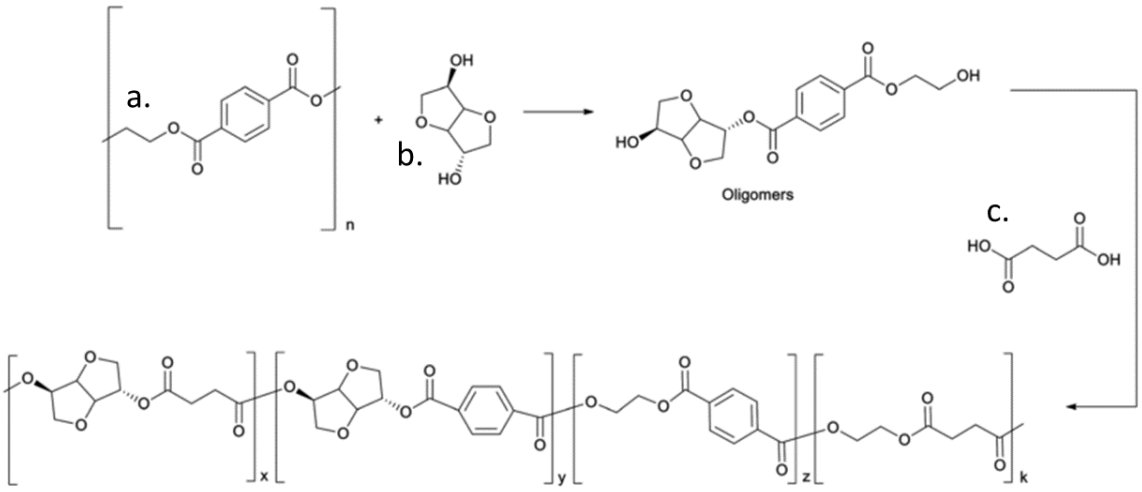

Figure 4.13: Synthesis route of polyester oligomers based on recycled PET (a.), isosorbide (b.) and succinic acid (c.) from [162]

Powder coatings were then obtained by reaction of the polyester oligomers with an epoxy hardener (exact composition was not disclosed by Gioia *et al*.). The resulting coatings displayed a good weatherability as well as high gloss.

A patent from Henkels & Holdings in 2016 [163] claimed the use of isosorbide for the synthesis of polyurethane-based methacrylate oligomers (see Figure 4.14) for coating and adhesives applications.

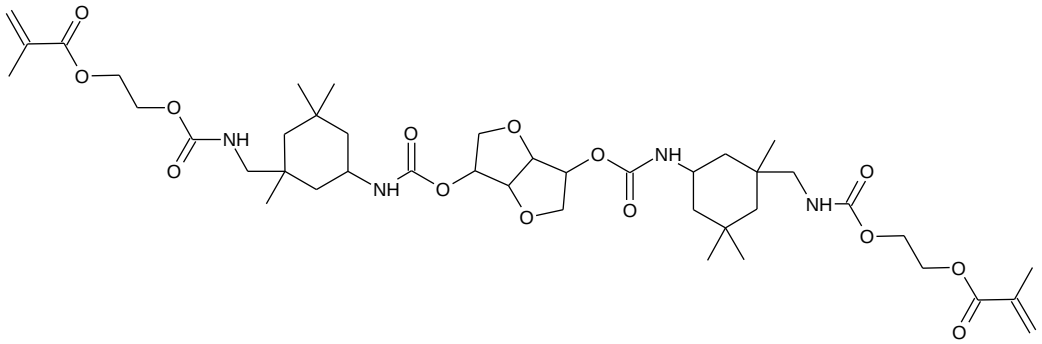

Figure 4.14: Example of IPDI and ISO-based methacrylate oligomer from [163]

Several examples have also been found that describe the reaction of various isosorbide-based hydroxyl-terminated oligomers with isocyanate hardeners such as diisocyanate trimers. In 2006 and 2011, Noordover *et al*. [164], [165] worked on polyester-urethane and polycarbonate-urethane networks for the synthesis of coatings. Oligo-polyesters based on isosorbide were obtained through reaction of isosorbide with succinic acid and a third monomer chosen among 2,3-butanediol, 1,3-propanediol or neopentyl glycol. The resulting linear oligomers were cross-linked by reaction with hexamethylene diisocyanate trimer (t-HDI) or isophorone diisocyanate trimer (t-IPDI), through a solvent borne deposition. The

coatings obtained were colorless and transparent and displayed better impact resistance as the molar mass of the oligomer increased due to the decrease in cross-link density. In the same fashion, oligocarbonates obtained from isosorbide were cross-linked with t-HDI and t-IPDI [165]. The polycarbonate oligomers were obtained through reaction of isosorbide and triphosgene (see Figure 4.15) and optionally a supplementary short alcohol chosen among 1,3-propanediol and glycerol.

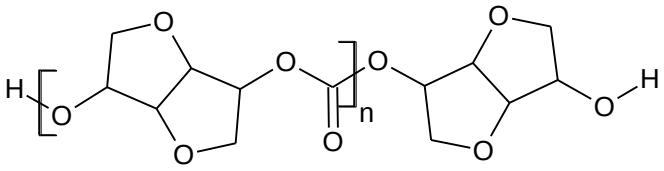

Figure 4.15: Example of structure obtained by reaction of isosorbide with triphosgene from [165]

The resulting polycarbonate-urethane coatings displayed good impact and solvent resistance and were additionally colorless and transparent.

Finally, polyester oligomers based on isosorbide and fatty acid dimers were also studied by Valspar Sourcing in a patent in 2011 [166]. The polyester was obtained by reaction of isosorbide, neopentyl glycol, ethylene glycol, fatty acid dimers and isophthalic acid. The resulting oligomers were cross-linked with isophorone diisocyanate trimer.

Isosorbide in coatings is mainly used as a component of the starting oligomers, however, scarce information was found on the intrinsic properties of the obtained coatings.

3.1.4.3. Isosorbide in waterborne polyurethane coating formulations

Only one patent mentioning the use of isosorbide in waterborne formulation was found. It is from Stichting Dutch Polymer Institute [167] and demonstrates the synthesis of polyurethane films based on isosorbide, DMPA and either DDI or lysine diisocyanate methyl ester (see Figure 4.16).

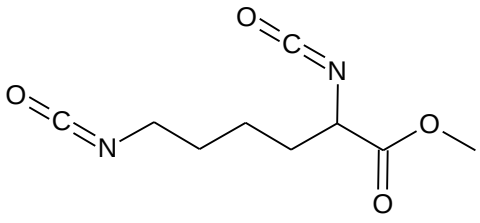

Figure 4.16: Structure of lysine diisocyanate methyl ester

Unfortunately, no information about the resulting coatings and films properties were reported.

3.1.4.4. Solvent borne polyurethane coatings containing isosorbide

One example reporting the use of isosorbide in solvent borne coatings was found. Patent [168] from 2016 owned by Nitto Denko illustrates adhesive compositions intended for

wound dressings. They invented acrylate compositions containing isosorbide, but also isosorbide-based polyurethane coatings. The formulations were based on a fatty acid dimer-based polyester similar to FADM, isosorbide and t-HDI. Their solvent of choice was a nontoxic and biocompatible diester of isosorbide (see Figure 4.17), it was also partly used as a plasticizer.

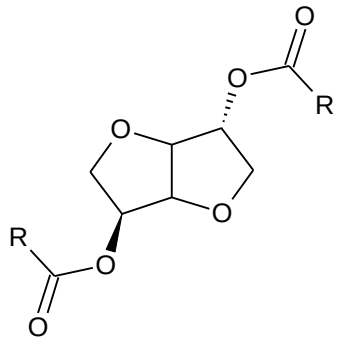

Figure 4.17: Example of isosorbide diester structure, with R being a linear carbon-based chain

Tested properties were skin adhesion and release of active substances comprised in the polyurethane coating.

3.1.5. Choice of a suitable formulation for use as a base for polyurethane coating formulations

It was chosen to work with one of the formulation studied in Chapter 3, based on the aliphatic IPDI, in order to design coating formulations. First of all, phase segregation is not desired for a clear coating synthesis, as it could hinder curing and induce opacity. As such, FADM-based formulations cannot be retained as they clearly showed phase segregation. The choice of one of the PTMEG-based formulations also has the advantage of getting an already clear and colorless material.

Poor mechanical properties of the IPDI-based materials will be enhanced by the incorporation of a diisocyanate trimer to obtain a PU thermoset material. The higher T_g brought by the use of ISO as a chain extender could allow to use smaller ratio of hard segments in the formulations. TII60 displayed a T_g of 70°C, and was then outside its rubbery state at room temperature and would then become very brittle after addition of a cross-linker. It was thus chosen to use TII45 as a base for the formulation of coatings with a target glass transition temperature between 60°C and 80°C.

3.1.6. Conclusion

The literature review allowed to obtain insight into the parameters influencing film formation in polyurethanes as well as the state of the art of the isosorbide integration in polyurethane coatings.

Isosorbide was integrated in various formulations ranging from powder to solvent borne coatings with a high content of renewable components. It seems moreover interesting to

note that the examples cited previously always integrated isosorbide with modifications either to change the type of reacting functions or to integrate it in oligomers. This means that the use of modified isosorbide could increase the carbon footprint due to the addition of synthesis steps. This seems counterintuitive to the need of producing renewable coatings.

This chapter will thus explore the synthesis of polyurethane coatings using pure unmodified isosorbide, and its impact on properties by comparison with 1,4-butanediol. Partially bio-sourced isocyanate trimers and a non-toxic solvent will also be used in order to increase renewable content.

Synthesis of transparent thermosetting coating for steel substrates, from a IPDI and ISO-based formulation chosen from those of Chapter 3, which should display minimal phase segregation, will be performed. Cross-links will be brought by replacement of some of the -NCO functions of the IPDI by -NCO functions from diisocyanate trimers, being either isophorone diisocyanate trimer or pentamethylene diisocyanate trimer. Homogenization method, film formation and cure will be explored and optimized. Solvent will be chosen as to minimize occupational toxicity. Effect of isosorbide on the coating properties will be compared to more classical 1,4-butanediol chain extender. This chapter will thus contain:

- Characterizations of the starting reactants
- A short study of the critical synthesis and film formation parameters: miscibility of components, choice of a suitable solvent, control of substrate wettability and cratering
- Optimization of the cure cycle in terms of reaction conversion, coating coloration, solvent evaporation and monomer stability
- Following this work on synthesis process, the study of 8 thermosetting polyurethane formulations based on a linear PTMEG/IPDI/ISO 1:3:2
- Characterization of the obtained coatings: glass transition temperature measurements and mechanical properties

3.2. SYNTHESIS OF POLYURETHANE COATINGS

This section focuses on the synthesis of cross-linked coatings using first extrusion, and then a solvent borne method. Critical parameters were surveyed in order to design a reliable procedure allowing the production of samples of known composition, defect-free surface for mechanical testing and a controlled cure. This section is not a systematic study of critical parameters at play in the synthesis of such coatings.

3.2.1. Substrates

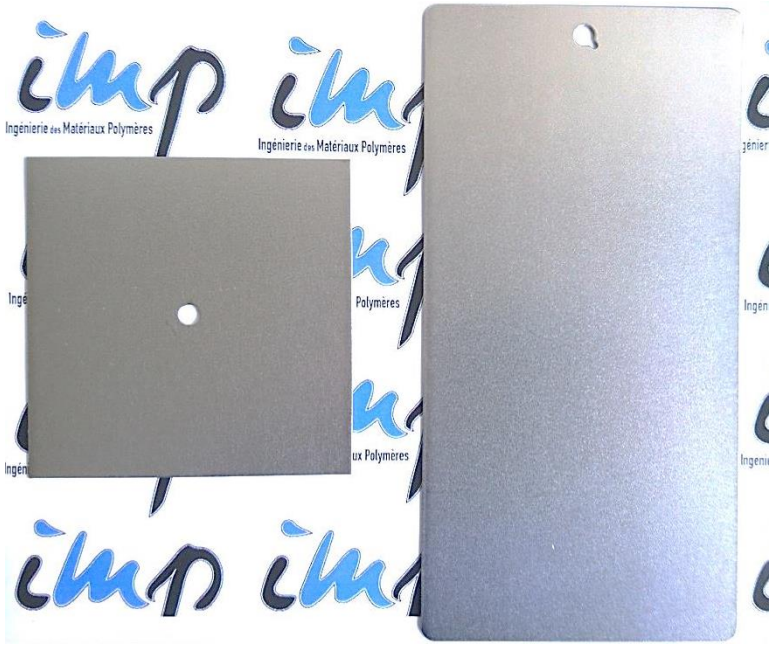

Figure 4.18: Q-Panel steel substrates chosen as the support for film deposition – Left: abrasion sample panel R-44-T type – Right: Panel used for all other characterization R-48 type

The chosen substrates were steel panel purchased from Q-Lab, and are shown in Figure 4.18. Their surface finish is matte and follows ISO 1514 standards for roughness and surface finish. The samples were either deposited on panels of dimensions 0.8x102x203 mm, and pierced 0.8x102x102 mm substrates specifically designed to be used with a Taber abrader.

3.2.2. Miscibility of components

One thermoplastic TPU formulation based on IPDI called TII30 was chosen from Chapter 3 as a base for coating formulations, as it displayed minimal phase segregation. The tests of section 4.2. for determination of synthesis method and deposition parameters were carried on using PTMEG 1000 or 650. This is indicated at the beginning of each section in the part related to the test condictions. However, the starting monomers are not all miscible, which means that a homogenization method must be found. Table 4.1 reports the miscibility of all building blocks used in this work. Miscibility tests were carried out at 80°C to ensure that all building blocks were in the liquid state. It is apparent that the hydroxy-terminated

components such as PTMEG, ISO and BDO are miscible. The same statement can be made for the –NCO terminated components as IPDI, t-IPDI and t-PMDI are miscible. However, those two types of building blocks are not miscible.

Table 4.1 : Miscibility of monomers and components of the coating formulations

Monomers	Physical state in standard conditions	Miscibility (yes : x / no : o)				
		PTMEG	ISO	BDO	IPDI	t-IPDI
PTMEG	Viscous liquid	X	X	X	O	O
Isosorbide	Crystalline pellets	X	X	X	O	O
1,4-Butanediol	Liquid	X	X	X	O	O
IPDI	Liquid	O	O	O	X	X
t-IPDI	Amorphous pellets	O	O	O	X	X
t-PMDI	Viscous liquid	O	O	O	X	X

In order to obtain a good conversion, it is required to homogenize the reacting mixture. Several methods will be tested in the following sections, such as reactive extrusion and solvation.

3.2.3. Reactive extrusion tests

Homogenization can be obtained by reaction of the monomers, with the same procedure used for the synthesis of thermoplastic polyurethanes in the previous chapters. However, since t-IPDI is an amorphous thermoplastic with a T_g of 72°C, mechanical stirring in a reactor is too weak to obtain a good mixing of the components. It was then chosen to first study the formation of cross-linked polymers by partial reaction of the components in a micro-extruder leading to homogenization followed by curing in a stove. This procedure is close to the synthesis process used to obtain powder coatings.

3.2.3.1. Preliminary exploration of the synthesis

Table 4.2 presents the composition of the sample series synthesized by micro-extrusion process. No catalyst was used in order to slow the reaction, as the extruder could become clogged by the cross-linked polymer at high conversion and become very difficult to clean. The extruder was heated at 110°C, with twin screws speed set at 100 rpm. The building blocks were then weighed and introduced in the barrel. The reaction was left to proceed in circulation mode for 30 min, as which point the polymer was extruded and put in aluminum

plates or silicon molds. Reaction was then carried out for 20 h in a stove at 110°C under vacuum (it was noticed that air presence resulted in yellowing of the exposed sample surfaces). PTMEG 1000 (M_n around 1000 $g.mol^{-1}$) was used for those extrusion tests.

Table 4.2: Compositions of cross-linked sample series synthesized by a one-shot procedure, based on PTMEG/IPDI/ISO 1 :3 :2 formulation. –NCO functions from IPDI were progressively replaced by –NCO functions from t-IPDI

Sample name	Mass (g)			
	PTMEG 1000	IPDI	t-IPDI	Isosorbide
0% t-IPDI	7.7	5.1	0	2.2
50% t-IPDI	6.4	2.2	4.6	1.8
100% t-IPDI	5.6	0	7.9	1.6

Figure 4.19: Clog of t-IPDI on one of the screws

It is however probable that the stoichiometry of the mix was not properly achieved because a clog of partially melted t-IPDI formed at the beginning of the screws, which prevented a proper integration of all the t-IPDI in the mixing zone as illustrated by Figure 4.19.

DSC scans where performed on the resulting samples, and the first heating scans are presented in Figure 4.20**.** It was immediately apparent that the reaction conversion under those conditions is not optimal: a large exothermic peak is present on the three curves between 100 and 230°C. The curves can be compared to sample TII30 which is the two-step thermoplastic sample used as a basis for the synthesis of the extruded samples. However, the curves of the extruded samples do not display any distinguishable glass transition. Sample 0%-IPDI which is similar to TII30 but obtained in a one shot procedure seems to display a T_g around 37°C, but no clear conclusion can be drawn.

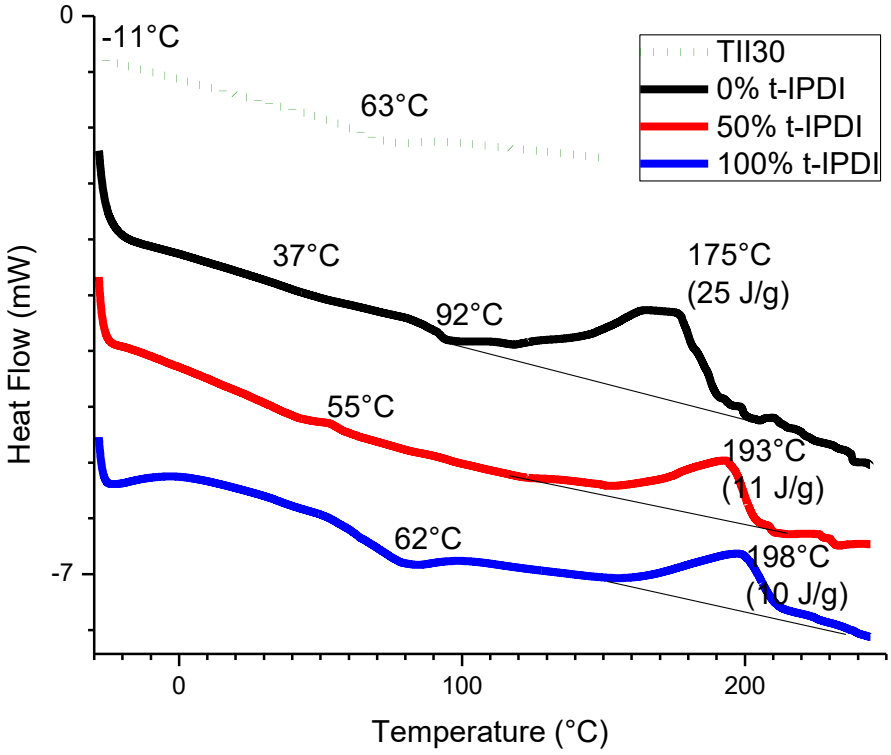

Figure 4.20: DSC heating scans (20°C/min) from -30 to 250°C of cross-linked sample series based on PTMEG/IPDI/ISO 1:3:2 formulations, with t-IPDI as the cross-linker

Table 4.3 : Infrared bands attribution in sample 50%-t-IPDI

Wavenumber (cm^{-1})	Functional groups
3329	-NH from polyurethane
2944	CH_2 asymmetrical elongation
2857	CH_2 symmetrical elongation
2262	free -NCO

This conclusion was confirmed by FT-IR measurements, presented in Figure 4.21, in which the –NCO peak is still present and displays a high absorbance. This proves that a lot of the isocyanate functions have not reacted. As such, the measured T_g are not relevant since the system is not completely reacted, even in the case of the linear system. Even though, the addition of IPDI trimer resulted in a 55°C increase of the T_g in the case of the sample 100% t-IPDI compared to sample TII45 from Chapter 3. It was however necessary to increase the curing temperature in order to obtain a better conversion, preferably in the range of 140°C to 180°C as the onset of the exotherm peak was found in this temperature range.

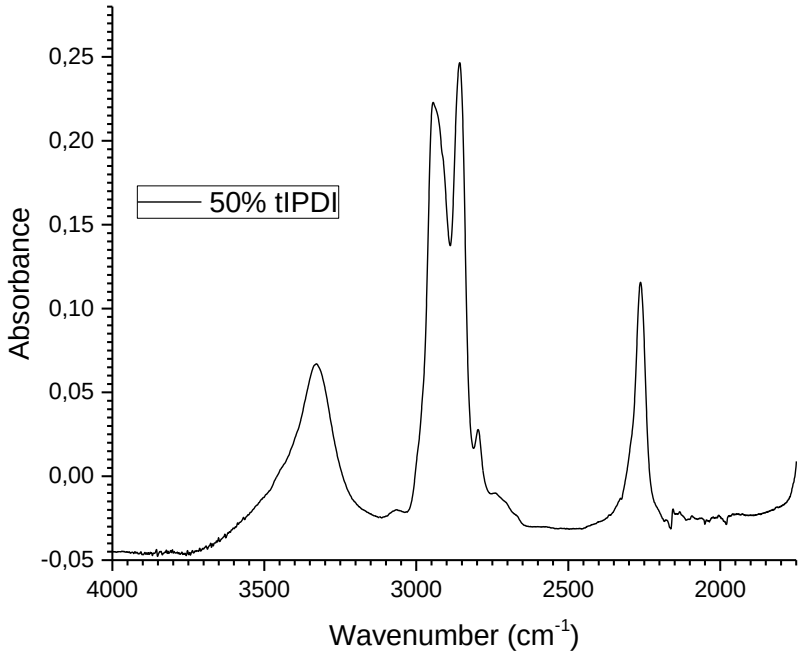

Figure 4.21: FT-IR ATR mode spectra measured on the 50%-t-IPDI sample

3.2.3.2. Reduction of trimer ratio

Table 4.4 presents the composition of the sample series synthesized by micro-extrusion process. No catalyst was used. The extruder was heated at 110°C, with twin screws speed set at 100 rpm. The building blocks were then weighed and introduced in the barrel. The reaction was left to proceed in circulation mode for 30 min, as which point the polymer was extruded and put in aluminum plates or silicon molds. Reaction was then carried out for 3 h in a stove at 160°C under vacuum. Smaller amounts of IPDI trimer were introduced in a TII30 formulation in order to retain the flexibility of the materials while still improving its thermal resistance, as such PTMEG 1000 was used in these tests.

Table 4.4 : Compositions of cross-linked sample series synthesized by a one-shot procedure, based on PTMEG/IPDI/ISO 1 :3 :2 formulation. –NCO functions from IPDI were replaced by –NCO functions from t-IPDI

Sample name	Mass (g)			
	PTMEG 1000	**IPDI**	**t-IPDI**	**Isosorbide**
10% t-IPDI	7.4	4.4	1.0	2.1
20% t-IPDI	7.1	3.8	2.0	2.0

DSC scans where performed on the resulting samples, and the first heating scans are presented in Figure 4.22**.** No exothermic peaks were present, which indicated that a better conversion of the reaction was reached. This was confirmed by FT-IR spectrometry,

presented in Figure 4.23**.** Indeed, there is no isocyanate peak remaining at 2260 cm^{-1}, and the shoulder of the –OH peak is not visible in the NH peak.

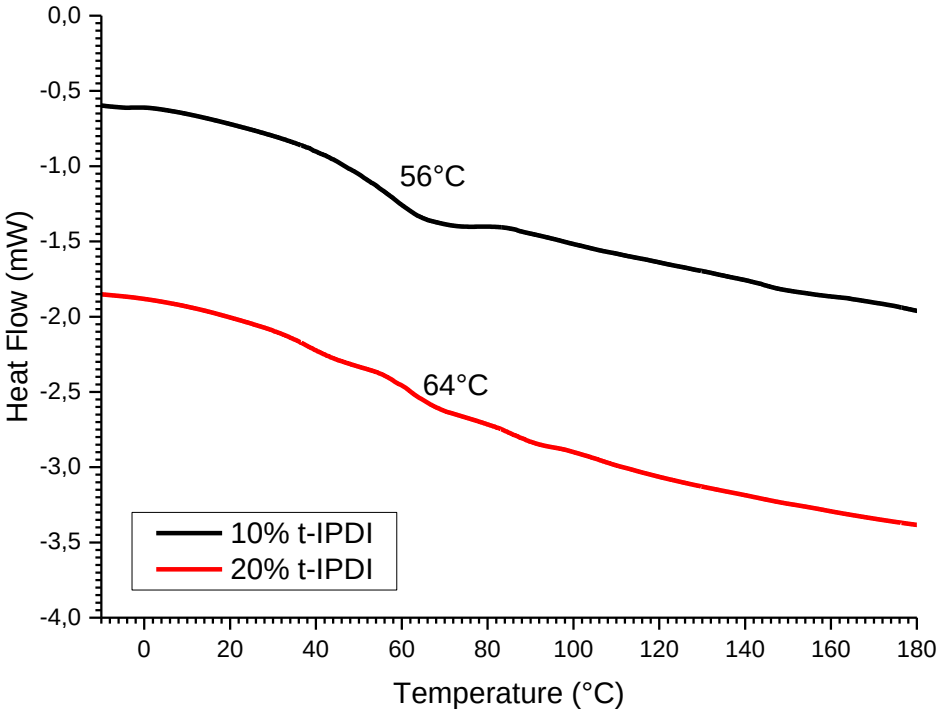

Figure 4.22 : DSC heating scans (20°C/min) from -30 to 200°C of cross-linked sample series based on PTMEG/IPDI/ISO 1:3:2 formulations, with t-IPDI as the cross-linker

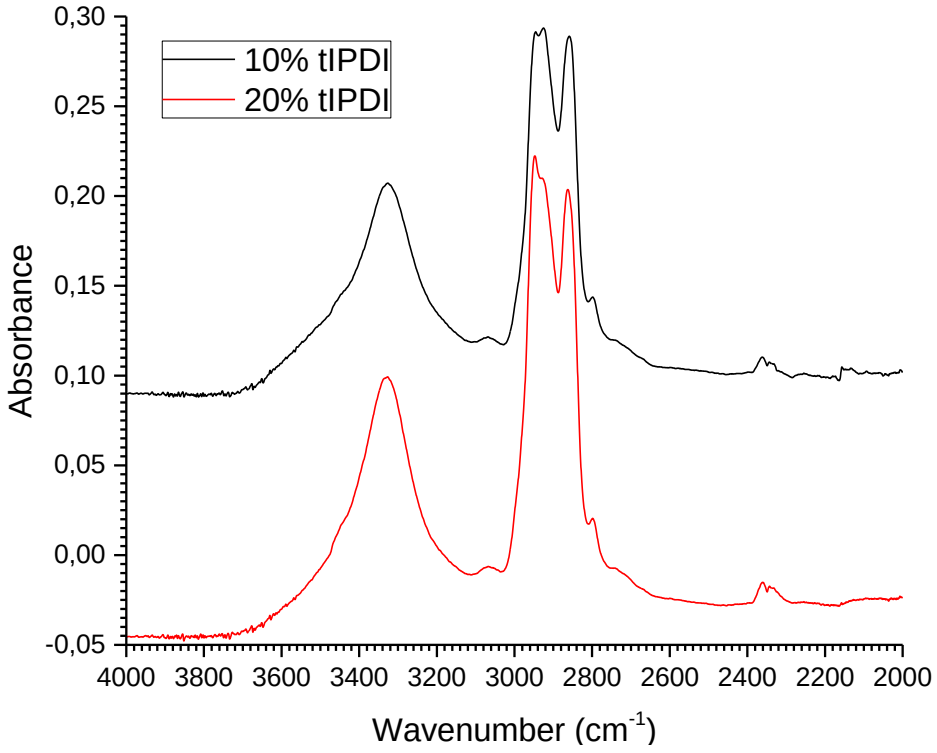

Figure 4.23 : FT-IR ATR mode spectra measured on sample 10%-t-IPDI and 20%-t-IPDI samples

Table 4.5 : Infrared bands attribution in sample 10%-t-IPDI and 20%-t-IPDI

Wavenumber (cm^{-1})	Functional groups
3327	-NH from polyurethane
2935	CH_2 asymmetrical elongation
2861	CH_2 symmetrical elongation
2340-2360	CO_2

Higher conversions also allowed obtaining T_g of the same order of magnitude as what was measured in the previous section for 100% t-IPDI, however with a greatly reduced ratio of cross-linker.

Table 4.6 : Summary of DMA results for the sample series based on cross-linked PTMEG/IPDI/ISO 1:3:2 formulation

Sample	**T_α**	**25°C**			**T_α + 50°C**		
	(°C)	**G' (MPa)**	**G''(MPa)**	**tan δ**	**G'(MPa)**	**G''(MPa)**	**tan δ**
10% t-IPDI	100	70	6.3	0.09	0.1	0.02	0.02
20% t-IPDI	108	93	6.4	0.07	3.9	0.2	0.05

In order to assess the effect of the cross-linker presence on the thermal resistance, DMA was performed on samples 10% t-IPDI and 20% t-IPDI. Results are presented in Table 4.6 and Figure 4.24**.**

The curves display a well-defined α transition as well as a long rubber plateau for both samples. As expected, the temperature of the α transition is a few degrees higher in the case of the 20%-t-IPDI sample.

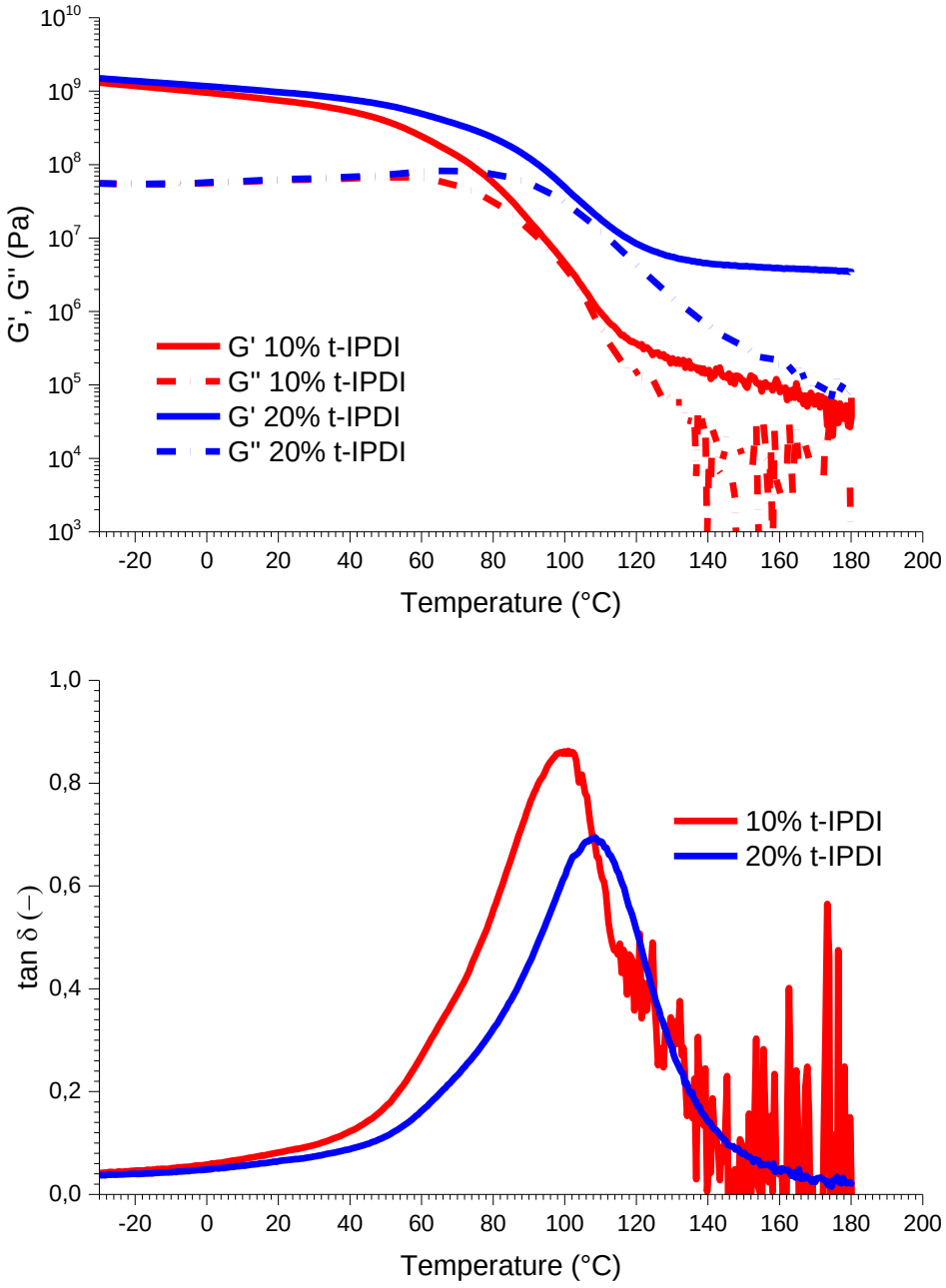

Figure 4.24: DMA heating scan from -30 to 180°C at 3°C/min C of cross-linked sample series based on PTMEG/IPDI/ISO 1:3:2 formulations, with t-IPDI as the cross-linker

In light of the results obtained with reactive extrusion, it was chosen to test coating formulations containing a maximum of 20% t-IPDI. However, the synthesis process carried out in the micro-extruder with 15 g batches did not allow to obtain highly accurate stoichiometry, as up to 2 g of trimer could be lost due to clogging. In order to obtain the accurate stoichiometry necessary for a meaningful review of the impact of isosorbide on such materials, it was thus chosen to design a solvent-borne deposition and synthesis for the isosorbide and IPDI-based coatings.

3.2.4. Choice of a suitable solvent for solvent borne coatings

A second choice to induce homogenization in the unreacted monomer mixture was to use a solvent. However, solvents are often a critical parameter for coating formulations as they can be expensive and harmful to both operator during processing and end-user in the event that some solvent is still present in the finished product.

Solvents type and concentration also allow controlling the viscosity and the wettability of the coating over the chosen substrate during deposition. Ideally, they must be totally evaporated at the end of the cure.

Table 4.7: Summary of tested solvent properties, isosorbide solubility and toxicity

Solvent	Type	Isosorbide solubility	Boiling point	Toxicity
		Yes (x)/no (o)	°C (760 mmHg)	
Acetone	Polar, aprotic	x	56	Irritant
Tetrahydrofuran (THF)	Polar, aprotic	x	66	Irritant, carcinogen
Butan-2-one (MEK)	Polar, aprotic	x	80	Irritant
1,4-Dioxane	Non-polar, aprotic	x	100	Irritant, carcinogen
Methylisobutylketone (MIBK)	Polar, aprotic	o	116	Irritant
Cyclopentanone (CPK)	Polar, aprotic	x	130	Irritant
Isosorbide dimethylether (DMI)	Non-polar, aprotic	x	234	Non-harmful
Dimethylsulfoxide (DMSO)	Polar, aprotic	x	191	Non-harmful

Isosorbide is soluble in most alcoholic solvents such as methanol, ethanol, isopropanol, etc. It is also very soluble in water. Obviously, those solvents cannot be used for the synthesis of polyurethanes through isocyanate route. Some results of the solubility tests carried out on isosorbide are presented in Table 4.7. ISO is thus soluble in very small molar mass ketones

and generally polar solvents. Notable exceptions are 1,4-dioxane and DMI that are non-polar. All other building blocks were soluble in the solvents presented in Table 4.7.

Butane-2-one, cyclopentanone and DMI were chosen as suitable candidates, as they were at least non-CMR (ideally being non-harmful), miscible with ISO and all the other monomers used in this chapter.

Curing tests as a function of the solvent were carried out on a coating formulation stoichiometry 1:3.05:2. The –NCO functions were brought by 80% from IPDI and 20% from t-PMDI. The diols were PTMEG 650 (as the trimer is t-PMDI, it was expected to lower the final T_g in comparison to t-IPDI, and therefore PTMEG 650 was preferred over PTMEG 1000 in first intention) as the soft segment, and ISO as the chain extender. DBTDL was used in order to fasten the reaction. The mass of building blocks and of the solvent used for the synthesis are reported in Table 4.8. The solution contained 25 wt% solvent. As the boiling point of the solvent used is high, it was preferred to work with a highly concentrated solution in order to be able to evaporate it all at the end of the curing cycle to avoid a plasticizing effect. Moreover, as the boiling temperature is high, it allows increasing the reaction temperature. This may induce a better conversion by avoiding vitrification of the coating during cure and thus allowing a better mobility of the unreacted monomers. However, this increase in temperature may also increase the evaporation rate of the solvent. A fast evaporation would not be beneficial for the conversion, as was shown by the literature review of the polyurethane film formation. That is why a sequenced cure cycle with a moderate temperature on a first step allowing onset of solvent evaporation combined to cure followed by a higher temperature step designed for complete evaporation of the solvent and post cure for total conversion, may be better for end-properties.

Table 4.8 : Composition of cure tests as a function of the solvent, solution 25 wt% of solvent

Sample	Mass (g)							
	PTMEG 650	ISO	IPDI	t-PMDI	DBTDL	MEK	CPK	DMI
Co1-MEK	3.8	1.7	3.2	1.3	0.002	3.3	0	0
Co2-CPK	3.8	1.7	3.2	1.3	0.002	0	3.3	0
Co3-DMI	3.8	1.7	3.2	1.3	0.002	0	0	3.3

ISO and DBTDL were first dissolved in the solvent before adding PTMEG and all the other isocyanates in order to avoid reaction before solvation and homogenization of the solution.

Deposition was carried out by using an Elcometer Film Applicator fitted with a 75 µm profile spiraled bar at speed 5.

Cure was carried out in a vacuum stove. In order to avoid immediate evaporation of the solvents, it was chosen to first cure 1h30 at 100°C, before post-curing 1h30 at 160°C.

The resulting sample surfaces are presented in Figure 4.25 to 4.27**.**

The substrate of sample Co1-MEK displays a very uneven surface: there are marbling and yellowing. Moreover, the sample was still sticky in places, showing that the reaction was not completed. From the aspect, it is highly probable that MEK evaporated too quickly at the beginning of the cure cycle, thus inducing a premature separation of the components and preventing reaction. However, the film formation at the initial deposition stage was good and the whole substrate was coated. This led us to keep MEK as a candidate for co-solvent as it could help wettability and is very volatile.

Figure 4.25 : Surface aspect of a coating Co1-MEK after cure at 100°C for 1h30 and 160°C for 1h30 under vacuum, with butan-2-one as the solvent.

Figure 4.26: Surface aspect of a coating Co2-CPK after cure at 100°C for 1h30 and 160°C for 1h30 under vacuum, with cyclopentanone as the solvent.

Sample Co2-CPK displays a film with no marbling or yellowing and good gloss, meaning that the rate of evaporation of CPK was more suitable to prevent segregation of the monomers and induce curing. However, the film displays lots of holes revealed in Figure 4.26.

A very similar result was obtained with DMI, as shown by Figure 4.27 that presents the substrate surface of sample Co3-DMI. The cure reaction seems to have been completed and no marbling separation is visible. However, the film formation is not perfect and holes (brown spots) are present.

Figure 4.27: Surface aspect of a coating Co3-DMI after cure at 100°C for 1h30 and 160°C for 1h30 under vacuum, with DMI as the solvent.

Such results could be due to several reasons. It was suspected that the holes could appear either early on in the cure cycle or at a later time during cure. As a matter of fact, as CPK and DMI evaporate and the cross-linking reaction proceeds, the viscosity of the coating increases and its surface energy increases as well, thus inducing local de-wetting of the steel surface. The defects could also appear later, as a skin with a higher T_g forms at the surface of the

coating and traps the solvent in the lower layer as described by Dusek et al. [136], bubbles may form and burst, as the cure proceeds under vacuum and there is a two-stage cure cycle.

In conclusion, as relatively high temperatures must be used to cure the IPDI and ISO-based coating, better results are obtained with solvents having higher boiling points. Similar results were obtained for CPK and DMI. It was thus chosen to focus the study on DMI-based formulations as this solvent has the advantage of being completely non-toxic.

3.2.5. Cure cycle of solvent borne coatings and reaction conversion

The cure cycle used in the previous section was 1h30 at 100°C followed by 1h30 at 160°C. It appeared however that some of the monomers have boiling points very close to 160°C as reported in Table 4.9, and it is very likely that those boiling points are lower under vacuum than they are at standard pressure.

Table 4.9: Fusion and boiling temperatures of monomers at standard temperatures

Monomer	T_f (°C)	T_b (°C)
Isosorbide	62	160 (at 10 mmHg)
1,4-Butanediol	16	235
IPDI	-60	158

It was suspected that some IPDI or ISO could evaporate during the 160°C heating cycle. It was thus chosen to make a quick test using a milder cure cycle described in Figure 4.28, in which an intermediate step at 140°C was added while reducing the duration of the 160°C post cure to 30 min. Tests were performed on the Co3-DMI formulation presented in the previous section.

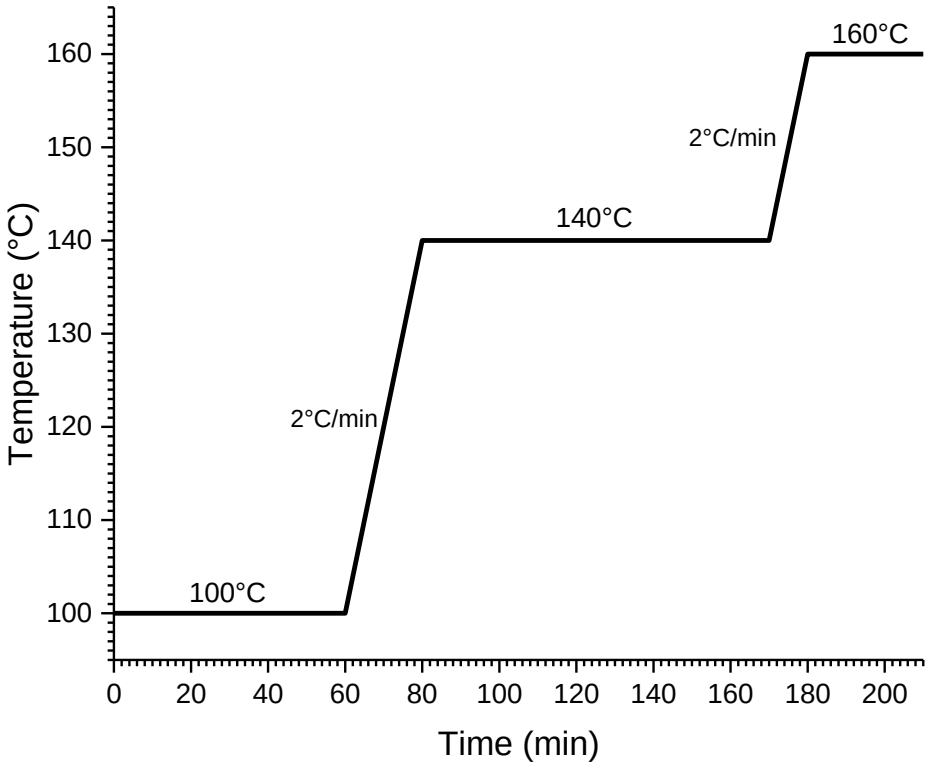

Figure 4.28 : Temperature cycle used for limiting evaporation of monomers

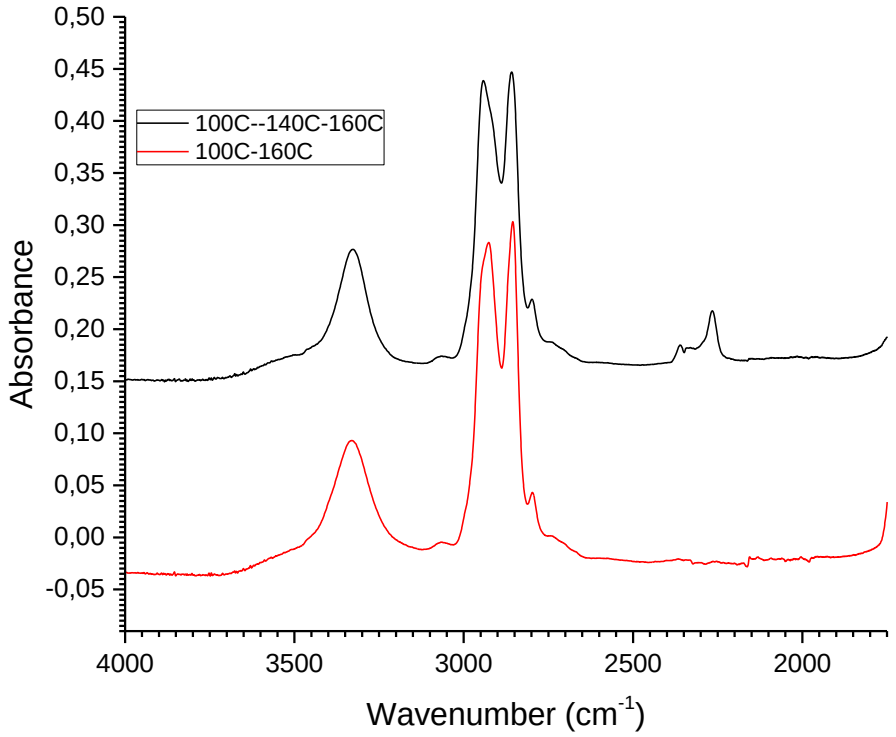

Figure 4.29: FT-IR recorded in ATR mode spectra measured on sample Co4-DMI as a function of the cure cycle

Table 4.10: Infrared bands attribution in sample Co4-DMI spectra

Wavenumber (cm^{-1})	Functional groups
3362	CO_2
3502	Free OH
3327	-NH from polyurethane
2942	CH_2 asymmetrical elongation
2859	CH_2 symmetrical elongation
2340-2360	CO_2
2266	free -NCO

The resulting coatings were assessed by ATR FT-IR. The results are shown in Figure 4.29 and Table 4.10. The –NCO peak at 2260 cm^{-1} has completely disappeared with the 100°C-160°C cure cycle, while a small intensity peak is remaining with the 100°C-140°C-160°C cure cycle. The complete disappearance of the isocyanate functions seems suspicious considering that the starting stoichiometry uses a small excess of 0.05 mol of NCO with respect to the –OH molar number. Moreover, as reaction conversion increases, mobility of the monomers should become hampered by solvent evaporation and network formation, so that reaching 100% conversion is not possible. This is supported by the fact that the shoulder due to free –OH functions appearing near the –NH peak (between 3700 and 3400 cm^{-1}) is still present on both FT-IR curves.

There are then only two possible explanations for the disappearance of –NCO without consumption of –OH: side reactions or evaporation. The latter is favored, as no significant difference between both spectra at lower wavenumbers was found. This question could be however clearly answered to by performing solid NMR or NMR on swollen coating and comparing the spectra to the material before cure.

The three-step cure cycle was chosen for the rest of the work performed in this chapter, as loss of IPDI could not be quantified with the 100°C-160°C. Moreover, if this IPDI loss is occurring too early in the cure cycle, it could significantly hamper end-properties of the coating such as lower the T_g. It is however obvious that this problem of residual –NCO functions will need to be evaluated if the material is produced commercially as it may be a toxicology matter for the end user, since both free IPDI and free -NCO can be irritating for the skin.

3.2.6. Wettability and cratering

Wetting and cratering were assessed on a coating formulation stoichiometry 1:3.05:2. The -NCO functions were brought by 80% from IPDI and 20% from t-PMDI. The diols were PTMEG 650 as the soft segment and ISO as the chain extender. DBTDL was used in order to fasten the reaction. As the exact origin of the above-mentioned defects (hole-like defects on the coated surface presented in section 4.2.5.) was not clear, it was in first intention chosen to improve wettability of the solution over the steel panel. DMI and MEK were used as solvent and co-solvent. The mass of building blocks and of the solvent used for the synthesis are reported in Table 4.11.

The resulting sample surfaces are presented in Figure 4.30 to Figure 4.32.

Table 4.11: Compositions used for wettability and cratering tests

Sample	Mass (g)							
	PTMEG 650	ISO	IPDI	t-PMDI	DBTDL	MEK	DMI	BYK 307
Co4-DMI	3.8	1.7	3.2	1.3	0.002	0	3.3	0
Co5-DMI	3.8	1.7	3.2	1.3	0.002	0.7	3.3	0
Co6-DMI	3.8	1.7	3.2	1.3	0.002	0.7	3.3	0.01

BYK 307 (a silicon additive presented in the materials section) was added to further control cratering in Co6-DMI sample only.

Sample Co4-DMI was very similar to Co3-DMI presented previously. The substrate surface displays a film with lots of holes that are due to poor wettability of the substrate by the solution.

Figure 4.30: Surface aspect of a coating Co4-DMI after cure cycle 100-140-160°C under vacuum.

It was thus decided to add 5% MEK as a co-solvent to improve film formation at the deposition step. The resulting sample is presented in Figure 4.31. The size and number of holes on the surface have been greatly reduced, but the coating is still showing defects after cure. Wettability at film deposition step was good and the defects are probably originating from the fast evaporation of MEK during the cure, inducing high viscosity, which then leads to bad wettability of the partially cured coating over the steel panel.

In order to improve the coating coverage, it was chosen to add 0.1% of BYK 307 to improve wettability and self-levelling of the coating. Concentration was chosen after a few quick tests in order to improve wettability without increasing foam stabilization which would be also a problem during deposition and curing.

Figure 4.31: Surface aspect of a coating Co5-DMI after cure cycle 100-140-160°C under vacuum.

Figure 4.32: Surface aspect of a coating Co6-DMI after cure cycle 100-140-160°C under vacuum.

The resulting sample surface is shown in Figure 4.32. Full coverage of the substrate was achieved. It is assumed that BYK 307 allowed to maintain good wetting of the substrate by the reacting coating as conversion and solvent evaporation occurred.

3.2.7. Summary of the chosen conditions

Cross-linked samples based on a PTMEG/IPDI/ISO aliphatic formulation, from which monomers are non-miscible, were successfully obtained by both reactive extrusion and solvent-borne process.

The poor control of the stoichiometry of the sample obtained by reactive extrusion, making the effect of isosorbide in coatings difficult to appreciate, led to the choice of a solvent borne synthesis.

A solvent-borne formulation allowing the production of cross-linked coatings based on the environmentally friendly DMI was designed by choice from a selection of suitable solvents.

Additives BYK 307 and MEK co-solvent concentrations were adjusted in order to obtain homogeneous surfaces and high gloss, leading to the following choices:

- Solutions of 25 wt% DMI and 5 wt% MEK
- 0.1 wt% of BYK 307 for wettability

Eventually, a three-step cure cycle consisting in 1h at 100°C, 1h30 at 140°C and 30 min at 160°C with 2°C/min heating ramps under vacuum, was chosen to limit the evaporation of monomers, as a removal too early in the curing cycle would lead to poor cross-linking reaction.

3.3. CHARACTERIZATION OF THE COATINGS

3.3.1. Synthesis plan

Using the method designed in the previous section, a series of 4 ISO-based formulations and their 4 BDO-based equivalents were synthesized. Name and compositions are reported in the Table 4.12 below.

Table 4.12: Names and compositions of coating sample series studied hereafter

Name	Introduced Mass (g)										
	PTMEG 650	PTMEG 1000	ISO	BDO	IPDI	t-IPDI	t-PMDI	DMI	MEK	DBTDL	BYK 307
1	8.0	0	3.6	0	0	0	13.4	8.9	1.8	0.006	0.025
2	9.6	0	4.3	0	8.0	0	3.2	8.9	1.8	0.006	0.025
3	0	11.9	3.4	0	6.3	3.4	0	8.9	1.8	0.006	0.025
4	8.8	0	3.9	0	5.5	3.9	2.9	8.9	1.8	0.006	0.025
11	8.5	0	0	2.3	0	0	14.2	8.9	1.8	0	0.025
22	10.3	0	0	2.8	8.5	0	3.4	8.9	1.8	0.006	0.025
33	0	12.5	0	2.2	6.7	3.5	0	8.9	1.8	0.006	0.025
44	9.4	0	0	2.6	5.8	4.1	3.1	8.9	1.8	0.006	0.025

Several compositions of the isocyanate fraction were explored. Samples 1 and 11 were composed exclusively of t-PMDI as the isocyanate fraction in order to evaluate the properties brought by this new cross-linker as well as increase the bio-sourced content. In samples 2 and 22 on one hand, and samples 3 and 33 on the other hand, 20% of the -NCO functions from IPDI were replaced by -NCO functions from a diisocyanate trimer in comparison to the TII30 formulation used as the starting base, being either t-PMDI or t-IPDI. In samples 4 and 44, combined effects of t-IPDI and t-PMDI were studied by replacing 40% the -NCO functions from IPDI by 20% of -NCO functions from t-IPDI and 20% of -NCO functions from t-PMDI.

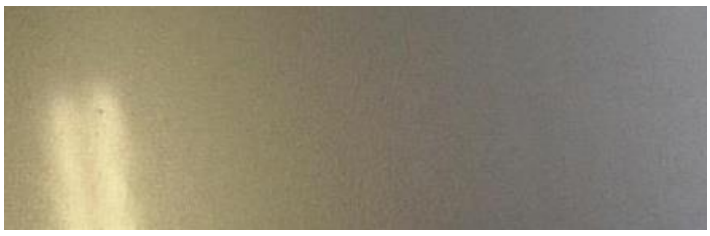

Figure 4.33: Surface aspect of sample 11 as an example

All obtained samples had very similar surface aspects, with very glossy coatings, without defects, as shown in Figure 4.33 as a representative example.

3.3.2. Thermal behavior

DSC heating scans were performed from -60°C to 250°C at a rate 20°C/min in order to measure the glass transition temperature of the samples. Results are presented in Table 4.13.

The ISO-based series displays on average higher T_g than the equivalent BDO-based sample series, which is in accordance with the conclusion of chapter 3 in which it was shown that isosorbide allows to increase the glass transition temperature. All T_g of the ISO-based samples are over 25°C, which results in samples without tackiness at room temperature. The glass transition of the BDO-based series is in general lower than room temperature. Tackiness of the coating was especially high for samples having a T_g close to 0°C such as samples 11 and 33.

Table 4.13: Compositions and glass transition temperatures of cross-linked sample series

Name	Macrodiol	Diisocyanate	Cross-linker	Chain extender	T_g
		% of NCO functions	% of NCO functions		(°C)
1	PTMEG 650	0%	100% t-PMDI	Isosorbide	30
2	PTMEG 650	80% IPDI	20% t-PMDI	Isosorbide	48
3	PTMEG 1000	80% IPDI	20% t-IPDI	Isosorbide	43
4	PTMEG 650	60% IPDI	20% t-IPDI + 20% t-PMDI	Isosorbide	53
11	PTMEG 650	0%	100% t-PMDI	1,4-butanediol	4
22	PTMEG 650	80% IPDI	20% t-PMDI	1,4-butanediol	14
33	PTMEG 1000	80% IPDI	20% t-IPDI	1,4-butanediol	-10
44	PTMEG 650	60% IPDI	20% t-IPDI + 20% t-PMDI	1,4-butanediol	26

The presence of IPDI-based HS in the coating composition increases the T_g, as can be seen by comparing samples 1 and 2 on the one hand, and samples 11 and 22 on the other hand. Even at lower cross-linking density, as is the case for sample 2 compared to sample 1, the presence of IPDI allows a large increase in T_g that can outmatch the effect of the t-PMDI cross-link density. This effect can also be seen on sample 4, for which a part of the IPDI was replaced by t-PMDI without resulting in a large difference in the glass transition in spite of the cross-link density increase. In the same BDO-based type of samples (samples 44 and 33), this replacement has a more marked effect.

The value of the glass transition temperature displayed the largest increase between samples 3 and 33 with a difference of 53°C between sample 3 and its BDO-based equivalent sample 33. The effect was not as marked for sample containing t-PMDI as the cross-linker. This is probably due to the fact that the structures obtained by reaction of t-IPDI with ISO display a higher T_g than the equivalent obtained by reaction of t-PMDI with ISO. Moreover, the glass transition temperature of the model thermoplastic polyurethane from Chapter 2 TII45 was -11°C. It was greatly enhanced by replacement of 20 mol% of –NCO functions from IPDI by functions from the IPDI trimer (sample 3). The same observation cannot be made for sample 33 and its thermoplastic equivalent TIB45, both examples displaying a T_g of -10°C.

3.3.3. Solvent evaporation

Solvent evaporation at the end of the cure cycle was evaluated by TGA. Samples were obtained by peeling off the coating from the surface when possible, and by chipping the surface coating when the adhesion was too good for peeling to be performed. By examination of the weight loss over the curve of the heating from room temperature to 150°C, one could obtain the order of magnitude of the amount of solvent still trapped in the cross-linked material.

The resulting curves are presented in Figure 4.34 and Figure 4.35**.** Degradation temperatures were not studied as polyurethanes have a complex thermal degradation. The urethane function starts to become unstable at 160-170°C, however no mass loss can usually be seen until 250°C. The evaporation of pure DMI was also tested, there is a 5 wt% loss at 82°C, and all the solvent is gone around 150°C.

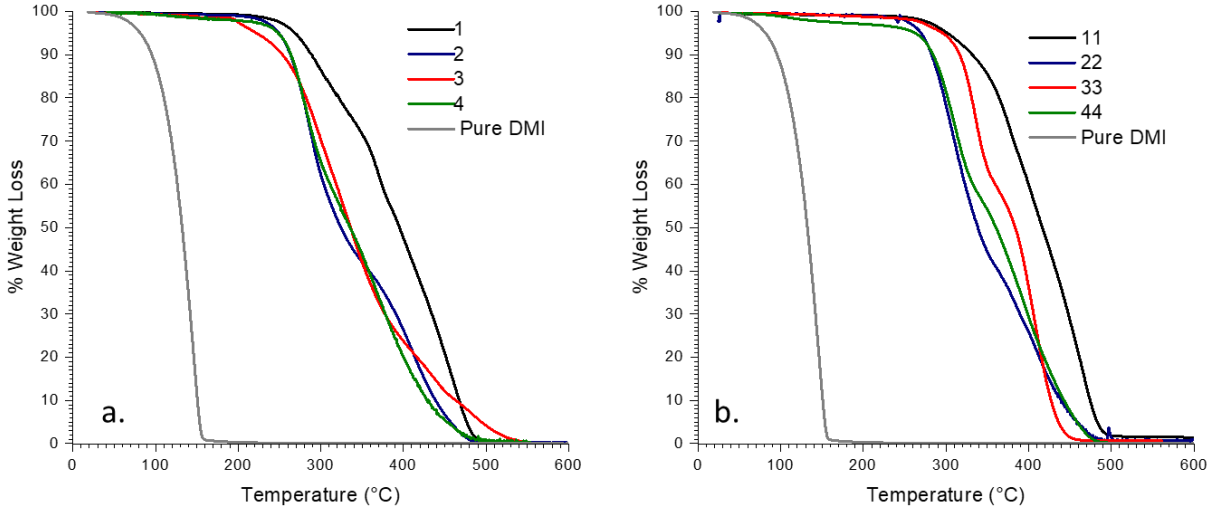

Figure 4.34: TGA curves performed on coating samples at a heating rate of 20°C/min – a. samples based on ISO – b. samples based on BDO

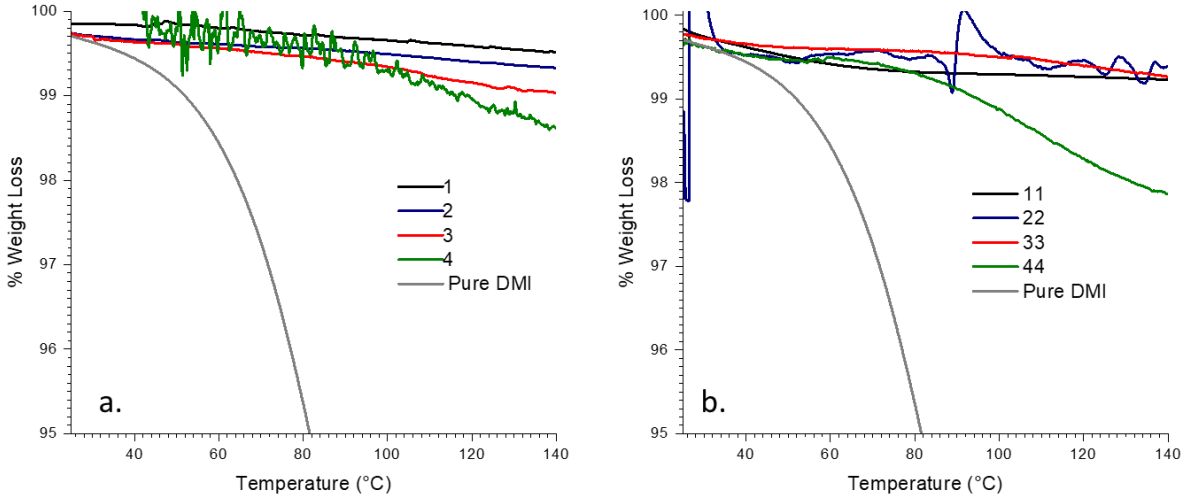

Figure 4.35: Magnification of the heating phase between room temperature and 140°C of the TGA curves – a. samples based on ISO – b. samples based on BDO

When looking more precisely at the start of the heating cycle from Figure 4.35, the mass loss is less than 1% for most samples. Exceptions are samples 4 and 44 for which there seems to be an accelerated mass loss starting at 90°C, however the exact nature of this loss is not clear, the most probable being evaporation of trapped DMI, but unreacted monomers or additives could also be involved.

In general, mass loss does not exceed 2% with on average less than 1%, which means that the cure cycle used efficiently removes the solvent.

3.3.4. Thickness

The thickness of the coatings was measured by profilometry on a step created by peeling a rectangular piece of the coating of average dimensions 8x25 mm, in order to expose the substrate.

Profiles of 25 mm length were then measured over the width or the exposed part and the step height evaluated. Results are reported in Table 4.14.

A large majority of samples displays very comparable thicknesses between 25 and 38 µm, which is rather thin compared to industrial standards of 100 to 300 µm film thickness. The only exception is sample 1 with a thickness of 85 µm. Variations can occur due to variable reactivity of the solutions arising from difference in composition. Both parameters induce a difference in viscosity of the deposited solutions which is crucial for thickness control.

Thickness has an impact on the properties of the coatings as a lower thickness usually induces better adhesion and better deformation resistance of the coating. It is also a critical parameter in the formation of a glassy layer at the surface of the coating, the thicker the coating, the more solvent trapped in the bulk. As such, since the DMI is not very volatile, it is best that the average film thickness is small, as the solvent evaporation will be easier. This may also be the reason why TGA measurements did not shown massive release of DMI.

Table 4.14: Composition and thickness of the synthetized coatings, solutions with 25 wt% of DMI

Name	Macrodiol	Diisocyanate	Cross-linker	Chain extender	Thickness	Standard deviation
		% of NCO function	% of NCO functions		µm	µm
1	PTMEG 650	0%	100% t-PMDI	Isosorbide	85	±3.1
2	PTMEG 650	80% IPDI	20% t-PMDI	Isosorbide	36	±0.2
3	PTMEG 1000	80% IPDI	20% t-IPDI	Isosorbide	31	±1.2
4	PTMEG 650	60% IPDI	20% t-IPDI + 20% t-PMDI	Isosorbide	26	±4
11	PTMEG 650	0%	100% t-PMDI	1,4-butanediol	35	±0.6
22	PTMEG 650	80% IPDI	20% t-PMDI	1,4-butanediol	35	±2
33	PTMEG 1000	80% IPDI	20% t-IPDI	1,4-butanediol	31	±3
44	PTMEG 650	60% IPDI	20% t-IPDI + 20% t-PMDI	1,4-butanediol	27	±0.9

3.3.5. Practical adhesion

In order to evaluate the quality of the adhesion between the steel substrate and the coating, adhesion grid tests following ISO 2409 standards, were performed. Results are classified on a scale of 0 to 5, 0 being a grid pattern showing no damage after peeling, while 5 is a very poor result with a majority of the test surface being damaged after peeling. Four tests were performed on each sample, and the lowest grid test score was kept if it was reproduced at least 3 times.

Detailed procedure is described in the experimental section.

As can be seen in Table 4.15, results of grid tests are on average better for ISO-based samples. This general trend is probably due to the higher T_g displayed by ISO-based samples that prevent tackiness and thus limits interactions with the scotch tape during the peeling phase of the grid test. Indeed, samples 11 and 33 have the lowest glass transition temperatures (4°C and -10°C respectively) and are those displaying the poorest grid test results of the series. It is also nonetheless probable that chemical composition-related phenomena are at play, but it is not possible to explore such parameters with grid testing alone.

Table 4.15 : Composition and adhesion grid tests results on ISO and BDO-based coatings

Name	Macrodiol	Diisocyanate	Cross-linker	Chain Extender	Grid test
		% of NCO function	% of NCO functions		ISO 2409
1	PTMEG 650	0%	100% t-PMDI	Isosorbide	1
2	PTMEG 650	80% IPDI	20% t-PMDI	Isosorbide	0
3	PTMEG 1000	80% IPDI	20% t-IPDI	Isosorbide	1
4	PTMEG 650	60% IPDI	20% t-IPDI + 20% t-PMDI	Isosorbide	1
11	PTMEG 650	0%	100% t-PMDI	1,4-butanediol	4
22	PTMEG 650	80% IPDI	20% t-PMDI	1,4-butanediol	1
33	PTMEG 1000	80% IPDI	20% t-IPDI	1,4-butanediol	4
44	PTMEG 650	60% IPDI	20% t-IPDI + 20% t-PMDI	1,4-butanediol	1

3.3.6. Impact resistance

The deformation resistance of the coatings was evaluated by performing direct and reverse impact tests on the coated substrates, following ISO 6272 standards. ISO 6272 standard describes how a limit of energy beyond which the coating is damaged can be measured by gradual increase of the fall height or increase of the indenter mass. However, for most of our samples, damage was never attained using the maximum possible falling indenter mass (1 kg) and fall height (1 m) available in the IMP lab. It was thus chosen to only use those maximum parameters for evaluation, performing 4 indentation tests on each coating formulation. Damage in the coating was revealed by application of a copper sulfate and HCl aqueous solution. The exact protocol is described in the experimental section.

Table 4.16: Composition and adhesion impact tests results on ISO and BDO-based coatings

Name	Macrodiol	Diisocyanate	Cross-linker	Chain extender	Direct Impact ISO 6272 1 kg – 1m Damaged : o	Reverse impact ISO 6272 1 kg – 1m Intact : x
		% of NCO function	% of NCO functions			
1	PTMEG 650	0%	100% t-PMDI	Isosorbide	x	x
2	PTMEG 650	80% IPDI	20% t-PMDI	Isosorbide	x	x
3	PTMEG 1000	80% IPDI	20% t-IPDI	Isosorbide	x	x
4	PTMEG 650	60% IPDI	20% t-IPDI + 20% t-PMDI	Isosorbide	x	x
11	PTMEG 650	0%	100% t-PMDI	1,4-butanediol	o	o
22	PTMEG 650	80% IPDI	20% t-PMDI	1,4-butanediol	x	o
33	PTMEG 1000	80% IPDI	20% t-IPDI	1,4-butanediol	x	x
44	PTMEG 650	60% IPDI	20% t-IPDI + 20% t-PMDI	1,4-butanediol	o	o

Figure 4.36 : Delamination at impact point on direct and reverse impact tests on sample 11

Excellent results (Table 4.16) were obtained for the ISO-based samples, while BDO-based sample series displays more heterogeneous results. BDO-based coatings failure was often due to peeling or delamination of the coating from the substrate at the impact point, as shown as an example in Figure 4.36. Those results may both result from a lower glass transition temperature as well as the higher reactivity of BDO which may have induced the formation of an amorphous skin early during the cure cycle and thus trapped some solvent at the interface with the steel panel. Inverse impact seems to be more detrimental that

direct impact, which could mean that the BDO-based series is more sensitive to tensile deformation (inverse impact) than in compression (direct impact).

Outstanding results obtained for the ISO-based samples can be explained by the glass transition temperatures of those samples, that even though being over 25°C are not very high either, with no temperatures higher than 55°C. This accounts for very flexible and deformable coatings.

3.3.7. Abrasion resistance

Abrasion resistance was evaluated using a Taber abrader. Exact measurement conditions are reported in the experimental section. As the mass loss was not quantifiable, roughness measurements were made by profilometry over the abraded coatings. Results are reported in Table 4.17 in term of roughness R_q and R_a, which equations are reported in Equation 2 and 3.

$$R_a = \frac{1}{n}\sum_{i=1}^{n}|y_i| \qquad \textbf{Equation 2}$$

$$R_q = \sqrt{\frac{1}{n}\sum_{i=1}^{n} y_i^2} \qquad \textbf{Equation 3}$$

With n the total number of data points, y_i is the vertical distance from the mean line to the i^{th} data point. R_a is the arithmetical mean roughness while R_q is the root mean squared roughness. R_q gives more importance to the large variations of height compared to R_a.

All coatings have a non-abraded surface roughness value of the same order of magnitude. No relation can really link roughness and abrasion resistance. However, from the data, one can see that the variation between abraded and non-abraded surface seems to be linked to the value of the glass transition temperature as well as to the chain extender type of the samples: as the T_g increases, so does the roughness variation, and the BDO-based series displays on average lower roughness variation values than the ISO-series.

Ashrafizadeh *et al*. [170] performed wear tests on polyurethane elastomers (T_g between -24°C and 10°C, which is in the same range as our samples despite being elastomers) at several temperatures in the range of 22°C to 100°C in order to study the effect of temperature on abrasion resistance. They showed that in general the studied polyurethanes displayed an improved resistance at 60°C and a fast degradation at 100°C, due to an initial enhanced recovery at 60°C and on the contrary, adversely affected mechanical properties at 100°C. Scanning electron microscopy (SEM) moreover allowed them to study the eroded surfaces. They thus showed that for low abrasion rates, small asperities are formed, while as abrasion increases, ridges perpendicular to the surface are formed. It is not clear at the moment if this phenomenon can also be found in cross-linked polyurethanes compositions.

Table 4.17: Roughness R_a and R_q as a function of coating formulation, and surface preparation performed on ISO and BDO-based coatings

Sample	R_q (μm)			R_a (μm)		
	Abraded	Non-abraded	% Variation	Abraded	Non-abraded	% Variation
Substrate	-	1.51	-	-	1.24	-
1	0.46	0.25	84	0.3	0.21	43
2	0.57	0.08	613	0.4	0.06	567
3	0.46	0.08	475	0.31	0.06	417
4	0.48	0.05	860	0.30	0.03	900
11	0.42	0.17	147	0.24	0.13	85
22	0.42	0.16	163	0.27	0.13	108
33	0.55	0.11	400	0.29	0.09	222
44	0.62	0.06	933	0.37	0.04	825

This observation could potentially mean that poor wear resistance induces a higher roughness of the surface in polyurethanes, but more information needs to be gathered in order to evaluate the abrasion resistance as a function of the composition and the T_g of the sample. This could be achieved by complementary information on the hardness and elastic moduli of the samples as well as study of the sample surface by scanning electron microscopy.

3.4. CONCLUSION

Syntheses of several novel polyurethane coatings containing isosorbide were successfully performed. Cross-links were obtained by integration of aliphatic diisocyanate trimers. Particular attention was paid to using partially bio-sourced building blocks.

Both reactive extrusion and solvent-borne processes were evaluated as homogenization means. However, poor control on the stoichiometry of the samples obtained by reactive extrusion led to the choice of a solvent borne synthesis.

A solvent-borne formulation allowing the production of cross-linked coatings based on the environmentally friendly DMI was designed by choice from a selection of suitable solvents. Film formation was optimized by addition of MEK and BYK 307. DBTDL was used to accelerate reaction between isosorbide and IPDI derived -NCO functions. Eventually, a three-step cure cycle consisting in 1h at 100°C, 1h30 at 140°C and 30 min at 160°C with 2°C/min heating ramps under vacuum, was chosen to limit the evaporation of monomers as removal early on the curing cycle would lead to poor cross-linking. However, a thorough study of the film formation of this system should be carried out in the manner of that led by Dusek [136] or Monaghan [139] in order to completely understand the synthesis, deposition and cure parameters that yield optimal properties.

Synthesized coatings contained less than 2 wt% of residual DMI, and glass transition temperatures ranging between 25 and 55°C were obtained for the ISO-based series of samples. Notably lower T_g values were obtained for BDO-based sample series. Incorporation of isosorbide had beneficial effects on mechanical properties such as impact resistance and practical adhesion.

CONCLUSION AND PERSPECTIVES

Conclusion and perspectives

During this thesis, bio-based isosorbide was integrated in thermoplastic and cross-linked polyurethanes compositions. Efforts were made to incorporate other bio-sourced building blocks along with isosorbide in some of the studied compositions. This allowed to get insight into the potential of isosorbide for design of polyurethanes with an optimized bio-sourced content. The chemical and thermo-mechanical properties of the resulting materials were evaluated and compared to compositions containing 1,4-butanediol.

Isosorbide has been first synthesized in the 50's, but due to its lower reactivity as a secondary alcohol and its high production cost, it did not rise interest in the industry until the early 2000's. Several authors showed that isosorbide based hard segments generally have high glass transition temperatures and crystallization seems to be more readily obtained when isosorbide is associated with MDI or HDI.

In this context, isosorbide was successfully used as a chain extender in compositions based on MDI and a soft segment chosen from PTMEG, PCL or FADM (fatty acid dimer-based polyester macrodiol). Synthesis parameters were carefully monitored as to maximize the molar mass of the material while keeping the process at a reasonable time scale. Molar masses of average 22.7 $kg.mol^{-1}$ were reached for isosorbide-based polyurethanes. Isosorbide and MDI-based polyurethanes did not reach very high molar masses on average compared to the model 1,4-butanediol, but they were sufficient to be considered comparable. This difference was not detrimental to their thermo-mechanical properties, as it was demonstrated that isosorbide induced higher melting temperature of the hard domains, measured between 174 and 208°C, thus providing a higher flow limit temperature in PCL and PTMEG-based systems. Furthermore, it was shown that phase segregation of ISO/MDI-based hard segments was more limited and not as stable as that of the BDO/MDI-based hard segments, at least when combined to the studied soft segments. It was also shown that the nature of the soft segments played a crucial role in this phenomenon, as the phase segregation quality and its thermal stability was much higher for the FADM-based polyurethanes. Finally, ISO-based polyurethanes were on average harder than their BDO counterpart and their water-uptake was not significantly higher either, with an uptake of less than 2% over 60 days.

As synthesis of thermoplastic polyurethanes from isosorbide, as well as the phase segregation of ISO-based hard segments were proved, isosorbide was used in other thermoplastic compositions based on the aliphatic IPDI. Its lower reactivity has been used to control kinetics of polymerization and IPDI has thus been used in various polyurethane compositions ranging from coatings to water-borne elastomers. It is known that its use in linear block-polyurethanes usually renders mechanically weak materials due to lack of phase segregation.

Pure hard segments based on IPDI and ISO were synthesized and were found to have a high glass transition at 121°C, compared to pure hard segments based on IPDI and BDO with a T_g of 24°C. Integration of isosorbide in IPDI-based thermoplastics was thus seen as a mean of obtaining clear elastomeric materials with potentially good thermal resistance. Several polyurethanes were thus synthetized from IPDI/ISO HS or IPDI/BDO HS associated with either PTMEG or FADM. Polymerization reactions were catalyzed by DBTDL and high molar masses were obtained, with values of average molar mass ranging from of 16 $kg.mol^{-1}$ to 60 $kg.mol^{-1}$ for ISO-based materials and from 44 $kg.mol^{-1}$ to 78 $kg.mol^{-1}$ for their BDO counterparts. From DMA, it was however seen that these molar masses were not sufficient for the appearance of a rubber plateau on a majority of the samples and it is believed that the molar masses were not high enough to induce entanglements.

Two qualities of phase segregation were obtained. PTMEG-based materials thus displayed weak and non-thermally stable phase segregation with ISO as the chain extender, while FADM-based polyurethanes displayed a more pronounced and thermally stable phase segregation. Both series of materials were amorphous and transparent. Glass transition temperatures of phases richer in hard segments were ranging between 65°C and 95°C for ISO-based samples, while they were between 25 and 60°C for the BDO equivalents. Those results suggest that transparent materials with a good thermal resistance could be obtained from ISO/IPDI-based polyurethanes if higher molar masses can be obtained.

After the successful integration of Isosorbide in transparent materials with limited phase segregation, its incorporation in aliphatic and low VOC coating formulations was explored. To our knowledge, integration of unmodified isosorbide in polyurethane coatings had never been reported. Formulations of cross-linked coatings were based on a known thermoplastic composition in a first intention. TII30 sample was thus selected as it displayed weak phase segregation, aliphatic structure and was amorphous.

Keeping in mind constraints such as components miscibility, stoichiometry, solvent toxicity, and film formation parameters, a solvent borne synthesis and deposition was designed. The final samples were thus obtained using a mix of DMI and MEK as the solvent. Cross-links were obtained by incorporation of trimers (either bio-sourced t-PMDI, or classical t-IPDI) in TII30 formulation. ISO was again demonstrated to significantly increase T_g of the considered materials compared to BDO. It moreover induced better adhesion and impact resistance on average.

Several perspectives for the continuation of this work can be proposed.

First, results obtained on the MDI/ISO-based elastomers have led to the observation of very characteristic microstructures as well as still partially misunderstood thermal transitions. One cannot help but wonder if more in-depth study of those phenomena could bring better understanding of the mechanism of phase segregation at the origin of the very homogeneous globular microstructure observed in FADM/ISO/MDI samples, and eventually

the impact of such microstructure on mechanical properties such as hardness or tensile resistance. This would however require systematic measurements in SAXS/WAXS diffraction combined to thermo-microscopy and AFM. At such, such study completely outranged the scope of this thesis.

Secondly, encouraging results were obtained concerning IPDI-based materials that could lead to the design of transparent and thermally stable materials. Indeed, FADM/IPDI/ISO-based samples seemed to display interesting phase segregation but suffered small molar mass values between 16 and 25 $kg.mol^{-1}$ which most probably did not allow for entanglements to occur.

Finally, the work carried out on coatings demonstrated that it is possible to design coating formulations with high bio-sourced content (between 60 and 85% for the studied systems), low VOC and using non-toxic solvent. From the theoretical approach presented on film formation phenomena, it could be of high interest to apply the model to this system to be able to predict properties depending on cure conditions. However, depending on the intended applications, higher T_g (ideally between 80 and 100°C), higher thickness, and in-depth characterization of those coatings in term of hardness, adhesion and abrasion resistance may be required.

In conclusion, this work showed that Isosorbide could become a highly useful building block for the design of bio-polyurethanes in the years to come, and it may also be used with non-conventional building blocks to obtain innovative materials such as those obtained with IPDI or bio-sourced isocyanurates. Technical applications may include automotive, pharmaceutical, clothing and sport industry.

EXPERIMENTAL SECTION

Experimental section

5.1. MATERIALS AND CHARACTERIZATION

5.1.1. Chain extenders

- ***Isosorbide***

The isosorbide used in this work was kindly supplied by Roquette Frères, and was subsequently dried for 4h under nitrogen flush at 100°C with magnetic agitation. Residual water content was measured by Coulometric Karl Fisher titration, as described in section 5.2.3. and was found to be 700 ppm (±10 ppm). I_{OH} was experimentally determined to be 766 mg/g by hydroxyl titration (theoretical value of I_{OH} is 768.6 mg/g), as described in 5.2.1.

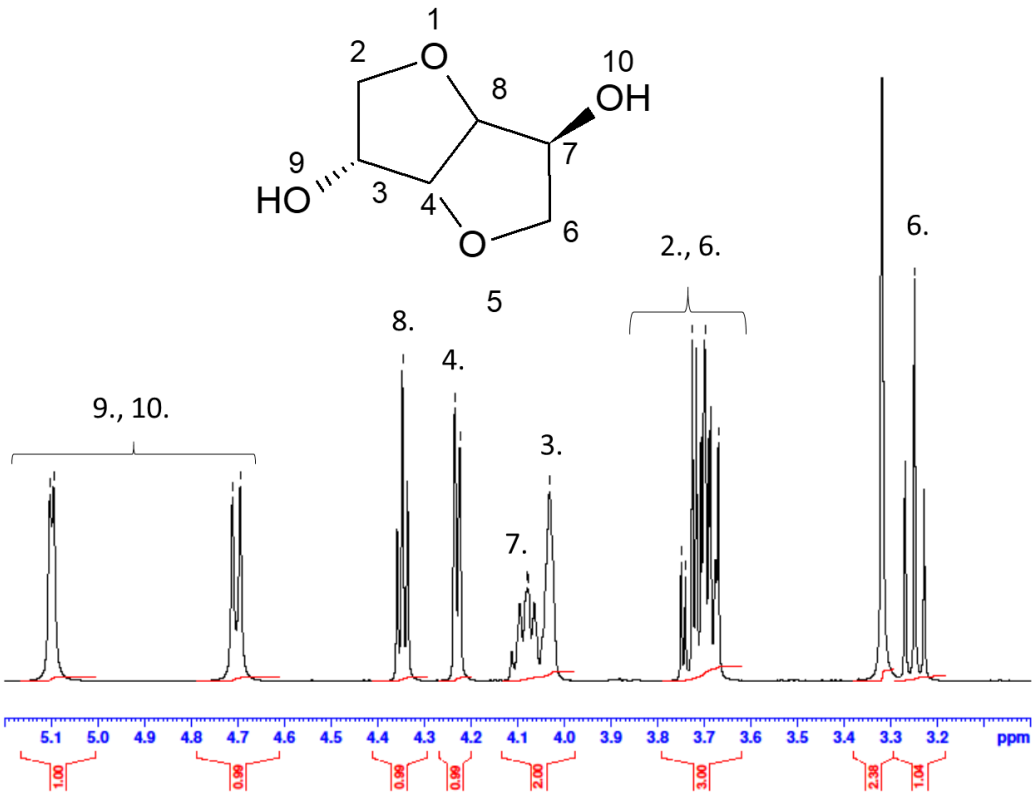

^{1}H NMR (400 MHz, DMSO-d6, δ, ppm): 3.25 (1H from C^{6}), 3.67-37 (2H from C^{2} and 1H from C^{6}), 4.03 (1H from C^{3}), 4.08 (1H from C^{7}), 4.22 (1H from C^{4}), 4.35 (1H from C^{8}), 4,71-5.10 (2x1H from $C^{9,10}$)

- ***1,4-Butanediol***

1,4-butanediol was purchased from Sigma-Aldrich, and was subsequently dried for 4h under nitrogen flush at 100°C with magnetic agitation. Residual water content was measured by Coulometric Karl Fisher titration, and was found to be 600 ppm (±20 ppm). I_{OH} was experimentally determined to be 1245 mg/g by hydroxyl titration (theoretical value of I_{OH} is 1246.7 mg/g).

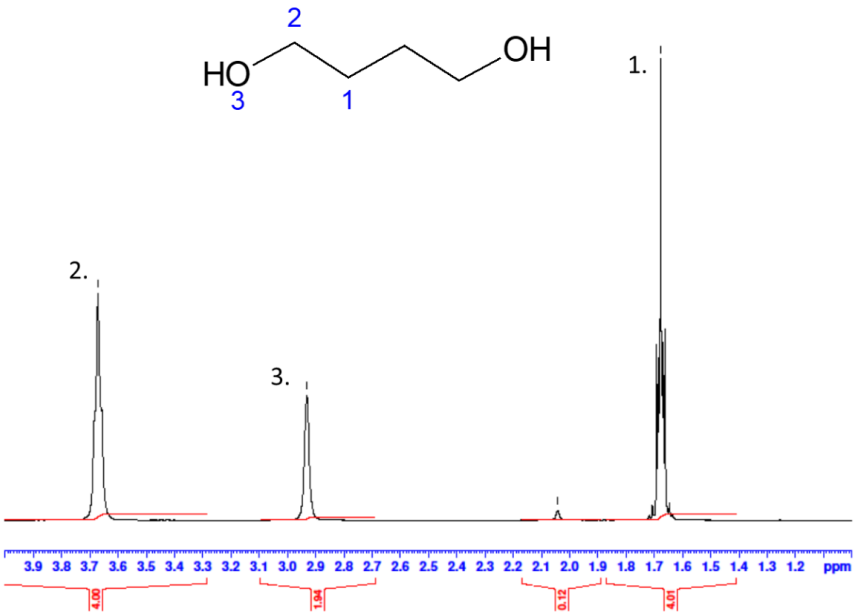

^{1}H NMR (400 MHz, $CDCl_3$, δ, ppm): 1.68 (2x2H from mid-chain CH_2[1]), 2.93 (2x1H from end chain OH[3]), 3.67 (2x2H from O adjacent CH_2[2])

- ***2,5-bis(hydroxymethyl)tetrahydrofuran (THFDM)***

The THFDM used in this work was kindly supplied by Roquette Frères and is a bio sourced monomer. It was subsequently dried for 4h under nitrogen flush at 100°C with magnetic agitation. Residual water content was measured by Coulometric Karl Fisher titration and was found to be 1870 ppm (±40 ppm). I_{OH} was experimentally determined to be 852 mg/g by hydroxyl titration (theoretical value being 849 mg/g). Its ^{1}H NMR spectrum is presented below. It allows to obtain the cis-trans ratio which is 94% cis for 6% trans (this measurement did not allow to discriminate between S/S, S/R and R/R isomers).

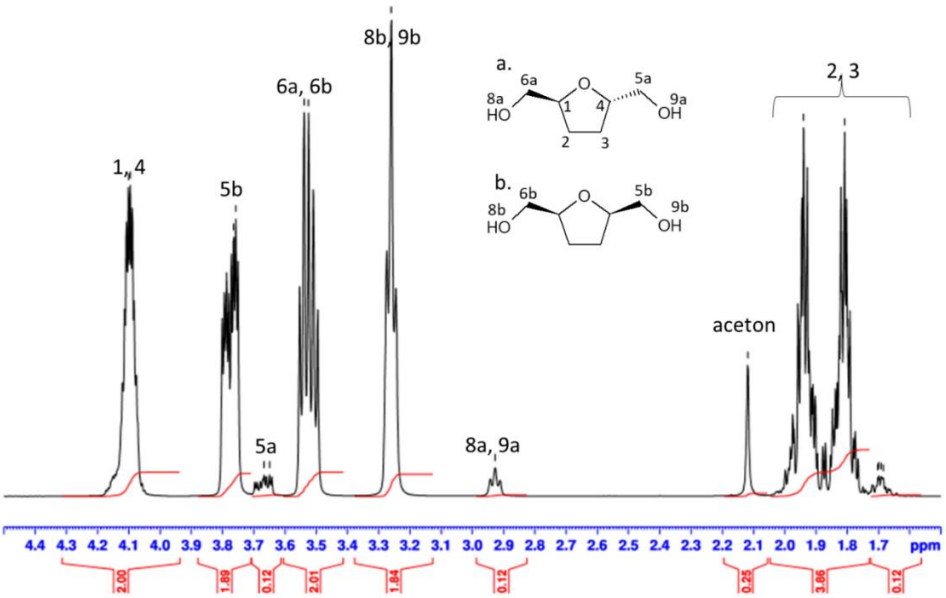

^{1}H NMR spectrum of THFDM in CDCl3, and structure of THFDM isomers a. Trans – b. Cis – (400 MHz, CDCl3, δ, ppm) 1.70-1.94 (4H from 2, 3, multiplet), 2.93 (1H from 8a and 9a, triplet), 2.26 (1H from 8b and 9b, triplet), 3.53 (2H from 6a, 6b, multiplet), 3.65 (2H from 5a, multiplet), 3.76 (2H from 5b, multiplet), 4.10 (2H from 1 and 4, multiplet)

- ***Polyether oligomer based on isosorbide (IsoOP)***

The polyether oligomer based on isosorbide used in this work was kindly supplied by Roquette Frères, and was subsequently dried for 4h under nitrogen flush at 100°C with magnetic agitation. Structure was monitored by the supplier by ^{1}H NMR. Residual water content was measured by Coulometric Karl Fisher titration and was found to be 785 ppm (±40 ppm). I_{OH} was experimentally determined to be 852 mg/g by hydroxyl titration.

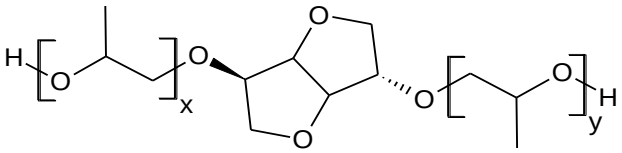

Figure 5.1: Structure of polyether oligomer based on isosorbide (IsoOP), with substitution indices x+y=2.4

5.1.2. Macrodiols

- ***Poly(ε-caprolactone) diol***

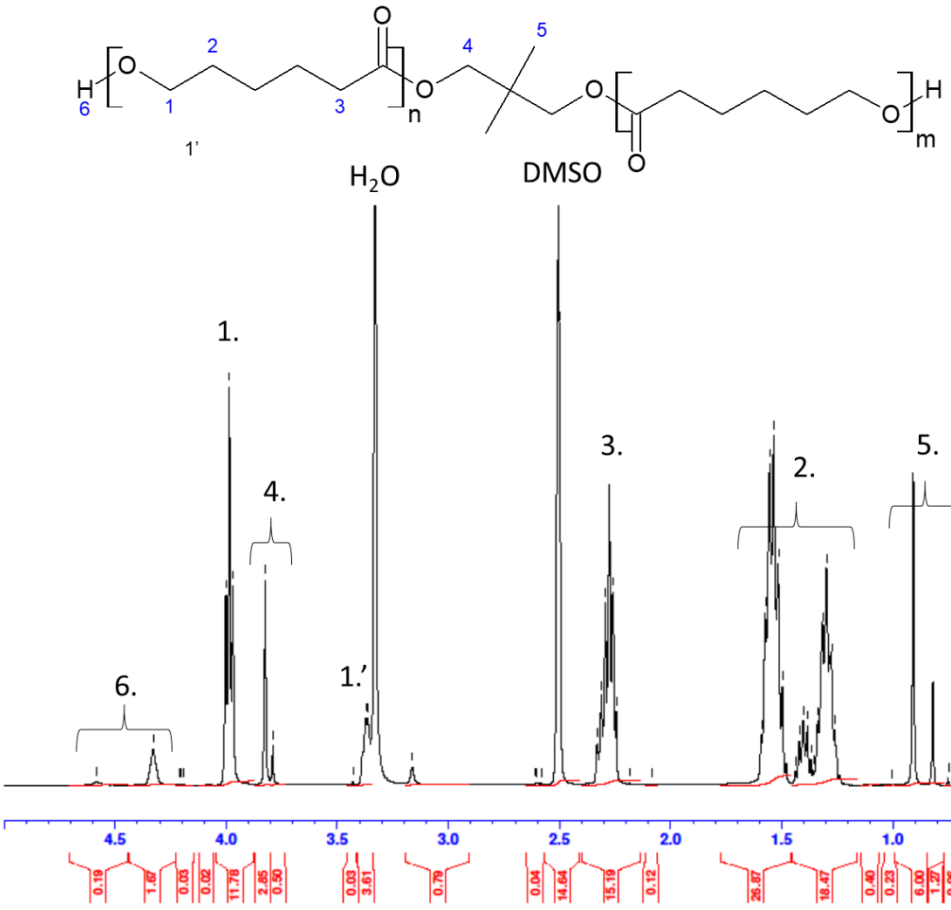

n+m=8

^{1}H NMR (400 MHz, DMSO-d6, δ, ppm): 0.90 (2x3H from C^{5}), 1.30-1.53 (24x2H from C^{2}), 2.27 (8x2H from C^{3}), 3.37 (2x2H from C^{1} next to –OH end functions), 3.82 (2x2H from C^{4}), 3.99 (6x2H from C^{1}, triplet), 4.33 (2x1H from end chain functions H6)

Poly(ε-caprolactone) of M_n around 1000 g.mol^{-1} (CAPA 2101A) was kindly supplied by Perstorp. The product was used without further treatment. Water content was measured by Coulometric Karl Fisher titration and was found to be 100 ppm (±20 ppm), it was therefore not necessary to dry this macrodiol. I_{OH} was experimentally determined to be 108 mg/g by hydroxyl titration (theoretical value of I_{OH} is 112 mg/g). Some peaks from 2,2'dimethyl-1,3-propanol (neopentyl glycol) were doubled in 1H NMR and the doublet displayed a shift around -0.09 ppm. It is supposed that some chains composing the PCL mix were asymmetrical and that the neopentyl glycol may sometime be located at the end of the PCL chain and does not compose the core.

- ***Poly(tetrahydrofurane) diol 1000***

Poly(tetrahydrofurane) of M_n around 1000 g.mol^{-1} was purchased from Sigma-Aldrich. The product was used without further treatment. Water content was measured by Coulometric Karl Fisher titration and was found to be 80 ppm (±20 ppm) and was thus used without drying. I_{OH} was experimentally determined to be 111 mgKOH/g by hydroxyl titration (theoretical value of I_{OH} is 112 mg/g).

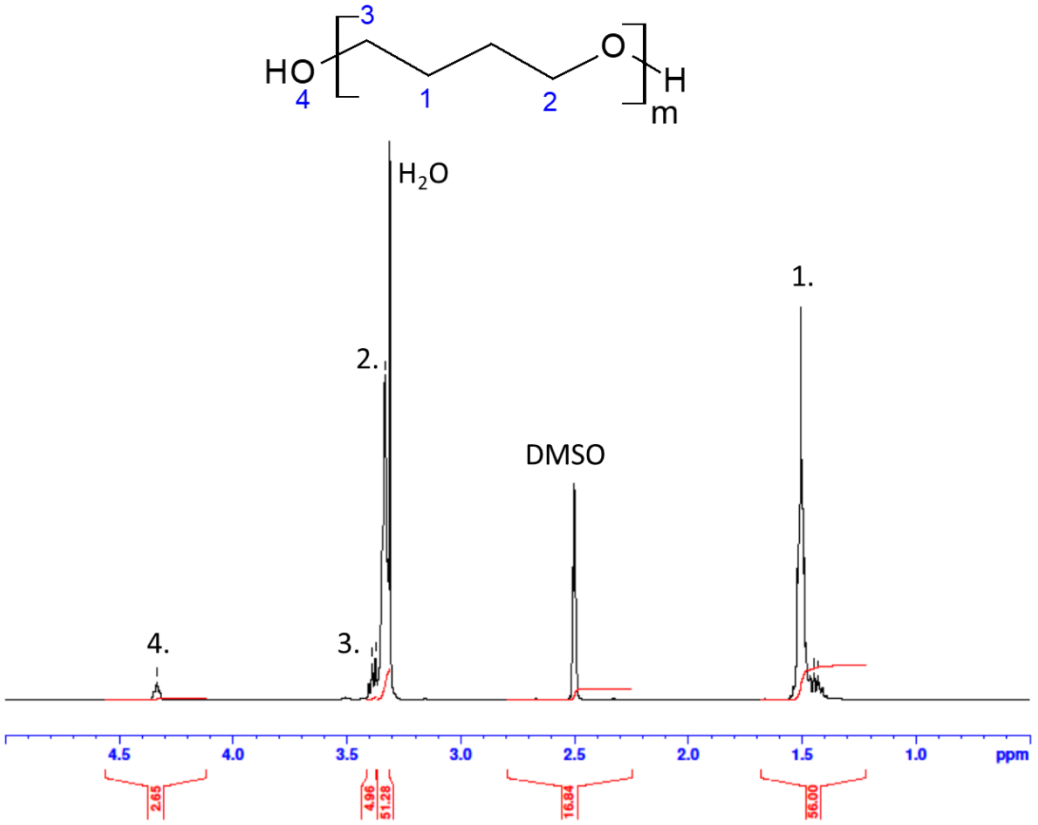

m=14

^{1}H NMR (400 MHz, DMSO-d6, δ, ppm): 1.51 (28x2H from C^{1}), 3.33 (26x2H from C^{2}), 3.37 (2x2H from C^{3} next to –OH end functions), 4.34 (2x1H from end chain functions H4)

- ***PTMEG 650***

Poly(tetrahydrofuran) with an average molar mass M_n=650 g.mol^{-1} was purchased from Sigma-Aldrich. The product was used without further treatment. I_{OH} was experimentally determined to be 170 mgKOH/g by hydroxyl titration (Theoretical value: I_{OH} =172.62 mgKOH/kg).

- ***Fatty acid dimers based oligoester diol (FADM)***

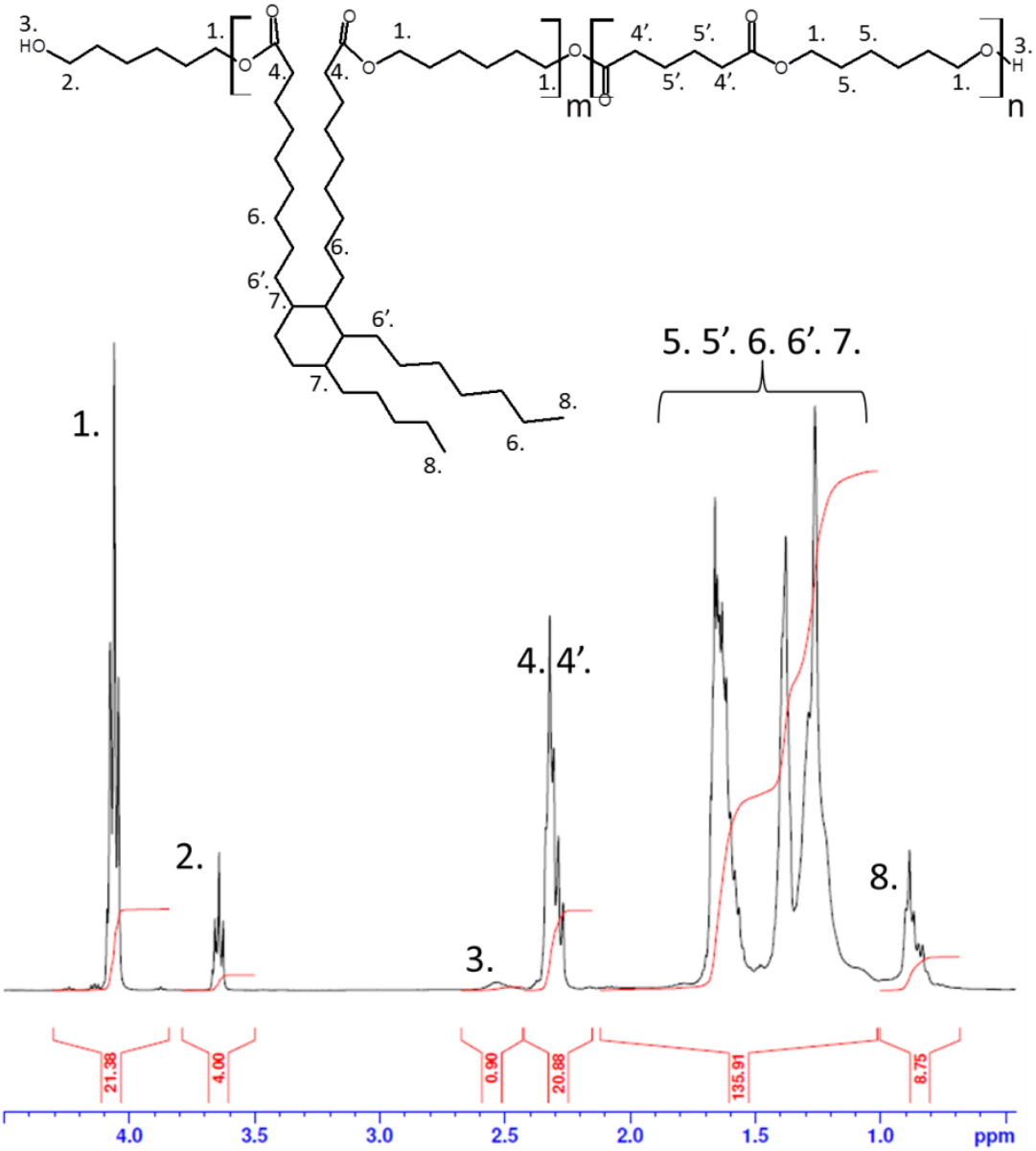

m=4.4 n=1.7

^{1}H NMR (400 MHz, CDCl3, δ, ppm): 0.88 (6H from 8.), 1.26-1.66 (middle chain hydrogens from fatty acid dimers, 1,6-hexanediol and adipic acid 5., 5'., 6., 6'., 7.), 2.32 (hydrogens from 4. And 4'.), 2.53 (H from end-chain hydroxyls 3.), 3.64 (4H from end-chain 2.), 4,06 (H from 1.)

Fatty acid dimer-based oligoester diol (Radia 7282) of M_n around 2200 g.mol^{-1} was supplied by Oleon. The product was used without further treatment. Water content was measured by Coulometric Karl Fisher titration and was found to be less than 40 ppm (±20 ppm). I_{OH} measured by the supplier was 57.9 mg/g. Our protocol used for hydroxyl function determination could not be used due to side-reaction of the polymer chains with one of the reactant used for the titration. This oligomer is a copolymer composed of a fatty acid dimer obtained from rapeseed oil associated to adipic acid and 1,6-hexanediol. The stoichiometry between the dimer and the adipic acid was estimated by ^{1}H NMR and is of 1 dimer out of 2.6 adipic acids.

5.1.3. Isocyanates

- ***4,4'-diphenylmethylene diisocyanate***

4,4'-diphenylmethylene diisocyanate was purchased from Sigma-Aldrich. The product was used without further treatment. I_{NCO} was measured by titration of the isocyanate functions as described in section 5.2.2, and was found to be 8.01 mol/kg.

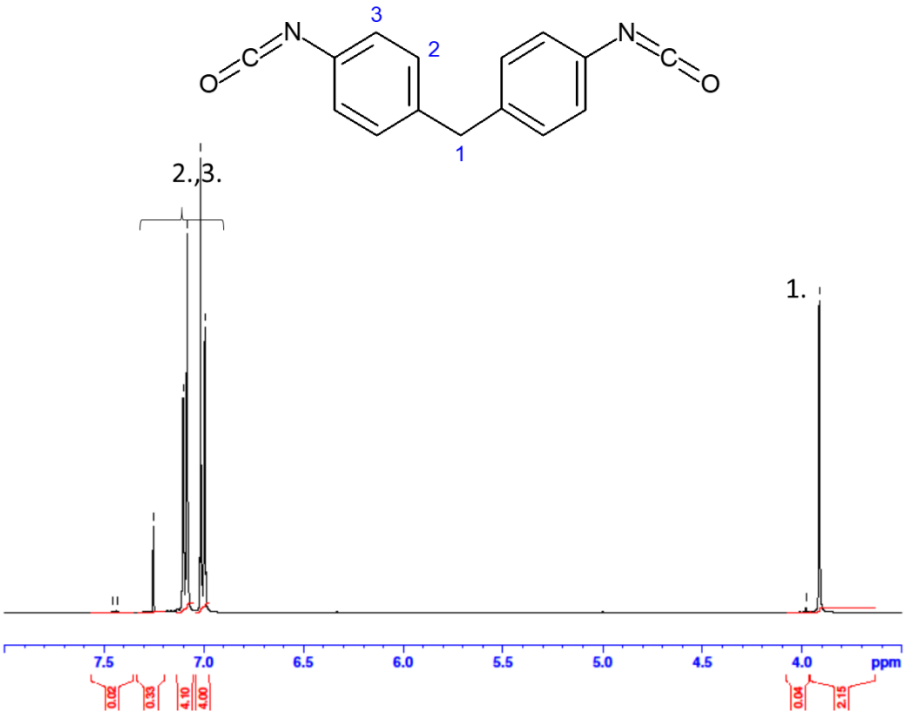

^{1}H NMR (400 MHz, $CDCl_3$, δ, ppm): 3.91 (2H from C^1, singlet), 6.99-7.10 (8H from $C^{2,3}$)

- ***Isophorone diisocyanate***

The IPDI used in this work was purchased from Sigma-Aldrich. The product was used without further treatment. I_{NCO} was measured by titration of the isocyanate functions and was found

to be 8.86 mol/kg (theoretical value being 9.0 mol/kg). Its ^{1}H NMR spectrum is presented below. It allows to obtain the cis-trans ratio which is 78% cis for 22% trans.

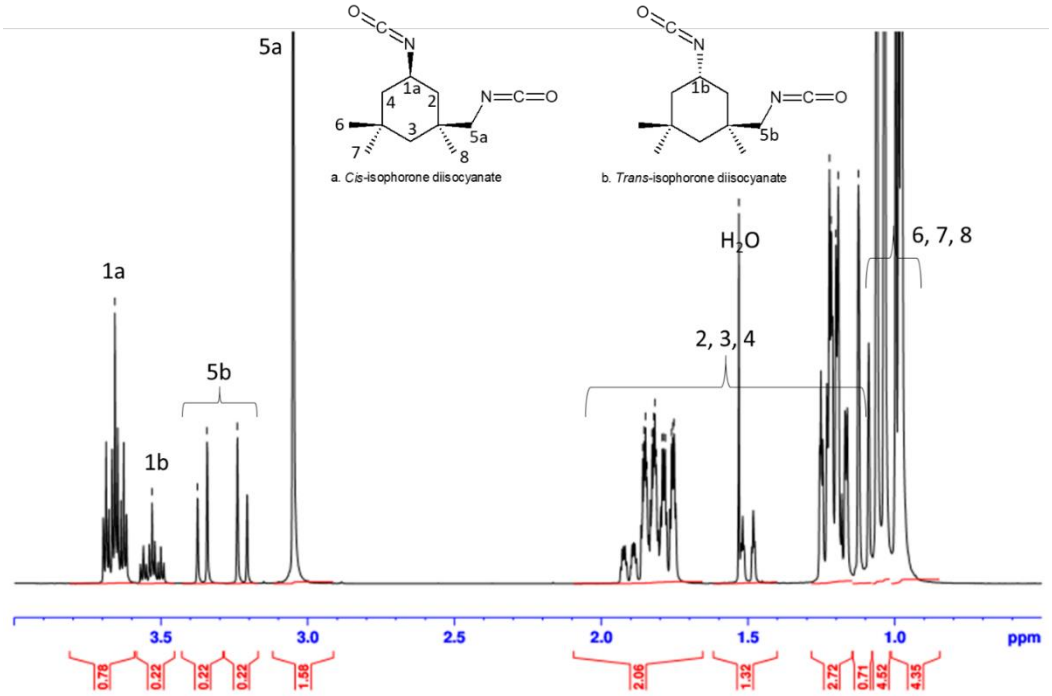

^{1}H NMR spectrum of IPDI in CDCl3, and structure of IPDI isomers a. Cis – b. Trans – (400 MHz, CDCl3, δ, ppm) 0.98-1.06 (9H from 6, 7 and 8, multiplet), 1.12-1.92 (6H from 2, 3, 4, multiplet), 3.05 (2H from 5a, singlet), 3.24-3.34 (2H from 5b, multiplet), 3.53 (1H from 1b, multiplet), 3.66 (1H from 1a, multiplet)

- ***Pentamethylene diisocyanate trimer***

Pentamethylene diisocyanate trimer (trade name: DESMODUR eco N7300) used in this work was kindly donated by Covestro. The product was used without further treatment. I_{NCO} was measured by titration of the isocyanate functions as described in 5.2.1., and was found to be 5.58 mol/kg (in the ideal case of a completely pure trimer, I_{NCO}= 6.49 mol/kg). At room temperature, it presented itself as a very viscous transparent liquid.

- ***Isophorone diisocyanate trimer***

Isophorone diisocyanate trimer (trade name: VESTANAT T1890/100) used in this work was kindly donated by Azelis. The product was used without further treatment. I_{NCO} was measured by titration of the isocyanate functions, and was found to be 4.2 mol/kg (in the ideal case of a completely pure trimer, I_{NCO}=4.51 mol/kg). At room temperature, the product was in the form of amorphous pellets. DSC analysis showed that it displays a glass transition temperature at 71°C.

In order to have more insight into the composition of both trimers, they were analyzed by SEC in THF. The results are presented in Figure 5.2 and Table 5.1.

From the SEC curves, it is apparent that both trimers contain molecules of different size distribution. The peaks of larger intensity appearing around 22 mL for t-IPDI or around 23 mL for t-PMDI, are in both cases the trimer peaks. The difference in retention volume for those two peaks is due to the difference in intrinsic molar mass and hydrodynamic volume of the trimers. Indeed, pure t-PMDI has a molar mass of 462 $g.mol^{-1}$, while pure t-IPDI has a molar mass of 666 $g.mol^{-1}$. The peaks appearing before those two peaks are due to the formation of higher homopolymers such as pentamers, heptamers, etc. which are frequently occurring during trimer synthesis [169]. The small peaks appearing right after the trimer peaks were attributed to dimers or monomers depending on their volume of retention.

By comparison of the areas under the curve of the different peaks and supposing that the refraction index of all products is the same, it was possible to calculate the weight percentage of each fraction composing t-PMDI and t-IPDI. The fraction of higher homopolymers is larger in the case of t-PMDI compared to t-IPDI, which explains the larger difference between the measured value of I_{NCO} and its theoretical value for this product.

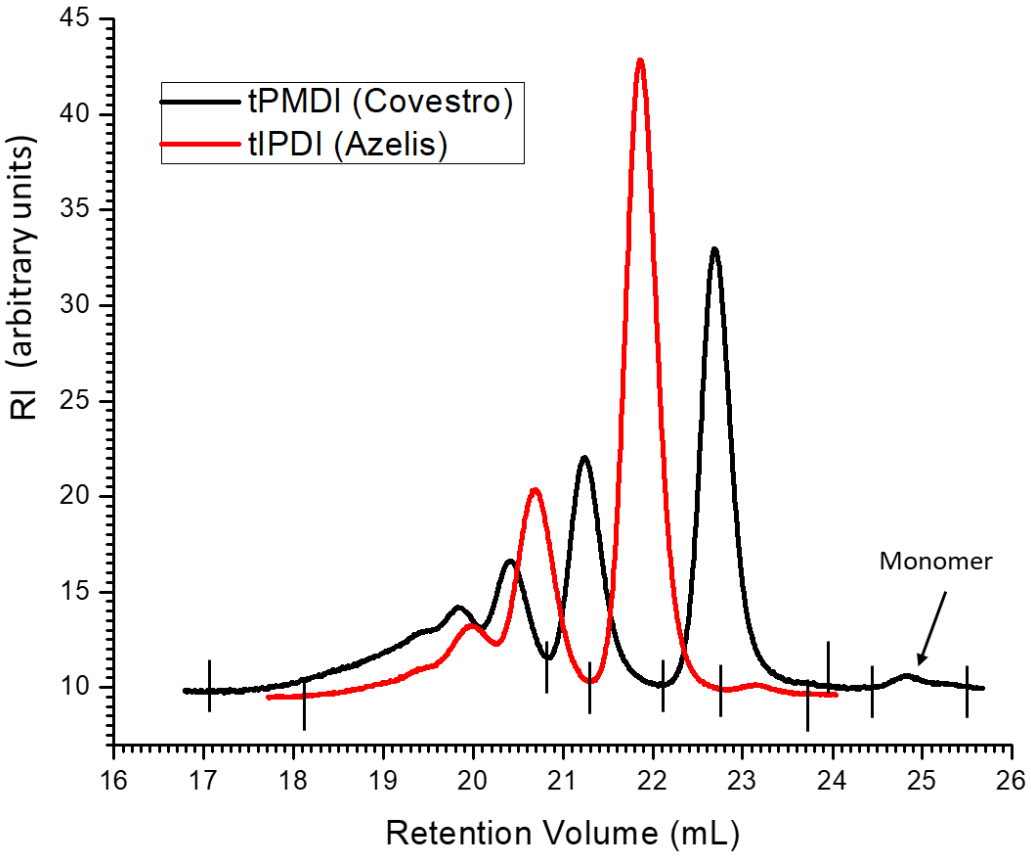

Figure 5.2 : SEC RI curves of the trimers of IPDI and PMDI in THF (1mL/min)

The distribution of the moieties of the t-IPDI were sensibly different from the results found by Burel *et al.* on a similar product [146]. Their sample did not contain any dimer, contrary to ours and they obtained a better separation on peaks appearing at smaller retention volume. They also reported a ratio of trimer at 71 wt%, which is higher than the percentage of pure

trimer found in our sample. Those differences most probably from the fact that the sample studied here is from a different source (and as such, the manufacturer probably does not use the same catalysts for the isocyanurate ring-formation, resulting in differing size distributions), as well as the fact that Burel *et al.* modified their samples with methanol which probably helped the separation of the higher mass peaks.

Table 5.1 : Ratio of constituents of trimers of IPDI and PMDI in weight percent obtained from refractometric signal of SEC in THF

		t-IPDI	t-PMDI
Monomer	(wt%)	0	1.7
Dimers	(wt%)	1.4	0
Trimers	(wt%)	62.5	41.2
Tetramers	(wt%)	36.2	25.2
Higher oligomers	(wt%)		32.7

5.1.4. Others

- ***Dimethyl ether of Isosorbide (DMI), 2-Butanone and Dibutyl tin dilaurate (DBTDL)***

Dimethyl ether of isosorbide was kindly supplied by Roquette Frères and was used as received. 2-butanone and DBTDL were purchased from Sigma-Aldrich and used as received.

- ***BYK 307***

BYK 307 is a solvent-free polyether-modified polydimethylsiloxane used as surfactant for solvent borne coatings. It is specifically designed for reducing cratering and lowering surface tension. It was obtained from BYK Additives and Instruments and used as received. It presents itself as a viscous liquid at room temperature.

5.2. METHODS

5.2.1. Chemical titrations

5.2.1.1. Titration of isocyanate functions

Reaction Scheme

The chemical titration of the isocyanate functions used in this work was carried out following AFNOR NF T52-132 standard. The titration is based on the reaction of N,N-dibutylamine (DBA) with the NCO functions in order to obtain urea, as explained in Figure 5.3.

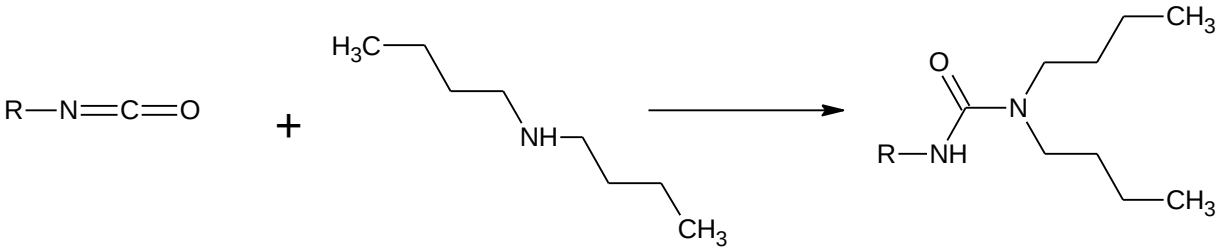

Figure 5.3: Reaction scheme of a compound R terminated by an isocyanate (NCO) moiety and dibutylamine (DBA) producing the corresponding urea compound

The excess amine is then back titrated with hydrochloric acid (HCl) by a simple pH titration.

Protocol

Around 0.5 g of –NCO containing sample is weighed, and 6 mL of 1 M DBA solution in THF is precisely added. The reaction is left to proceed with magnetic stirring at room temperature for 1h.

Then, 20 mL of pure THF is added in order to increase the sample volume and prevent miscibility problems with the HCl aqueous solution.

The excess DBA amine is then titrated by an aqueous HCl solution 1M by pH follow-up with an automated titration device.

Results

The isocyanate concentration was calculated as an isocyanate index which is commonly used in the polyurethane industry. This index stands for the mass percentage of NCO functions in the material, and is defined as shown in Equation 4.

$$I_{NCO} = 100 \times \frac{42.02 \times f_n}{M} \qquad \textbf{Equation 4}$$

with M the molar mass of the material and f_n the isocyanate average functionality.

In the case of this titration, I_{NCO} can be obtained by application of Equation 5

$$I_{NCO} = \frac{(V_0 - V) \times N_{HCl} \times 4.202}{m} \quad \textbf{Equation 5}$$

with V_0 the equivalent volume of HCl solution obtained for the blank sample in mL, V is the equivalent volume of HCl solution obtained for the sample in mL, N_{HCl} the titer of the HCl solution in mol.L^{-1} and m the mass of the dry sample in g.

Another value can be used for evaluation of isocyanate concentration in the material, named the equivalent NCO Eq_{NCO}. It represents the number of NCO functions per mass unit of the material and is calculated in mol.kg^{-1}, as shown by Equation 6.

$$Eq_{NCO} = \frac{(V_0 - V) \times N_{HCl}}{m} \quad \textbf{Equation 6}$$

5.2.1.2. Titration of alcohol functions

Reaction Scheme

The chemical titration of the alcohol functions used in this work was derived from the protocol for the isocyanate titration described in the previous section and is a double back titration. The first step is based on the reaction of the hydroxyl functions with a monofunctional isocyanate, p-toluenesulfonyl isocyanate (p-TSI) in order to obtain a urethane function, as shown in Figure 5.4.

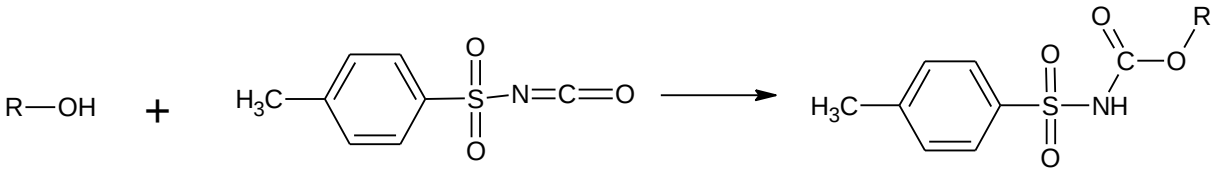

Figure 5.4: Reaction scheme of a compound R terminated by a hydroxyl moiety and p-toluenesulfonyl isocyanate (p-TSI) producing the corresponding urethane compound

The excess p-TSI is then reacted with DBA and the remaining DBA is subsequently back titrated with hydrochloric acid (HCl) by pH titration.

Protocol

Between 0.5 g and 2 g of polyol sample is weighed, and 6 mL of solution of p-TSI 1 M in THF is precisely added. The reaction is left to proceed with magnetic agitation at room temperature for 1h.

Then, 8 mL of 1M DBA solution in THF is precisely added. This second reaction is left to proceed at room temperature for 1h with magnetic agitation.

Then, 20 mL of pure THF is added in order to increase the sample volume and prevent miscibility problems with the HCl aqueous solution in the following steps.

The excess DBA is then titrated by an aqueous HCl solution at 1M by pH follow-up with an automated titration device.

Results

The hydroxyl concentration (I_{OH}) was calculated as a hydroxyl index which is commonly used in the polyurethane industry. This index stands for the mass in milligram of potassium hydroxide which would be needed to neutralize the acetic acid that combines by esterification to 1g of the sample, it is given in mgKOH/g. It can be calculated from the equivalent volumes obtained by titration as shown in Equation 7.

$$I_{OH} = \frac{(V_0 - V) \times M_{KOH} \times N_{HCl}}{m_{polyol}} \quad \textbf{Equation 7}$$

with V_0 the equivalent volume of HCl solution obtained for the blank sample in mL, V is the equivalent volume of HCl solution obtained for the sample in mL, M_{KOH} the molar mass of potassium hydroxide (M_{KOH}= 56.1 g.mol^{-1}), N_{HCl} the titer of the HCl solution in mol.L^{-1} and m_{polyol} the mass of the dry sample in g.

I_{OH} is also linked to the molar mass of the polyol by the Equation 8.

$$I_{OH} = \frac{1000 \times M_{KOH} \times f_n}{M_n} \quad \textbf{Equation 8}$$

with f_n the hydroxyl average functionality, M_n the average molar mass of the polyol.

5.2.2. Measurement of the MDI contents by refractometry

In order to check the completion of the reaction of MDI with macrodiols in prepolymers (especially for the prepolymer based on FADM since FADM has a side reaction with DBA), it was in some cases necessary to measure the quantity of remaining MDI by a non-destructive method.

Methodology

By separation analysis methods such as SEC, it is possible to precisely separate the fractions of non-reacted monomers in a mix such as prepolymers, and subsequently quantify that fraction.

The detectors found on a SEC device are usually viscometers and differential refractometers. The Refraction Index increases linearly with the concentrations in most cases. This property can be used in order to build a calibration curve with several pure MDI solutions and compare this result with a prepolymer sample in order to measure its MDI concentration.

Protocol

Four solutions of MDI in THF with a toluene marker were prepared at the following concentrations: 0.05 $mg.mL^{-1}$, 0.50 $mg.mL^{-1}$, 1.00 $mg.mL^{-1}$, and 5.00 $mg.mL^{-1}$. A solution of the prepolymer was prepared as well in THF at a concentration around 1 $mg.mL^{-1}$.

Size-Exclusion Chromatography of MDI solutions and prepolymer solutions was then performed in tetrahydrofuran (THF) at 35°C, using a Shimadzu LC-20AD pump equipped with a Shimadzu DGU-20A3 auto-sampler, differential refractive index detector (Shimadzu RID-10A), UV detector (Shimadzu SPD-20A) and a viscometer (Viscotek 270 Dual Detector). Three Styragel columns from Waters, with porosity 10^3, 10^5 and 10^3 Å, including a precolumn, were used at a flow rate of 1.0 mL/min.

Results

The results are obtained as SEC curves. By calculating the area of the peak corresponding to the free MDI (peak b. on Figure 5.5) on the RI signal curve of the MDI solutions, it is possible to build the calibration curve presented in Figure 5.6.

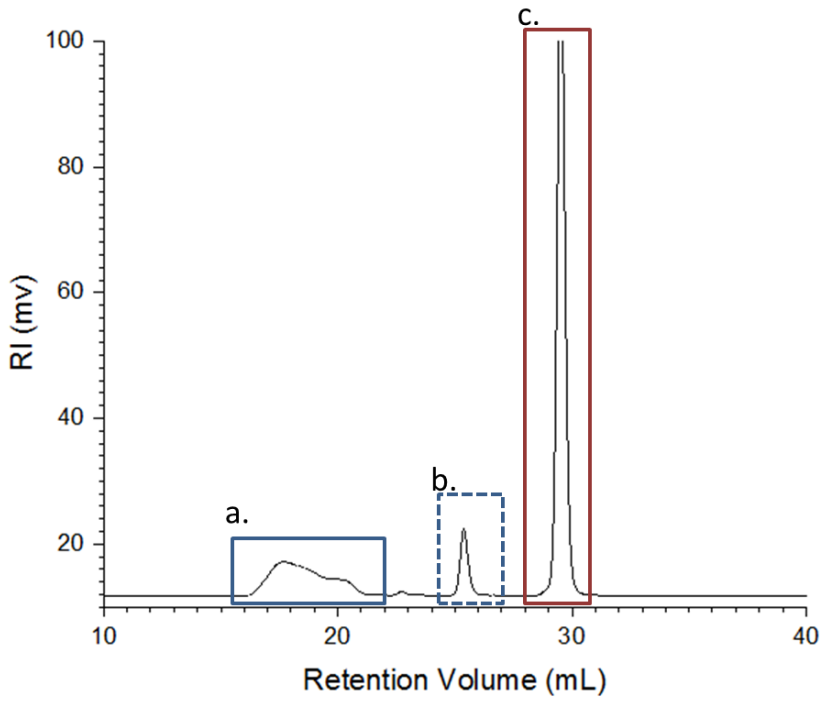

Figure 5.5: Example of a SEC curve measured on a PTMEG-MDI prepolymer sample. The peak a. is the PTMEG terminated by –NCO moieties, peak b. is the free MDI and peak c. is the toluene flow marker.

As the relationship between concentration of the solutions and MDI peak area is linear, it is possible to simply calculate the equation of the calibration curve.

The area of the MDI peak of the prepolymer sample is as well calculated, and the concentration in free MDI (c_{MDI}) of the prepolymer solution can be derived from the calibration curve equation in mg/mL.

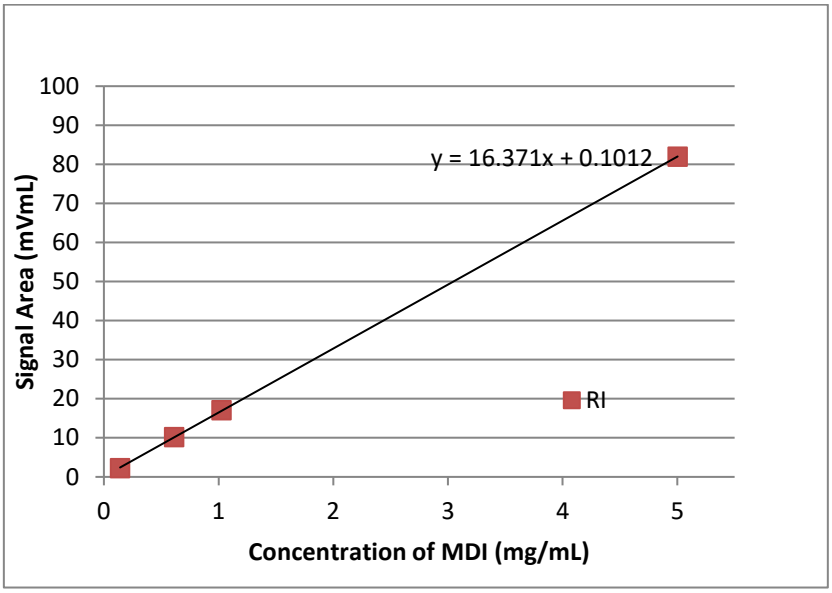

Figure 5.6: Calibration curves of solutions of MDI in THF for refractometer at 35°C.

The effective percentage of free MDI in the sample can then be calculated by in Equation 9, it is given as a mass percentage of free MDI over the prepolymer mass.

$$Ef_{MDI} = \frac{c_{MDI} \times m_b \times V}{m \times m_{MDI}} \times 100 \qquad \text{Equation 9}$$

with m_b the mass of the synthesized bulk sample in g, c_{MDI} the concentration in MDI of the prepolymer solution in g.mL^{-1}, V the volume of the prepared prepolymer solution in THF in mL, m the mass of sample dissolved in the THF prepolymer solution in g, m_{MDI} the mass of MDI used for the synthesis of the bulk sample in g.

5.2.3. Measurement of the water content – Karl Fisher titration

The water content was measured by Coulometric Karl Fischer Titration on a TiTouch 917 from Metrohm, using Hydranal Coulomat AG Oven reactant from Honeywell.

The titration is based on the following chemical equation:

$$SO_2 + I_2 + 2\,H_2O \rightarrow H_2SO_4 + 2\,HI$$

However, this reaction is reversible. A base is thus usually added in order to catch the H^+ ions produced during the reaction and thus displace the equilibrium toward the formation of I^- anions and the consumption of all available water. Imidazole is usually used for this purpose. The titrant solution also contains methanol as it allows to increase the reaction sensibility.

The water titration reaction is thus modified as follows by the addition of imidazole (RN) and methanol (MeOH):

$$MeOH + SO_2 + 3\ RN + I_2 + H_2O \rightarrow [(RN\text{-}H)^+ (SO_4)^-\text{-}Me] + 2\ [RN\text{-}H^+]\ I^-$$

In a coulometric Karl Fischer, the iodine is produced by an anode from iodide anion while at the cathode H^+ is reduced into H_2. The reaction is monitored by amperometry with a third electrode. The end of the reaction is signaled by a sharp decrease of the electric potential.

Samples that are solids at room temperature were usually dissolved in dry methanol at a 60% concentration and a reference measurement was done on a methanol sample in order to calculate water content of the sample. Liquid samples were simply introduced in the measurement cell without other treatment. Water content was measured four times for each sample in order to obtain the standard deviation.

5.2.4. Size Exclusion Chromatography (SEC)

Size-Exclusion Chromatography of prepolymers was performed in tetrahydrofuran (THF) at 35°C, using a Shimadzu LC-20AD pump equipped with a Shimadzu DGU-20A3 auto-sampler, differential refractive index detector (Shimadzu RID-10A), an UV detector (Shimadzu SPD-20A) and a viscometer (Viscotek 270 Dual Detector). Three Styragels columns from Waters, of porosity 10^3, 10^5 and 10^3 Å, including a precolumn, were used at a flow rate of 1.0 mL/min.

Size Exclusion Chromatography of prepolymers and chain-extended polyurethanes was performed in a 0.01M solution of bis(trifluoromethane)sulfonimide lithium salt ($LiNTf_2$) in dimethyl formamide (DMF) at 50°C as eluent, using a Viscotek pump (VE 1122 solvent delivery and VE 5111 Injector), and differential refractive index (RI) detector (Viscotek VE 3580 RI detector). Three porous styrene-divinylbenzene copolymer columns from Malvern, with porosity 10^3, 10^5 and 10^3 Å, including a precolumn, were used at a flow rate of 1.0 mL/min. Conventional calibration used polystyrene standards from Shodex. Polymer solution concentration was 3 $mg.mL^{-1}$.

Injection volumes of both devices were 100 µL. The sample solutions in DMF were prepared 14 days prior to the measurement in order to obtain a good solubility (see Annex A.). Sample solutions in DMF or THF were filtered through 0.2 µm PTFE porous membranes prior to measurement.

5.2.5. ^{1}H NMR

Proton NMR spectroscopy was used to study the structure and composition of reactants, as well as a mean to monitor synthesis. The ^{1}H spectra were recorded at 400 MHz, in either deuterated chloroform ($CDCl_3$), deuterated DMSO or deuterated DMF, with a Bruker Advance III 400 (5 mm), at 298 K, acquisition time 2 s, pulse delay 4 s, and 128 scans.

5.2.6. Thermal Characterizations

5.2.6.1. Differential Scanning Calorimetry (DSC)

Thermal behavior was assessed by means of a TA Instruments DSC Q20 equipment, calibrated with Indium standard. Samples of 3 to 5 mg were sealed in hermetic aluminum pans. They were subjected to a first cooling stage from room temperature to -150°C, followed by a first heating ramp from -150°C to 250°C. A second cycle of cooling and heating in the -150°C to 250°C temperature range was performed additionally. All steps were carried out at 20°C.min^{-1} under helium (flow rate 25 mL.min^{-1}).

5.2.6.2. Dynamic Mechanical Analysis (DMA)

Dynamic mechanical analysis (DMA) was performed on an ARES G2 rheometer from TA Instruments, with temperature scans of 3°C.min^{-1} from -100°C to 180°C. Rectangular samples of average 2.5x11x7mm were cut from bulk sheet samples and used to perform rectangular torsion tests. Parameters were set such that frequency was 1 Hz, and strain was 0.01%.

5.2.7. Mechanical Characterizations

5.2.7.1. Hardness

Hardness tests were performed on TPU materials with a manual Rockwell Shore D durometer from Zwick-Roell on 10 mm-thick cylindrical bulk samples, following standard DIN 53505. Shore D hardness was determined at room temperature, as the average of fifteen measurements, spaced by at least 5 mm and at a margin of 5 mm from the edges of the sample.

5.2.7.2. Compression Set

Compression set tests were made after standard NF ISO 815-1 and were performed with a simple apparatus made of two square steel plates of thickness 20 mm and 200x200 mm dimensions, secured by four screws and bolts in each corner. The two plates are separated by two steel spacers of dimensions 9.40x20x200 mm, as shown in Figure 5.7. Samples were obtained by piling 6 discs of diameter 29 mm, cut in the 2 mm TPU sheets, in order to get cylinders of diameter 30 mm and thickness 12.5 mm. After careful measurement of the exact thickness of the cylindrical samples with a caliper, they were installed in the compression set apparatus which was screwed up to the steel spacers to obtain a 25% strain. The apparatus was placed in a stove at 70°C for 24h, at which point the samples were taken out of the stove and released from the apparatus. After 30 min, the final thickness was measured. The compression set was computed as follows: $\%CPS = \frac{T_i - T_f}{T_i - T_s} \times 100$, with T_i the initial thickness of the sample, T_f the final thickness of the sample and T_s the thickness of the steel spacer. A result close to 100% means that the sample did not retain its shape at all during the thermal treatment, while a result close to 0% is the sign of a perfectly reversible deformation in the test conditions.

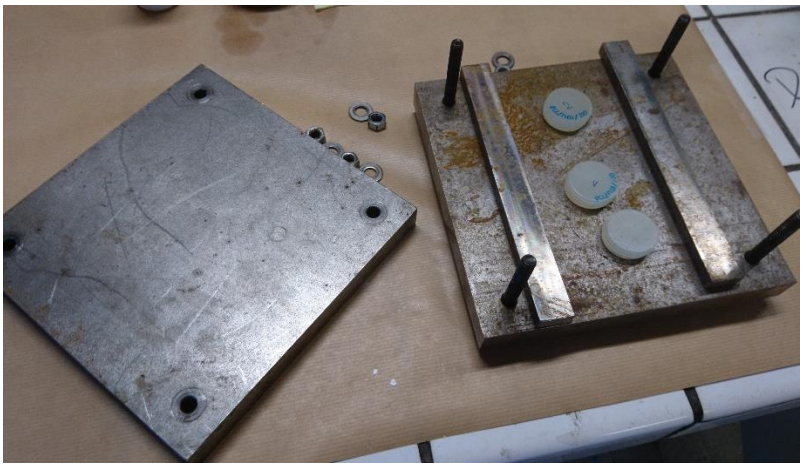

Figure 5.7 : Compression Set test apparatus and samples

5.2.7.3. Direct and reverse impact

Direct and reverse impact tests were performed on coated steel panels following standard ISO 6272 on an impact column from Sheen, as shown in Figure 5.8. The indenter was a sphere of diameter 20 mm and equipped with a mass of 1 kg. Tests were performed at a height of 100 cm and repeated 4 times in direct impact as well as 4 times on reverse impact. An aqueous solution composed of copper sulfate and hydrochloric acid was used to reveal defects in the coating after impact.

Figure 5.8: A Sheen Impact column

Any visible mark or spot of rust in or around the indentation after use of the revealing solution was considered a damage. Only one damaged test out of the 4 performed in direct or reverse impact on the sample was considered a damaged result for the whole series of 4 tests.

5.2.7.4. Abrasion

Abrasion resistance was evaluated on polyurethane coatings. Tests were performed using a 5135 Taber Abraser equipped with a CS-17 millstone and 1 kg weights on the fixtures in

order to apply a 12.7N force on the samples, as shown in Figure 5.9. From the standard, abrasion tests were performed with 200 rotations at a speed of 60 rpm. Since mass loss was too small to be measurable, the abrasion was qualified by performing a profilometry scan to obtain the roughness value of the abraded and non-abraded surfaces.

Figure 5.9: A Taber Abraser

5.2.7.5. Practical adhesion

Practical adhesion was evaluated by performing cross-hatch tests using a Labomat CC2000 grid cutter, and following ISO 2409 standard. Grid spacing of the cutter was specifically chosen following the standard directives: for coatings of thickness less than 60 µm, the grid spacing is 1 mm, and for thicknesses between 61 and 120 µm, the grid spacing is 2 mm. Cross-hatch at an angle of 90° were performed in order to obtain a grid pattern. The pattern is then brushed lightly along both diagonals in order to remove eventual chips, and then a tape with an adherence force to steel of 4.3N/cm was stuck to the pattern. After 10s, the tape was peeled with an angle of 45° and the resulting pattern was observed. Evaluation was done following the directives of ISO 2409 standard presented in Table 5.2.

Four tests were performed on each sample, preferably in the middle of the panel within a distance of more than 3 cm from the edges, and the lowest grid test score was kept if it was reproduced at least 3 times.

Table 5.2 : Classification of damage following ISO 2409

ISO score	0	1	2	3	4	5
Surface Aspect	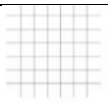	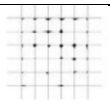	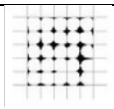	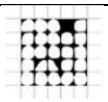	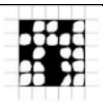	
Description	Cut marks are smooth, no tile of the grid is absent or damaged.	Light peeling at cut intersections, the damaged area is not over 5% or the total test area.	Peeling of the coating along the cuts and/or the cut intersections, the damaged area is comprised between 5 and 15 % of the total test area.	Partial or total peeling of the coating along the cuts in large bands and/or partial or total peeling of tiles from the grid, the damaged area is comprised between 15 and 35 % of the total test area.	Peeling of the coating along the cuts in large bands and/or partial or total peeling of tiles from the grid, the damaged area is comprised between 35 and 65 % of the total test area.	Peeling of such an extent that it cannot be classified in any of the other categories.

5.2.8. Others

5.2.8.1. Swelling in water

Samples of TPU material of around 20x20x2mm were weighed and submerged in separated bottles containing around 40 mL de-ionized water at room temperature. They were then periodically taken out, dried on paper towel and weighed in order to plot water uptake over time.

5.1.1.1. Profilometry

Profilometer allowed to record topographical scans of the surfaces of coatings. Scans were performed on a Dektak 150 instrument equipped with a 2.5 µm radius stylus, over a length between 3 to 4 cm, with a scan speed of 250 µm/s.

5.1.1.2. Transmission Electron Microscopy (TEM)

Transmission electron microscopy samples were prepared by cryo-ultramicrotomy at -100°C. The obtained ultrathin sections of 80 nm were observed using a PHILIPS CM120 transmission electron microscope (TEM) at an acceleration voltage of 120KV.

5.1.1.3. Atomic Force Microscopy (AFM)

Atomic Force Microscope (AFM) allowed observing phase contrast images of the smooth flat surfaces obtained by cryo-ultramicrotomy. Scans were performed in tapping mode on a Nano-observer CSInstruments equipped with a cantilever with a stiffness of 40N/m and a resonance frequency of 300 KHz purchased from APPNANO. A setpoint of 6V was used in order to increase the oscillation amplitude of the cantilever. This resulted in more contrast on the phase image at the expense of the topography image.

REFERENCES

References

[1] M. F. Sonnenschein, *Polyurethanes, Science, Technology, Markets, and Trends*, 1st Editio. Hoboken (NJ, USA): John Wiley & Sons, Ltd, 2015.

[2] Covestro, “Polyurethanes,” *European Coatings Journal*, pp. 1–108, 2016.

[3] E. Delebecq, J. Pascault, B. Boutevin, and F. Ganachaud, “On the Versatility of Urethane/Urea Bonds: Reversibility, Blocked Isocyanate, and Non-isocyanate Polyurethane,” *Chem. Rev.*, vol. 113, no. 1, pp. 80–118, 2013.

[4] M. F. Sonnenschein, V. V. Ginzburg, K. S. Schiller, and B. L. Wendt, “Design, polymerization, and properties of high performance thermoplastic polyurethane elastomers from seed-oil derived soft segments,” *Polymer*, vol. 54, no. 4, pp. 1350–1360, 2013.

[5] Y. Ni, F. Becquart, J. Chen, and M. Taha, “Polyurea-urethane supramolecular thermo-reversible networks,” *Macromolecules*, vol. 46, no. 3, pp. 1066–1074, 2013.

[6] R. G. Arnold, J. A. Nelson, and J. J. Verbanc, “Recent Advances in Isocyanate Chemistry,” *Chem. Rev.*, vol. 57, no. 1, pp. 47–76, 1957.

[7] K. C. Frisch, “The ICI polyurethanes book, Second Edition by George Woods, Wiley, New York, 1990, 362 pp.,” *J. Polym. Sci. Part A Polym. Chem.*, vol. 29, no. 12, pp. 1834–1835, 1991.

[8] Z. Wirpsza, *Polyurethanes: Chemistry, Technology and Applications*, 1st Ed. Ellis Horwood Polymer Science Series, 1993.

[9] K. Schwetlick and R. Noack, “Kinetics and Catalysis of Consecutive Isocyanate Reactions. Formation of Carbamates, Allophanates and lsocyanurates,” *J. Chem. Soc.*, vol. 1, no. 3, pp. 395–402, 1995.

[10] G. Anzuino, A. Pirro, O. Rossi, and L. Polo Friz, “Reaction of Diisocyanates with Alcohols. I. Uncatalyzed reactions,” *J. Polym. Sci. Polym. Chem. Ed.*, vol. 13, pp. 1657–1666, 1975.

[11] M. Spirkova, M. Kubin, and K. Dusek, “Side reactions in the formation of polyurethanes: Model reactions between phenylisocyanate and 1 -butanol,” *J. Macromol. Sci. Part A - Chem.*, vol. 24, no. 10, pp. 1151–1166, 1987.

[12] A. Lapprand, F. Boisson, F. Delolme, F. Méchin, and J. P. Pascault, “Reactivity of isocyanates with urethanes: Conditions for allophanate formation,” *Polym. Degrad. Stab.*, vol. 90, no. 2, pp. 363–373, 2005.

[13] G. Oertel, *Polyurethane Handbook*, 2nd editio. Hanser Publishers, 1994.

[14] L. Thiele and R. Becker, “Catalytic mechanism of polyurethane formation,” in *Advances in Urethane: Science & Technology vol 12*, K. C. Frisch and D. Klempner, Eds.

Technomic, 1993.

[15] S. Dabi and A. Zilkha, “Effect of polar aprotic solvents on the trimerization of aliphatic isocyanates by organometallic catalysts,” *Eur. Polym. J.*, vol. 16, no. 6, pp. 471–473, 1980.

[16] G. Woods, *The ICI polyurethanes book*, Second Edi. Wiley, 1991.

[17] D. K. Chattopadhyay and D. C. Webster, “Thermal stability and flame retardancy of polyurethanes,” *Prog. Polym. Sci.*, vol. 34, no. 10, pp. 1068–1133, 2009.

[18] B. A. Dombrow, *Polyurethanes*. Reinhold, 1965.

[19] W. P. Yang, C. W. Macosko, and S. T. Wellinghoff, “Thermal degradation of urethanes based on 4,4’-diphenylmethane diisocyanate and 1,4-butanediol (MDI/BDO),” *Polymer*, vol. 27, pp. 1235–1240, 1986.

[20] M. Tanaka and T. Nakaya, “Liquid crystalline polyurethane. Polyurethanes containing bis-(*p* -oxymethylphenyl) terephthalate,” *J. Macromol. Sci. Part A - Chem.*, vol. 24, no. 7, pp. 777–785, 1987.

[21] L. H. Peebles, “Sequence Length Distribution in Segmented Block Copolymers,” *Macromolecules*, vol. 7, no. 6, pp. 872–882, 1974.

[22] L. H. Peebles, “Hard Block Length Distribution in Segmented Block Copolymers,” *Macromolecules*, vol. 9, pp. 58–61, 1976.

[23] S. L. Cooper and A. V. Tobolsky, “Properties of linear elastomeric polyurethanes,” *J. Appl. Polym. Sci.*, vol. 10, no. 12, pp. 1837–1844, 1966.

[24] T. Ohta and K. Kawasaki, “Equilibrium Morphology of Block Copolymer Melts,” *Macromolecules*, vol. 19, pp. 2621–2632, 1986.

[25] L. Leibler, “Theory of Microphase Separation in Block Copolymers,” *Macromolecules*, vol. 13, no. 6, pp. 1602–1617, 1980.

[26] G. H. Fredrickson and E. Helfand, “Fluctuation effects in the theory of microphase separation in block copolymers,” *J. Chem. Phys.*, vol. 87, no. 1, pp. 697–705, 1987.

[27] H. Benoit and G. Hadziioannou, “Scattering Theory and Properties of Block Copolymers with Various Architectures in the Homogeneous Bulk State,” *Macromolecules*, vol. 21, no. 5, pp. 1449–1464, 1988.

[28] Y. Camberlin, J. P. Pascault, J. M. Letoffe, and P. Claudy, “Synthesis and DSC study of model hard segments from diphenyl methane diisocyanate and butane diol,” *J. Polym. Sci. Polym. Chem. Ed.*, vol. 20, no. 2, pp. 383–392, 1982.

[29] Y. Camberlin and J.-P. Pascault, “Quantitative DSC Evaluation of Phase Segregation Rate in Linear Segmented Polyurethanes and Polyurethaneureas,” *J. Polym. Sci. Polym. Chem. Ed.*, vol. 21, pp. 415–423, 1983.

[30] Y. Camberlin and J.-P. Pascault, “Phase Segregation Kinetics in Segmented Linear Polyurethanes : Relations between Equilibrium Time and Chain Mobility and between Equilibrium Degree of Segregation and Interaction Parameter,” *J. Polym. Sci. Polym. Phys. Ed.*, vol. 22, pp. 1835–1844, 1984.

[31] J. T. Koberstein and T. P. Russell, “Simultaneous SAXS-DSC Study of Multiple Endothermic Behavior in Polyether-Based Polyurethane Block Copolymers,” *Macromolecules*, vol. 19, pp. 714–720, 1986.

[32] M. F. Sonnenschein, N. Rondan, B. L. Wendt, and J. M. Cox, “Synthesis of transparent thermoplastic polyurethane elastomers,” *J. Polym. Sci. Part A Polym. Chem.*, vol. 42, no. 2, pp. 271–278, 2004.

[33] S. Oprea, “Effect of the long chain extender on the properties of linear and castor oil cross-linked PEG-based polyurethane elastomers,” *J. Mater. Sci.*, vol. 46, no. 7, pp. 2251–2258, 2011.

[34] K. Gisselfält and B. Helgee, “Effect of soft segment length and chain extender structure on phase separation and morphology in poly(urethane urea)s,” *Macromol. Mater. Eng.*, vol. 288, no. 3, pp. 265–271, 2003.

[35] C. Bueno-Ferrer, E. Hablot, F. Perrin-Sarazin, M. C. Garrigós, A. Jiménez, and L. Averous, “Structure and Morphology of New Bio-Based Thermoplastic Polyurethanes Obtained From Dimeric Fatty Acids,” *Macromol. Mater. Eng.*, vol. 297, no. 8, pp. 777–784, 2012.

[36] S. Sartori, M. Boffito, P. Serafini, A. Caporale, A. Silvestri, E. Bernardi, M. P. Sassi, F. Boccafoschi, and G. Ciardelli, “Synthesis and structure–property relationship of polyester-urethanes and their evaluation for the regeneration of contractile tissues,” *React. Funct. Polym.*, vol. 73, no. 10, pp. 1366–1376, 2013.

[37] C. E. Hoyle, Y. G. No, K. G. Malone, S. F. Thames, and D. Creed, “Laser flash photolysis of a 4,4’-methylene bis(phenyl isocyanate) (MDI) based polyurethane and model carbamates,” *Macromolecules*, vol. 21, no. 9, pp. 2727–2730, 1988.

[38] T. Calvo-Correas, M. D. Martin, A. Retegi, N. Gabilondo, M. A. Corcuera, and A. Eceiza, “Synthesis and Characterization of Polyurethanes with High Renewable Carbon Content and Tailored Properties,” *ACS Sustain. Chem. Eng.*, vol. 4, no. 10, pp. 5684–5692, 2016.

[39] L. Gustini, C. Lavilla, L. Finzel, B. A. J. Noordover, M. M. R. M. Hendrix, and C. E. Koning, “Sustainable coatings from bio-based, enzymatically synthesized polyesters with enhanced functionalities,” *Polym. Chem.*, vol. 7, pp. 6586–6597, 2016.

[40] Y. Li, B. A. J. Noordover, R. A. T. M. Van Benthem, and C. E. Koning, “Chain extension of dimer fatty acid- and sugar-based polyurethanes in aqueous dispersions,” *Eur. Polym. J.*, vol. 52, pp. 12–22, 2014.

[41] “DuPont Launches DuPont™ Cerenol,” 2007. [Online]. Available:

http://www.duponttateandlyle.com/news_060407.

[42] M. Vasiliu, K. Guynn, and D. A. Dixon, “Prediction of the Thermodynamic Properties of Key Products and Intermediates from Biomass,” *J. Phys. Chem. C*, vol. 115, no. 31, pp. 15686–15702, 2011.

[43] Y. Jiang, A. J. J. Woortman, G. O. R. Alberda van Ekentein, D. M. Petrovic, and K. Loos, “Enzymatic Synthesis of Biobased Polyesters Using 2,5- Bis(hydroxymethyl)furan as the Building Block,” *Biomacromolecules*, vol. 15, pp. 2482–2493, 2014.

[44] N. Karak, *Vegetable oil-based polymers. Properties, processing and applications*. WoodHead Publishing, 2012.

[45] J. Y. Jadhav, “Castor Oil Based Prepolymers and Thermoplastic Urethane Polymers,” *Int. J. Polym. Mater. Polym. Biomater.*, vol. 11, pp. 151–158, 1986.

[46] H. Caupin, “Products from castor oil: Past, present and future,” in *Lipid Technologies and Applications*, Marcel Dek., F. Gunstone and F. Padley, Eds. 1997.

[47] D. Montarnal, P. Cordier, C. Soulié-Ziakovic, F. Tournilhac, and L. Leibler, “Synthesis of self-healing supramolecular rubbers from fatty acid derivatives, diethylene triamine, and urea,” *J. Polym. Sci. Part A Polym. Chem.*, vol. 46, no. 24, pp. 7925–7936, 2008.

[48] C. Bueno-Ferrer, E. Hablot, M. D. C. Garrigós, S. Bocchini, L. Averous, and A. Jiménez, “Relationship between morphology, properties and degradation parameters of novative biobased thermoplastic polyurethanes obtained from dimer fatty acids,” *Polym. Degrad. Stab.*, vol. 97, no. 10, pp. 1964–1969, 2012.

[49] C. Carré, H. Zoccheddu, S. Delalande, P. Pichon, and L. Avérous, “Synthesis and characterization of advanced biobased thermoplastic nonisocyanate polyurethanes, with controlled aromatic-aliphatic architectures,” *Eur. Polym. J.*, vol. 84, pp. 759–769, 2016.

[50] C. Carré, L. Bonnet, and L. Avérous, “Solvent- and catalyst-free synthesis of fully biobased nonisocyanate polyurethanes with different macromolecular architectures,” *RSC Adv.*, vol. 5, no. 121, pp. 100390–100400, 2015.

[51] C. Carré, L. Bonnet, and L. Avérous, “Original biobased nonisocyanate polyurethanes: solvent- and catalyst-free synthesis, thermal properties and rheological behaviour,” *RSC Adv.*, vol. 4, no. 96, pp. 54018–54025, Oct. 2014.

[52] I. Yilgör, E. Yilgör, and G. L. Wilkes, “Critical parameters in designing segmented polyurethanes and their effect on morphology and properties: A comprehensive review,” *Polymer*, vol. 58, no. 1–36, pp. A1–A36, 2015.

[53] A. Lapprand, “Modification chimique des polyurethanes thermoplastiques: étude des réactions chimiques menant à l’autoreticulation et de la microorgansation physique, pour le contrôle des propriétés.,” PhD Thesis, INSA Lyon, Université de Lyon, 2005.

[54] D. Howell, “Technology, Formulation and Application of powder coatings,” in

Wiley/Sita Series in Surface Coatings technology, J. D. Sanders, Ed. New York: John Wiley & Sons, Ltd, 2000.

[55] H. W. Wolfe, "Aqueous Polyurethane Dispersions," US 4,183,836, 1961.

[56] H. G. Fletcher and R. M. Goepp, "1,4;3,6-Hexitol dianhydride L-Isoidide," *J. Am. Chem. Soc.*, vol. 67, no. 6, pp. 1042–1043, 1945.

[57] R. Montgomery and L. F. Wiggins, "The anhydrides of polyhydric alcohols. Part IV. The constitution of dianhydro sorbitol," *J. Chem. Soc.*, pp. 390–393, 1946.

[58] F. Fenouillot, A. Rousseau, G. Colomines, R. Saint-Loup, and J. P. Pascault, "Polymers from renewable 1,4:3,6-dianhydrohexitols (isosorbide, isomannide and isoidide): A review," *Prog. Polym. Sci.*, vol. 35, no. 5, pp. 578–622, 2010.

[59] G. Flèche and M. Huchette, "Isosorbide, Preparation, Properties and Chemistry," *Starch/Stärke*, vol. 38, no. 1, pp. 26–30, 1986.

[60] G. Flèche, P. Fuertes, R. Tamion, and H. Wyart, "Method for purifying a composition containing at least one internal dehydration product of a hydrogenated sugar," US 0110969, 2002.

[61] F. J. Hopton and G. H. S. Thomas, "Conformations of some dianhydrohexitols," *Can. J. Chem.*, vol. 47, no. 13, pp. 2395–2401, 1969.

[62] J. C. Goodwin, J. E. Hodge, and D. Weisleder, "Preparation of bicyclic hexitol anhydrides by using acidic cation-exchange resin in a binary solvent. 13C-N.m.r. spectroscopy confirms configurational inversion in chloride displacement of methanesulfonate in isomannide and isosorbide derivatives," *Carbohydr. Res.*, vol. 79, no. 1, pp. 133–141, 1980.

[63] F. Jacquet, R. Audinos, M. Delmas, and A. Gaset, "Analytical Techniques Suitable for the Study of the Oxidation of a Biomass-Issued Substrate : 4,8-dihydroxy-2,6-dioxabicyclo(3.3.0)octane(IR, 4S, 5R, 8R)," *Biomass*, vol. 6, pp. 193–209, 1985.

[64] L. W. Wright and J. D. Brandner, "Catalytic Isomerization of Polyhydric Alcohols. II. The Isomerization of Isosorbide to Isomannide and Isoidide," *J. Org. Chem.*, vol. 29, no. 10, pp. 2979–2982, 1964.

[65] E. Cognet-Georjon, "Synthèse et caractérisation de prépolymères fonctionnels et de matériaux à partir d'isosorbide," PhD Thesis, INSA Lyon, 1995.

[66] M. Ionescu, Z. S. Petrović, M. D. Sandhu, I. Javni, N. Bilić, and E. Eastwood, "New Isosorbide Derivatives for Bio-based Polyurethanes," in *Polyurethanes 2011 Technical Conference*, pp. 144–155, 2011.

[67] E. Cognet-Georjon, F. Méchin, and J.-P. Pascault, "New polyurethanes based on diphenylmethane diisocyanate and 1,4:3,6-dianhydrosorbitol, 1. Model kinetic studies and characterization of the hard segment," *Macromol. Chem. Phys.*, vol. 196, pp. 3733–3751, 1995.

[68] Y. Li, B. A. J. Noordover, R. A. T. M. van Benthem, and C. E. Koning, “Reactivity and Regio-Selectivity of Renewable Building Blocks for the Synthesis of Water-Dispersible Polyurethane Prepolymers,” *ACS Sustain. Chem. Eng.*, vol. 2, no. 4, pp. 788–797, 2014.

[69] S. K. Dirlikov and C. J. Schneider, “Polyurethanes based on 1;4-3;6-dianhydrohexitols,” US4443563, 1984.

[70] J. Thiem and H. Lüeders, “Synthesis and properties of polyurethanes derived from diaminodianhydroalditols,” *Makromol. Chemie*, vol. 187, no. 12, pp. 2775–2785, 1986.

[71] M. Beldi *et al.*, “Characterization of cyclic and non-cyclic poly-(ether-urethane)s bio-based sugar diols by a combination of MALDI-TOF and NMR,” *Eur. Polym. J.*, vol. 43, no. 8, pp. 3415–3433, 2007.

[72] C.-H. Lee, H. Takagi, H. Okamoto, M. Kato, and A. Usuki, “Synthesis , Characterization , and Properties of Polyurethanes Containing 1,4:3,6-Dianhydro-D-sorbitol,” *J. Polym. Sci. Part A Polym. Chem.*, vol. 47, pp. 6025–6031, 2009.

[73] R. Marìn, A. Alla, A. Martinez de Ilarduya, and S. Munoz-Guerra, “Carbohydrate-Based Polyurethanes : A Comparative Study of Polymers Made from Isosorbide and 1,4-Butanediol,” *J. Appl. Polym. Sci.*, vol. 123, pp. 986–994, 2012.

[74] M. D. Zenner, Y. Xia, J. S. Chen, and M. R. Kessler, “Polyurethanes from isosorbide-based diisocyanates.,” *ChemSusChem*, vol. 6, no. 7, pp. 1182–1185, 2013.

[75] E. Cognet-Georjon, F. Méchin, and J. Pascault, “New polyurethanes based on 4.4’-diphenylmethane diisocyanate and 1,4:3,6 dianhydrosorbitol, 2: Synthesis and properties of segmented polyurethane elastomers,” *Macromol. Chem. Phys.*, vol. 197, pp. 3593–3612, 1996.

[76] I. Javni *et al.*, “Thermoplastic polyurethanes with isosorbide chain extender,” *J. Appl. Polym. Sci.*, vol. 132, no. 47, p. 45830, 2015.

[77] I. Javni *et al.*, “Thermoplastic polyurethanes with controlled morphology based on methylenediphenyldiisocyanate/isosorbide/butanediol hard segments,” *Polym. Int.*, vol. 64, no. 11, pp. 1607–1616, 2015.

[78] H.-J. Kim, M.-S. Kang, J. C. Knowles, and M.-S. Gong, “Synthesis of highly elastic biocompatible polyurethanes based on bio-based isosorbide and poly(tetramethylene glycol) and their properties.,” *J. Biomater. Appl.*, vol. 29, no. 3, pp. 454–464, 2014.

[79] K. Gorna and S. Gogolewski, “Biodegradable porous polyurethane scaffolds for tissue repair and regeneration,” *J. Biomed. Mater. Res. A*, vol. 79A, no. 1, pp. 128–138, 2006.

[80] Y. K. Tsui and S. Gogolewski, “Microporous biodegradable polyurethane membranes for tissue engineering.,” *J. Mater. Sci. Mater. Med.*, vol. 20, no. 8, pp. 1729–1741, 2009.

[81] S. Gogolewski, K. Gorna, E. Zaczynska, and A. Czarny, “Structure-property relations and cytotoxicity of isosorbide-based biodegradable polyurethane scaffolds for tissue

repair and regeneration.," *J. Biomed. Mater. Res. A*, vol. 85A, no. 2, pp. 456–465, 2008.

[82] R. Marìn and S. Muñoz-Guerra, "Carbohydrate-Based Poly(ester-urethane)s: A Comparative Study Regarding Cyclic Alditols Extenders and Polymerization Procedures," *J. Appl. Polym. Sci.*, vol. 114, pp. 3723–3736, 2009.

[83] H.-S. Park, M.-S. Gong, and J. C. Knowles, "Catalyst-free synthesis of high elongation degradable polyurethanes containing varying ratios of isosorbide and polycaprolactone: physical properties and biocompatibility.," *J. Mater. Sci. Mater. Med.*, vol. 24, no. 2, pp. 281–294, 2013.

[84] M. J. Donnelly, "Polyurethanes from renewable resources. III: synthesis and characterisation of low molar mass polytetrahydrofuran diols and their glucosides," *Polym. Int.*, vol. 37, no. 1, pp. 1–20, 1995.

[85] J. V. Koleske and R. D. Lundberg, "Lactone Polymers I. Glass transition temperature of poly-e-caprolactone by means of compatible polymer mixtures," *J. Polym. Sci. Part A2*, vol. 7, pp. 795–807, 1969.

[86] S.-Y. Oh, M.-S. Kang, J. C. Knowles, and M.-S. Gong, "Synthesis of bio-based thermoplastic polyurethane elastomers containing isosorbide and polycarbonate diol and their biocompatible properties," *J. Biomater. Appl.*, vol. 30, no. 3, pp. 327–337, 2015.

[87] V. Besse *et al.*, "Synthesis of isosorbide based polyurethanes: An isocyanate free method," *React. Funct. Polym.*, vol. 73, no. 3, pp. 588–594, 2013.

[88] M. Charlon, B. Heinrich, Y. Matter, E. Couzigné, B. Donnio, and L. Avérous, "Synthesis, structure and properties of fully biobased thermoplastic polyurethanes, obtained from a diisocyanate based on modified dimer fatty acids, and different renewable diols," *Eur. Polym. J.*, vol. 61, pp. 197–205, 2014.

[89] M. Z. Oulame, F. Pion, S. Allauddin, K. V. S. N. Raju, P.-H. Ducrot, and F. Allais, "Renewable alternating aliphatic-aromatic poly(ester-urethane)s prepared from ferulic acid and bio-based diols," *Eur. Polym. J.*, vol. 63, pp. 186–193, 2015.

[90] V. Besse, F. Camaraa, F. Méchin, E. Fleury, S. Caillol, J.-P. Pascault and B. Boutevin, "How to explain low molar masses in PolyHydroxyUrethanes (PHUs)," *Eur. Polym. J.*, vol. 71, pp. 1–11, 2015.

[91] L. Cuvé, J. P. Pascault, G. Boiteux, and G. Seytre, "Synthesis and properties of polyurethanes based on polyolefine: 1 . Rigid polyurethanes and amorphous segmented polyurethanes prepared in polar solvents under homogeneous conditions," *Polymer*, vol. 32, no. 2, pp. 343–352, 1991.

[92] J. T. Koberstein and A. F. Galambos, "Multiple Melting in Segmented Polyurethane Block Copolymers," *Macromolecules*, vol. 25, no. 21, pp. 5618–5624, 1992.

[93] C. Li, J. Liu, J. Li, F. Shen, Q. Huang, and H. Xu, "Studies of 4,4'-diphenylmethane diisocyanate (MDI)/1,4-butanediol (BDO) based TPUs by in situ and moving-window two-dimensional correlation infrared spectroscopy: Understanding of multiple DSC endotherms from intermolecular interactions and motions level," *Polymer*, vol. 53, no. 23, pp. 5423–5435, 2012.

[94] A. Saiani, W. A. Daunch, H. Verbeke, J.-W. Leenslag, and J. S. Higgins, "Origin of Multiple Melting Endotherms in a High Hard Block Content Polyurethane. 1. Thermodynamic Investigation," *Macromolecules*, vol. 34, no. 26, pp. 9059–9068, 2001.

[95] A. Saiani, C. Rochas, G. Eeckhaut, W. A. Daunch, J.-W. Leenslag, and J. S. Higgins, "Origin of Multiple Melting Endotherms in a High Hard Block Content Polyurethane . 2. Structural Investigation," *Macromolecules*, vol. 37, pp. 1411–1421, 2004.

[96] A. Saiani, A. Novak, L. Rodier, G. Eeckhaut, J.-W. Leenslag, and J. S. Higgins, "Origin of Multiple Melting Endotherms in a High Hard Block Content Polyurethane: Effect of Annealing Temperature," *Macromolecules*, vol. 40, no. 20, pp. 7252–7262, 2007.

[97] B. Fernández-d'Arlas, J. Balko, R. P. Baumann, E. Pöselt, R. Dabbous, B. Eling, T. Thurn-Albrecht and A. J. Müller, "Tailoring the Morphology and Melting Points of Segmented Thermoplastic Polyurethanes by Self-Nucleation," *Macromolecules*, vol. 49, pp. 7952–7964, 2016.

[98] J. Balko, B. Fernández-d'Arlas, E. Pöselt, R. Dabbous, A. J. Müller, and T. Thurn-Albrecht, "Clarifying the Origin of Multiple Melting of Segmented Thermoplastic Polyurethanes by Fast Scanning Calorimetry," *Macromolecules*, vol. 50, no. 19, pp. 7672–7680, 2017.

[99] L. Cuvé, J. Pascault, and G. Boiteux, "Synthesis and properties of polyurethanes based on polyolefin: 2 . Semicrystalline segmented polyurethanes prepared under heterogeneous or homogeneous synthesis conditions," *Polymer (Guildf).*, vol. 33, no. 18, pp. 3957–3967, 1992.

[100] D. B. Klinedinst, I. Yilgör, E. Yilgör, M. Zhang, and G. L. Wilkes, "The effect of varying soft and hard segment length on the structure–property relationships of segmented polyurethanes based on a linear symmetric diisocyanate, 1,4-butanediol and PTMO soft segments," *Polymer.*, vol. 53, no. 23, pp. 5358–5366, 2012.

[101] C. P. Christenson, M. A. Harthcock, M. D. Meadows, H. L.Spell, W. L. Howard, M. W. Creswick, R. E. Guerra, R. B. Turner, "Model MDI/butanediol polyurethanes: Molecular structure, morphology, physical and mechanical properties," *J. Polym. Sci. Part B Polym. Phys.*, vol. 24, no. 7, pp. 1401–1439, 1986.

[102] K. K. S. Hwang, D. J. Hemker, and S. L. Cooper, "Phase diagrams and morphology of a urethane model hard segment and polyether macroglycols," *Macromolecules*, vol. 17, no. 3, pp. 307–315, 1984.

[103] L. M. Leung and J. T. Koberstein, "DSC annealing study of microphase separation and

multiple endothermic behavior in polyether-based polyurethane block copolymers," *Macromolecules*, vol. 19, no. 3, pp. 706–713, 1986.

[104] T. R. Hesketh, J. W. C. Van Bogart, and S. L. Cooper, "Differential scanning calorimetry analysis of morphological changes in segmented elastomers," *Polym. Eng. Sci.*, vol. 20, no. 3, pp. 190–197, 1980.

[105] S. Pongkitwitoon, R. Hernández, J. Weksler, A. Padsalgikar, T. Choi, and J. Runt, "Temperature dependent microphase mixing of model polyurethanes with different intersegment compatibilities," *Polymer*, vol. 50, no. 26, pp. 6305–6311, 2009.

[106] S. Desilets, S. Villeneuve, M. Laviolette, and M. Auger, "13C-NMR spectroscopy study of polyurethane obtained from azide hydroxyl-terminated polymer cured with isophorone diisocyanate (IPDI)," *J. Polym. Sci. Part A Polym. Chem.*, vol. 35, pp. 2991–2998, 1997.

[107] A. V. Cunliffe, A. Davis, M. Farey, and J. Wright, "The Kinetics of the Reaction if Isophorone Di-isocyanate with Mono-alcohols," *Polymer*, vol. 26, pp. 301–306, 1985.

[108] H.-K. Ono, F. N. Jones, and S. P. Pappas, "Relative Reactivity of Isocyanate Groups of Isophorone Diisocyanate. Unexpected High Reactivity of the Secondary Isocyanate Group," *J. Polym. Sci. Polym. Lett. Ed.*, vol. 23, pp. 509–515, 1985.

[109] F. M. B. Coutinho and M. C. G. Rocha, "Kinetic Study of the reactions between hydroxylated polybutadiene and isocyanates in chlorobenzene. IV. Reactions with tolylene diisocyanate, 3-isocyanatomethyl-3,5,5-trimethylcyclohexyl isocyanate and hexamethylene diisocyanate," *Eur. Polym. J.*, vol. 27, no. 2, pp. 213–216, 1991.

[110] N. Bialas, H. Höcker, M. Marschner, and W. Ritter, "13C NMR studies on the relative reactivity of isocyanate groups of isophorone diisocyanate isomers," *Makromol. Chemie*, vol. 191, pp. 1843–1852, 1990.

[111] "Isophorone Diisocyanate," *Center for Disease Control and Prevention*, 2017. [Online]. Available: https://www.cdc.gov/niosh/ipcsneng/neng0499.html.

[112] R. Teissier and G. Martino-Gauchi, "Continuous process for the manufacture of 3,5,5-trimethylcyclohexa-3-en-one(beta-isophorone)," US6274772B1, 2001.

[113] J. C. Thunberg and W. B. Begonis, "Process for the preparation of 3-cyano-3,5,5-trimethylcyclohexanone by addition of hydrogen cyanide to isophorone," US5011968, 1991.

[114] M. Schwarz, A. Merkel, J.-J. Nitz, and G. Grund, "Process for preparing 3-cyano-3,5,5-trimethylcyclohexanone," US2014/0114085A1, 2014.

[115] D. Thorpe and R. C. Smith, "Process for making aliphatic and cycloaliphatic polyisocyanates," EP0327231, 1989.

[116] A. Otterbach H. V. Schwarz, F. Lerger, W. Schwarz, E. Brandt, P. Magnussen, O. Mattner, “Multistep, continuous preparation of organic polyisocyanates,” US5386053, 1995.

[117] C. Cascella, M. Malinconico, E. Martuscelli, A. Piermattei, G. Ragosta, and A. Rizzo, “Physical, dynamic-mechanial and thermogravimetric analysis of aromatic and cycloaliphatic-based poly(urethaneurea)s,” *Angew. Makromol. Chemie*, vol. 231, pp. 79–89, 1995.

[118] D. E. Nikles, J.-L. Liang, J. L. Cain, A. P. Chacko, R. I. Webb, and K. Belmore, “Amine-Quinone Polyurethanes. I. Preparation of Polyurethane Block Copolymers Containing 2,5-Bis(N-2-hydroxyethyl-N-methylamino)-1,4-benzoquinone Diol Monomer,” *J. Polym. Sci. Part A Polym. Chem.*, vol. 33, no. 17, pp. 2881–2886, 1995.

[119] J. Y. Jang and J. Y. Do, “Synthesis and evaluation of thermoplastic polyurethanes as thermo-optic waveguide materials,” *Polym. J.*, vol. 46, no. 6, pp. 349–354, 2014.

[120] W. Xue, L. Zhang, H. Chen, J. Wang, H. Na, and J. Zhu, “Synthesis of polyurethane containing carbon – carbon double bonds to prepare functionalizable ultrafine fibers via electrospinning,” *Polym. Chem.*, vol. 6, pp. 3858–3864, 2015.

[121] W. Xu, R. Zhang, W. Liu, J. Zhu, X. Dong, H. Guo and G.-H. Hu, “A Multiscale Investigation on the Mechanism of Shape Recovery for IPDI to PPDI Hard Segment Substitution in Polyurethane,” *Macromolecules*, vol. 49, no. 16, pp. 5931–5944, 2016.

[122] S. Srivastava, A. Biswas, S. Senapati, B. Ray, D. Rana, V. K. Aswal and P. Maiti, “Novel shape memory behaviour in IPDI based polyurethanes: Influence of nanoparticle,” *Polymer*, vol. 110, pp. 95–104, 2017.

[123] Y. Lu, L. Tighzert, P. Dole, and D. Erre, “Preparation and properties of starch thermoplastics modified with waterborne polyurethane from renewable resources,” *Polymer*, vol. 46, pp. 9863–9870, 2005.

[124] Y. Zhang, B. Fan, P. Zhang, Y. Leng, M. Zhu, and Q. Wu, “Thermoplastic starches modified with polyurethane microparticles : The effects of isocyanate types in polyurethane,” *Starch/Stärke*, vol. 63, pp. 700–708, 2011.

[125] T. Gurunathan and S. K. Nayak, “The influence of reactive organoclay on a biorenewable castor oil-based polyurethane prepolymers toughened polylactide nanocomposites,” *Polym. Adv. Technol.*, vol. 27, no. 11, pp. 1484–1493, 2016.

[126] S. M. You, K. R. Sun, I. D. Chung, and B. K. Kim, “Polyurethane-amide hybrid dispersions,” *J. Polym. Eng.*, vol. 29, no. 1–3, pp. 63–78, 2009.

[127] H. G. Fang, H. L. Wang, J. Sun, H. B. Wei, and Y. S. Ding, “Tailoring elastomeric properties of waterborne polyurethane by incorporation of polymethyl methacrylate with nanostructural heterogeneity,” *RSC Adv.*, vol. 6, no. 16, pp. 13589–13599, 2016.

[128] T. Wan and D. Chen, “Synthesis and properties of self-healing waterborne

polyurethanes containing disulfide bonds in the main chain," *J. Mater. Sci.*, vol. 52, no. 1, pp. 197–207, 2017.

[129] S. Hajializadeh, M. Barikani, and S. M. Bellah, "Synthesis and characterization of multiwall carbon nanotube/waterborne polyurethane nanocomposites," *Polym. Int.*, vol. 66, no. 7, pp. 1074–1083, 2017.

[130] R. Ménard, S. Caillol, and F. Allais, "Chemo-enzymatic synthesis and characterization of renewable thermoplastic and thermoset isocyanate-free poly(hydroxy)urethanes from ferulic acid derivatives," *ACS Sustain. Chem. Eng.*, vol. 5, no. 2, pp. 1446–1456, 2017.

[131] W. W. Graessley, "The entanglement concept in polymer rheology," in *Advances in Polymer Science*, Berlin/Heidelberg: Springer-Verlag, 1974, pp. 1–179.

[132] S. Wu, "Predicting chain conformation and entanglement of polymers from chemical structure," *Polym. Eng. Sci.*, vol. 32, no. 12, pp. 823–830, 1992.

[133] J. Huybrechts and K. Dušek, "Star Oligomers for Low VOC Polyurethane Coatings," *Surf. Coatings Int.*, vol. 3, pp. 117–127, 1998.

[134] M. Duškova-Smrčkova and K. Dušek, "Processes and states during polymer film formation by simultaneous crosslinking and solvent evaporation," *J. Mater. Sci.*, vol. 37, pp. 4733–4741, 2002.

[135] K. Dušek and M. Duškova-Smrčkova, "Vapor pressure over stressed coating films," *Polym. Bull.*, vol. 45, pp. 83–88, 2000.

[136] M. Duškova-Smrčkova, K. Dušek, and P. Vlasák, "Solvent activity changes and phase separation during crosslinking of coating films," *Macromol. Symp.*, vol. 198, pp. 259–270, 2003.

[137] S. Kiil, "Mathematical modelling of simultaneous solvent evaporation and chemical curing in thermoset coatings: A parameter study," *Prog. Org. Coatings*, vol. 70, no. 4, pp. 192–198, 2011.

[138] S. Kiil, "Quantification of simultaneous solvent evaporation and chemical curing in thermoset coatings," *J. Coatings Technol. Res.*, vol. 7, no. 5, pp. 569–586, 2010.

[139] S. Monaghan and R. A. Pethrick, "Solvent effects on cure in a 2K polyurethane-mechanical and dielectric studies," *Ind. Eng. Chem. Res.*, vol. 51, no. 34, pp. 11038–11044, 2012.

[140] S. Monaghan and R. A. Pethrick, "Solvent Effects in Polyurethane Cure: A Model Study," *Macromolecules*, vol. 45, no. 9, pp. 3928–3938, 2012.

[141] C. J. Hilado and E. M. Olcomendy, "Ignitability of rigid foam insulation," *J. Therm. Insul.*, vol. 2, pp. 87–89, 1978.

[142] L. N. Boretzky, K. E. Best, D. C. McClurg, and A. I. Wallace, "Chip resistant

polyurethane coating," US5250650, 1993.

[143] A. M. Kaminski and M. W. Urban, "Interfacial studies of crosslinked urethanes: Part II. The effect of humidity on waterborne polyurethanes; a spectroscopic study," *J. Coatings Technol.*, vol. 69, no. 10, pp. 113–121, 1997.

[144] S. Allmaras, "Worker exposure to 1,3,5-triglycidyl isocyanurate (TGIC) in powder paint coating operations," *Appl. Occup. Environ. Hyg.*, vol. 18, no. 3, pp. 151–153, 2003.

[145] L. E. Katz, E. A. Barsa, B. W. Tucker, and P. V. Grosso, "Catalyst and process for producing isocyanate trimers," US5691440, 1997.

[146] F. Burel, A. Feldman, C. Loutelier-Bourhis, and C. Bunel, "Characterization of an isophorone-based polyisocyanate," *e-Polymers*, vol. 1, no. 11, pp. 1–9, 2004.

[147] T. Nagakawa, H. Takeuchi, K. Sato, and S. Yamasaki, "Pentamethylene diisocyanate, methods for producing pentamethylene diisocyanate, polyisocyanate composition, polyurethane resin, and polyurea resin.," EP2684867A1, 2014.

[148] S. Lawrenson, M. North, F. Peigneguy, and A. Routledge, "Greener solvents for solid-phase synthesis," *Green Chem.*, vol. 19, no. 4, pp. 952–962, 2017.

[149] F. Aricò, A. S. Aldoshin, and P. Tundo, "One-Pot Preparation of Dimethyl Isosorbide from d-Sorbitol via Dimethyl Carbonate Chemistry," *ChemSusChem*, vol. 10, no. 1, pp. 53–57, 2017.

[150] P. Tundo, F. Aricò, G. Gauthier, L. Rossi, A. E. Rosamilia, H. S. Bevinakatti, R. L. Sievert and C. P. Newman, "Green synthesis of dimethyl isosorbide," *ChemSusChem*, vol. 3, no. 5, pp. 566–570, 2010.

[151] C. Burger, M. Gerber, J. L. Du Preez, and J. Du Plessis, "Optimised transdermal delivery of pravastatin," *Int. J. Pharm.*, vol. 496, no. 2, pp. 518–525, 2015.

[152] D. Mohammed, P. J. Matts, J. Hadgraft, and M. E. Lane, "In vitro-in vivo correlation in skin permeation," *Pharm. Res.*, vol. 31, no. 2, pp. 394–400, 2014.

[153] M. Durand, V. Molinier, T. Féron, and J. M. Aubry, "Isosorbide mono- and di-alkyl ethers, a new class of sustainable coalescents for water-borne paints," *Prog. Org. Coatings*, vol. 69, no. 4, pp. 344–351, 2010.

[154] I. D. C. Rood, K. J. H. Kruithof, and K. J. Van den Berg, "Use of Derivatives of Dianhydrohexitol in the Preparation of Resins," EP2143743A1, 2010.

[155] G. Messant and F. Viez, "Utilisation d'un vernis biosourcé comme système de protection anti-graffitis," FR2987364A1, 2013.

[156] J. Nordstrom, L. Nordstrom, and S. Sheariss, "Curable Nail Composition and Methods for Strengthening and Repairing Nails," US 20140261512A1, 2014.

[157] S. Ma, D. C. Webster, and F. Jabeen, "Hard and Flexible, Degradable Thermosets from

Renewable Bioresources with the Assistance of Water and Ethanol," *Macromolecules*, vol. 49, pp. 3780–3788, 2016.

[158] X. Pan, P. Sengupta, and D. C. Webster, "High biobased content epoxy-anhydride thermosets from epoxidized sucrose esters of fatty acids," *Biomacromolecules*, vol. 12, no. 6, pp. 2416–2428, 2011.

[159] T. Modjinou, D. Versace, S. Abbad-andallousi, N. Bousserrhine, J. Babinot, and E. Renard, "Antibacterial Networks Based on Isosorbide and Linalool by Photoinitiated Process," *ACS Sustain. Chem. Eng.*, vol. 3, pp. 1094–1100, 2015.

[160] C. Lorenzini *et al.*, "Photoinduced Development of Antibacterial Materials Derived from Isosorbide Moiety," *Biomacromolecules*, vol. 16, pp. 683–694, 2015.

[161] C. Gioia, M. Vannini, A. Celli, M. Colonna, and A. Minesso, "Chemical recycling of post-consumer compact discs towards novel polymers for powder coating applications," *RSC Adv.*, vol. 6, pp. 31462–31469, 2016.

[162] C. Gioia, M. Vannini, P. Marchese, A. Minesso, R. Cavalieri, M. Colonna and A. Cellia, "Sustainable polyesters for powder coating applications from recycled PET , isosorbide and succinic acid," *Green Chem.*, vol. 16, pp. 1807–1815, 2014.

[163] D. P. Dworak, D. Gustafson, D. Mullen, A. D. Messana, A. Hynes, D. Ledwith and R. O'Kane, "(Meth)Acrylate-functionalized extended isosorbide," WO2016160135 A1, 2016.

[164] B. A. J. Noordover, V. G. van Staalduinen, R. Duchateau, C. E. Koning, R. A.T.M. van Benthem, M. Mak, A. Heise, A. E. Frissen and J. van Haveren, "Co- and Terpolyesters Based on Isosorbide and Succinic Acid for Coating Applications : Synthesis and Characterization," *Biomacromolecules*, vol. 7, pp. 3406–3416, 2006.

[165] B. A. J. Noordover, D. Haveman, R. Duchateau, R. A. T. M. van Benthem, and C. E. Koning, "Chemistry, functionality, and coating performance of biobased copolycarbonates from 1,4:3,6-dianhydrohexitols," *J. Appl. Polym. Sci.*, vol. 121, no. 3, pp. 1450–1463, 2011.

[166] P. Stenson, B. Prouvost, J. Niederst, D. G. Wind, R. H. Evans, C. Skillman, P. E. Share and J. Robinson, "Polymer having polycyclic groups and coating compositions thereof," US20110290696A1, 2011.

[167] R. A. T. M. van Benthem, J. van Heveren, C. E. Koning, and Y. Li, "Polyurethane Prepolymer and Aqueous Polyurethane Dispersion," WO2011098272A2, 2011.

[168] G. De Visscher and M. Takeiri, "Wound Dressing," WO2016135038A1, 2016.

[169] L. E. Katz, E. A. Barsa, B. W. Tucker, and P. V. Grosso, "Catalyst and process for producing isocyanate trimers," US5691440, 1997.

[170] H. Ashrafizadeh, P.Mertiny and A.McDonald, "Evaluation of the effect of temperature on mechanical properties and wear resistance of polyurethane elastomers," *Wear,*

vol. 368-369, pp 26-38, 2016

[171] N. D. Hann, “Effects of lithium bromide on the gel-permeation chromatography of polyester-based polyurethanes in dimethylformamide.,” *J. Polym. Sci. Polym. Chem. Ed.*, vol. 15, no. 6, pp. 1331–1339, 1977.

[172] I. A. Shkrob, T. W. Marin, Y. Zhu, and D. P. Abraham, “Why bis(fluorosulfonyl)imide is a ‘magic anion’ for electrochemistry,” *J. Phys. Chem. C*, vol. 118, no. 34, pp. 19661–19671, 2014.

APPENDICES

Annex A. SEC Measurements: Solubilization and stability of polyurethanes in Dimethylformamide

Size-Exclusion Chromatography of thermoplastic polyurethanes was performed in a 0.01M solution of bis(trifluoromethane)sulfonimide lithium salt ($LiNTf_2$) in dimethyl formamide (DMF) at 50°C, using a Viscotek pump (VE 1122 solvent delivery and VE 5111 Injektor Value Bracket), differential refractive index detector (Viscotek VE 3580 RI detector). Three porous styrene/divinylbenzene copolymer columns from Malvern, of porosity 10^3, 10^5 and 10^3 Å, including a precolumn, were used at a flow rate of 1.0 mL/min. Conventional calibration was used for both methods using polystyrene standards from Shodex. Volumes of 100 µL of solutions with 3 $mg.mL^{-1}$ concentration were injected.

1.1. SEC IN 0.01 M LITHIUM SALT DIMETHYLFORMAMIDE SOLUTION

Polyurethanes are highly polar polymers due to the inherent presence of the urethane or urea functions along their chains. As such, DMF is usually one of the few solvents in which high HS ratio TPUs are soluble due to its polar nature. SEC of polyester-based polyurethanes in DMF was studied by Hann *et al.* [171]. They have however shown that pure DMF used as the elution solvent imparts very strong interactions of the polymer with the stationary phase.

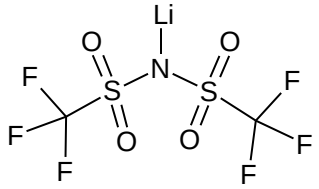

Figure A.1: Bis(trifluoromethane)sulfonimide lithium salt ($LiNTf_2$)

The addition of lithium salts in the DMF allows a better control of this phenomenon and more accurate measurements. Classically, LiBr and LiCl salts are used. However our equipment used $LiNTf_2$ (Figure A.1), as NTf_2^- is widely used to compose ionic liquid solvents [172]. It is indeed a non-coordinating anion, and thus easily dissociates from Li^+. This allowed to have a polyvalent SEC device in our laboratory.

1.2. REPRODUCIBILITY OF SEC MEASUREMENTS

The measurements obtained with DMF/$LiNTf_2$ SEC were however poorly reproducible and very high dispersity values (over 4) were obtained on some TPU formulations containing high ratio of HS, usually BDO-MDI-based HS. As the synthesis protocol was kept as similar as possible between BDO and ISO-based material, higher dispersity values for BDO were not expected. The reliability of the SEC measurement was thus explored. It was suspected that this dispersity difference and poor reproducibility could be due to interchain H-bond interactions from urethane functions.

In order to get insight into the phenomenon taking place, polyurethane solutions of around 2.5 mg/mL in 0.01 $LiNTf_2$ DMF solutions were made. Chosen samples were TMB50 and TMI50 synthesized through Method F, both presented in Chapter 2. SEC was performed 4 days and 11 days after the making of the solutions as dissolution of the PU materials was slow and could take up to one week in some cases. The clear solutions were filtered through a 0.20 µm porosity filter prior to SEC measurement. In order to check the stability of the separation columns, a freshly made polystyrene standard solution was tested the same day as the polyurethane solutions.

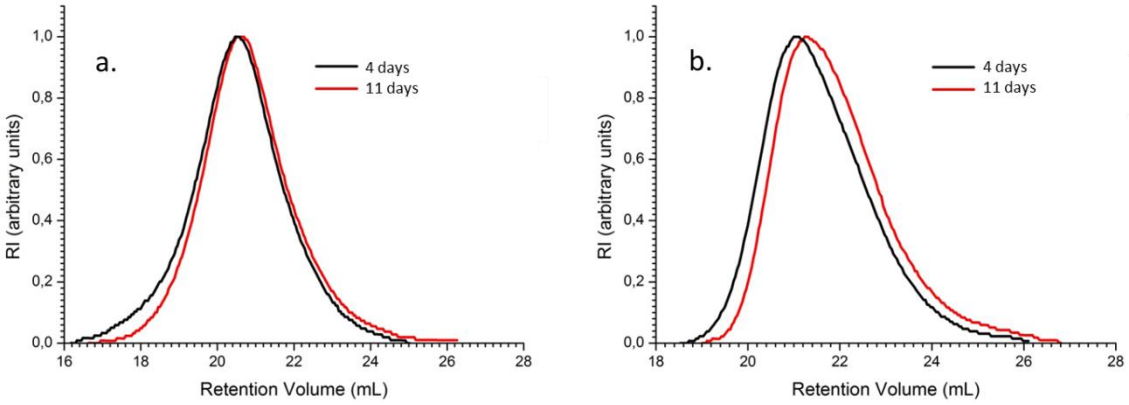

Figure A.2: SEC curves of PTMEG based polyurethanes, in DMF 0.01 $LiNTf_2$ – a. TMB50 with BDO as the chain extender – b. TMI50 synthesized by method F with ISO as the chain extender

The SEC results are presented in Figure A.2 and Table A.1; from the results obtained on the polystyrene (PS) standard, the separation column is stable, and the difference between day 4 and 11 cannot be explained by a drift of the column or bad calibration.

Table A.1 : Composition and molar mass of poly(tetrahydrofuran) and MDI-based polyurethanes – obtained by SEC in $LiNTf_2$ 0.01 M solution at 1 mL/min and calculated from polyestyrene standards

Sample	Chain extender	wt% HS	Time (days)	M_n (kg.mol^{-1})	M_w (kg.mol^{-1})	Đ (M_w/M_n)
TMI50 – Method F	ISO	51	4	23 ±2	60 ±6	2.6
			11	17 ±2	48 ±5	2.8
TMB50	BDO	48	4	78 ±8	273 ±27	3.5
			11	37 ±4	130 ±13	3.5
Polystyrene (PS) standard M_w=53 kg.mol^{-1}	*As PS degrades in DMF, a new solution was made right before each SEC run		4*	44 ±4	53 ±5	1.2
			11*	42 ±4	53 ±5	1.3

From the SEC curves of Figure A.2, TMB50 high volume retention curves overlap. However, there is a significant decrease of entities appearing at smaller retention volume from day 4 to day 11. TMI50 is overall shifted toward the higher retention volumes as time goes. This is reflected by the values in Table A.1. Molar masses of TMI50 have decreased of around 25% while the molar masses of TMB50 have decreased by half. It is then understood that such a drop could account for large measurement errors. The fact that the dispersity index stays constant is also surprising, and it is probable that no degradation occurs.

In the following sections, a longer study of the molar mass evolution will be presented, as well as an investigation on possible degradation of the polyurethanes in the DMF solution.

1.3. STABILITY STUDY OF POLYURETHANE SOLUTIONS IN DMF

The same test as presented in the previous section was performed over a longer time on TMB50, and TMI50 synthesized with original and F method. Results are presented in the following Figure A.3 and Figure A.4**.**

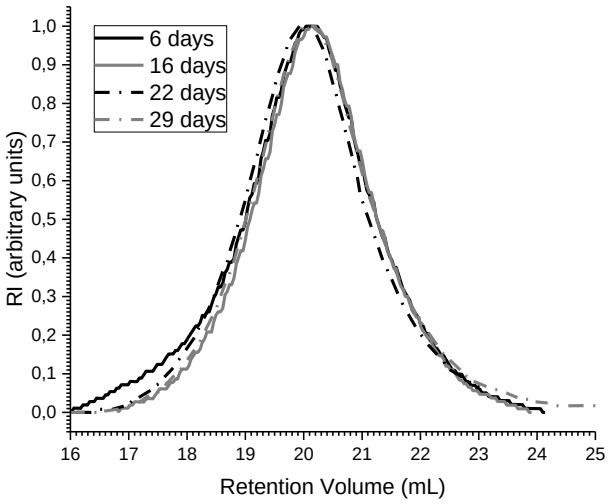

Figure A.3 : SEC curves of PTMEG and BDO based polyurethanes TMB502 followed for 1 month, in DMF 0.01 $LiNTf_2$

The same results as presented in the previous section were reproduced with TMB50 over the first 16 days of the test. Curves were then overlapping from 16 to 29 days, as can be also seen from the stabilization of value of the molar mass curve on Figure A.4. Both TMI50 samples however showed rather small variation over the time span of the test. On Figure A.4 b, the untypical curve of day 22 probably originates from a bad SEC run, as all the other tests run on this sample are otherwise consistent between themselves.

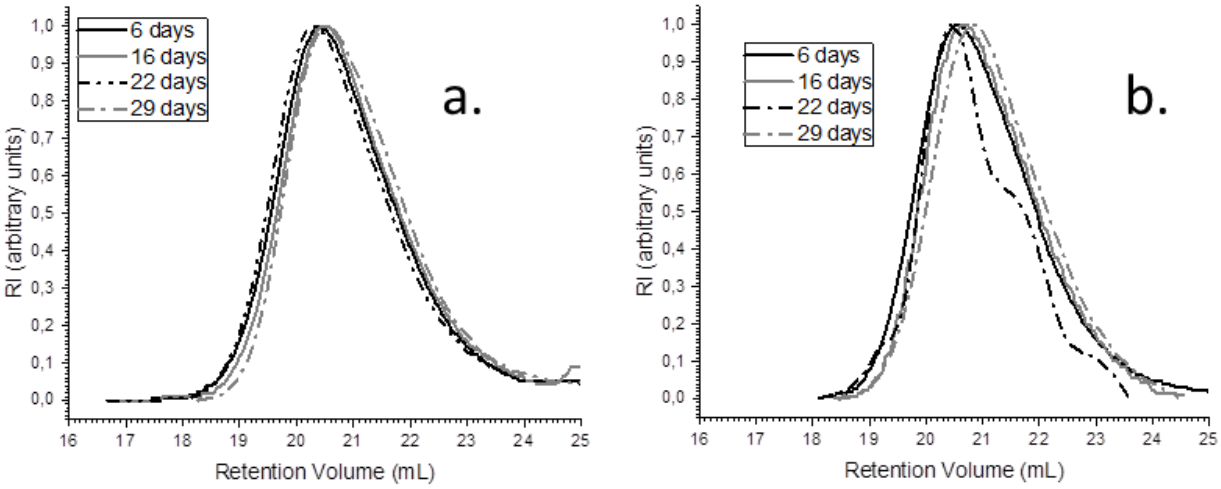

Figure A.4: SEC curves of PTMEG based polyurethanes, in DMF 0.01 $LiNTf_2$ – a. TMI50 synthesized by original method with ISO as the chain extender – b. TMI50 synthesized by method F with ISO as the chain extender

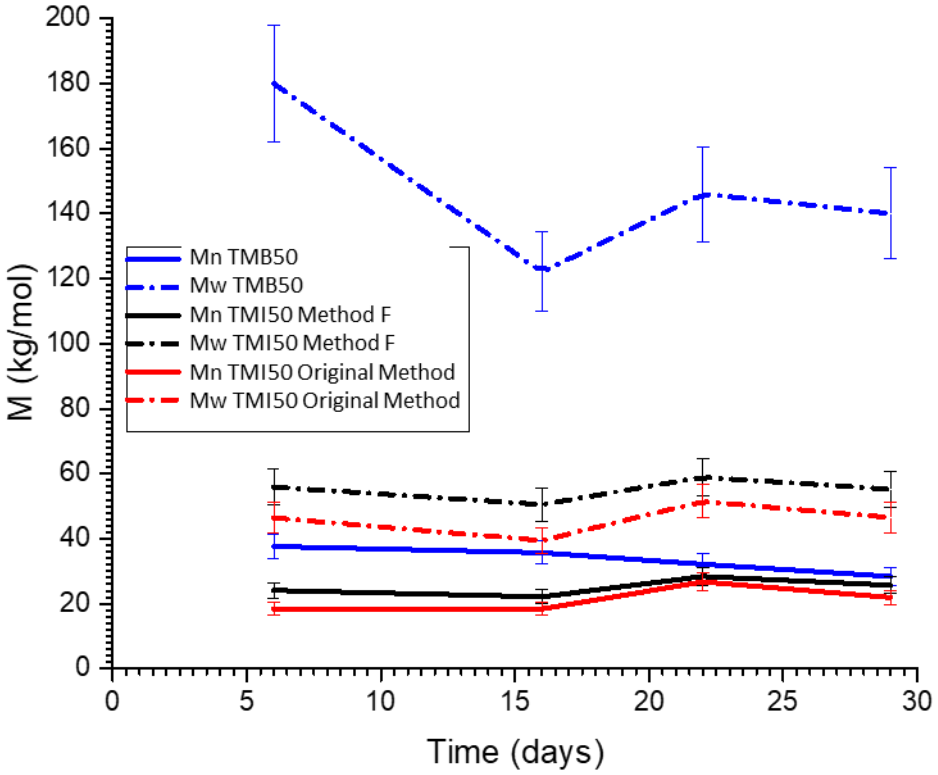

Figure A.5: Average molar masses M_n and M_w, as a function of time in 0.01M $LiNTf_2$ DMF solution

In summary, it is probable that the stabilization of the ISO-based samples occurs between 4 and 6 days, while for the BDO-based samples, stabilization seems to occur between 6 and 14 days. However, the very slow dissolution of the samples in DMF could also be due to slow degradation of the sample. ^{1}H NMR was then used in order to rule out degradation as the origin of the molar mass decrease and stabilization observed in this test.

1.4. DEGRADATION STUDY OF POLYURETHANE IN DMF

Degradation in 0.01M $LiNTF_2$ in DMF-d7 was assessed by making 30 mg/mL solutions of the studied polyurethanes in the solvent. Chemical shifts of TMB50 and TMI50 spectra were attributed and results are presented in Figure A.6 and A.7 and Table A.2 and Table A.3**.**

Table A.2 : Chemical shifts and attributions for sample TMB50 in DMF-d7 with 0.01M of $LiNTf_2$

Chemical Shift δ(ppm)	Attribution
1.58-1.68	1. (middle chain CH_2 from PTMEG and BDO)
2.74-2.91	DMF
3.39	2. (-CH_2 adjacent to ether O from PTMEG)
3.48	H_2O
3.86	3.
4.13	4. (CH_2 adjacent to O from urethane function)
6.59-7.51	5. and 5’ (aromatic CH from MDI)
8.02	DMF
9.47	6.

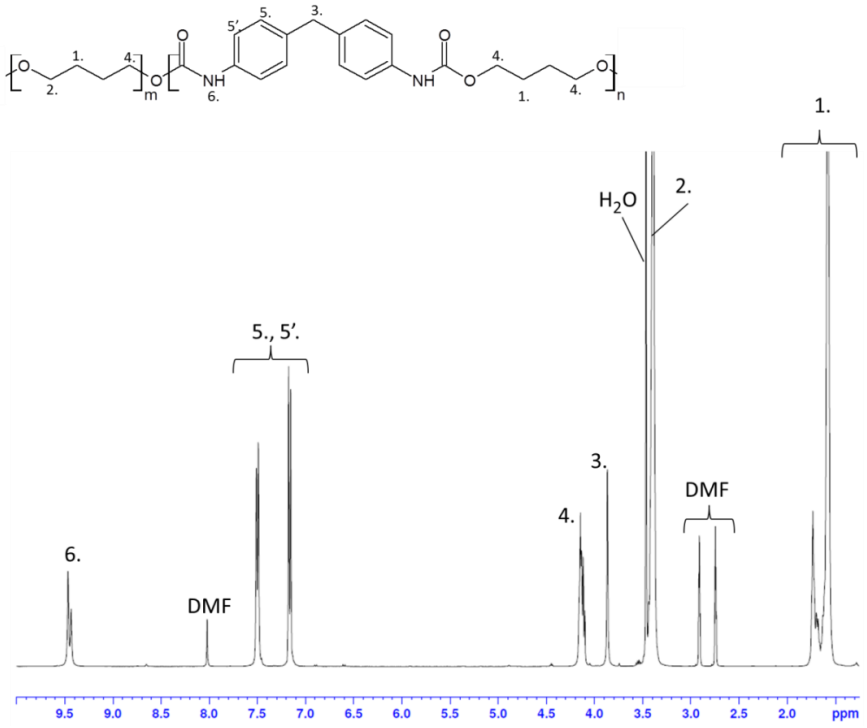

Figure A.6:^{1}H NMR spectrum of polyurethane based on PTMEG, MDI and BDO TMB50, and chemical structure in DMF-d7 with 0.01M of $LiNTf_2$.

Table A.3: Chemical shifts and attributions for sample TMI50 (synthesis with original method) in DMF-d7 with 0.01M of $LiNTf_2$

Chemical Shift δ(ppm)	Attribution
1.58-1.68	1. (middle chain CH_2 from PTMEG)
2.74-2.91	DMF
3.39	2. (-CH_2 adjacent to ether O)
3.47	H_2O
3.88	3.
3.81-3.98	4. and 5.
4.12	6. (CH_2 adjacent to O from urethane function)
4.54	7. (inner ring -CH)
4.80	7. from end-chain isosorbide
4.88	8. (inner ring -CH)
5.11	9. (-CH adjacent to exo-OH)
5.20	10. (-CH adjacent to endo-OH)
6.59-7.51	11. and 12’ (aromatic CH from MDI)
8.02	DMF
9.44	13.
9.71	14.

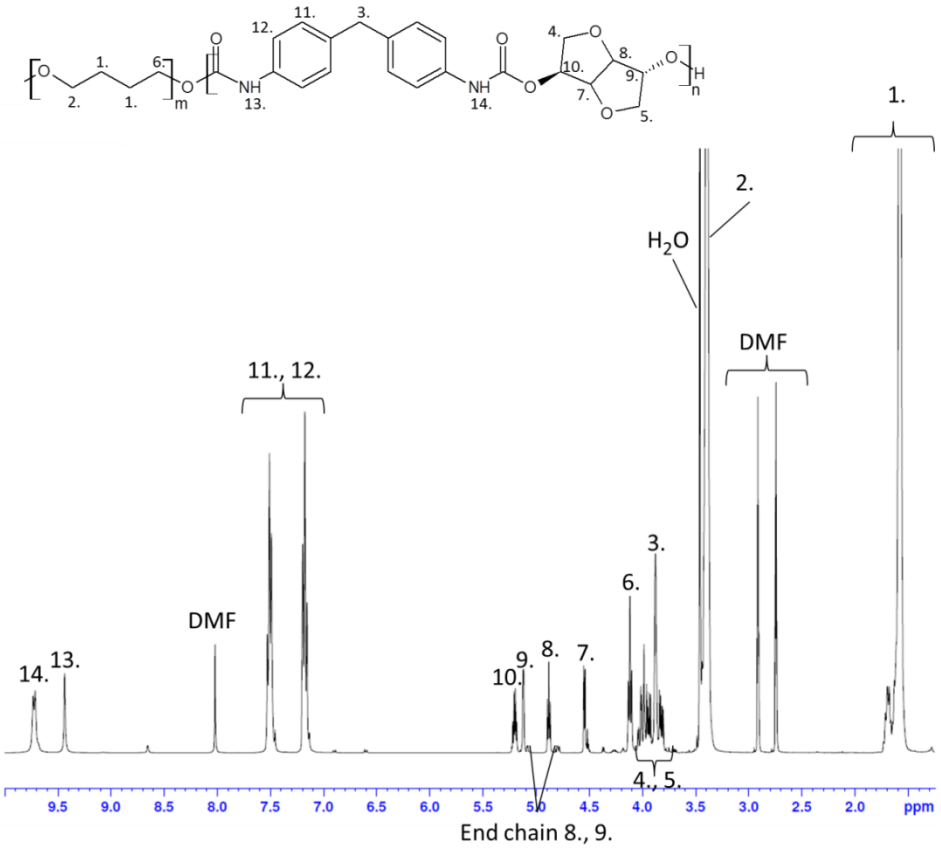

Figure A.7: ^{1}H NMR spectrum of polyurethane based on PTMEG, MDI and ISO TMI50 (original synthesis method), and chemical structure in DMF-d7 with 0.01M of $LiNTf_2$.

NMR analysis was then performed periodically over a period of 3 weeks after the making of the sample solutions. Spectra are presented in Figure A.8 to A.10. No peak shifting nor peak appearance or disappearance over time was observed in any of the sample spectra. Peak integrals were stable over time as well. No evidence of chemical degradation could be found from this study.

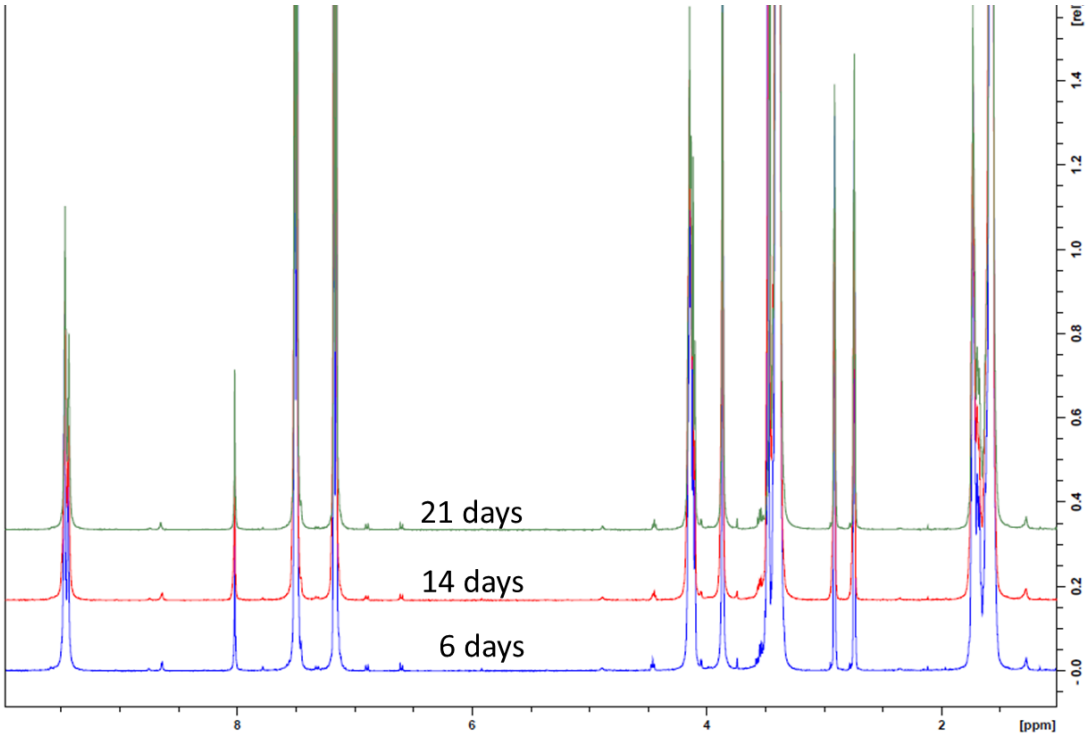

Figure A.8: ^{1}H NMR spectra of polyurethane based on PTMEG, MDI and BDO TMB50, and chemical structure in DMF-d7 with 0.01M of $LiNTf_2$.

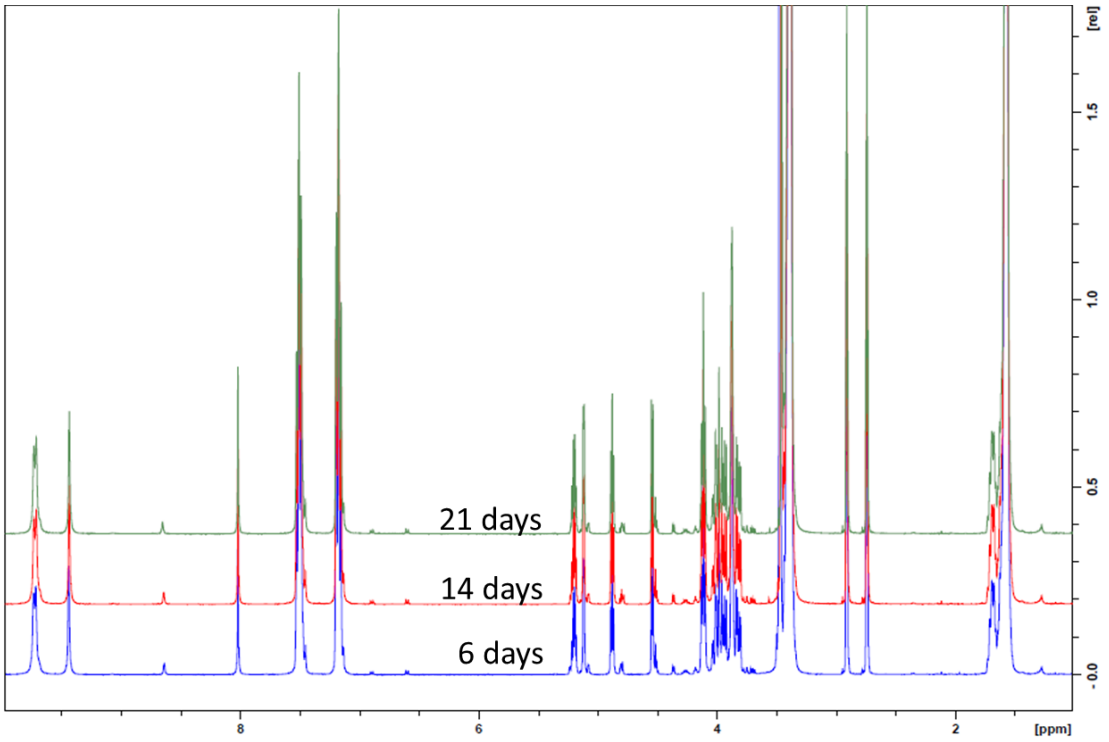

Figure A.9: ^{1}H NMR spectra of polyurethane based on PTMEG, MDI and ISO TMI50 (original synthesis method), and chemical structure in DMF-d7 with 0.01M of $LiNTf_2$.

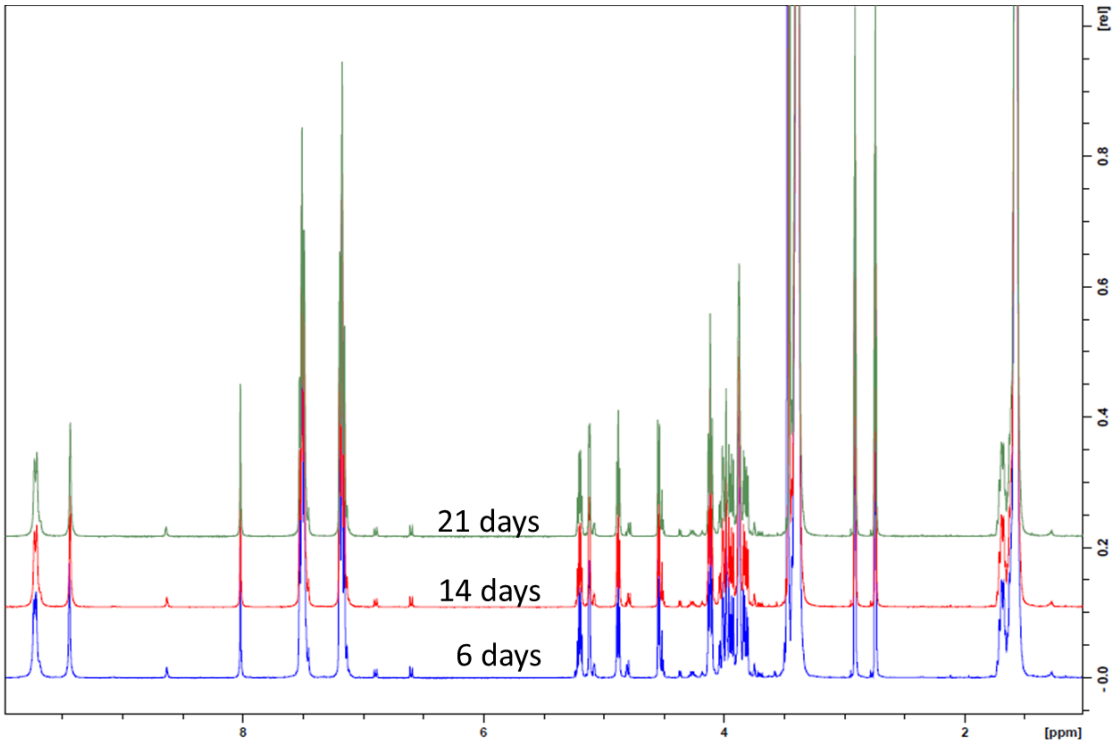

Figure A.10: ^{1}H NMR spectrum of polyurethane based on PTMEG, MDI and ISO TMI50 (synthesis method F), and chemical structure in DMF-d7 with 0.01M of $LiNTf_2$.

1.5. CONCLUSION

From the SEC tests and NMR analysis, it seems that the decrease in molar mass observed by SEC is not due to degradation. Dispersity is as well constant over time. This phenomenon thus most probably originates from slow breakage of H-bonds over time, as it is especially high in highly segregated and crystalline materials such as BDO/MDI based samples.

However, it often results in inconsistent and poorly reproducible molar mass measurements. It was then decided to always perform SEC runs 14 days after the making of the polyurethane solutions.

Annex B. List of Symbols and Abbreviations

%mol	Molar percentage
wt%	Mass Percentage
δ	NMR Chemical shift
ΔC_p	Variation of thermal capacity at standard pressure
ΔH_f	Enthalpy of fusion
Đ	Dispersity
ω^{HS}	Weight fraction of hard segment
ω^{SS}	Weight fraction of soft segment
AFM	Atomic Force Microscopy
AQD	2,5-bis(N-2-hydroxymethyl-N-methylamino)-1,4-benzoquinone diol
BDO	1,4-Butanediol
$CDCl_3$	Deuterated chloroform
CPK	Cyclopentanone
DBTDL	Dibutyltin dilaurate
DDI	2-Heptyl-3,4-bis(9-isocyanatononyl)-1-pentylcyclohexane
DMA	Dynamic Mechanical Analysis
DMF	N,N-Dimethylformamide
DMI	Dimethylether of isosorbide
DMSO	Dimethylsulfoxide
DSC	Differential Scanning Calorimetry
Eq_{NCO}	NCO Index of prepolymer ($mol.kg^{-1}$)
EELDI	Ethyl ester L-lysine diisocyanate
FADM	Fatty Acid dimer based macrodiol
FTIR	Fourier Transform Infrared Spectroscopy
G'	Storage Modulus
G''	Loss Modulus

HCl	Hydrochloric acid
HDI	Hexamethylene diisocyanate
HQEE	Hydroquinone bis(2-hydroxyethyl) ether
HMDI	Hydrogenated 4,4'-diphenylmethylene diisocyanate
HS	Hard Segment
I_{OH}	Hydroxyl Index
I_{NCO}	NCO Index of diisocyanates ($mol.kg^{-1}$)
IPDI	Isophorone diisocyanate
ISO	Isosorbide
IsoOP	Polyether oligomer based on isosorbide
$LiNTf_2$	Bis(trifluoromethane)sulfonimide lithium salt
MDI	4,4'-diphenylmethylene diisocyanate
MEK	Butan-2-one
MIBK	Methylisobutylketone
MME	Multiple Melting Endotherms
M_n	Number Average Molar Mass
M_w	Weight Average Molar Mass
MWCNT	Multi-walled carbon nanotube
NMR	Nuclear Magnetic Resonance
OTPDM	3,5-bis(1,3-oxathiolan-2-yl)- 1,2-cyclopentanedimethanol
PCD	Polycarbonate Diol
PCL	Poly(ε-caprolactone)
PEO	Polyethylene oxide
PMDI	Pentamethylene diisocyanate
ppm	part per million
PPO	Polypropylene oxide
PTMEG	Poly(tetrahydrofuran)
PU	Polyurethane
RI	Refraction index

SAXS	Small Angle X-Ray Scattering
SEC	Size Exclusion Chromatography
SS	Soft Segment
T_α	Temperature of the principal mechanical transition (α transition)
tan δ	Damping factor
T_b	Boiling temperature
T_f	Melting temperature
T_g	Glass transition Temperature
T_g^{SP}	Glass transition Temperature of soft phase
T_g^{HP}	Glass transition Temperature of hard phase
T_g^{HS}	Glass transition Temperature of hard segments
T_g^{SS}	Glass transition Temperature of soft segments
TDI	Toluene Diisocyanate
THF	Tetrahydrofuran
THFDM	Tetrahydrofuran dimethanol
t-IPDI	Isophorone diisocyanate trimer
t-PMDI	Pentamethylene diisocyanate trimer
TPU	Thermoplastic polyurethane